NASA Contractor Report 3729

Aeroelastic Analysis for Propellers

Mathematical Formulations and Program User's Manual

R. L. Bielawa, S. A. Johnson,
R. M. Chi, and S. T. Gangwani
United Technologies Research Center
East Hartford, Connecticut

NASA

National Aeronautics
and Space Administration

Scientific and Technical
Information Branch

1983

PREFACE

The G400PROP mathematical formulations and resulting computer code described herein were developed by United Technologies Research Center (UTRC) under contract NAS3-22753, "Development of a Comprehensive Aeroelastic Analysis for Propellers". This contract was through the Lewis Research Center of NASA with Mr. Oral Mehmed acting as contract monitor. The initial development of the G400 analysis was conducted at UTRC by Dr. Richard L. Bielawa under Corporate sponsored independent research and development. Extensive refinements to the analysis were made under sponsorship of the Langley Research Center of NASA and the U.S. Army Mobility R&D Laboratory, Langley Directorate as part of Contract NAS1-10960. Subsequently, further development was supported by Sikorsky and Hamilton Standard Divisions of United Technologies Corporation as well as the Structures Laboratory of the USRTL (AVRADCOM) under contract NAS1-16058. Sally Ann Johnson was responsible for developments in the expanded eigensolution, the PANPER interfacing and sample calculation portions of the report. She furthermore shared with Dr. Ray M. Chi in the development of the unstalled unsteady airloads development. Dr. Santu T. Gangwani was responsible for the extentions of the UTRC stalled airloads theory to the higher subsonic Mach numbers.

Aeroelastic Analysis for Propellers -
Mathematical Formulations and Program User's Manual

TABLE OF CONTENTS

Aeroelastic Analysis for Propellers -
Mathematical Formulations and Program
User's Manual*

by

Richard L. Bielawa,
Sally A. Johnson,
Ray M. Chi,
Santu T. Gangwani

United Technologies Research Center

SUMMARY

Mathematical development is presented for a specialized propeller
dedicated version of the United Technologies Corporation G400 Rotor Aero-
elastic Analysis. This specialized analysis, G400PROP, simulates aeroelastic
characteristics particular to propellers such as structural sweep, aerodynamic
sweep and high subsonic unsteady airloads (both stalled and unstalled).
Detailed formulations are presented for these expanded propeller related
methodologies. Results are presented of limited application of the analysis
to realistic blade configurations and operating conditions which include
stable and unstable stall flutter test conditions.

Sections are included for enhanced program user efficiency and expanded
utilization. This material includes (1) a detailed description of the
structuring of the G400PROP FORTRAN coding, (2) a detailed description of
the required input data, (3) a detailed description of the output results,
and (4) general information to facilitate operation and improve efficiency.

INTRODUCTION

With recent renewed interest in propellers has come a redirection of
design innovation and a need to advance the state-of-the-art in this
technology. Major advances in materials and construction techniques on one
hand, and the increasing ability to optimize basic aerodynamic efficiency
on the other, are producing propeller designs which now require greater
attention to analysis. A notable example is the so-called prop-fan which
has extensive structural and aerodynamic sweep, relatively thin sections and
operates in transonic flow conditions. This general acceleration in the growth
of propeller state-of-the-art has especially increased the importance of
structural integrity in a dynamic and/or aeroelastic environment. It is this
aspect of propeller development to which the subject matter of this report is
directed.

Definition of Problem

The assurance of satisfactory structural dynamic behavior and in particular
aeroelastic (flutter) stability requires an accurate aeroelastic analysis
specifically directed to the particular characteristics of advanced propeller
designs. The purpose of this document is to describe the more important
details of the G400PROP aeroelastic analysis developed to satisfy the analysis
requirements of advanced propeller designs.

The specific characteristics of advanced technology propellers as they
relate to aeroelasticity can be readily identified. First, these propellers
will generally continue to have sufficiently high aspect ratios, thereby
justifying the treatment of them as beams for most aeroelastic problem areas.
It is to be expected that, for some configurations with relatively low
aspect ratio and high structural sweep, the beam theory formulation may have
to be abandoned in favor of a more comprehensive plate theory formulation
for some aeroelastic problem areas. The relatively low-cost advantages of
beam theory formulations, however, together with the sustained applicability
to configurations which do have high aspect ratios clearly justify develop-
ment of a comprehensive aeroelastic analysis for propellers using beam theory.

A second relevant characteristic of advanced technology propellers is
the departure from the usual straight, torsionally rigid planforms. Within
the technology available to build them, propellers are being designed with
large sweeps and thinner sections to be rotated at significantly increased
tip speeds in order to capitalize on the aerodynamic efficiencies which
result. Structural sweep in a propeller blade is a relatively new and
important aeroelastic consideration and clearly must be dealt with. The prime

2

importance of sweep is the large degree of coupling it introduces between bending and torsion. Based on experience with fixed wing sweep, this coupling must necessarily alter the aeroelastic behavior of propellers. The degree of aeroelastic involvement will also increase for these propellers due to the relative torsional softening caused by the thinner sections. Of particular significance is the increased susceptibility of these propellers to stall flutter, a condition usually experienced at the high thrust (high pitch angle) static flow conditions at take off.

With the exception of structural sweep, the established validity of a beam formulation and the requirement to analyze known rotary wing aeroelastic phenomena (including stall flutter) form justifications for using a helicopter rotor aeroelastic analysis as a basis for advanced propeller aeroelastics. To this end, a highly successful helicopter and wind turbine aeroelastic analysis, the United Technologies Corporation (UTC) G400 Rotor Aeroelastic Analysis, was selected for enhanced development appropriate to advanced technology propellers. Two features of this analysis made it especially attractive to this application: First, it already had an advanced method for analyzing stall flutter, and second, it was formulated elastomechanically in a manner as to accommodate readily the inclusion of built-in structural sweep. Under NASA sponsorship, a development effort was therefore undertaken to modify a copy of the UTC G400 analysis into a comprehensive aeroelastic analysis dedicated to the requirements of both general aviation and advanced technology propellers.

Figure 1 presents an overview of this resulting computer code, G400PROP. The three principal types of inputs to the code are the physical description of the propeller (geometry, inertia, and elastic properties), the flight condition as defined by air density, speed of sound, propeller airspeed, and control (pitch) angle and, finally, an optional description of the detailed flow field resulting from nacelle blockage and wake/nacelle interaction considerations. The analysis generates dynamic equations of motion, which use a beam theory, normal modes basis and incorporates the higher order aeroelastic characteristics of structural sweep, structural twist, and unsteady airloads. For these dynamic equations, two principal solution types are produced: (1) eigensolutions, as defined in the Laplace Transform variable domain, and (2) time-history solutions appropriate to the calculation of transients. The principal uses of the eigensolution are the calculations of vacuum coupled modes (frequencies and mode shapes), and of those aeroelastic stability phenomena which can be readily linearized. The principal uses of the time-history solution are the calculations of transients resulting either from strongly nonlinear aeroelastic stability phenomena or control inputs, of aerodynamic performance, and of harmonic responses of both hub loads and blade stresses resulting from harmonic aerodynamic excitation.

3

FLIGHT CONDITION
(AIRSPEED, CONTROL ANGLE)

PROPELLER CONFIGURATION
(PHYSICAL DESCRIPTION)

INFLOW
CHARACTERISTICS

G400PROP AEROELASTIC
ANALYSIS

- BEAM BENDING & TORSION MODES
- STRUCTURAL SWEEP & TWIST
- UNSTEADY AIRLOADS

EIGENSOLUTION
- VACUUM
- NONVACUUM

TIME HISTORY
SOLUTION

COUPLED MODES
& FREQUENCIES

(LINEAR)
AEROELASTIC
STABILITY

TRANSIENTS,
(NONLINEAR)
AEROELASTIC
STABILITY,
CONTROL INPUTS

HARMONIC
RESPONSES,
STRESSES

PERFORMANCE

Figure 1. Overview of G400PROP Aeroelastic Analysis

The version of the G400 used as a basis for the development of G400PROP was already structured in the form shown in Figure 1. However, several specific modifications and enhancements were required to develop G400PROP. Principal areas in which modifications were required consisted of the following:

1. All specific helicopter and wind turbine related modelings were to be stripped.

2. The eigensolution portion of the analysis was to be upgraded to include both structural and aerodynamic sweep.

3. The established UTRC unsteady stalled airloads methodology was to be extended to include high subsonic Mach number data.

4. A differential equation (transfer function) modeling of unsteady unstalled airloads was to be developed and implemented.

5. The analysis was to be configured to interact with an existing variable inflow analysis which describes the propeller/nacelle interactive flow field.

Review of Existing Documentation

The G400PROP propeller aeroelastic analysis described herein represents a specialization of an ongoing aeroelastic analysis development originally formulated for the unique aeroelastic characteristics of the composite bearingless rotor. It represented an advancement in the state-of-the-art with regard to the modeling of rotors with time-variable, nonlinear structural twist and multiple structural redundancy, as described in Reference 1. Since the publication of that report, the basic G400 program has evolved into a family of analyses with a completely general range of applicability in rotor type (articulated, hingeless, teetered) and vehicle application (helicopters, propellers, wind turbines).

Most of the major documentation available on the G400 technology is contained in References 1 through 3. A review of their existing literature with regard to analytical alternatives to the G400 approach is contained in Reference 1 and a review of such alternate approaches now would be inappropriate. Reference 1 presents most of the basic ideas inherent in the G400 methodology upon which the present continuing development was made. The primary purpose of the present report, therefore, is to present the additional formulations required to meet the special requirements of analyzing advanced technology propellers. In addition, the development of this propeller oriented code coincidentally resulted in enhanced general program efficiency and capability. Therefore, a secondary purpose of this report is to increase

program user efficiency and to facilitate integration of G400PROP into industrial propeller design processes.

Summary of New Technology

All of the objectives identified for this development, as itemized in the first subsection above, were successfully met. The first major section to follow summarizes the unified theory developed for extending the original G400 twist related transformations to the more general case including structural sweep. The next four sections deal with elements of advanced aerodynamic modeling especially important to propellers. The first and fourth of these, which deal with aerodynamic sweep and inflow, respectively, are related more to aerodynamic "geometry" and are applicable even to steady flow conditions. The second and third of these aerodynamic sections deal with truly unsteady airloads and are those most directly related to propeller aeroelasticity. The following section presents the salient features of the enhanced eigensolution which include details of the modeling of perturbational sweep and unstalled unsteady related airloads. The following section presents details of limited application of the analysis to realistic propeller designs and appropriate operating conditions. The remaining four sections provide detailed program user information for the actual G400PROP computer program which implements the formulations presented herein.

LIST OF SYMBOLS AND FORTRAN EQUIVALENTS

Symbol	FORTRAN Equiv.	Description
A	ARATE, AUNST	Nondimensional aerodynamic section angle-of-attack time derivative ($=\dot{\alpha}c/2U_n$)
[A]	AA	Inertia coupling matrix
A_1, A_2, A_3	CLA1, CLA2, CLA3, (CMA1, CMA2, CMA3)	Coefficients for inflow angle Padé augmented state variables, for either lift (or pitching moment) coefficients, (ND)
a, b, c, d, e, f	(None)	Coefficients defining Padé approximant functionality
a_{oL}	AO	Aerodynamic section static lift curve slope, deg^{-1}
a_∞	SPSD	Sonic velocity at freestream conditions, fps
B	TL	Tip loss factor
[B]	BB	Damping matrix for blade eigensolution
B_1, B_2, B_3, B_4	CLB1, CLB2,...., (CMB1, CMB2,...)	Coefficients for pitching angle Padé augmented state variables, for either lift (or pitching moment) coefficients, (ND)
b	BL	Number of blades
[C]	CC	Stiffness matrix for blade eigensolution
C_A, C_w, C_α	(CADM, CARE), (CWDM, CWRE), CATE	Empirical coefficients multiplying A, α_w and α, respectively, in dynamic stalled airloads functionality, (ND)
C_{Ds}, C_{Ls}, C_{Ms}	CDS, CLS, CMS	Aerodynamic section static drag, lift and pitching moment coefficients, respectively, as used in unsteady stalled airloads modeling
C_{Du}, C_{Lu}, C_{Mu}	UNCD, UNCL, UNCM	Aerodynamic section unsteady drag, lift and pitching moment coefficients, respectively, (ND)
$-C_{L1}, \Delta C_{L2}$	DELC1, DELC2	Incremental lift coefficients (ND)
c	CHORD, CHORDB	Blade section chord, ft and (ND)
c_d	CD, ACD, CDTOT	Section aerodynamic drag coefficient, (ND)
c_{d_p}, c_{d_s}	CDP, (CDS, CDSKNF)	Section aerodynamic pressure and skin friction drag coefficients, respectively, (ND)
c_ℓ	CL, ACL	Section aerodynamic lift coefficient, (ND)
$c_{\ell_\alpha}, c_{m_\alpha}$	(None)	Unsteady aerodynamic section lift and pitching moment coefficients, respectively, due to pitching motion
c_{ℓ_h}, c_{m_h}	(None)	Unsteady aerodynamic section lift and pitching moment coefficients, respectively, due to plunging motion
c_{ℓ_o}, c_{m_o}	(None)	Steady-state section lift and pitching moment coefficients, respectively, to be used in conjunction with the incremental Padé section lift and moment coefficients, (ND)
$c_m, c_{m_{c/4}}$	CM, ACM	Section aerodynamic pitching moment about the quarter chord, (ND)

7

LIST OF SYMBOLS AND FORTRAN EQUIVS. (Cont'd)

Symbol	FORTRAN Equiv.	Description
$c_{L_0}, c_{L_1}, c_{L_2}$	CLOPAN, CL1PAN, CL2PAN	Quadratic components of the lift coefficient required by PANPER routine
$c_{D_0}, c_{D_1}, c_{D_2}$	CDOPAN, CD1PAN, CD2PAN	Quadratic components of the drag coefficient required by PANPER routine
c_4	CRDPAN	Blade section chord in the 4-coordinate system, (ND)
Δc	(None)	Generalized incremental lift or pitching moment coefficient, defined by Padé theory, (ND)
$\Delta c_\ell, \Delta c_m$	DCL, DCM	Incremental section lift, or pitching moment, coefficients defined by Padé theory, (ND)
D_p, D_s	(None)	Section aerodynamic pressure and skin friction drags, respectively, lb/in.
$DUEAE_k, DUEAF_i$	DUEAE, DUEAF	Radial foreshortening of blade element point due to linear variations of k'th edgewise and i'th flatwise bending modes, respectively, (ND)
DUEAO	DUEAO	Radial foreshortening of blade element point due to built-in sweep
[DFDZ]	DFDZ	Partial derivative matrix of aerodynamic loadings with respect to intermediary perturbation vector
EB_1	EB1B	Nonlinear torsion stiffness parameter (to be multiplied by twist rate cubed), lb-ft^4
EB_2	EB2B	Torsion to edgewise elastic coupling stiffness (to be multiplied by twist rate), lb-ft^3
EI_y, EI_z	EIYB, EIZB	Section bending stiffness in flatwise and edgewise directions, respectively lb-in.^{2} or (ND)
e	ER	x_2 coordinate of coincident flat-lag hinge or hingeless blade offset point, in.
1E	(None)	1st blade edgewise mode
1F, 2F, 3F, 4F, 5F	(None)	1st through 5th blade flatwise modes
GJ	GJ, GJT, GJEFF	St. Venant (linear) torsion stiffness, lb-in.^{2}
I_E	(None)	Edgewise area moment of inertia distribution, in.^{4}
I_F	(None)	Flatwise area moment of inertia distribution, in.^{4}
$\lceil I_m \rfloor$	(None)	Identify matrix of dimension m
i	(None)	Square root of -1.
k	(None)	Aerodynamic section reduced frequency (= $\omega c/2U_N$)
k_A	PRGS	Area radius of gyration of tension carrying portion of blade section, in.
$k_{y_{10}}, k_{z_{10}}$	KY10, KZ10	Mass radii of gyration of blade section about axes through and perpendicular to the spanwise (x_5) axis and in the chordwise and thicknesswise directions, respectively, in.

8

Symbol	FORTRAN Equiv.	Description
L	(None), ELL	Alternately (section aerodynamic lift distribution), and local radius of intersection of blade section midchord with section boundary, measured from axis $\mathcal{Q}$, (ND)
M	MACH	Mach number
M_x	(None)	Section aerodynamic pitching moment distribution, in.-lb/in.
$\bar{m}$	XMASSB	Blade mass distribution (ND)
m_o	XMO	Reference blade mass distribution, taken to be that of the 5th blade segment, $lb\text{-}sec^2/ft^2$
NEM,NFM,NTM	(Same)	Numbers of assumed flatwise, edgewise, and torsion natural "uncoupled" primitive modes, respectively
n	N	Blade segment index
$\bar{n}_1, \bar{n}_2, \bar{n}_3$	(None)	Unit vectors defining aerodynamically swept coordinate system, (ND)
O( )	(None)	Denotes order of magnitude
P	(None)	Per rotor revolution, (ND)
P_1, P_2, P_3	P1,P2,P3	Empirical coefficients for C_{Lu} functionality
p	(None)	Aerodynamically nondimensional Laplace transform variable
$P_{x_5}, P_{y_5}, P_{z_5}$	SX5,SY5,SZ5	Section shear load distributions in directions of axes in the 5-coordinate system, (ND)
P_1, P_2	CLP1,CLP2 (CMP1,CMP2)	Padé poles for pitching, for either lift or pitching moment coefficients, (ND)
$\hat{P}_1, \hat{P}_2$	CLP1C,CLP2C, (CMP1C,CMP2C)	Padé poles for plunging for either lift or pitching moment coefficients, (ND)
$Q_1, Q_2, \ldots Q_7$	Q1,Q2,...Q7	Empirical coefficients for C_{Lu} functionality
{Q}	Q	Vector of blade degrees-of-freedom
q	Q	General expression for a response variable deflection
q_{v_k}	QVL(K)	Blade k'th edgewise modal response variable
q_{w_i}	QWL(I)	Blade i'th flatwise modal response variable
$q_{x_5}, q_{y_5}, q_{z_5}$	XM5,YM5,ZM5	Section moment load distributions about axes in the 5-coordinate system, (ND)
q_{θ_j}	QTL(J)	Blade j'th torsion modal response variable
R	R	Rotor radius, ft
R_n	(None)	Reynolds number
$R_1, R_2, \ldots R_8$	ARE1,ARE2,...ARE8	Empirical coefficients for C_{Du} functionality
$\bar{r}$	X	Blade spanwise coordinate, measured from offset, e, in x_5 direction (ND)

Symbol	FORTRAN Equiv.	Description
$\Delta r_i, \Delta x_i$	DX,QUAD	i'th blade spanwise segment (arc) length, (ND)
s	SSS	Aerodynamic time
s_m	SSSM	Nondimensional time measured from instant of stall onset
T	TENSB,TENST	Tension at an arbitrary spanwise station, (ND)
[TAS]	TAS	Coordinate transformation matrix relating "5" and "6" coordinate systems, due to structural sweep, (ND)
$[TAS^{(A)}]$	ATAS	Coordinate transformation matrix relating "5" and "8" coordinate systems, due to aerodynamic sweep, (ND)
$[TR_{45}]$	TR45	Coordinate transformation matrix relating "4" and "5" coordinate systems, (ND)
1T,2T	(None)	1st and 2nd blade torsion modes
t	T	Time, sec
t_{dm}	(None)	Time when dynamic stall first occurs
U	U	Total aerodynamic section inflow velocity, (ND)
U_N	UN	Vector sum of U_T and U_P aerodynamic section, inflow velocities, (ND)
U_R, U_T, U_P	UR,UT,UP	Total aerodynamic section inflow velocities in "6" coordinate system radial, tangential and upflow directions, respectively, (ND)
$U_{R_5}, U_{T_5}, U_{P_5}$	UR5QC,UT5QC, UP5QC	Aerodynamic section inflow velocities in "5" coordinate system radial, tangential and upflow directions, respectively, excluding blade motion, (ND)
$UELSET_{kj}, UELSFT_{ij},$ $UELASE_{kj}, UELASF_{in}$	UELSET,UELSFT, UELASE,UELASF	Radial foreshortening of blade element due to nonlinear variations of edgewise, flatwise and torsion modes, (ND)
u_e	UE	Inward radial (x_5) foreshortening of blade element point due to combination of built-in sweep and elastic deformation, (ND)
V_T	VEL,VELBAR	Trimmed rotor flight speed, kts and (ND)
w'	WDIS	Blade mass distribution, lb/in.
$\Delta V, \Delta W$	(None)	Deflection correction terms due to second order twist effects, (ND)
$\bar{v}_e, \bar{w}_e$	VE,WE	Elastic deflections in the edgewise and flatwise directions, respectively, (ND)
v_{y6_e}, v_{z6_e}	(None)	Components of aerodynamic section inflow velocities in "6" coordinate system tangential and upflow directions, respectively, due to blade motions, (ND)
$\Delta v, \Delta w$	(None)	Deflection correction functions due to first order twist effects, (ND)
$\Delta v_{B_i}, \Delta v_{e_{ij}},$ Δv_{EA_j}	DVB,DVE,DVEA	Edgewise motion deflection correction functions, (ND)
v_{im}	VO,VINDND,PANVO	Induced velocity based on momentum balance considerations, fps or (ND)
$\Delta w_{B_k}, \Delta w_{e_{kj}}, \Delta w_{EA_j}$	DWB,DWE,DWEA	Flatwise motion deflection correction functions, (ND)

10

Symbol	FORTRAN Equiv.	Description
X_n, Y_n	XALFW, YALFW	Time variables used to calculate α_w using a recursion formula
x, y, z, w	XN, YN, ZN, WN, (XNM, YNM, ZNM, WNM)	Padé augmented state variables, for either lift (or pitching moment)
x_5, y_5, z_5	XX5, YY5, ZZ5	Components of the 5-coordinate system, defined to be rotating with the hub, but at the blade coned and lagged position, (ND)
x_4, y_4, z_4	(None)	Components of the 4-coordinate system, defined by vectors taken locally at the cylindrically-oriented segment boundaries, (ND)
$x_{4LEB}, y_{4LEB}, z_{4LEB}$	X4LEB, Y4LEB, Z4LEB	Components of the 4-coordinate system, taken at the intersection of the segment leading edge with the segment boundary (ND)
$x_{4QC}, y_{4QC}, z_{4QC}$	X4QC, Y4QC, Z4QC	Components of the 4-coordinate system, taken at the intersection of the segment quarter chord with the segment center, (ND)
x_8, y_8, z_8	(None)	Components of the 8-coordinate system, defined similar to 6-coordinate system, but displaced by bending and oriented by the aerodynamic sweep angle
y_6, z_6	YY6, ZZ6	Displacements in the 6-coordinate system, defined locally normal to built-in elastic axis
y_{10}, z_{10}	(None)	Chordwise and thicknesswise position coordinate, respectively, of an arbitrary point within a blade section, (ND)
y_{10EA}, z_{10EA}	Y10EA, Z10EA	Built-in offset distances of elastic axis from x_5 axis, in edgewise and flatwise directions, respectively, (ND)
$\Delta y_{10EA}, \Delta z_{10EA}$	Y10EAC, Z10EAC	Changes per segment (arc) length of built-in elastic axis edgewise and flatwise offsets, respectively
y_{10CG}	Y10CG	Chordwise distance of blade section mass center forward from the elastic axis, (ND)
$y_{10c/4}, y_{103c/4}$	Y10QC, Y103QC	Chordwise distances of blade section quarter chord and three quarter chord locations, respectively, forward from the elastic axis, (ND)
$\{z\}$	(None)	Vector of intermediary aerodynamic variables
α	AL, ALF, ALTAB	Section angle-of-attack, deg and rad
α_{Dm}	ALDM	Aerodynamic section dynamic stall angle-of-attack, deg
α_E	ALTAB	Effective aerodynamic section angle-of-attack, including effects of unsteady decay parameter, deg
α_{RE}	ALRTCH	Aerodynamic section reattachment angle-of-attack, deg
α_{SS}	ALFSS	Aerodynamic section static stall angle-of-attack, deg
α_{TE}	(None)	Section angle-of-attack when vortex nears the trailing edge
α_w	ALFW	Aerodynamic section unsteady decay parameter, rad
α_o	(None)	Mean angle-of-attack for oscillating airfoil, deg
$\bar{\alpha}$	(None)	Angular amplitude for oscillating airfoil, deg
$\Delta\alpha_1, \Delta\alpha_2$	DELA1, DELA2	Aerodynamic section angle-of-attack shifts to account for unsteady effects

11

LIST OF SYMBOLS AND FORTRAN EQUIVS. (Cont'd)

Symbol	FORTRAN Equiv.	Description
β	BETAT,FACPGT	Alternately, total cone angle, rad, and Prandtl-Glauert transformation factor, $(=\sqrt{1-M^2})$
β_B	PREC,BETAB, BTAERO	Built-in Blade precone, deg or radians, as appropriate
β_1	BETA1	Empirical constant, normally equals 0.18
$[\Gamma_B]$	SHAPE	Galerkin method integration weighting matrix
$\Gamma_{y_{\theta_j}}, \Gamma_{z_{\theta_j}}$	GTNLY,GTNLZ	Nonlinear j'th torsion modal weighting function for torsion excitation due to edgewise and flatwise force loadings, respectively, (ND)
$\tilde{\Gamma}_{y_{\theta_j}}, \tilde{\Gamma}_{z_{\theta_j}}$	GTNLYP,GTNLZP	Nonlinear j'th torsion modal weighting functions for torsion excitation due to flatwise and edgewise moment loadings, respectively, (ND)
γ	GAMMA	Total aerodynamic sweep angle consisting of built-in and radial flow contributions, rad
γ_{v_k}	GV	Deflection mode shape for the k'th edgewise normal mode, (ND)
γ_{w_i}	GW	Deflection mode shape for the i'th flatwise normal mode, (ND)
γ_{θ_j}	GT	Deflection mode shape for the j'th torsion normal mode, (ND)
$\tilde{\gamma}_{\theta_j}$	(None)	Effective torsion mode shape due to integration of cosine components, (ND)
δ	DELTAB,DELTAT	Total blade lead angle, radians
$\delta(\ )$		Denotes perturbational quantity
δ_B	PREL,DELTB, DLAERO	Built-in blade prelead, deg or rad, as appropriate
$\delta_1, \delta_2, \delta_3, \delta_4$	DELLC1,DELLC2, DELLC3,DELLC4	Dynamic parameters used in dynamic stalled airloads functionality, (ND)
η	(None)	The approximate distance measured from the G400 5-coordinate system segment boundary to the 4-coordinate system segment boundary, at a generalized blade chordwise location
η_{LE}, η_{TE}	ETALE,ETATE	The approximate distances measured from the G400 5-coordinate system segment boundary to the 4-coordinate system segment boundary, at the blade leading and trailing edges, respectively, (ND)
$\eta_1, \eta_2, \ldots, \eta_8$	ETA1,ETA2,..., ETA8	Empirical coefficients for C_{M_u} functionality
θ	TH	Total local blade pitch angle, radians
θ_B	THETA	Built-in blade pitch angle (structural twist), deg or rad
θ_B'	TW	Built-in twist rate, (ND)
θ_e	THE	Elastic torsion deflection angle, radians
θ_o	THAO, (TH75,THETAO)	Alternately, local static blade pitch angle, as defined by Padé filtering technique, or pitch angle due to input control angle, deg and rad
θ_4	PCHPAN	Local blade pitch angle in the 4-coordinate system, radians

12

Symbol	FORTRAN Equiv.	Description
$\tilde{\theta}$	THTIL	Local blade perturbational pitch angle, as defined by Padé filtering technique, rad
κ	CAPPA	Aerodynamic pitch damping parameter, (ND)
Λ_{e_5}	GME5	Structural sweep angle projection onto x_5-y_5 plane, rad
$\Lambda_{e_5}^{(A)}$	AGME5	Aerodynamic sweep angle projection onto x_5-y_5 plane, rad
Λ_{f_5}	GMF5	Structural sweep angle projection onto x_5-z_5 plane, rad
$\Lambda_{f_5}^{(A)}$	AGMF5	Aerodynamic sweep angle projection onto x_5-y_5 plane, rad
Λ_s	SWPLAM	Aerodynamic section sweep angle of midchord measured in edgewise direction, (+) aft, deg
$\Delta\Lambda$	DGAM	Difference in sweep angle between midchord and elastic axis, as measured in local chordwise direction, deg and rad
λ	LAMBDA, (NONE)	Alternately, aerodynamic rotor inflow, and eigenvalue (= $\sigma \pm i\omega$)
$\{\Xi\}$	XI	Vector of excitations for the degrees-of-freedom
ξ	ZETA	Angle which the radius measured from the hub to the intersection point of the section midchord with the section boundary, makes with the preconed and prelead-lagged feathering axis.
ξ_{MC}	ZETAMC	Angle which the radius, measured from the hub to the intersection point of the section midchord with the section center, makes with the preconed and prelead-lagged feathering axis.
ρ	RHO	Air density, lb-sec^2/ft^4
σ	SIGMA, ROOTE	Alternately, rotor solidity, and real part of eigenvalue
$\sigma_{ij}^{(x)}, \sigma_{ij}^{(y)}, \sigma_{ij}^{(z)}, \sigma_{ij}^{(w)}$	SIGXL, SIGYL, SIGZL, SIGWL, (SIGXM, SIGYM, SIGZM, SIGWM)	Integrations of Padé pole distributions for lift (and moment)
τ	(NONE)	Alternately, section thickness ratio, (= section thickness/semichord), (ND), and blade torsion stress, psi
ϕ	PHI	Total local blade inflow angle, radians
ϕ_o	PHIO	Local blade static inflow angle, as defined by Padé filtering technique, deg or rad
$\tilde{\phi}$	PHTILN	Local blade perturbational inflow angle, as defined by Padé filtering technique, rad
ϕ_c	(NONE)	Generalized Wagner function with compressibility corrections
ψ	PSI (PSIREF)	Blade azimuthal (angular) position, rad and (deg)
$\Delta\psi$	DP	Nondimensional time (azimuthal) step, rad
ω	(NONE), ROOTI	Alternately, frequency of motion, (Hz), and imaginary part of eigenvalue
$\bar{\omega}_{w_i}, \bar{\omega}_{v_k}, \bar{\omega}_{\theta_j}$	FF, EF, TF	(Nondimensional) uncoupled natural frequencies of i'th flatwise bending mode, k'th edgewise bending mode, and j'th torsion mode, respectively

13

Symbol	FORTRAN Equiv.	Description
Ω	OMEGA,PRPM	Rotor rotational frequency or speed (rpm)

Subscripts

$(\ )_a$	Arising from aerodynamic loading
$(\ )_B$	Structurally built-in parameter, or conditions of blade immediately outboard of juncture
$(\ )_D$	Effects of dynamic origin
$(\ )_{EA}$	Defined at the elastic axis
$(\ )_e$	Due to elastic deformation
$(\ )_k$	Pertaining to particular time step
$(\ )_{LE}$	Defined at the blade leading edge
$(\ )_{LEB}$	Defined at the intersection of the section leading edge with the section boundary
$(\ )_{MC}$	Defined at the intersection of the section midchord with the section center
$(\ )_{MCB}$	Defined at the intersection of the section midchord with the section boundary
$(\ )_N$	Components of vector quantities normal to segment midchord, or about local elastic axis
$(\ )_{QC}$	Defined at the blade quarter chord
$(\ )_{TE}$	Defined at the blade trailing edge
$(\ )_u$	Pertaining to unsteady stalled aerodynamic effects

Superscripts

$(\ )^{(A)}$	Pertaining to aerodynamic as opposed to structural
$(\ )^{(L)}$	Relating to Padé lift coefficient
$(\ )^{(M)}$	Relating to Padé pitching moment coefficient
$(\ )^{(1)}, (\ )^{(2)}$	Pertain to first and second integrals defining the deflection correction function, respectively
$(\bar{\ })$	Nondimensionalization by combinations of m_o, R and/or Ω
$(\overset{*}{\ })$	Differentiation with respect to (Ωt)
$(\ )'$	Differentiation with respect to (r/R)
$(\hat{\ })$	Denotes evaluation at zero collective angle

14

STRUCTURAL TWIST AND SWEEP

Principal Assumptions

The aeroelastic analysis presented herein represents a specialization of the G400 analysis described in References 1 and 3. Since the publication of the initial documentation (Reference 1), various of the principal assumptions enunciated therein have been either relaxed and/or extended. Most significant are the specific extensions which have been made to account for the more stringent modeling demands of high performance propellers (e.g. the prop-fan). Insofar as is practical within the scope of this report, the principal assumptions used herein are presented below:

1. The rotor is rotating at a constant angular velocity, has infinite hub impedance, and is in steady translational flight. The orientation of the rotor in space is specified by appropriate Euler angles (pitch and roll). The orientation relative to the freestream is specified by means of a rotor angle-of-attack and a yaw angle.

2. The elasto-mechanics of the blade are describeable within a beam theory framework with corrections of a kinematic nature to account for structural twist and sweep (see Figures 2a and b). The elements of beam theory analysis pertinent to the development, are the concepts of an elastic axis, the relationship of elastic bending to elastic torsion, and the definitions of these two elastic deformations.

3. The elastic (torsion) axis is defined as the spanwise locus of shear centers of the two-dimensional blade (beam) sections taken perpendicular to this spanwise locus. Note that this definition treats the elastic axis as an abstracted section property, as contrasted with what one would measure in a bench test of an actual curved beam. In such a test, the locus of points where bending loads produce no torsion deflection (at the points of load application) would conform to the usual interpretation of the "elastic axis." This axis, however, would be different from the herein usage of the term to denote the locus of section shear centers. The built-in structural sweep (elastic axis offset), together with the elastic bending deflections, defines an elastic axis which is generally a space curve about which the local torsion deflections must take place. Thus, as shown in Figure 2a, each spanwise beam segment will not in general be defined parallel to the other segments. For the analysis of the beam-like elastic properties, the structurally swept blade (Figure 2a) is assumed to have its so-defined elastic axis "straightened out". This artificial straightening defines an

BEAM PROPERTIES DEFINED
NORMAL TO E.A.

LOCUS OF SHEAR
CENTERS (ELASTIC
AXIS,E.A.)

PITCH BEARING

PITCH AXIS

TYPICAL SEGMENT
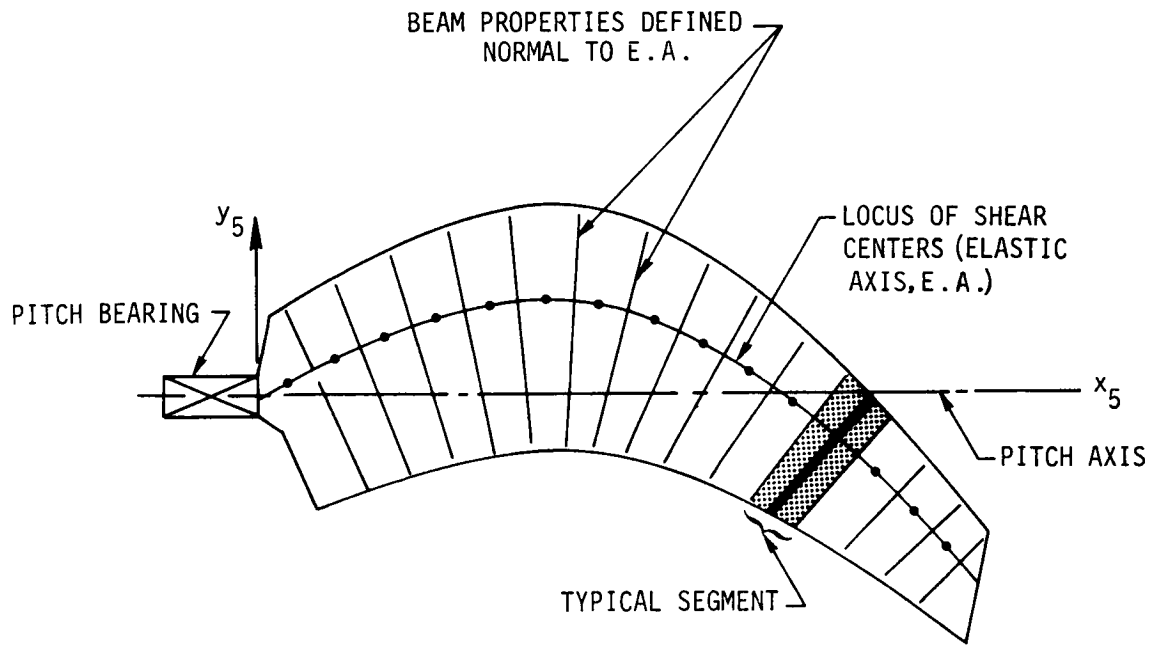
a) LOCUS OF SHEAR CENTERS DEFINING ELASTIC AXIS

BEAM SECTIONS
REMAIN THE SAME

TYPICAL SEGMENT
AFTER STRAIGHTENING

STRAIGHTENED ELASTIC AXIS
WITH ARC LENGTH MAINTAINED
CONSTANT
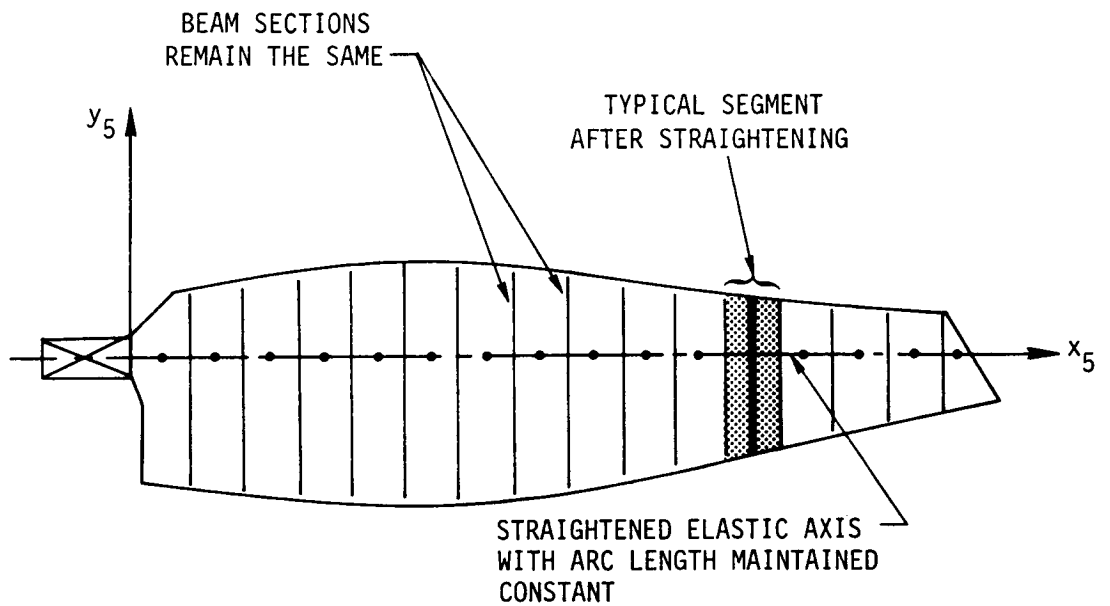
b) EQUIVALENT BEAM FOR DEFINING BEAM ELASTOMECHANICS

Figure 2. Basis for Use of Beam Theory for Structurally Swept Blade

16

"equivalent beam" whose (straight) elastic axis has the same arc length as the original swept blade (see Figure 2b).

4. The blade elasticity is described by the conventional (linear) beam bending and (nonlinear) bar torsion characteristics, as formulated by Houbolt and Brooks in Reference 4, for the above defined "equivalent beam". It is recognized that various deficiencies have been identified in these and other earlier formulations, both with respect to their adequacy for moderate to large bending deflections (References 5 and 6) and with respect to the proper modeling of pretwisted beams under tension (References 7-9). However, there is not yet well established agreement either on the impact of these deficiencies on propeller elasticity or, more importantly, on a final proper reformulation. Thus, the continued use herein of the Houbolt and Brooks elastic formulations must be viewed as an eventually correctable deficiency of uncertain importance, to be addressed at some future date.

5. The elastic bending and torsion deflections are "small" and respectively defined in a local sense normal to and along the space curve as defined by the built-in elastic axis. These deflections are defined as "small" in the sense that the elastic bending slopes and torsion deflection angles conform to the usual definition for "small" angles.

6. The elastic bending and torsion deflections are describable using the "uncoupled" normal bending and torsion modes of the "equivalent beam". Thus, the deflections in the flatwise and edgewise directions are respectively given by:

$$\overline{w}_e = \sum_{i=1}^{NFM} \gamma_{w_i}(\overline{r}) q_{w_i}(t) \tag{1a}$$

$$\overline{v}_e = \sum_{k=1}^{NEM} \gamma_{v_k}(\overline{r}) q_{v_k}(t) \tag{1b}$$

, and the elastic torsion deflections are given by:

$$\theta_e = \sum_{j=1}^{NTM} \gamma_{\theta_j}(\overline{r}) q_{\theta_j}(t) \tag{1c}$$

17

Uncoupled modes are herein defined to be those beam vibration modes calculated assuming zero precone, prelag, pitch, twist, center-of-gravity offset and elastic axis offset. Thus γ_{w_i}, γ_{v_k}, and γ_{θ_j} are all mutually uncoupled from each other.

7. Blade elastic bending is defined by the conventional beam bending differential equations (as developed in Reference 4) wherein the usual independent spanwise variable is taken to be the arc length along the elastic axis. Furthermore, these bending differential equations are defined locally using the loadings locally normal to the built-in elastic axis. Within this context, explicit elastic bending-torsion coupling due to structural sweep is omitted in favor of implicit coupling due to inertial, aerodynamic and gravitational loadings taken with appropriate sweep related kinematics.

8. The blade aerodynamic and structural twist distributions are non-linear. Additionally, the total (integrated) angle of structural twist is negligible beyond second order; cases of large local twist rates over short sections of span are not denied, however.

9. Local radial foreshortening is defined relative to the equivalent beam defined in Figure 2. Contributions to radial foreshortening accrue from (a) the built-in structural sweep, i.e. that which restores the equivalent beam to the original swept planform (shown in Figure 2a), (b) first order (linear) functions of bending, arising from built-in structural sweep, (c) second order (nonlinear) functions of bending each with elastic torsion arising from built-in structural sweep, and (d) second order functions each of both flatwise and edgewise bending. Note that this greatly relaxes principal assumption number 6 given in Reference 1.

10. The elastic axis is coincident with the feathering (pitch) axis at the root of the blade. The built-in elastic is furthermore defined relative to the feathering axis.

11. The blade flapping and lead-lag degrees-of-freedom used in Reference 1 are assumed to be fixed at the built-in values. Thus, pinned root conditions are denied. It is to be noted that this assumption pertains only to the propeller dedicated aeroelastic analysis described herein.

12. The blade distributions of center-of-gravity, aerodynamic center and center-of-tension (intersection of flatwise and edgewise neutral axes) are defined in two dimensional sections normal to the space curve elastic axis. These distributions are furthermore generally

18

noncoincident with the elastic axis and measured relative to the elastic axis.

13. The blade sections have finite thicknesswise mass, but generally the thicknesswise location of the section center-of-gravity away from the chordwise principal axis is negligible.

The above assumptions are used for the mechanical developments in the subsections which immediately follow. Assumptions regarding the basic implementation of aerodynamic sweep are described in the next chapter.

Basic Methodology for Structural Twist

The present aeroelastic theory is characterized to a large extent by the kinematic modeling selected to describe the bending deflections of a pretwisted, prebent beam (elastic axis taken as a space curve). The material presented draws heavily on the development of Reference 1 subject to above assumptions 5 through 10.

As shown in Figure 3, the "5" coordinate system is defined by the preconed and prelead-lagged feathering axis. The "6" coordinate system is defined by unit vectors taken locally normal to the preswept elastic axis with the y_6 direction arbitrarily taken parallel to the $x_5 - y_5$ plane.

In the presence of only blade pitch angle, Θ, the "5" and "6" coordinate systems would be the same and the resulting "5" coordinate system deflections would be simple trigonometric resolutions of the flatwise and edgewise deflections as given by Equations (1a) and (1b). With the addition of (arbitrary) structural twist, however, a simple trigonometric resolution transformation of flatwise and edgewise <u>deflections</u> is incapable of satisfying the beam "force" boundary conditions at the blade tip and an "integrated" trigonometric transformation is required.

As is shown in Reference 1, the required integrated effect can be achieved by means of a trigonometric resolution transformation not on deflections, but instead on the second spanwise derivatives of the deflection, i.e. the <u>curvatures</u>:

$$\bar{y_6}'' = \bar{v_e}'' \cos\Theta - \bar{w_e}'' \sin\Theta \qquad (2a)$$

$$\bar{z_6}'' = \bar{v_e}'' \sin\Theta + \bar{w_e}'' \cos\Theta \qquad (2b)$$

19
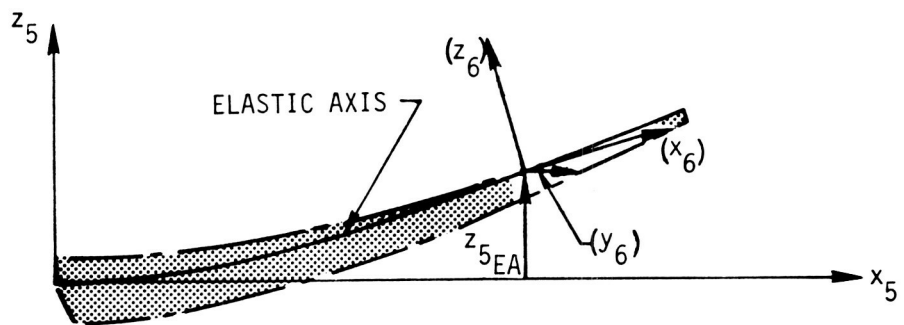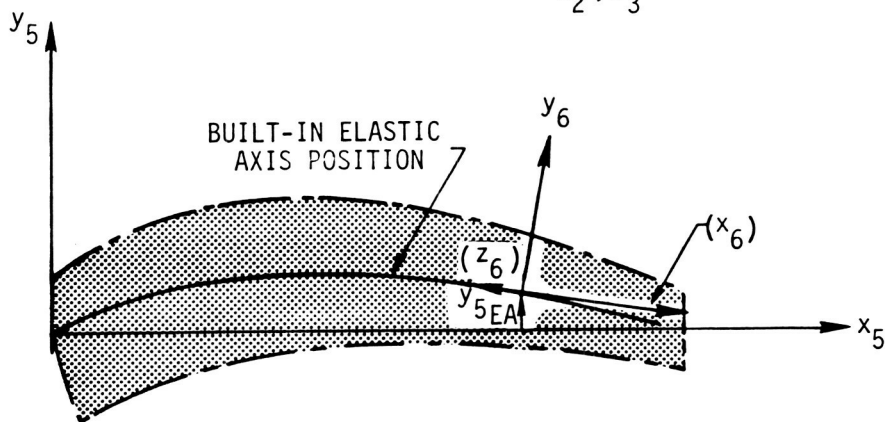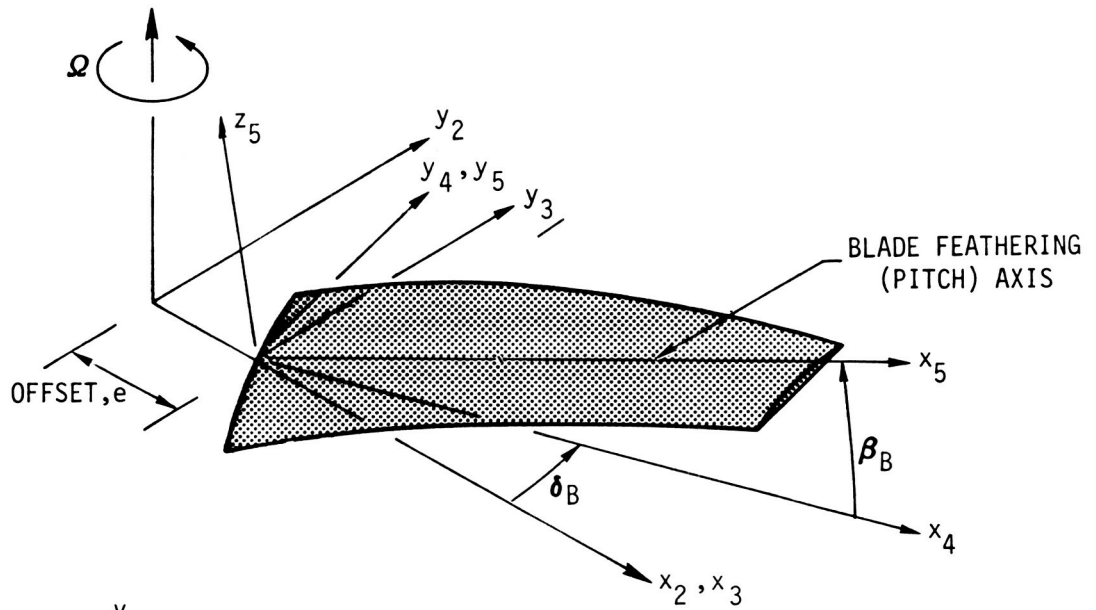
( ): INDICATES PROJECTIONS

Figure 3. Schematics of the "5" and "6" Coordinate Systems

This basic coordinate system transformation has the advantage that the aforementioned boundary conditions are always satisfied. In of themselves, however, trigonometric resolutions of curvatures are not directly useful for defining the blade kinematics. Instead, they serve as a starting point for deriving such a deflection based transformation. The required blade kinematic coordinate system transformation for deflections can then be derived from Equations (2) using integrations by parts and invocation of assumption 8. While the details of this integration procedure is straightforward, it is sufficiently tedious to be inappropriate to the scope of the present report. The integration yields a trigonometric resolution coordinate transformation in the usual form, as given in Reference 4 and elsewhere in the literature, but with the addition of various "deflection correction" functions due to twist:

$$\bar{y}_6 = (\bar{v}_e + \Delta v - \underline{\Delta V})\cos\Theta - (\bar{w}_e - \Delta w - \underline{\Delta W})\sin\Theta + O(\Theta'^3) \tag{3a}$$

$$\bar{z}_6 = (\bar{v}_e + \Delta v - \underline{\Delta V})\sin\Theta + (\bar{w}_e - \Delta w - \underline{\Delta W})\cos\Theta + O(\Theta'^3) \tag{3b}$$

where the underlined terms are, by assumption, negligible and where the deflection correction functions are defined by the following expressions:

first order in twist:

$$\Delta v = \int_0^{\bar{r}} \Theta' w_e \, d\bar{r} + \int_0^{\bar{r}} \int_0^{\bar{r}_1} \Theta' w_e' \, d\bar{r}_2 d\bar{r}_1 \tag{4a}$$

$$\Delta w = \int_0^{\bar{r}} \Theta' v_e \, d\bar{r}_1 + \int_0^{\bar{r}} \int_0^{\bar{r}_1} \Theta' v_e' \, d\bar{r}_2 d\bar{r}_1 \tag{4b}$$

second order in twist:

$$\Delta V = \int_0^{\bar{r}} \Theta' \Delta w \, d\bar{r}_1 + \int_0^{\bar{r}} \int_0^{\bar{r}_1} \Theta' \Delta w^{(2)'} \, d\bar{r}_2 d\bar{r}_1 \tag{5a}$$

$$\Delta W = \int_0^{\bar{r}} \Theta' \Delta v \, d\bar{r}_1 + \int_0^{\bar{r}} \int_0^{\bar{r}_1} \Theta \Delta v^{(2)'} \, d\bar{r}_2 d\bar{r}_1 \tag{5b}$$

21

It is to be noted that the total twist rate, θ', contains the built-in twist, θ'_B, and the time dependent elastic deflection, θ'_e $(= \gamma'_{\theta_j} \cdot q_{\theta_j})$. Thus, the deflection correction functions, Δv, Δw, ΔV, and ΔW, nominally contain both linear and nonlinear combinations of the modal time variables (q_{w_i}, q_{v_k}, and q_{θ_j}). Specifically, the linear ones involve the built-in twist angle and are denoted with a "B" subscript. The nonlinear combinations involve the elastic twist angle and hence, are proportional to the product of q_{θ_j} with either q_{w_i} or q_{v_k}. Herein, the products $q_{\theta_j} \cdot q_{w_i}$ and $q_{\theta_j} \cdot q_{v_k}$ are retained only in the Δv and Δw (first order) correction functions and are denoted with an "e" subscript. The ΔV and ΔW (second order) correction terms retain only the contributions due to built-in twist rate, θ_B, and hence, are strictly linear. Thus, the deflection correction functions defined generally in Equation (4) are given specifically as follows:

first order in twist:

$$\Delta v = \Delta v_B + \Delta v_e \tag{6a}$$

$$\Delta w = \Delta w_B + \Delta w_e \tag{6b}$$

where:

$$\Delta v_B = \sum_{i=1}^{NFM} \Delta v_{B_i} q_{w_i} \tag{7}$$

$$\Delta v_e = \sum_{i=1}^{NFM} \sum_{j=1}^{NTM} \Delta v_{e_{ij}} \cdot q_{w_i} q_{\theta_j} \tag{8}$$

$$\Delta w_B = \sum_{k=1}^{NEM} \Delta w_{B_k} q_{v_k} \tag{9}$$

$$\Delta w_e = \sum_{k=1}^{NEM} \sum_{j=1}^{NTM} \Delta w_{e_{kj}} q_{v_k} q_{\theta_j} \tag{10}$$

second_order_in_twist:

$$\Delta V = \Delta V_B \qquad\qquad (11a)$$

$$\Delta W = \Delta W_B \qquad\qquad (11b)$$

where:

$$\Delta V_B = \sum_{k=1}^{NEM} \Delta V_{B_k} q_{v_k} \qquad\qquad (12)$$

$$\Delta W_B = \sum_{i=1}^{NFM} \Delta W_{B_i} q_{w_i} \qquad\qquad (13)$$

Additional deflection correction functions are defined with the consideration of structural sweep given in the following subsection.

Kinematic Representation for Structural Sweep

Approximations for Small Sweep

Structural sweep is defined in a general sense wherein both chordwise and thickness offsets of the built-in elastic axis, $y_{10_{EA}}$ and $z_{10_{EA}}$, respectively, are admitted (see Figure 3). Within the context of the material in the preceeding subsection an approximation to the effects of structural sweep, for "small" values, can be obtained heuristically by considering the structural sweep to be "pre-bends" in the elastic axis. Within this context, the deflection correction functions defined by Equations (4) and (5) would be modified by the following substitutions:

$$\gamma_{w_i} q_{w_i} \longrightarrow z_{10_{EA}}$$

$$\gamma_{w_i'} q_{w_i} \longrightarrow z_{10_{EA}}' \qquad\qquad (14a)$$

$$\gamma_{v_k} q_{v_k} \longrightarrow y_{10_{EA}}$$

$$\gamma_{v_k'} q_{v_k} \longrightarrow y_{10_{EA}}'$$

where only those terms involving the elastic modal variables would be retained. For example, those terms involving only built-in twist and built-in sweep would be omitted. Thus, for small structural sweep Equations (6) and (11) would be modified as follows:

$$\Delta v \longrightarrow \Delta v + \Delta v_{EA}$$

$$\Delta w \longrightarrow \Delta w + \Delta w_{EA}$$

$$\Delta V \longrightarrow \Delta V + \Delta V_{EA} \tag{14b}$$

$$\Delta W \longrightarrow \Delta W + \Delta W_{EA}$$

where:

$$\left\{ \begin{array}{c} \Delta v_{EA} \\ \Delta w_{EA} \\ \Delta V_{EA} \\ \Delta W_{EA} \end{array} \right\} = \sum_{j=1}^{NTM} q_{\theta_j} \left\{ \begin{array}{c} \Delta v_{EA_j} \\ \Delta w_{EA_j} \\ \Delta V_{EA_j} \\ \Delta W_{EA_j} \end{array} \right\} \tag{15}$$

and where:

$$\Delta v_{EA_j} = \int_0^{\bar{r}} \gamma'_{\theta_j} z'_{10_{EA}} \, d\bar{r}_1 + \int_0^{\bar{r}} \int_0^{\bar{r}_1} \gamma'_{\theta_j} z'_{10_{EA}} \, d\bar{r}_2 d\bar{r}_1 \tag{16}$$

$$\Delta w_{EA_j} = \int_0^{\bar{r}} \gamma'_{\theta_j} y'_{10_{EA}} \, d\bar{r}_1 + \int_0^{\bar{r}} \int_0^{\bar{r}_1} \gamma'_{\theta_j} y'_{10_{EA}} \, d\bar{r}_2 d\bar{r}_1 \tag{17}$$

$$\Delta V_{EA_j} = \int_0^{\bar{r}} \theta'_B \, \Delta w_{EA_j} \, d\bar{r}_1 + \int_0^{\bar{r}} \int_0^{\bar{r}_1} \theta'_B \, \Delta w_{EA_j}^{(2)'} \, d\bar{r}_2 d\bar{r}_1 \tag{18}$$

$$\Delta W_{EA_j} = \int_0^{\bar{r}} \theta'_B \, \Delta v_{EA_j} \, d\bar{r}_1 + \int_0^{\bar{r}} \int_0^{\bar{r}_1} \theta'_B \, \Delta v_{EA_j}^{(2)'} \, d\bar{r}_2 d\bar{r}_1 \tag{19}$$

24

Coordinate Transformation Appropriate for Large Sweep

For the general case of moderate to large structural sweep, the material in the preceeding subsection is inappropriate, but serves as an introduction to the material which follows. A successful modeling of structural sweep must account for the fact that the sweep angles defining elastic axis offset orientation are Euler angles and must be carefully defined.

Inplane and Out-of-plane Position Vector Components

The general modeling of the blade y_5 and z_5 kinematics due to combined structural twist and sweep is accomplished in the following steps:

1. The elastic axis of the "equivalent beam" described in an above subsection is "distorted" back to the original planform defined by the built-in structural sweep and segment arc length distributions. This step essentially defines the position in space of the elastic axis space curve. This positioning requires the x_5, y_5 and z_5 offset distances of the centers of the segments as well as projections onto the x_5-y_5 and x_5-z_5 planes of the swept elastic axis line segments.

    These projections define the sweep angle distributions, Λ_{e_5} and Λ_{f_5}, as shown in Figure 4.

2. The orientations of the elastic axis line segments define the local "6" coordinate system. x_6 is defined parallel to the axis of the elastic axis line segment; y_6 is defined parallel to the x_5-y_5 plane, (+) in leading edge direction; z_6 is orthogonal to x_6 and y_6, (+) in the normally positive thrusting motion. It should be stressed that the result of step 1 is to produce, in addition to the inplane and out-of-plane offsets (Δy_5 and Δz_5) of the elastic axis from the (reference) x_5 pitch axis, a radial foreshortening (Δx_5) due to the constancy of the total arc length of the elastic axis. Mathematically, this Δx_5 kinematic foreshortening is modeled differently and separately from the Δy_5 and Δz_5 kinematic modeling.

3. The blade segments of the blade configuration resulting from steps 1 and 2 are then pitched and twisted about their respective elastic axis line segments (x_6 axis) to restore the blade back to its original built-in, but undeflected position. The pitch and twist angles for each segment are defined relative to the y_6 axis.

DISPLACED AIRFOIL
SECTION DEFINING
PITCH AND PRINCIPAL
BENDING DIRECTIONS

z_6

(FLATWISE)
w_e, Δw

TE

(EDGEWISE)
v_e, Δv

x_6

P

LE

θ

y_6

z_5

PITCH
BEARING

TE

FEATHERING
(PITCH) AXIS

LE

y_5

z_6

ELASTIC AXIS

Λ_{f_5}

$y_{5_{EA}}$

x_6

x_5

$z_{5_{EA}}$

P

BLADE SEGMENT
ARC LENGTH, Δr

Λ_{e_5}

y_6

(PARALLEL TO x_5-y_5 PLANE)
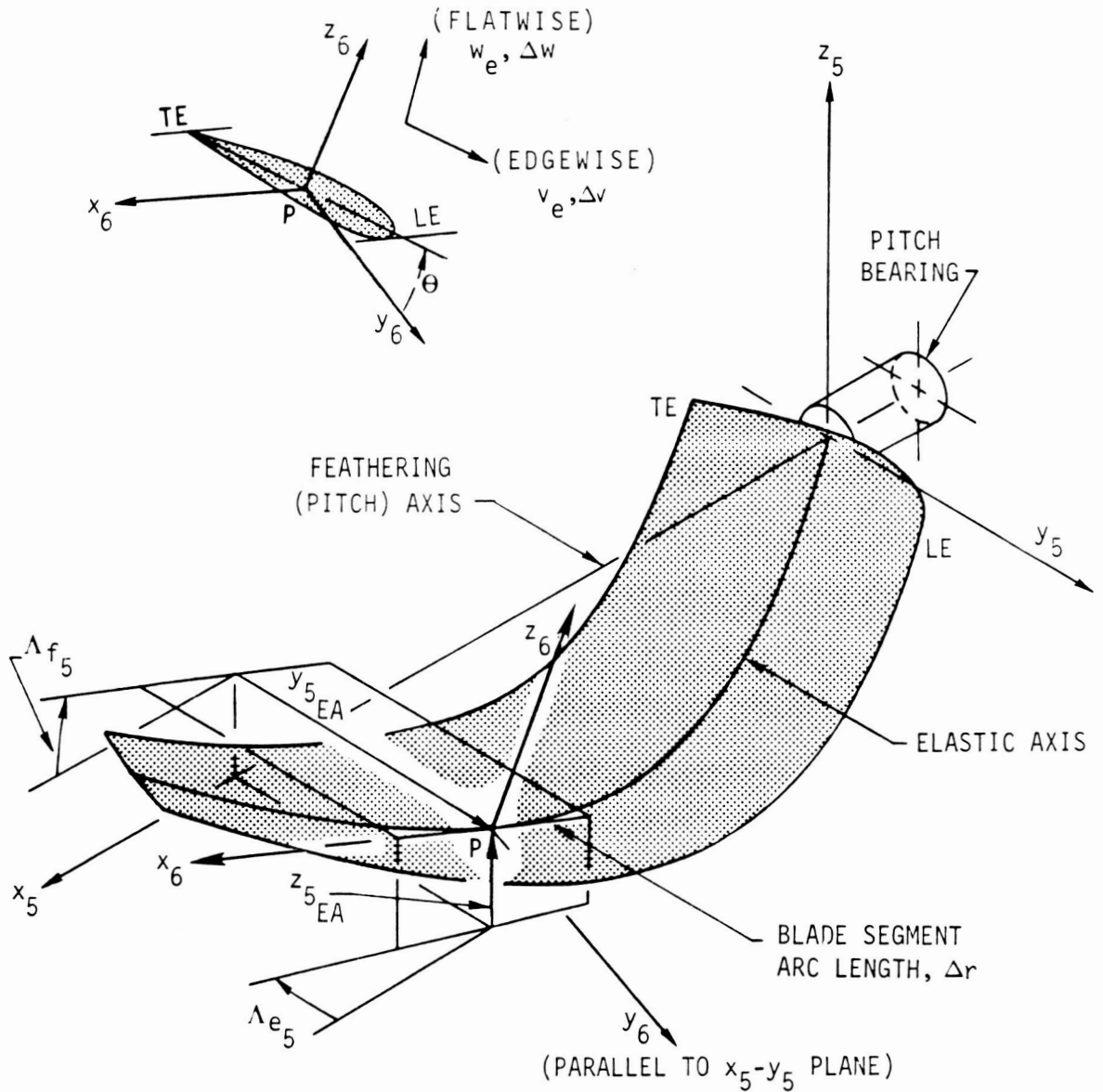
Figure 4. Euler Angles Defining Structural Sweep Transformation and Section Pitch

26

4. The blade is then elastically deflected in torsion about the built-in space curve elastic axis to define a first set of "small" incremental y_5 and z_5 deflections. This first set of small incremental deflections is governed by Equations (15) through (19).

5. The blade is then elastically deflected in flatwise and edgewise bending (in the presence of the torsion deflection) to define a second set of small incremental deflections. This second set of incremental deflections is measured in the "6" coordinate system and is governed by the basic deflection transformations defined by Equations (3) through (5).

6. The second set of small incremental "6" coordinate system deflections defined in step 5 is transformed to the "5" coordinate system using a Euler angle transformation derived from sweep angle projections Λ_{e_5} and Λ_{f_5}, discussed in above step 1.

7. The results of steps 1, 4 and 6 are combined to define the y_5 and z_5 position vector components. These results are summarized by the development which follows.

First, the sweep angle projection distributions are defined using the built-in elastic axis line segment changes per segment length, the (invariant) segment arc lengths, Δr, together with changes to the projection angles caused by elastic torsion deflection:

$$\Lambda_{e_5} = \sin^{-1}\left\{ -\frac{\Delta y_{5_{EA}}}{\Delta r} - \left[\left(\Delta v_{EA_j}^{(2)'} - \Delta v_{EA_j}^{(2)'} \right)\cos\Theta + \left(\Delta w_{EA_j}^{(2)'} + \Delta w_{EA_j}^{(2)'} \right)\sin\Theta \right] q_{\theta_j} \right\} \qquad (20)$$

$$\Lambda_{f_5} = \sin^{-1}\left\{ \frac{\Delta z_{5_{EA}}}{\Delta r} + \left[-\left(\Delta w_{EA_j}^{(2)'} + \Delta w_{EA_j}^{(2)'} \right)\cos\Theta + \left(\Delta v_{EA_j}^{(2)'} - \Delta v_{EA_j}^{(2)'} \right)\sin\Theta \right] q_{\theta_j} \right\} \qquad (21)$$

where $\Delta y_{5_{EA}}$ and $\Delta z_{5_{EA}}$ are the built-in changes per segment length. For consistency with the definitions used for other previously defined radial

27

distributions these spanwise variable quantities are considered to be "derived" quantities calculated from the corresponding quantities defined in the chordwise and thicknesswise directions, $\Delta y_{10_{EA}}$ and $\Delta z_{10_{EA}}$, respectively.

In practice, however, the "5" coordinate system quantities are the more accurately known and the "10" coordinate system quantities are derived using the "5" quantities according to:

$$\Delta y_{10_{EA}} = \Delta y_{5_{EA}} \cos \theta_B + \Delta z_{5_{EA}} \sin \theta_B \tag{22a}$$

$$\Delta z_{10_{EA}} = - \Delta y_{5_{EA}} \sin \theta_B + \Delta z_{5_{EA}} \cos \theta_B \tag{22b}$$

Accordingly, $\Delta y_{10_{EA}}$ and $\Delta z_{10_{EA}}$ are input to the program and $\Delta y_{5_{EA}}$ and $\Delta z_{5_{EA}}$ are calculated internally using the inverse transformation of Equations (22).

The coordinate system transformation relating the pitch axis ("5") coordinate system with the swept ("6") coordinate system makes use of the sweep angle projections given in Equations (20) and (21):

$$\{x_6\} = [TAS] \{x_5\} \tag{23}$$

$$\{x_5\} = [TAS^{-1}] \{x_6\} = [TAS^T] \{x_6\} \tag{24}$$

$$[TAS] = \begin{bmatrix} X & -\sin\Lambda_{e_5} & \sin\Lambda_{f_5} \\[2mm] \dfrac{\sin\Lambda_{e_5}}{\cos\Lambda_{f_5}} & \dfrac{X}{\cos\Lambda_{f_5}} & 0 \\[2mm] \dfrac{-X\sin\Lambda_{f_5}}{\cos\Lambda_{f_5}} & \dfrac{\sin\Lambda_{f_5}\sin\Lambda_{e_5}}{\cos\Lambda_{f_5}} & \cos\Lambda_{f_5} \end{bmatrix} \tag{25}$$

where:

$$X = \sqrt{1 - \sin^2\Lambda_{e_5} - \sin^2\Lambda_{f_5}} \tag{26}$$

Equations (3), (15) through (19), (22), and (24) through (26) can then be combined to yield the required expressions for inplane and out-of-plane displacement:

$$\begin{Bmatrix} y_5 \\ z_5 \end{Bmatrix} = \begin{Bmatrix} y_{IO_{EA}}\cos\theta_B - z_{IO_{EA}}\sin\theta_B \\ y_{IO_{EA}}\sin\theta_B + z_{IO_{EA}}\cos\theta_B \end{Bmatrix}$$

$$+ \sum_{j=1}^{NTM} \begin{Bmatrix} (\Delta v_{EA_j} - \Delta V_{EA_j})\cos\Theta + (\Delta w_{EA_j} + \Delta W_{EA_j})\sin\Theta \\ (\Delta v_{EA_j} - \Delta V_{EA_j})\sin\Theta - (\Delta w_{EA_j} + \Delta W_{EA_j})\cos\Theta \end{Bmatrix} q_{\theta_j}$$

$$+ [E][TAS^{-1}] \begin{Bmatrix} 0 \\ (v_e + \Delta v - \Delta V)\cos\Theta - (w_e - \Delta w - \Delta W)\sin\Theta \\ (v_e + \Delta v - \Delta V)\sin\Theta + (w_e - \Delta w - \Delta W)\cos\Theta \end{Bmatrix} \tag{27}$$

where:

$$[E] = \begin{bmatrix} 0 & 1 & 0 \\ 0 & 0 & 1 \end{bmatrix} \tag{28}$$

29

and where v_e, w_e, Δv, Δw, ΔV, ΔW are linear and nonlinear combinations of q_{w_i}, q_{v_k} and q_{θ_j}, as per Equations (6) through (14).

Radial Position Vector Component

The modeling of the radial, x_5, kinematics is accomplished in accordance with assumptions 3 and 9. The basis of the radial position modeling is the assumption of arc length constancy for each blade segment. Figure 5 presents a pictorial representation for a typical segment of the steps followed in this modeling process:

1. The elastic axis of the "equivalent beam" segment is rotated to the built-in swept positions defined by the projection sweep angles, $\Lambda_{e_{5_o}}$ and $\Lambda_{f_{5_o}}$, (given by Equations (20) and (21), with $q_{\theta_j} = 0$). The cosine foreshortening that results from this step is the built-in (constant) value and, for each segment, this "first" foreshortening is referred to as $(d\Delta x)_1$.

2. The elastic axis orientation sweep projection angles are modified due to the elastic torsion deflections, in accordance with Equations (20) and (21).

3. The results of step 2 (with the q_{θ_j} dependency linearized) are combined with the elastic bending deflections, y_{6_e} and z_{6_e}, to produce the "second" foreshortening referred to as $(d\Delta x)_2$, as shown in Figure 5. This second foreshortening contribution is linear in the bending deflection variables, q_{w_i} and q_{v_k} but contains nonlinear (quadratic) combinations of these variables with the torsion deflection, q_{θ_j}.

4. Using the built-in projection sweep angles, $\Lambda_{e_{5_o}}$ and $\Lambda_{f_{5_o}}$, the cosine foreshortening due to bending away from the undeflected elastic axis position is the "third" contribution to the foreshortening and is referred to as $(d\Delta x)_3$. This third foreshortening contribution is nonlinear in both the bending deflection variables, q_{w_i} and q_{v_k}.
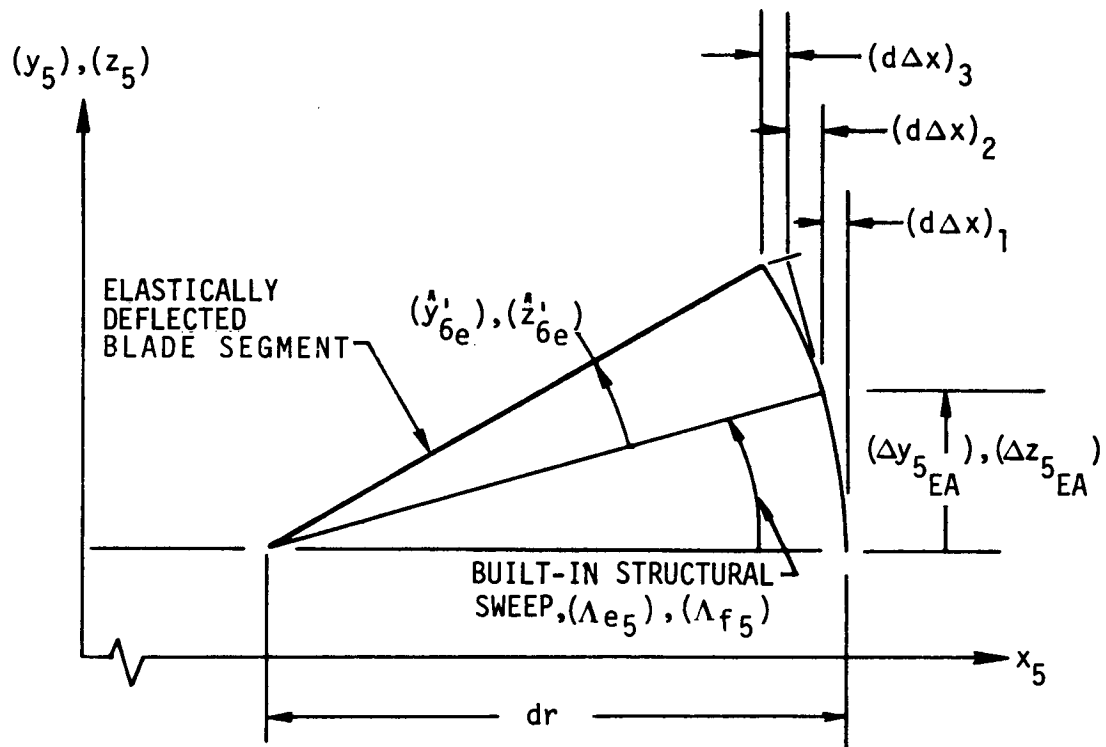
Figure 5. Contributions to Incremental Radial Foreshortening Due to Sweep and Elastic Deformations

5. The results of steps 1 through 4 define the total incremental fore-shortening over an arbitrary blade segment, $(d\Delta x)$. The total x_5 deflection for any segment is obtained by integrating the increments inboard of that location. These steps are summarized by the development given below:

Built-in Contribution

Reference to Figure 5 gives

$$(d\Delta x)_1 = dr - dx = dr - \sqrt{dr^2 - \Delta y_{5_{EA}}^2 - \Delta z_{5_{EA}}^2}$$
$$= dr\left[1 - \sqrt{1 - (\Delta y_{10_{EA}}/\Delta r)^2 - (\Delta z_{10_{EA}}/\Delta r)^2}\right] \tag{29}$$

Contribution Linear in Bending

The second foreshortening contribution is obtained by taking components of the bending deflection in the x_5 direction:

$$(d\Delta x)_2 = dr\left[\sin\Lambda_{f_5}\cos\Lambda_{e_5}\hat{z}_{6_e}' - \sin\Lambda_{e_5}\cos\Lambda_{f_5}\hat{y}_{6_e}'\right] \tag{30}$$

where the ($\hat{}$) superscript denotes evaluation with zero collective angle since foreshortening relative to the pitch axis is invariant with collective angle. Each of the trigonometric functions of the sweep angle projections is then linearized with respect to q_{θ_j} as are the bending shapes, $\hat{y}_{6_e}$ and $\hat{z}_{6_e}$. The details of this linearization are straightforward, but sufficiently tedious to be beyond the intent of this report. After this operation, Equation (3) can be rewritten as:

$$(d\Delta x)_2 = \left[d(DUEAF_i) \cdot q_{w_i} + d(DUEAE_k) \cdot q_{v_k}\right. \tag{31}$$
$$\left. + d(UELSFT_{ij}) \cdot q_{w_i}q_{\theta_j} + d(UELSET_{kj}) \cdot q_{v_k}q_{\theta_j}\right]$$

32

Contribution Nonlinear in Bending

The third foreshortening contribution is obtained by calculating the cosine foreshortening and taking components in the x_5 direction:

$$(d\Delta x)_3 = \cos\Lambda_{e_{5_0}} \cos\Lambda_{f_{5_0}} \left[1 - \sqrt{1 - v_e'^2 - w_e'^2} \right] dr \qquad (32)$$

$$\cong \cos\Lambda_{e_{5_0}} \cos\Lambda_{f_{5_0}} \cdot \frac{1}{2}(v_e'^2 + w_e'^2) dr$$

$$\therefore (d\Delta x)_3 = \cos\Lambda_{e_{5_0}} \cos\Lambda_{f_{5_0}} \cdot \frac{1}{2}\left[\gamma_{v_k}' \gamma_{v_m}' q_{v_k} q_{v_m} + \gamma_{w_i}' \gamma_{w_n}' q_{w_i} q_{w_n} \right] dr \qquad (33)$$

where summations over i, k, m and n are implied.

Combination of Contributions

All of the three contributions to the incremental radial position deflection must be integrated:

$$x_{5_n} = r_n - u_{e_n} \qquad (34)$$

where r_n is the radial location of the nth segment of the "equivalent beam" and is the summation of segment arc-lengths up to the center of the nth segment,

33

and where

$$u_{e_n} = \int_0^{r_n} \left[(d\Delta x)_1 + (d\Delta x)_2 + (d\Delta x)_3 \right] \qquad (35)$$

Symbolically, u_e is given by:

$$\begin{aligned}
u_e &= (DUEAO) + (DUEAF_i)q_{w_i} \\
&\quad + (DUEAE_k) \cdot q_{v_k} \\
&\quad + (UELSET_{k_j}) \, q_{v_k} q_{\theta_j} + (UELSFT_{i_j}) \, q_{w_i} q_{\theta_j} \\
&\quad + \frac{1}{2} (UELASE_{km}) q_{v_k} q_{v_m} + \frac{1}{2} (UELASF_{in}) q_{w_i} q_{w_n}
\end{aligned} \qquad (36)$$

where variation in all terms with radial station is implied.

34

Torsion Excitation for Elastic Axis
As A Space Curve

As given in Reference 1, and as recognized elsewhere in the literature, the torsion differential equation is comprised of three basic parts. The first part consists of the usual elastic stiffening terms, and the second consists of combinations of distributed <u>moment</u> loadings. The third part is the wholly nonlinear torsion loadings accruing from distributed <u>force</u> loadings acting on moment arms provided by curvature in the elastic axis. As given in Reference 1, the torsion equation is given by:

$$\left[GJ\theta_e' + \Theta k_A^2 T + \frac{1}{2} EB_1(\Theta'^2 - \theta_B'^2)\Theta' - EB_2\theta_B'v_e'' \right]' \text{\textcircled{\scriptsize I}}$$

$$\underbrace{}$$

elastic stiffening

$$= \left[-q_{x_5} - y_5' q_{y_5} - z_5' q_{z_5} \right] \text{\textcircled{\scriptsize II}}$$

$$\underbrace{}$$

(37)

moment loadings

$$+ \left\{ y_5'' \int_r^1 \left[z_{5_1}' \int_{r_1}^1 P_{x_5}(r_2)\,dr_2 - \int_{r_1}^1 P_{z_5}(r_2)\,dr_2 + q_{y_5}(r_1) \right] dr_1 \right.$$

$$\left. - z_5'' \int_r^1 \left[y_{5_1}' \int_{r_1}^1 P_{x_5}(r_2)\,dr_2 - \int_{r_1}^1 P_{y_5}(r_2)\,dr_2 - q_{z_5}(r_1) \right] dr_1 \right\} \text{\textcircled{\scriptsize III}}$$

$$\underbrace{} \quad \underbrace{}$$

curvatures   functions of force loadings

35

In Reference 1, the curvatures used in the (nonlinear) third portion of the torsion equation were assumed to arise entirely from the elastic bending deflections, v_e'' and w_e'', as per Equation (2). As such, it can be shown that the nonlinear excitation term in Equation (37) can be reduced to the familiar difference of bending stiffness, ΔEI ($= EI_z - EI_y$), term:

$$\{\cdots\}_{\text{(III)}} = \left[(EI_z - EI_y) v_e'' w_e'' - (e_A T + EB_2(\theta_B' + \tfrac{1}{2}\theta_e')\theta_e') w_e'' \right] \tag{38}$$

This method for including the effect is attractive principally because of its simplicity and has been used to good advantage by numerous investigators. Three difficulties exist with this method of implementation, however. The first difficulty relates to the fact that the implementation of Equation (38) is based on a "mode deflection" description of internal bending moment. The difficulty with a mode deflection formulation per se is two-fold. Studies of the characteristics of "mode deflection" (References 10 and 11) have established that convergence to accurate representations of internal bending moment is often not assured with a small number of modes. This accuracy problem is then compounded by the fact that the two components of this nonlinear excitation are subtractive. This is evidenced by the differencing of the section bending stiffnesses as indicated above.

A second difficulty with using the ΔEI method relates to the assumed space curve character of the elastic axis. As such, torsion deflections are seen to contribute to inplane and out-of-plane deflections in the presence of bending (see Equations (8) and (10)). Thus, an analogous nonlinear excitation effect exists in both the flatwise and edgewise bending equations. In the framework of the G400 analysis, these nonlinear excitations in the bending equations are most practically implemented using a "force integration" approach. Consequently, the use of a ΔEI mode deflection implementation in the torsion equation together with a force integration implementation in the bending equations results in a (coupled) modal mass matrix which is generally nonsymmetric. A nonsymmetric mass matrix is not intrinsically a weakness for isolated rotor simulation and has been successfully used for years in that mode. However, the potential exists for spurious divergent response conditions caused by an inertia matrix becoming nonpositive-definite due to this deflection dependent nonsymmetry.

The third difficulty with the Equation (38) formulation is that it is difficult to include the built-in curvature due to structural sweep. Equation (38) requires curvature information which is not generally available for the built-in geometry

Because of these difficulties, the conventional ΔEI approach of Equation (38) was abondoned in favor of a "force integration" approach. Accordingly, the Galerkin approach is applied to the nonlinear excitation term and integration by parts is used to achieve an intermediary step needed to eliminate the explicit curvature terms:

$$\int_0^1 \gamma_{\theta_j} \left\{ \cdots \right\}_{\text{(III)}} dr = \int_0^1 \left\{ -P_{z_5} \int_0^{\bar{r}} \int_0^{\bar{r}_1} \gamma_{\theta_j} y_5'' dr_2 dr_1 \right.$$

$$+ P_{y_5} \int_0^r \int_0^{r_1} \gamma_{\theta_j} z_5'' dr_2 dr_1 + (z_5'T + q_{y_5}) \int_0^{\bar{r}} \gamma_{\theta_j} y_5'' dr_1$$

(39)

$$\left. - (y_5'T - q_{z_5}) \int_0^{\bar{r}} \gamma_{\theta_j} z_5'' dr_1 \right\} d\bar{r}$$

Since this term represents the nonlinear effects, it is reasonable to use a zeroth order approximation to the curvature terms wherein the structural sweep in assumed to be "small". With this assumption, all the integrals in Equation (39) can be evaluated using the deflection correction functions defined in the above subsections. Thus, Equation (39) becomes:

$$\int_0^1 \gamma_{\theta_j} \left\{ \cdots \right\}_{\text{(III)}} dr = \int_0^1 \left\{ \Gamma_{y_{\theta_j}} \left[P_{y_5} \cos\Theta + P_{z_5} \sin\Theta \right] \right.$$

$$- \Gamma_{z_{\theta_j}} \left[P_{z_5} \cos\Theta - P_{y_5} \sin\Theta \right]$$

(40)

$$+ \tilde{\Gamma}_{z_{\theta_j}} \left[T(w_e' - \Delta w^{(2)'} - \Delta w^{(2)'}) + q_{y_5} \cos\Theta + q_{z_5} \sin\Theta \right]$$

$$\left. - \tilde{\Gamma}_{y_{\theta_j}} \left[T(v_e' + \Delta v^{(2)'} - \Delta v^{(2)'}) - q_{z_5} \cos\Theta + q_{y_5} \sin\Theta \right] \right\} dr$$

37

where:

$$\Gamma_{y_{\theta_j}} = \gamma_{\theta_j}(w_e + z_{10_{EA}} - \Delta w - \Delta W) - (\Delta v_{EA_j} - \Delta V_{EA_j}) \tag{41a}$$

$$\Gamma_{z_{\theta_j}} = \gamma_{\theta_j}(v_e + y_{10_{EA}} + \Delta v - \Delta V) - (\Delta w_{EA_j} + \Delta W_{EA_j}) \tag{41b}$$

$$\tilde{\Gamma}_{y_{\theta_j}} = \gamma_{\theta_j}(w'_e + z'_{10_{EA}} - \Delta w^{(2)'} - \Delta W^{(2)'}) - (\Delta v_{EA_j}^{(2)'} - \Delta V_{EA_j}^{(2)'}) \tag{41c}$$

$$\tilde{\Gamma}_{z_{\theta_j}} = \gamma_{\theta_j}(v'_e + y'_{10_{EA}} + \Delta v^{(2)'} - \Delta V^{(2)'}) - (\Delta w_{EA_j}^{(2)'} + \Delta W_{EA_j}^{(2)'}) \tag{41d}$$

Equation (40) represents the required form of the "force integration" implementation of the nonlinear torsion excitation term. To conclude this subsection, three observations can be made of the above formulation:

1. Equations (41) all reduce to zero for zero structural sweep and zero elastic deflection, as would be expected from the behavior of Equation (38).

38

2. In Equation (40), the terms multiplying the nonlinear torsion weighting functions ($\Gamma_{y\theta_j}$,...) are actually the force and moment loadings defined for the linear excitations of the bending equations. The nonlinear torsion weighting functions, Equations (41), thus serve in effect, as the virtual deflection functions arising from <u>torsion</u> deflections appropriate to the <u>bending</u> generalized loads.

3. The validity of the force integration approach is substantiated by the fact that the resulting terms in the torsion equation which represent rows of the inertia matrix (reflecting the integration of inertia forces) produce complete mass matrix symmetry and consequently insure positive-definiteness.

AERODYNAMIC SWEEP

Principal Assumptions

The unsteady airloads formulation incorporated in the G400PROP analysis is based on aerodynamic concepts originally developed for helicopter rotor blades. A characteristic of the aerodynamics of helicopter rotor blades is the generally large variability in local air velocities due to a combination of rotation with translational motion within the plane of the rotor. As a result, the aerodynamic formulations which have evolved are typically of a "strip theory" type with varying degrees of refinement to account for unsteady and swept flow effects. Such refinements typically are two-dimensional and applied in a heuristic manner based on the strip theory assumption. This is generally the approach followed herein. In addition to the basic strip theory assumption, the following specific sweep related assumptions are made.

1. The local aerodynamic section sweep angle is defined by the angle the local airflow direction makes with the blade section taken normal to the midchord line (see Fig. 6).

2. The section angle-of-attack is defined by the inflow and pitch angles measured within the section taken normal to the midchord line.

3. For those cases wherein the "quasi-static" option is invoked, the effective angle-of-attack is defined (using above assumption 2) as the sum of the pitch and inflow angles. For this case, inflow angle is evaluated using local flow velocities at the 3/4 chord control point.

4. For those cases wherein either of the specific, more advanced unsteady methods of the next two sections are invoked, the angle-of-attack or plunge variables are also defined using above assumption 2, but with inflow angle evaluation at the 1/4 chord control point.

5. Airfoil drag is divided into two vectorial components (pressure drag, and skin friction drag) which are vectorially added to give the total drag. Pressure drag is that generally associated with compressibility and lift, and locally acts in the direction normal to midchord line, whereas skin-friction drag acts in the direction of the local flow velocity.

PLAN FORM VIEW

TYPICAL BLADE
SEGMENT

y_5

MID-CHORD
LINE

U_R

A

U

U_{T_5}

$U_T(U_N)$

U_{R_5}

D_p

D_s

Δr

A

CONTROL POINT,
(QUARTER CHORD OR THREE
QUARTER CHORD FOR VELOCITIES),
(QUARTER CHORD FOR LOADS)

LE

$\Lambda_{e_5}^{(A)}$

TE

SKIN FRICTION
DRAG

x_5
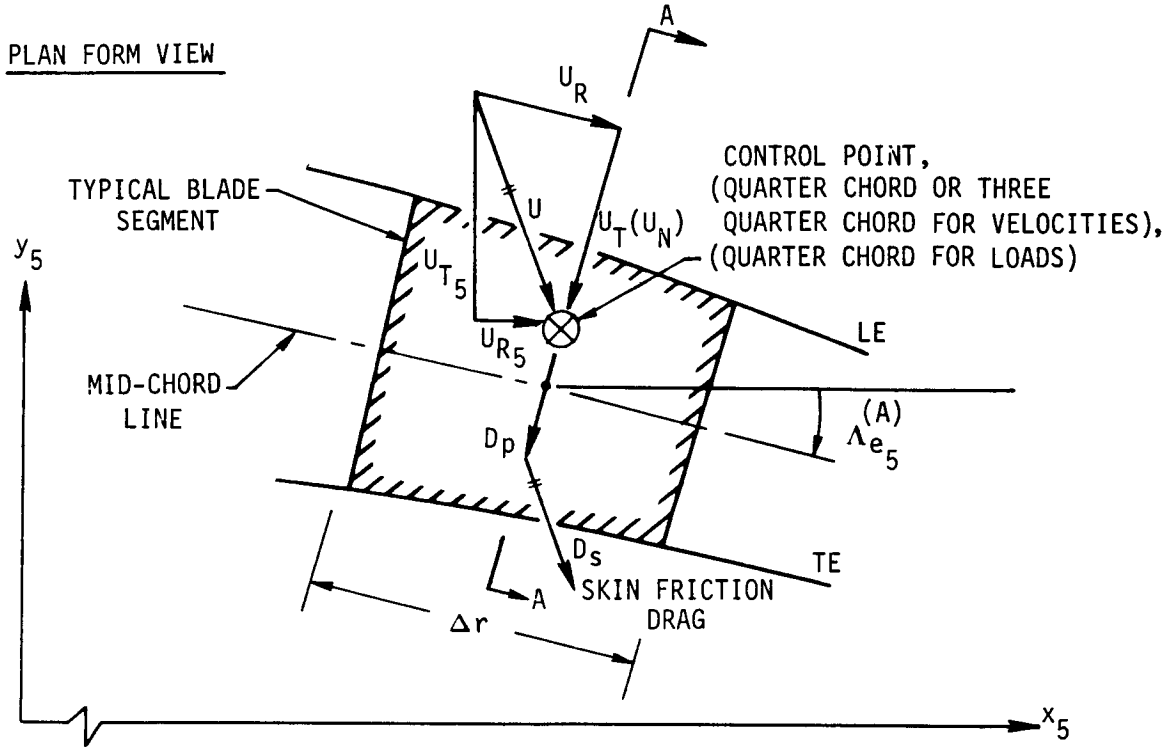
NORMAL AIRFOIL SECTION A-A

NORMAL SECTION
ANGLE-OF-ATTACK, α_N

M_x

LIFT,
L

CONTROL
POINT

PRESSURE DRAG,
D_p

z_8

U_n

U_p

U_T

MIDCHORD
POINT

INFLOW ANGLE , ϕ

TOTAL PITCH
ANGLE, θ_N

y_8
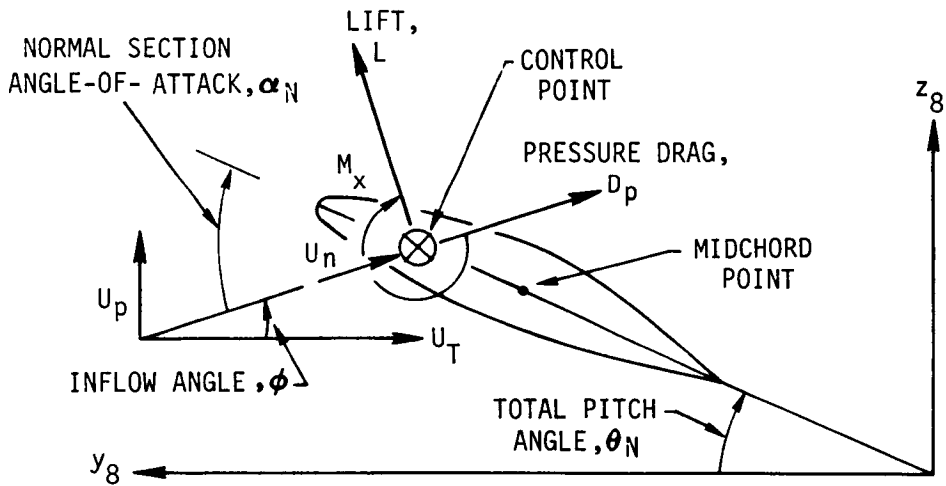
Figure 6. Geometric Details of Typical Aerodynamically Swept Section

41

6. Skin friction drag varies with span (and hence Mach number) but is invariant with angle-of-attack.

7. Lift, pitching moment, and pressure drag coefficients are determined by the angle-of-attack and Mach number measured in the section normal to the midchord line. The lift, pitching moment, and pressure drag are determined by their so-defined coefficients and the dynamic pressure based on the velocity components normal to the midchord line.

8. Skin friction drag is determined by the Mach number and dynamic pressure based upon the total vector sum of all components of the local total flow.

These assumptions form the basis of the development which follows.

Basic Modeling Characteristics

Aerodynamic Sweep Angle Projections

As was developed in the previous section, the appropriate axis for defining structural sweep is the elastic axis. The appropriate axis for defining aerodynamic sweep, however, is, by assumption 1, the locus of midchords. Therefore, the aerodynamic sweep angles are defined as:

$$\Lambda_{e_5}^{(A)} = \Lambda_{e_5} + (\cos\theta \, \Delta\Lambda - y_{6e}') \tag{42}$$

$$\Lambda_{f_5}^{(A)} = \Lambda_{f_5} + (-\sin\theta \, \Delta\Lambda + z_{6e}') \tag{43}$$

where $\Delta\Lambda$ is the difference in sweep angle between the midchord and the elastic axis, as measured in the local chordwise direction, and can reasonably be assumed to be a "small" angle. Since the elastic bending slopes of

42

y_6' and z_6' , are also assumed to be small, the small angle assumption can
$_e _e$

safely be used on the parenthetical terms in Equations (42) and (43).

Similar to the coordinate system transformation developed in the previous section (Equations (23) through (26)) and pictorially defined in Figure 4, a coordinate system transformation can be formulated for aerodynamic sweep. In particular, such an aerodynamic sweep transformation is needed to relate velocity and loading components in the "5" coordinate system to those quantities in the "8" coordinate systems. The "8" coordinate system is defined similarly to the "6" coordinate system but is additionally displaced by the elastic bending deflections, and is rotated relative to the "5" coordinate system by the aerodynamic sweep angles,
$\Lambda_{e_5}^{(A)}$ and $\Lambda_{f_5}^{(A)}$, given by Equations (42) and (43), respectively. Using the vector decompositions shown in Figure 7, the following definitions are made for an arbitrary spanwise element:

$\vec{n}_1 \equiv$ unit vector along the span of the midchord of the blade element

$\vec{n}_2 \equiv$ unit vector perpendicular to $\vec{n}_1$ and parallel to the x_5-y_5 plane, positive forward

$\vec{n}_3 \equiv$ unit vector mutually perpendicular to both $\vec{n}_1$ and $\vec{n}_2$, righthand rule.

Similar to Equation (24) the following relationship can be written:

$$\left\{ \begin{matrix} \vec{n}_1 \\ \vec{n}_2 \\ \vec{n}_3 \end{matrix} \right\} = \left[TAS^{(A)} \right] \left\{ \begin{matrix} \vec{i} \\ \vec{j} \\ \vec{k} \end{matrix} \right\} \tag{44}$$

where the elements of $[TAS^{(A)}]$ are defined using Equations (25) and (26), but with the aerodynamic sweep angles.

Velocity Decompositions

As shown in Figure 7, the local velocity vector including only environmental effects (i.e., neglecting blade motion) can be expressed in either

43
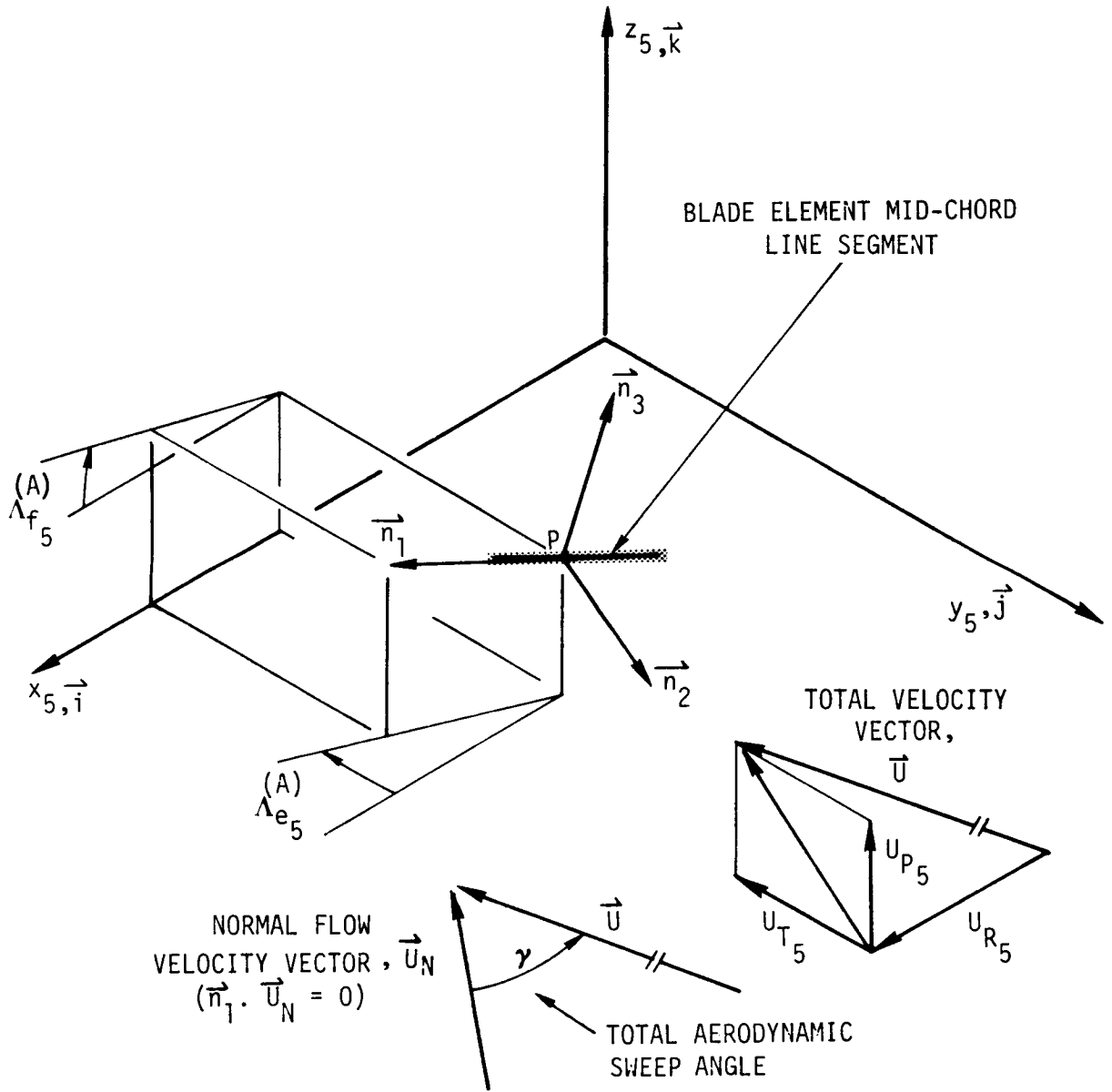
Figure 7. Pictorial Representations of Coordinate Systems and Velocity Decomposition Relating to Aerodynamic Sweep

44

coordinate system:

$$\vec{U} = U_{R_5}\vec{i} - U_{T_5}\vec{j} + U_{P_5}\vec{k}$$

$$= U_{R_0}\vec{n}_1 - U_{T_0}\vec{n}_2 + U_{P_0}\vec{n}_3 \tag{45}$$

Use of the above coordinate system transformation together with the local velocities due to blade motion, v_{y_6} and v_{z_6}, yields the following useful form:

$$\begin{Bmatrix} U_R \\ -U_T \\ U_P \end{Bmatrix} = \begin{bmatrix} TAS^{(A)} \end{bmatrix} \begin{Bmatrix} U_{R_5} \\ -U_{T_5} \\ U_P \end{Bmatrix} - \begin{Bmatrix} 0 \\ v_{y_{6e}} \\ v_{z_{6e}} \end{Bmatrix} \tag{46}$$

Note the U_{R_5}, U_{T_5}, and U_{P_5} can include not only the components due to axial flow and variable inflow distortion, as discussed in a later section, but any perturbation which might accrue from hub motion. Consideration of such hub motion is presently outside the scope of the study, however.

Other relationships which are needed to formulate the airloading distribution are the magnitude of the total velocity, U, and the component normal to the midchord, U_N:

$$U = (sgn\ U_T)\sqrt{U_T^2 + U_P^2 + U_R^2} \tag{47}$$

$$U_N = (sgn\ U_T)\sqrt{U_T^2 + U_P^2} \tag{48}$$

45

Airload Distributions

Using standard strip theory techniques, the local lift, pitching moment, pressure drag, and skin friction drag distributions can, respectively, be written as:

$$L = \rho \frac{c}{2} \cdot \Delta r \, U_N^2 \, c_\ell (\alpha_N, M_N) \tag{49a}$$

$$M_x = \rho \frac{c^2}{2} \Delta r \, U_N^2 \, c_{m_{c/4}} (\alpha_N, M_N) \tag{49b}$$

$$D_p = \rho \frac{c}{2} \Delta r \, U_N^2 \, c_{dp} (\alpha_N, M_N) \tag{49c}$$

$$D_s = \rho \frac{c}{2} \Delta r \, U^2 \, c_{d_s} (M) \tag{49d}$$

where:

$$\alpha_N = \theta_N + \tan^{-1}(U_p/U_T) \tag{50}$$

$$M_N = U_N / a_\infty \tag{51}$$

$$M = U/a_\infty \tag{52}$$

$$c_{d_p} = c_d (\alpha_N, M_N) - c_{d_s} (M_N) \tag{53}$$

The pitch angle seen in the "8" coordinate system, θ_N, is obtained from the nominal pitch angles with consideration of the integrated effect of the cosine components:

46

$$\theta_N = \theta_0 + \theta_B + \sum_{j=1}^{NTM} \tilde{\gamma}_{\theta_j} \cdot q_{\theta_j} \qquad (54)$$

where:

$$\tilde{\gamma}_{\theta_j} = \left[\gamma_{\theta_j} + \int_0^r \gamma'_{\theta_j} (\cos \Lambda^{(A)}(r_I) - 1) dr_I \right] \cos \Lambda^{(A)} \qquad (55)$$

$$+ \left[\int_0^r \gamma'_{\theta_j} \sin \Lambda^{(A)}(r_I) dr_I \right] \sin \Lambda^{(A)}$$

and where:

$$\Lambda^{(A)} = \sin^{-1} \frac{\Delta y_{IO_{EA}}}{\Delta r} + \Delta \Lambda \qquad (56)$$

Components in the "8" coordinate system

The airload distributions given by Equations (49) are then resolved to the "8" coordinate system using the components of the inflow velocity:

$$p_{a_{x_8}} = \rho_{\bar{2}} c \Delta r \, U U_R c_{d_s} \qquad (57)$$

$$p_{a_{y_8}} = -\rho_{\bar{2}} c \Delta r \left[U_N (c_{d_p} U_T - c_\ell U_P) + U U_T c_{d_s} \right] \qquad (58)$$

$$p_{a_{z_8}} = \rho_{\bar{2}} c \Delta r \left[U_N (c_\ell U_T + c_{d_p} U_P) + U U_P c_{d_s} \right] \qquad (59)$$

$$q_{a_{x_8}} = \rho_{\bar{2}} c^2 \Delta r \left[U_N^2 \, c_{m_{c/4}} - U \kappa \overset{*}{\theta} \right] + y_{IO_{c/4}} (p_{a_{z_8}} \cos \Theta - p_{a_{y_8}} \sin \Theta) \qquad (60)$$

47

and where:

$$K = \frac{\pi}{4} c(\text{sgn } U) \begin{cases} 0 & : \text{using advanced unsteady airloads option} \qquad (61) \\[2em] 1 - \frac{2}{c} y_{10_{c/4}} & : \text{forward flow, quasi-static option} \\[2em] \frac{2}{c} y_{10_{c/4}} & : \text{reversed flow, quasi-static option} \end{cases}$$

Components in the "6" coordinate system

Above Equations (57) through (60) define the airload components with directions aligned with the deflected blade segments. The appropriate airloads needed are those defined in the "6", or undeflected coordinate system:

$$p_{a_{x_6}} = p_{a_{x_8}} + p_{a_{y_8}} (\cos \Theta \, \Delta \Lambda - y_{6_e}') - p_{a_{z_8}} (-\sin \Theta + z_{6_e}') \qquad (62)$$

$$p_{a_{y_6}} = p_{a_{y_8}} - p_{a_{x_8}} (\cos \Theta \Delta \Lambda - y_{6_e}') \qquad (63)$$

$$p_{a_{z_6}} = p_{a_{z_8}} + p_{a_{x_8}} (-\sin \Theta \Delta \Lambda + z_{6_e}') \qquad (64)$$

$$q_{a_{x_6}} = q_{a_{x_8}} \qquad (65)$$

48

Remarks Concerning Application

Above Equations (63) through (65) define the most general information of the airload distributions to be used in the bending equations and in the nonlinear excitation term of the torsion equation (see Equation (41)). These expressions for airloadings are very nonlinear and, in the above form, are only suitable for utilization in the time-history solution. For eigensolution purposes, they must be completely expanded to yield all explicit linearized perturbations of the modal variables and their derivatives, δq_{w_i}, δq_{v_k}, δq_{θ_j}, $\delta \overset{*}{q}_{w_i}$ ... The details of this perturbational expansion are straightforward, but sufficiently tedious to warrant excluding them from the present report.

UNSTEADY STALLED AIRLOADS

A detailed analysis of dynamic stall experiments has led to a semi-analytic methodology characterized by a set of relatively compact analytical expressions, called synthesized unsteady airfoil data, which accurately describe in the time-domain the unsteady aerodynamic characteristics of stalled airfoils (Reference 12). Under the present study, the unsteady stalled airloads methodology was expanded for propeller applications by synthesizing similar unsteady loops at subsonic Mach numbers which are higher, more relevant than those used in the earlier study. More specifically, the high Mach number data contained in References 13 and 14 were reduced to synthesized form within the established Reference 12 framework.

Review of Basic Methodology

Dynamic Stall Model

The analytical model of dynamic stall, described herein, includes the main physical features of the dynamic stall phenomenon as observed in oscillationing airfoil tests. A brief description of dynamic stall events is given below.

When an airfoil experiences an unsteady increase in angle-of-attack beyond the static stall angle, a vortex starts to grow near the leading edge region. As the angle continues to increase, the vortex detaches from the leading edge and is convected downstream near the surface. These events are shown schematically in Figure 8. The suction associated with the vortex normally causes an initial increase in lift. The magnitude of the increase depends on the strength of the vortex and its distance from the surface. The streamwise movement of the vortex depends on the airfoil shape and the pitch rate. The relative distance between the vortex and the airfoil varies according to the kinematics of the airfoil. That is, it depends on characteristics such as the pitch rate and the instantaneous angle-of-attack. As the vortex leaves the trailing edge, a peak negative pitching moment is obtained. The airfoil then remains stalled until the angle-of-attack drops sufficiently so that reattachment of the flow can occur. The present method incorporates all of these events. For example, the strength of the vortex is made a function of the angle when the vortex leaves the leading edge (moment stall angle). The higher the moment stall angle, the higher the strength of the vortex.
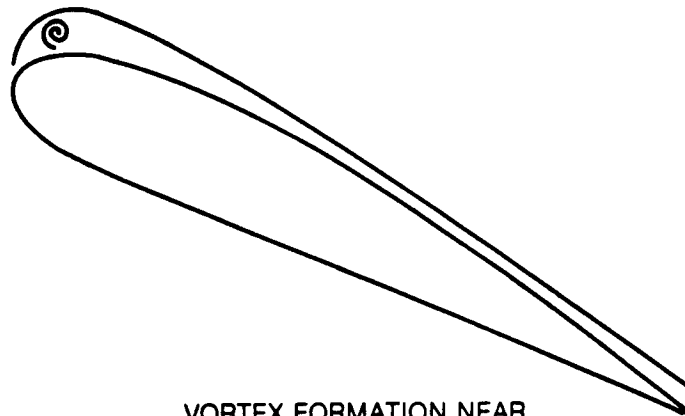
VORTEX FORMATION NEAR
LEADING EDGE
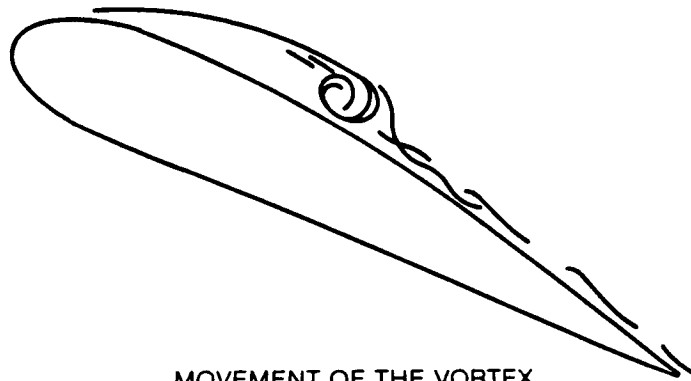
MOVEMENT OF THE VORTEX
OVER THE AIRFOIL

Figure 8. Dynamic Stall Modeling

Parameters Influencing Dynamic Stall

The unsteady lift, drag, and pitching moment coefficients of the airfoils obtained from the two-dimensional oscillating airfoil tests show a large degree of hysteresis when plotted as functions of angle-of-attack, particularly when the reduced frequency and the maximum angle-of-attack are sufficiently high. Figures 9a, 9b, and 9c show an example of typical loop data obtained from the oscillating airfoil test. The amount of hysteresis and the shape of the loops vary in a highly nonlinear fashion with such test parameters as amplitude, mean angle, and reduced frequency.

The results of the oscillation airfoil tests clearly indicate that the dynamic characteristics of an airfoil depend on the following main parameters: (1) airfoil shape and sweep; (2) Mach number; (3) Reynolds number; (4) reduced frequency, k; (5) oscillation amplitude, $\bar{\alpha}$; and (6) mean angle-of-attack, α_o.

The first three of these parameters affect both the static and the dynamic characteristics of the airfoil, while the last three parameters represent purely dynamic parameters. Since most rotor aeroelastic analyses employ time-history solution techniques for computation of the aerodynamic loading acting on the rotor blades, frequency domain parameters such as reduced frequency or amplitude, etc., are inappropriate for use in these time domain simulations. Moreover, for arbitrary motion it is difficult to describe the reduced frequency, the amplitude of oscillation, or the mean angle-of-attack of a rotor blade section in a precise manner. As a result, an alternative set of dynamic parameters, which are appropriate for the time domain simulations, is defined. The parameters replacing k, $\bar{\alpha}$, and α_o in the present method are: (4) the instantaneous angle-of-attack, α; (5) the nondimensional pitch rate, A; and (6) the unsteady decay parameter, α_w, which accounts for the time history effects of the change in α, and is based upon the Wagner function.

For the sinusoidally oscillating airfoil, these three parameters can be easily expressed in terms of the reduced frequency, the amplitude, and the mean angle-of-attack. Also, they can be easily evaluated for rotor blade sections in a stepwise manner and are very convenient to use for the prediction of the onset of dynamic stall and for the determination of the unsteady airloads. Thus, the present method determines, through the synthesization process, the effect of these selected parameters (α, A, α_w) on the dynamic stall characteristics of the airfoils by utilizing the data from the oscillating airfoil tests. The synthesization process used herein essentially involves curve-fitting of the test loop data to the prescribed analytical expressions, with the objective of determining the unknown parameters or coefficients embedded in the analytical expressions. The analytical expressions are

52
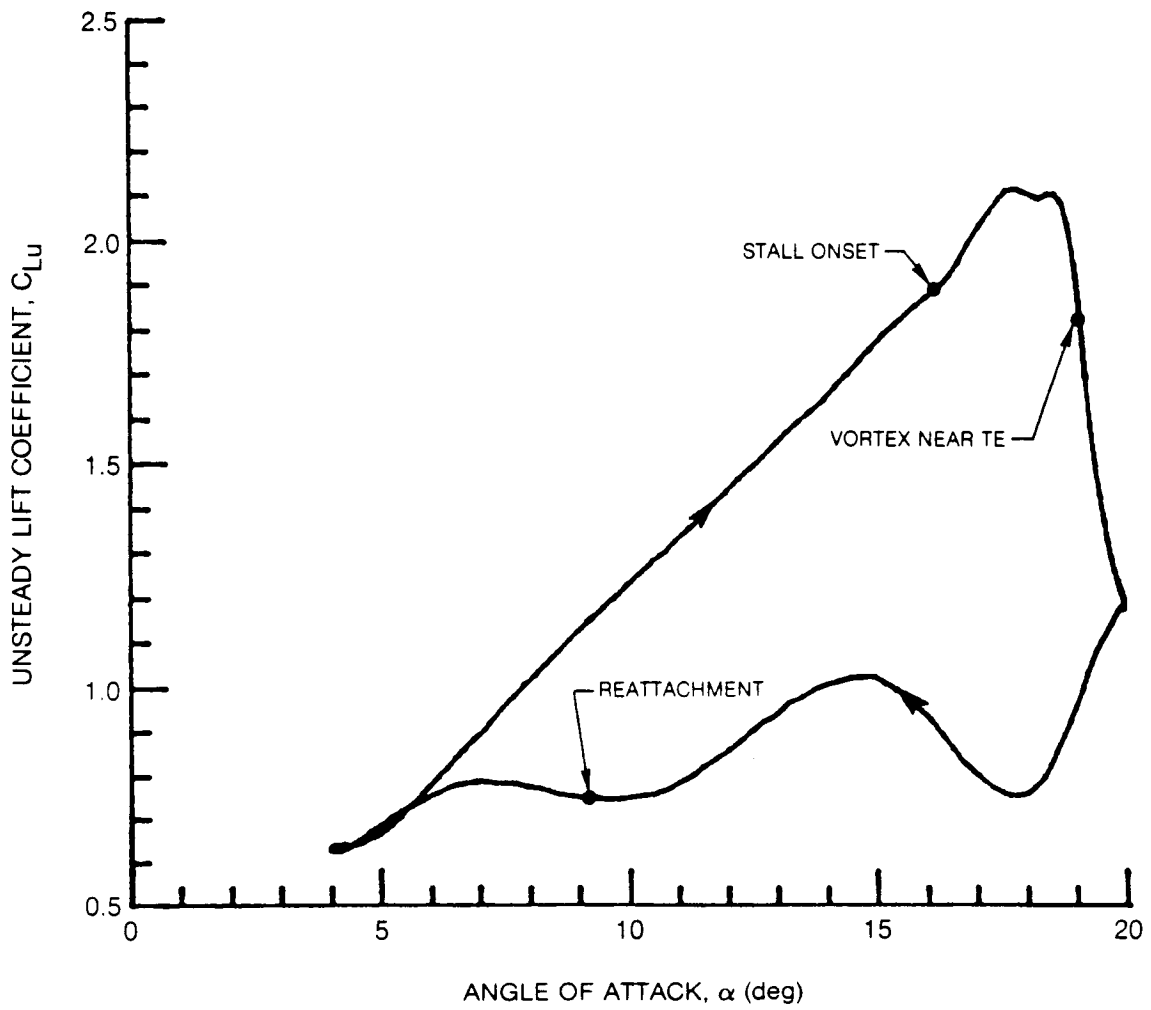
Figure 9a. Typical Unsteady Lift Coefficient Loop Data, SC 1095 Airfoil, M = 0.3, α_o = 12.0 deg, $\bar{\alpha}$ = 8.0 deg, k = 0.1
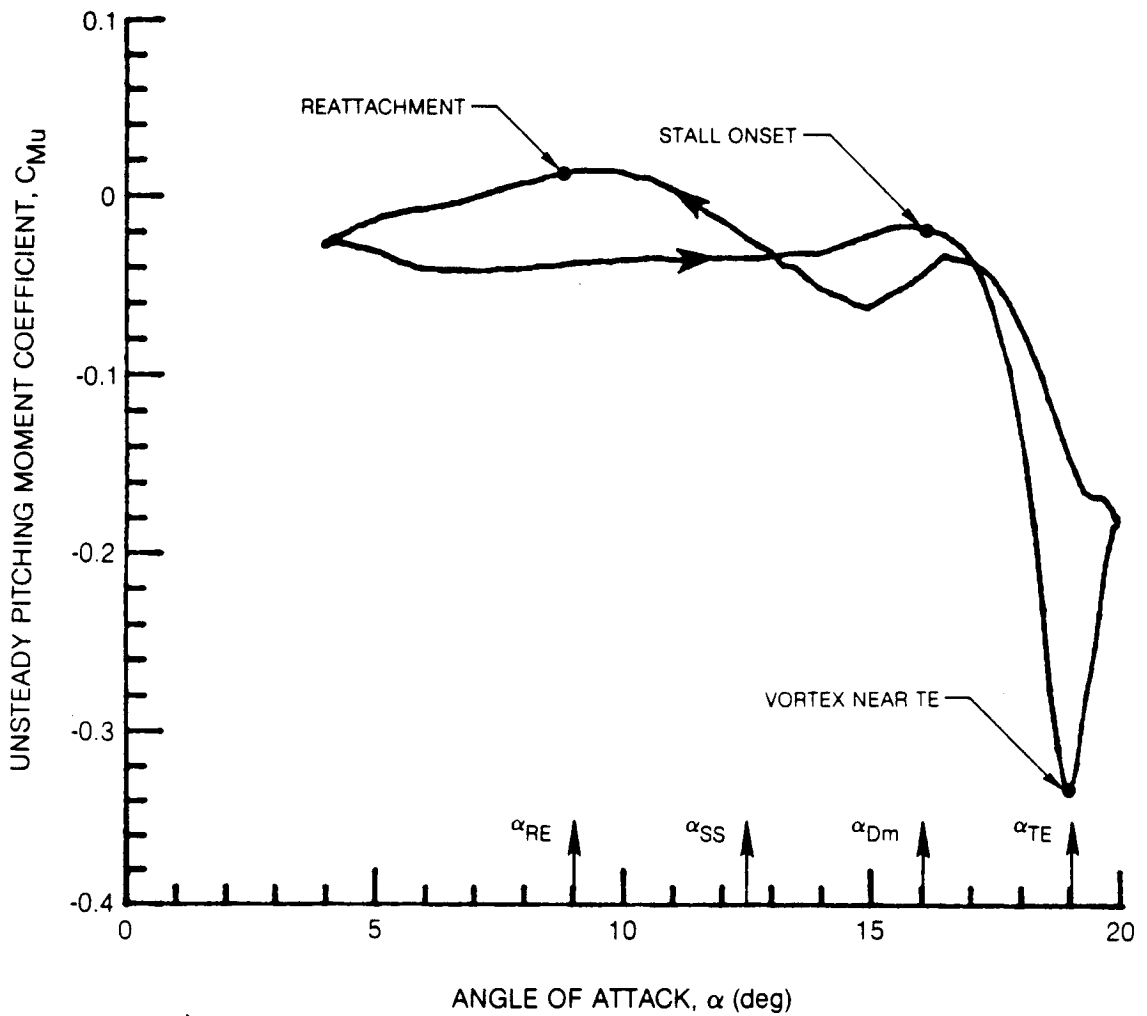
Figure 9b. Typical Unsteady Pitching Moment Loop Data, SC 1095 Airfoil, M = 0.3, α_o = 12.0 deg, $\bar{\alpha}$ = 8.0 deg, k = 0.1
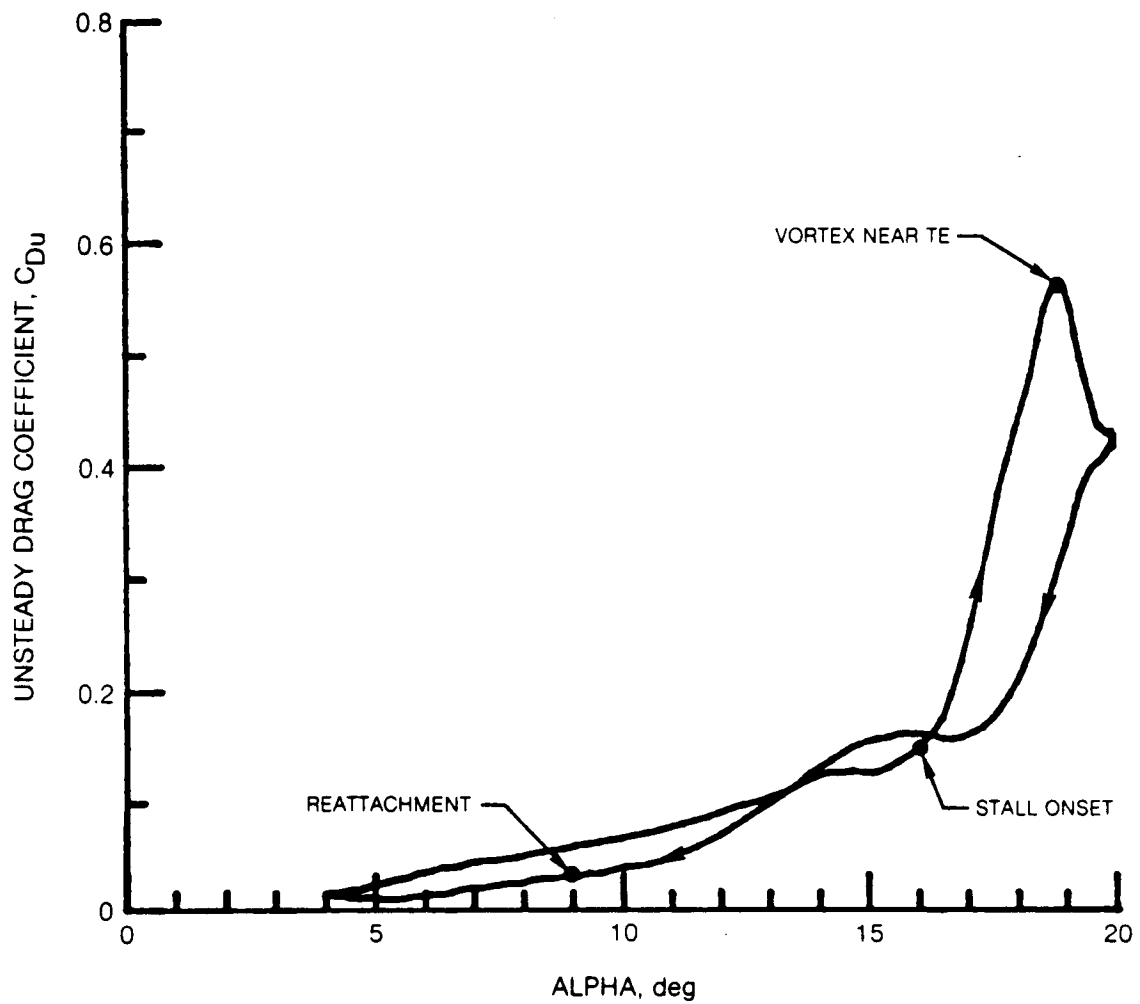
Figure 9c. Typical Unsteady Drag Coefficient Loop Data, SC 1095 Airfoil, M = 0.3, α_o = 12.0 deg, $\tilde{\alpha}$ = 8.0 deg, k = 0.1

obtained mostly by mathematical or empirical means and in general they represent simple quantitative approximations to the various observed physical features of the dynamic stall phenomenon.

Definition of the Unsteady Decay Parameter, α_w

For a two-dimensional airfoil going through an arbitrary change in angle-of-attack, one can describe an instantaneous effective angle-of-attack, α_E, by using Duhamel's integral (Reference 10) as given below:

$$\alpha_E (s) = \alpha (0) \phi_C (s,M) + \int_0^s \frac{d\alpha}{d\sigma} \beta \phi_C (s-\sigma, M) \, d\sigma \tag{66}$$

where $\alpha(0)$ corresponds to the initial angle-of-attack, M represents Mach number, $\phi_C(s,M)$ is the response to step change in α (a compressibility corrected form of the Wagner function), and s is the nondimensional time as given by:

$$s = \frac{2}{C} \int_0^t U \, dt_1 \tag{67}$$

The unsteady decay parameter, α_w, to be used extensively in the present method, is defined as follows:

$$\alpha_w = \alpha (s) - \alpha_E (s) \tag{68}$$

The α_w parameter physically represents the difference between the instantaneous angle, α and the effective angle, α_E, and therefore accounts for the time-history effects of the change in α. This physical description of α_w is valid for attached flow conditions only. In the present method, the α_w parameter is most useful for predicting the onset of dynamic stall, and for convenience, it is also used to describe approximately the unsteady coefficients after the stall.

The effects of compressibility are incorporated in the definitions of α_w by the use of the general or compressible Wagner function (see also Reference 15) obtained from the following approximate relationship

$$(69)$$

$$\phi_C \; (s,M) = \left[1.0 - 0.165 e^{-0.0455\,s\,(1-M^2)} - 0.335\, e^{-0.3s\,(1-M^2)} \right] / \sqrt{1-M^2}$$

Computation of Dynamic Parameters

For the sinusoidally oscillating airfoil, where the motion of the airfoil is completely known, the parameters α, A, and α_w can be obtained analyticaly as given below:

$$\alpha = \bar{\alpha} \sin ks \tag{70}$$

$$A = k \bar{\alpha} \cos ks \tag{71}$$

$$\alpha_w = \gamma_1 \; (k,M)\, k \bar{\alpha} \cos ks + \gamma_2 (k,M)\, \bar{\alpha} \sin ks \tag{72}$$

where k, s, and M represent reduced frequency, nondimensional time, and Mach number, respectively. The γ_1 and γ_2 functions are described by:

$$\gamma_1 \; (k,M) = \frac{0.165\,(1-M^2)(0.0455)}{k^2 + (1-M^2)^2\,(0.0455)^2} + \frac{0.335\,(1-M\;)(0.3)}{k^2 + (1-M^2)^2(0.3)^2} \tag{73}$$

$$\gamma_2 \; (k,M) = \frac{0.165\,k^2}{k^2 + (1-M^2)^2\,(0.0455)^2} + \frac{0.335\,k^2}{k^2 + (1-M^2)^2\,(0.3)^2} \tag{74}$$

In contrast to the closed form evaluations obtainable for sinusoidal motion, numerical evaluations of these three section dynamic parameters must be obtained for arbitrary motion in the time domain. This is accomplished in a stepwise manner utilizing the following recursive relationships at (time) step n:

$$\alpha_n = \theta_n + \phi_n \tag{75}$$

$$A_n = \left[\frac{\partial \theta_n}{\partial \psi} + \frac{\partial \phi_n}{\partial \psi}\right] \frac{\Delta \psi}{(\Delta s)_n} \tag{76}$$

$$(\alpha_w)_n = X_n + Y_n \tag{77}$$

where:

$$X_n = X_{n-1} e^{-0.0455(1-M^2)(\Delta s)_n} + 0.165(\alpha_n - \alpha_{n-1}) \tag{78a}$$

$$Y_n = Y_{n-1} e^{-0.3(1-M^2)(\Delta s)_n} + 0.335(\alpha_n - \alpha_{n-1}) \tag{78b}$$

$$(\Delta s)_n = \frac{2U_n}{\Omega c} (\Delta \psi) \tag{79}$$

Here $\Delta \psi$ is azimuthal stepsize, Ω is rotor speed, c is chord length, and U_n is streamwise velocity.

The instantaneous angle-of-attack, α_n, is described in the section normal to the midchord, θ_n and ϕ_n being the pitch angle and inflow angle, respectively. The numerical calculation of the nondimensional angle-of-attack rate, A, poses special problems. The nondimensional time derivative of pitch angle in Equation (76), $\partial\theta_n / \partial\psi$, may be computed analytically from the known control angle and elastic torsion response rates, whereas the time derivative of ϕ must be computed using some form of numerical differentiation. The nominal method suggested in Reference 12 is a backward difference scheme. However, in some applications, this method was found to give violent numerical instabilities and an alternate method was required. The alternate method selected is based on the assumption of a predominantly oscillatory response at some user selected frequency, $\bar{\omega}$, which typically would be taken as the dominant blade torsion natural frequency. These two numerical results are given below:

$$\frac{\partial\phi_n}{\partial\psi} = \begin{cases} \frac{1}{\Delta\psi}(1.5\,\phi_n - 2\,\phi_{n-1} + .5\,\phi_{n-2}); & \bar{\omega} = 0 \\[2ex] \frac{\bar{\omega}\cos\bar{\omega}\,\Delta\psi}{\sin\bar{\omega}\,\Delta\psi}(\cos\bar{\omega}\,\Delta\psi \cdot \phi_n - \phi_{n-1}); & \bar{\omega} > 0 \end{cases}$$

(80)

Prediction of Dynamic Stall Events

In the present method it is considered important to accurately predict three major events associated with dynamic stall. These events, as shown in Figure 9b, are the stall onset, the vortex at the trailing edge, and the reattachment. The next section describes the semi-empirical equations that are used to predict these events.

Onset of Stall

Because the dynamic stall airloads acting on an airfoil are highly influenced by the leading edge vortex, an accurate prediction of the instant the vortex breaks away from the leading edge (moment stall point) becomes very important. The occurrence of moment stall depends on factors such as Mach number, the airfoil shape and the pitch rate.

Under the conventional quasi-static theory formulation, the stall is assumed to occur when the effective angle-of-attack reaches the static stall angle,

$$\alpha_{Em} = \alpha_{ss}$$

(81)

In general, α_{ss} is assumed to vary with the airfoil shape, Mach number and Reynolds number. To some extent, the value of α_{ss} also depends on the criterion followed for stall.

Under the present formulation, the relationship represented by Equation (81) is extended to include dynamic stall effects, and an assumption is made that at the dynamic stall point, in general, the effective angle of attack, α_{Em}, is not only a function of α_{ss}, but also depends on the pitch rate at stall, A_m, and the instantaneous angle-of-attack at stall. That is,

$$\alpha_{Em} = F(\alpha_{ss}, A_m, \alpha_{Dm})$$ (82)

The actual functionality F depends on the type of stall and on the criterion followed for stall. It is assumed that F varies with airfoil shape, Mach number, and Reynolds number, and can be established empirically. Linearization of the relationship of Equation (82) with respect to parameters A_m and α_{Dm} around quasi-steady conditions, $\alpha_{ss}(1+\epsilon)$, leads to the following simple expression for α_{Dm}, the angle at which dynamic moment stall first occurs:

$$\alpha_{Dm} = (1 + \epsilon + C_{Am} A_m + C_{wm} \alpha_{wm}) \alpha_{ss}$$ (83)

Here, α_{w_m} represents the value of the parameter, α_w, at the point of moment stall. Thus, instead of the function F, one can determine empirically the coefficients ϵ, C_{Am}, and C_{wm} for various Mach numbers, Reynolds numbers, and airfoils. In Equation (83), the last two terms represent the delay in dynamic stall when compared with quasi-static stall. Other available methods (References 15, 16) represent this delay in stall by a constant time delay. However, Equation (83) is a much more general relationship which predicts the onset of dynamic stall quite accurately for airfoils experiencing unsteady motion.

Vortex at Trailing Edge

Normally, after the occurrence of moment stall, there is a significant increase in negative pitching moment due to the travel of the stall vortex.

The maximum negative pitching moment occurs when the vortex is near the trailing edge of the airfoil. For the case shown in Figure 9b the instant when the vortex leaves the trailing edge is marked by 'TE'. Preliminary results have led to the following empirical relationship for predicting the instant when the vortex leaves the airfoil:

$$S_{mt} = 1.0/(C_{At} A_{pm} + C_{\alpha t} \alpha_{pm}) \tag{84}$$

Here s_{mt} is the total nondimensional time for the vortex to travel from the leading edge to the trailing edge. Once again, the coefficients C_{A_t} and C_{α_t} vary with Mach number, airfoil shape, sweep, and Reynolds number.

Reattachment

The instant when the reattachment of the flow occurs is marked in Figure 9b. Normally, for low Mach numbers ($M \leq 0.4$) the reattachment occurs at an angle α_{RE} which is less than the static stall angle. At higher Mach numbers, where the static stall may be induced by shocks, the reattachment angle α_{RE} can be higher than the static stall angle, α_{ss}. In the present formulation, a general expression for α_{RE} is assumed and is given by:

$$\alpha_{RE} = (1 - \epsilon + C_{AR} A_{Dm} + C_{WR} \alpha_{WM}) \alpha_{ss} \tag{85}$$

In general, for a given airfoil, the values of C_{AR} and C_{wR}, as used in Equation (85) for reattachment, are quite different from C_{Am} and C_{wm} used for stall onset. However, the value of the parameter ϵ is the same in both of these equations.

This completes the description of all the events associated with dynamic stall that are required to compute the unsteady stall aerodynamic characteristics of an airfoil. It should be noted that the present formulation does not require explicit prediction of so-called 'dynamic lift stall'. Normally a sudden loss of lift occurs due to increase in the relative distance between the stall vortex and the airfoil surface. These effects are included

implicitly in the formulation of the unsteady lift coefficient which is described next.

<div align="center">Unsteady Section Coefficients</div>

Unsteady Lift Coefficient

The unsteady lift coefficient, C_{Lu}, of an airfoil in the time domain under the present synthesization is described by the following expressions:

$$C_{Lu} = C_{Ls}(\alpha - \Delta\alpha_1 - \Delta\alpha_2) + \alpha_{0L}\,\Delta\alpha_1 + \Delta C_{L1} + \Delta C_{L2} \tag{86}$$

$$\Delta\alpha_1 = (P_1\,A + P_2\,\alpha_w + P_3)\,\alpha_{ss} \tag{87}$$

$$\Delta\alpha_2 = \delta_2\,\alpha_{ss} \tag{88}$$

$$\Delta C_{L1} = Q_1\,A + Q_2\,\alpha_w + Q_3\,(\alpha/\alpha_{ss}) + Q_4\,(\alpha/\alpha_{ss})^2 \tag{89}$$

$$\Delta C_{L2} = Q_5\,\delta_1 + Q_6\,\Delta\alpha_2 + Q_7\,(\alpha_{Dm})^2\left[\frac{1 - e^{-(\beta_1\,s_m)^3}}{(\beta_1\,s_m)^2}\right] \tag{90}$$

$$s_m = \frac{2U(t - t_{dm})}{C} \qquad (91)$$

$$\delta_1 = \begin{cases} 0 & \alpha \leq \alpha_{ss} \\ (\alpha/\alpha_{ss} - 1) & \alpha_{ss} \leq \alpha \leq \alpha_{Dm} \\ (\alpha_{Dm}/\alpha_{ss} - 1)\left[1.0 - (s_m/s_{mt})^2\right] & 0 \leq s_m \leq s_{mt} \\ 0 & s_m > s_{mt} \end{cases} \qquad (92)$$

$$\delta_2 = \begin{cases} 0 & \alpha \leq \alpha_{ss} \\ (\alpha/\alpha_{ss} - 1) & \alpha_{ss} \leq \alpha \leq \alpha_{Dm} \\ (\alpha_{Dm}/\alpha_{ss} - 1) & 0 \leq s_m \leq s_{mt} \\ (\alpha_{Dm}/\alpha_{ss} - 1)\dfrac{\alpha - \alpha_{RE}}{\alpha_{TE} - \alpha_{RE}} & \alpha_{RE} \leq \alpha \leq \alpha_{TE} \\ 0 & \alpha \leq \alpha_{RE} \end{cases} \qquad (93)$$

The synthesized unsteady lift coefficient (Equation (86)) has been expressed as a sum of static C_{LS} at some shifted angle $(\alpha - \Delta\alpha_1 - \Delta\alpha_2)$ plus an incremental lift coefficient ($\Delta C_{L1} + \Delta C_{L2}$). The shift in angle is given by Equations (87) and (88) and the incremental lift coefficient by Equations (89) and (90). (The quantity a_{oL} in Equation (86) is the conventional static lift curve slope.) The $\Delta\alpha_1$ shift in angle (Equation (87)) is present even when no stall occurs, and the $\Delta\alpha_2$ shift in angle (Equation (88)) is mainly associated with the occurrence of dynamic stall and subsequent reattachment. Similarly, the ΔC_{L1} (Equation (89)) represents essentially the unsteady effects over static C_{LS} for dynamically unstalled airfoils, and ΔC_{L2} (Equation (90)) represents the effects associated with the dynamic stall events such as vortex formation and reattachment. In fact, the last term in Equation (90) represents explicitly the suction effects of the leading edge vortex and equals zero when no vortex exists.

Thus, Equation (86) is a general expression for unsteady C_L even when no dynamic stall occurs. For unstalled cases, the magnitudes of $\Delta \alpha_2$ and ΔC_{L2} are essentially zero.

The β_1 parameter in Equation (90) is an empirically determined constant and is nominally equal to 0.18. The quantity s_m, as described by Equation (91), represents the nondimensional time measured from the instant of the occurrence of dynamic moment stall. The unknown parameters P_1 through P_3 and Q_1 through Q_7 are determined empirically by means of a least-squares curve-fitting of Equation (86) with the test data. It should be noted that most of the terms in Equation (86) are linear in parameters α, A, and α_w.

Unsteady Moment Coefficient

The unsteady pitching moment coefficient, C_{Mu}, has been formulated using relationships similar to those for C_{Lu} and is described below:

$$C_{Mu} = C_{MS}(\alpha - \Delta \alpha_2) + a_{0m} \Delta \alpha_2 + \Delta C_M$$

(94)

$$\Delta C_M = \eta_1 A + \eta_2 \alpha_w + \eta_3 (\alpha / \alpha_{ss}) + \eta_4 |\alpha_w|$$
$$+ \eta_5 \delta_1 + \eta_6 \Delta \alpha_2 + \eta_7 \alpha_{Dm} A_{Dm} s_m$$

(95)

Here a_{0m} represents the static pitching moment slope at zero angle-of-attack and it normally equals zero. The last term in Equation (95) represents the vortex effects. For unstalled airfoils, the last three terms in Equation (95) are zero. The unknown parameters η_1 through η_7 once more are determined by the least-square curve-fitting of Equation (94) to the test data.

Unsteady Drag Coefficient

The unsteady drag coefficient, C_{Du}, appears to vary with the dynamic parameters in the same way as C_{Mu} and is described as follows:

$$C_{Du} = C_{Ds}(\alpha - \Delta\alpha_2) + \Delta C_D \qquad (96)$$

$$\Delta C_D = R_1 A + R_2 \alpha_w + R_3(\alpha/\alpha_{ss}) + R_4 |\alpha_w|$$
$$+ R_5 \delta_3 + R_6 \delta_4 + R_7 \Delta\alpha_2 + R_8 \alpha_{Dm} A_{Dm} S_m \qquad (97)$$

where:

$$\delta_3 = \begin{cases} 0 & \alpha \leq \alpha_{ss} \\ (\alpha/\alpha_{ss} - 1) & \alpha_{ss} \leq \alpha \leq \alpha_{Dm} \\ (\alpha_{Dm}/\alpha_{ss} - 1)\left[1. - (s_m/s_{mt})^{.25}\right] & 0 \leq s_m \leq s_{mt} \\ 0 & s_m > s_{mt} \end{cases} \qquad (98)$$

$$\delta_4 = \begin{cases} 0 & \alpha \leq \alpha_{ss} \\ (\alpha/\alpha_{ss} - 1)^2 & \alpha_{ss} \leq \alpha \leq \alpha_{Dm} \\ (\alpha_{Dm}/\alpha_{ss} - 1)^2\left[1. - (s_m/s_{mt})^{.25}\right] & 0 \leq s_m \leq s_{mt} \\ 0 & s_m > s_{mt} \end{cases} \qquad (99)$$

The last term in Equation (97) represents the effects of the stall vortex on the unsteady drag. For unstalled conditions, the last four terms in Equation (97) are essentially equal to zero. Once more, the unknown parameters R_1 through R_8 are computed using the linear least-squares curve-fitting of Equation (97) to the unsteady drag test data.

65

Because the higher Mach number unsteady data used to synthesize the coefficients in the G400PROP code did not include unsteady drag, the use of unsteady drag is not available to this version of G400. The description of unsteady drag coefficient given above was included herein for completeness.

Description of Additional Synthesization

The empirical relationships, for the prediction of stall events (Equations (83) through (85)) and for the description of unsteady airfoil characteristics (Equations (86) through (99)), have been established by utilizing a large number of available oscillatory airfoil test data sets. Furthermore, by illustrating the excellent correlation between the test and synthesized results, the generality of these empirical relationships to adequately represent the effects of variations in Mach number, sweep, and airfoil shape has been clearly demonstrated (References 12 and 17). This section describes the similar correlation results obtained under the present study, which relates mainly to the synthesization of the high subsonic Mach number data.

Test Data Used for Present Synthesis

The first step in the procedure for synthesis normally involves preparing a data set consisting of the loop data obtained for an airfoil at the same Mach number, Reynolds number, and sweep angle. Normally, a set of fifteen loops, consisting of both unstalled and stalled data, is found to be sufficient to establish the values of the empirical coefficients. The second step of the synthesis procedure consists of determining the empirical coefficients through least-squares fitting. The final step involves reconstructing the data from the empirical relations and comparing the synthesized data with test data.

Table I provides a list of all the data sets that were successfully synthesized under the present study. The data sets listed in Table I were acquired from two different sources (1) NASA CR-2915 (Reference 13) containing data sets 1 through 3, and (2) USAAVLABS TR-68-13B (Reference 14) containing data sets 4 through 7.

Each of the seven data sets represents a unique combination of test conditions. As a result, the values of the various empirical coefficients obtained are, in general, different for each of these data sets. Also, it should be noted that each of these data sets have, in general, a different static airfoil characteristic associated with them (steady state C_L, C_M, C_D variation with α).

TABLE I: TEST DATA SETS USED IN AIRFOIL UNSTEADY STALL SYNTHESIZATION

Data Set No.	Source Ref. No.	Airfoil Type	Mach No.	Reynolds No. $\times 10^{-6}$	Parameter Range of Test Data Used		
					k	α_o	$\bar{\alpha}$
1	13	NLR-1	0.5	6.3	0.07-0.22	0.0-12.5	2.5-7.5
2	13	NLR-1	0.6	9.1	0.06-0.18	0.0-12.5	2.5-7.5
3	13	NLR-1	0.7	10.1	0.05-0.16	0.0-12.5	2.5-7.5
4	14	V0012	0.4	4.8	0.0-0.31	5.0-15.0	2.5-7.5
5	14	V0012	0.6	6.2	0.0-0.25	5.0-10.0	2.5-7.5
6	14	V2301-158	0.4	4.8	0.0-0.25	5.0-15.0	2.5-7.5
7	14	V2301-158	0.6	6.2	0.0-0.25	5.0-10.0	2.5-7.5

Comparison of Synthesized Loop Data With Test Data

This subsection discussed the results obtained from the curve-fitting of Equations (86) and (94) to the test loop data corresponding to lift coefficient and pitching moment coefficient, respectively. As a typical case, consider all the lift coefficient loop data contained in data set number 3 (see Table I). When these loop data are curve fitted to Equation (86) in a least-squares sense, the values of unknown parameters P_1 through P_3 and Q_1 through Q_7 are obtained. When the values of the P_1 through P_3 and Q_1 through Q_7 parameters are inserted in Equations (86) the resulting time domain equation represents the two-dimensional unsteady lift coefficient of the NLR-1 airfoil at Mach number 0.7 for essentially all dynamic conditions.

To illustrate the accuracy of the resulting equation, a sample of the loop data for this case has been reconstructed from the equations and the comparisons of these synthesized C_{Lu} loops with test data are shown in Figure 10a. The differences between the test data and the synthesized are small and these differences are comparable to test data accuracy.

Similarly, when all the pitching moment coefficient loops contained in the data set number 3 in Table I are curve-fitted to Equation (94), the values of unknown parameters n_1 through n_7 are obtained. The comparison of the synthesized C_{Mu} loops with test data is shown in Figure 10b. Once again, the reconstructed loops match very well with the test data. The maximum negative C_{Mu} is generally predicted accurately for all the stalled loops.

Similar computations for the six other data sets contained in Table I have been successfully carried out. Figures 10a through 12b illustrate the good agreement obtained between the synthesized loop data and the test data corresponding to the highest Mach number data sets for each of the three airfoils. These figures correspond to the published data contained in References 13 and 14 as obtained in the Boeing two-dimensional, variable-density wind tunnel. It should be noted that Figures 10 through 12 present only lift and pitching moment loops because no drag data were included in these references.

68

DATA, ———— ———— COMPUTED

ALPHA, deg

C_{Lu}
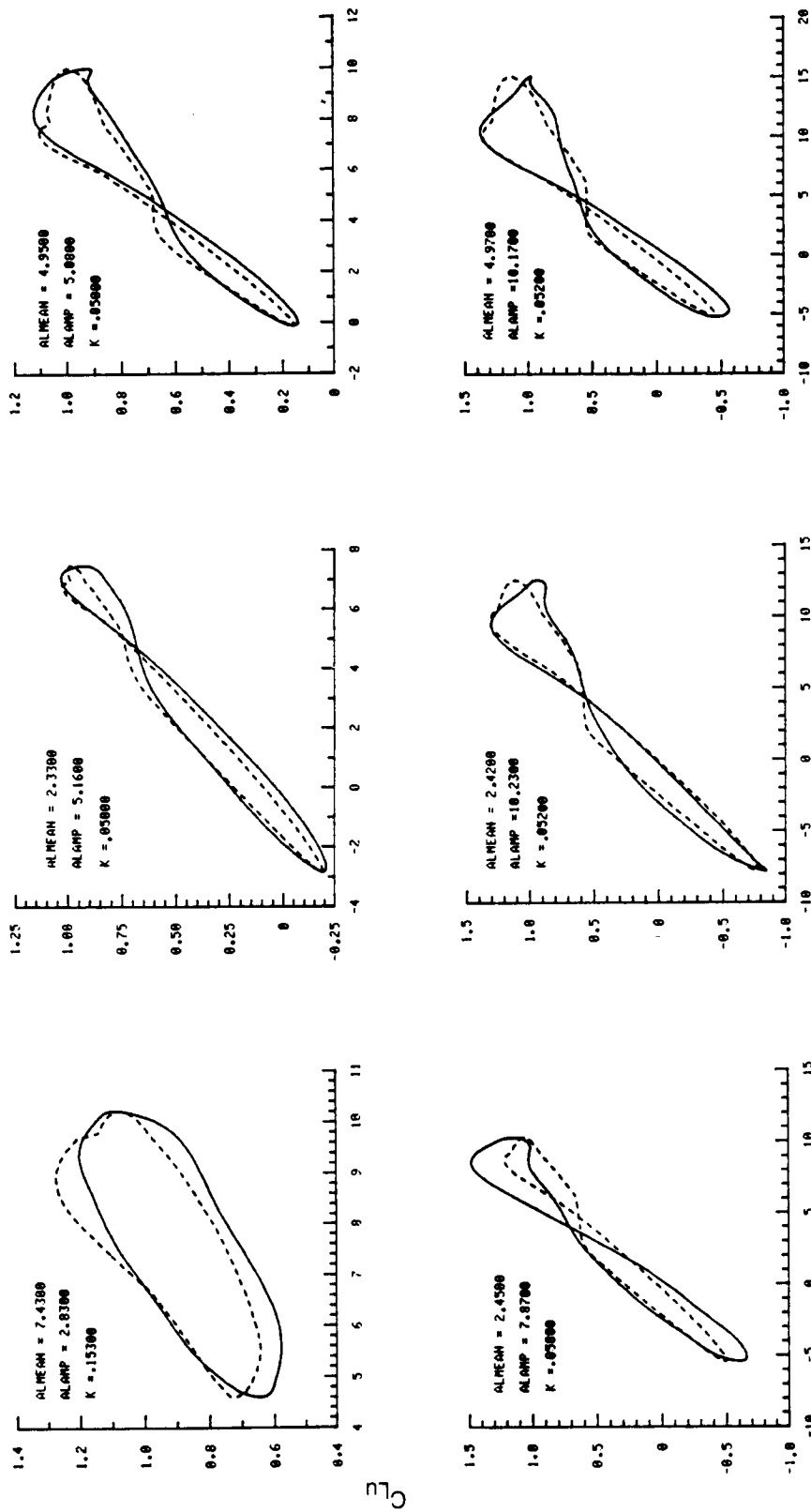
Figure 10a. Comparison of Synthesized Lift Coefficient Loops with Test Data, NLR-1 Airfoil,
M = 0.7, R_n = 10.0 × 10⁶ Data Set No. 3 in Table I

69
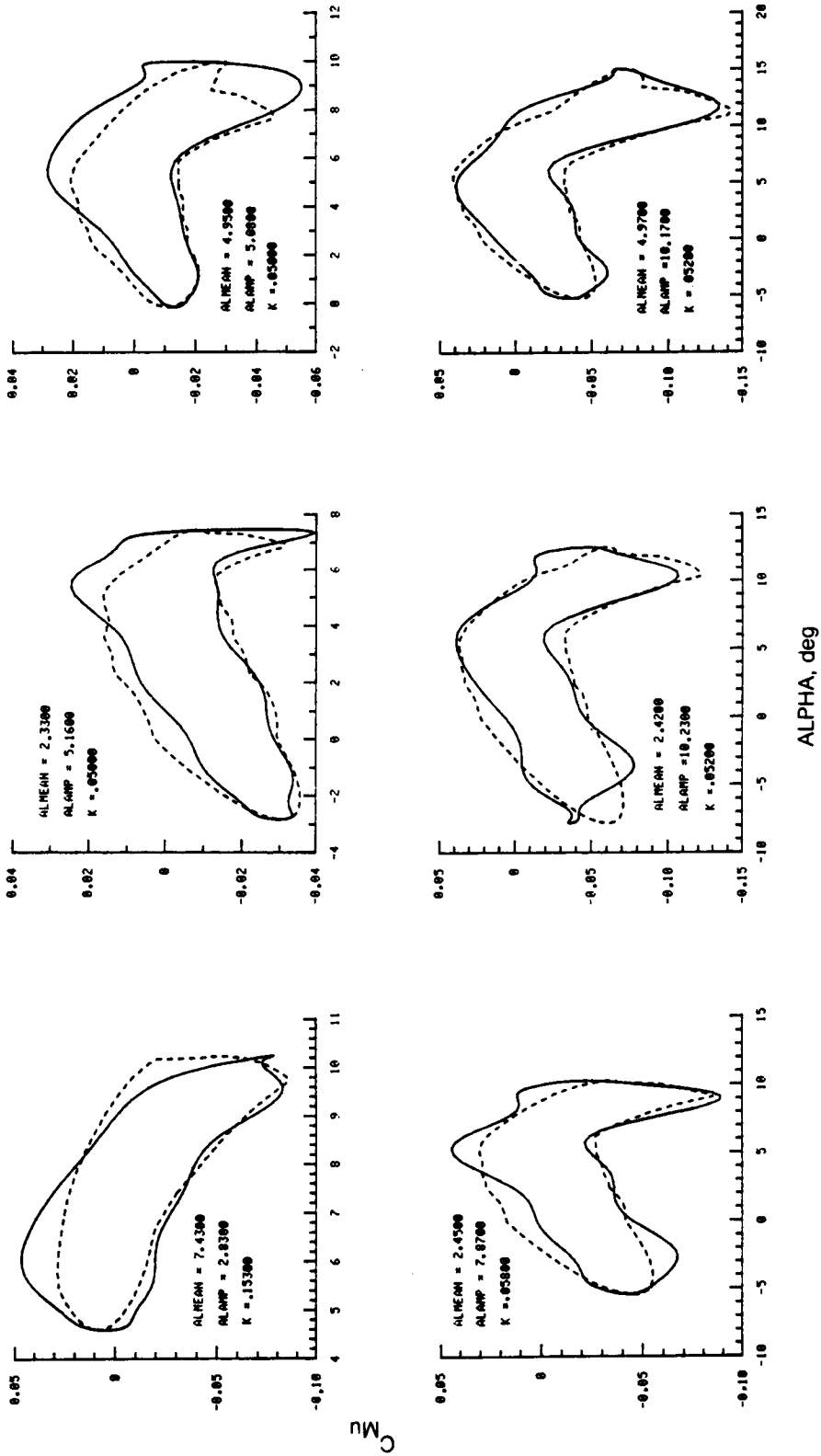
Figure 10b. Comparison of Synthesized Pitching Moment Coefficient Loops with Test Data, NLR-1 Airfoil, $M = 0.7$, $R_n = 1.0 \times 10^6$ Data Set No. 3 in Table I

70
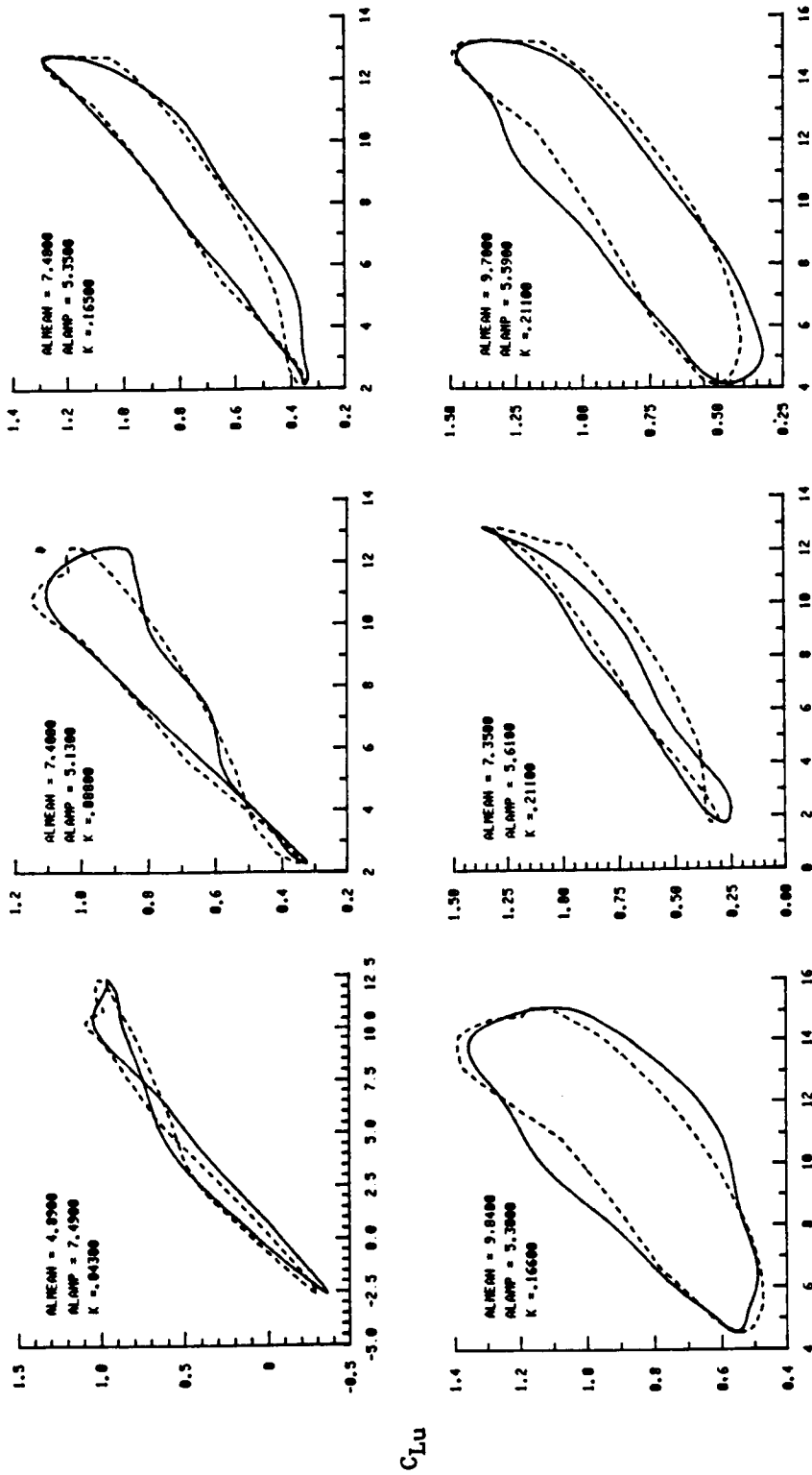
Figure 11a. Comparison of Sythesized Lift Coefficient Loops with Test Data Vertol Modified
NACA 0012 Airfoil, M = 0.60, R_n = 6.2 × 10^6 Data Set No. 5 in Table I

71
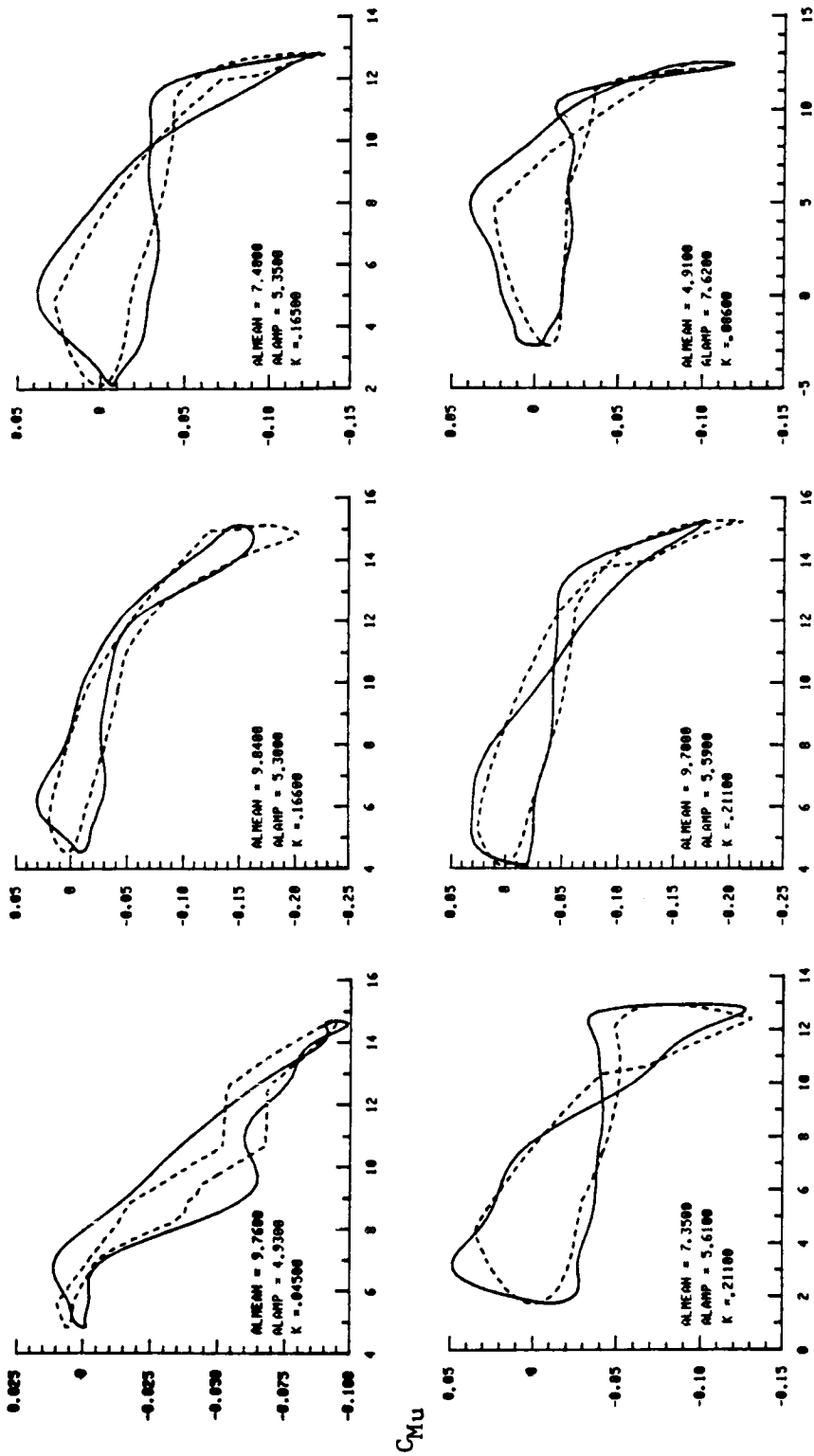
Figure 11b. Comparison of Synthesized Pitching Moment Coefficient Loops with Test Data Vertol
Modified NACA 0012 Airfoil, $M = 0.60$, $R_n = 6.2 \times 10^6$ Data Set No. 5 in Table I
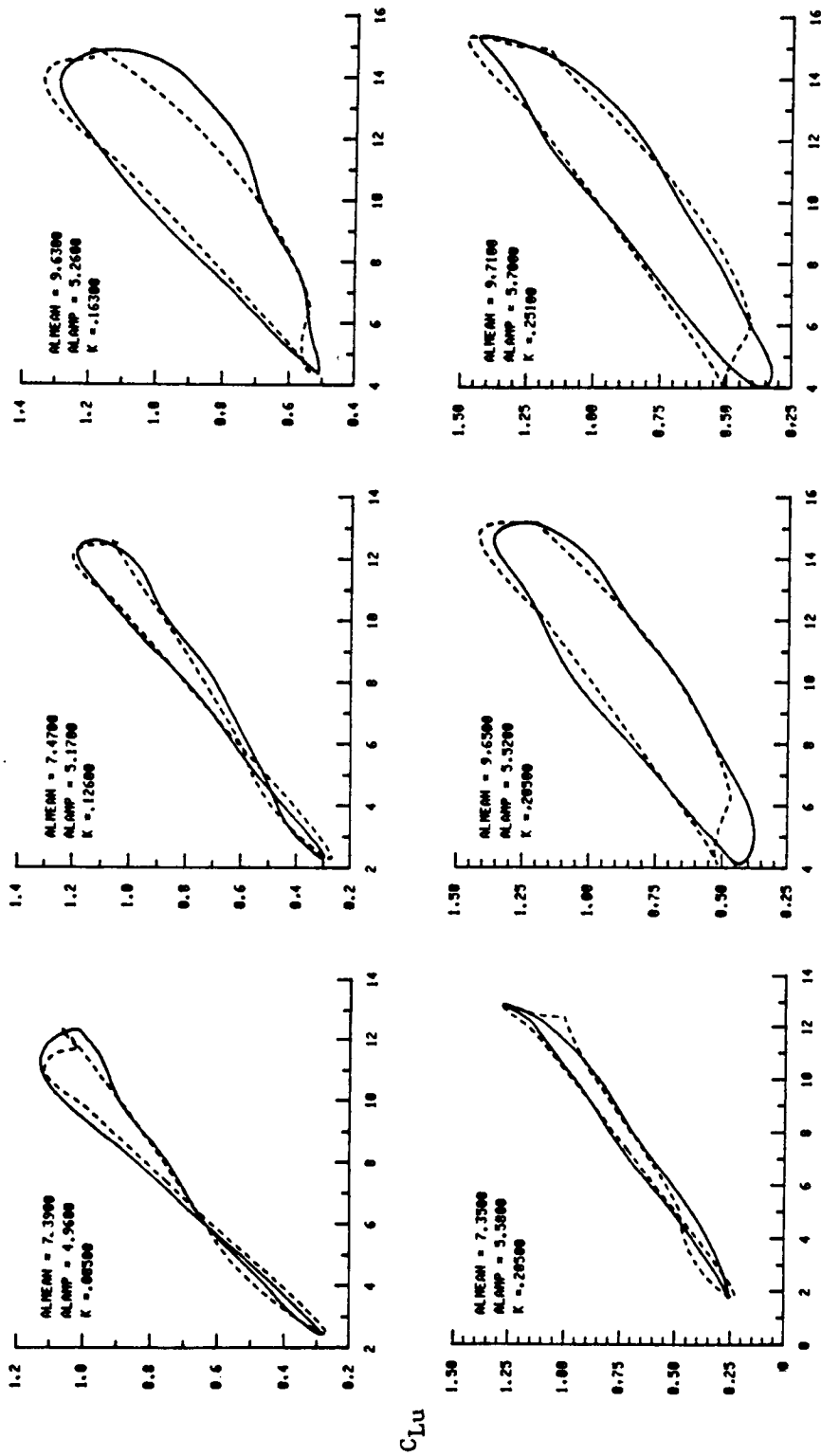
Figure 12a. Comparison of Synthesized Lift Coefficient Loops with Test Data V2301-1.58 Airfoil, $M = 0.60$, $R_n = 6.2 \times 10^6$ Data Set No. 7 in Table I
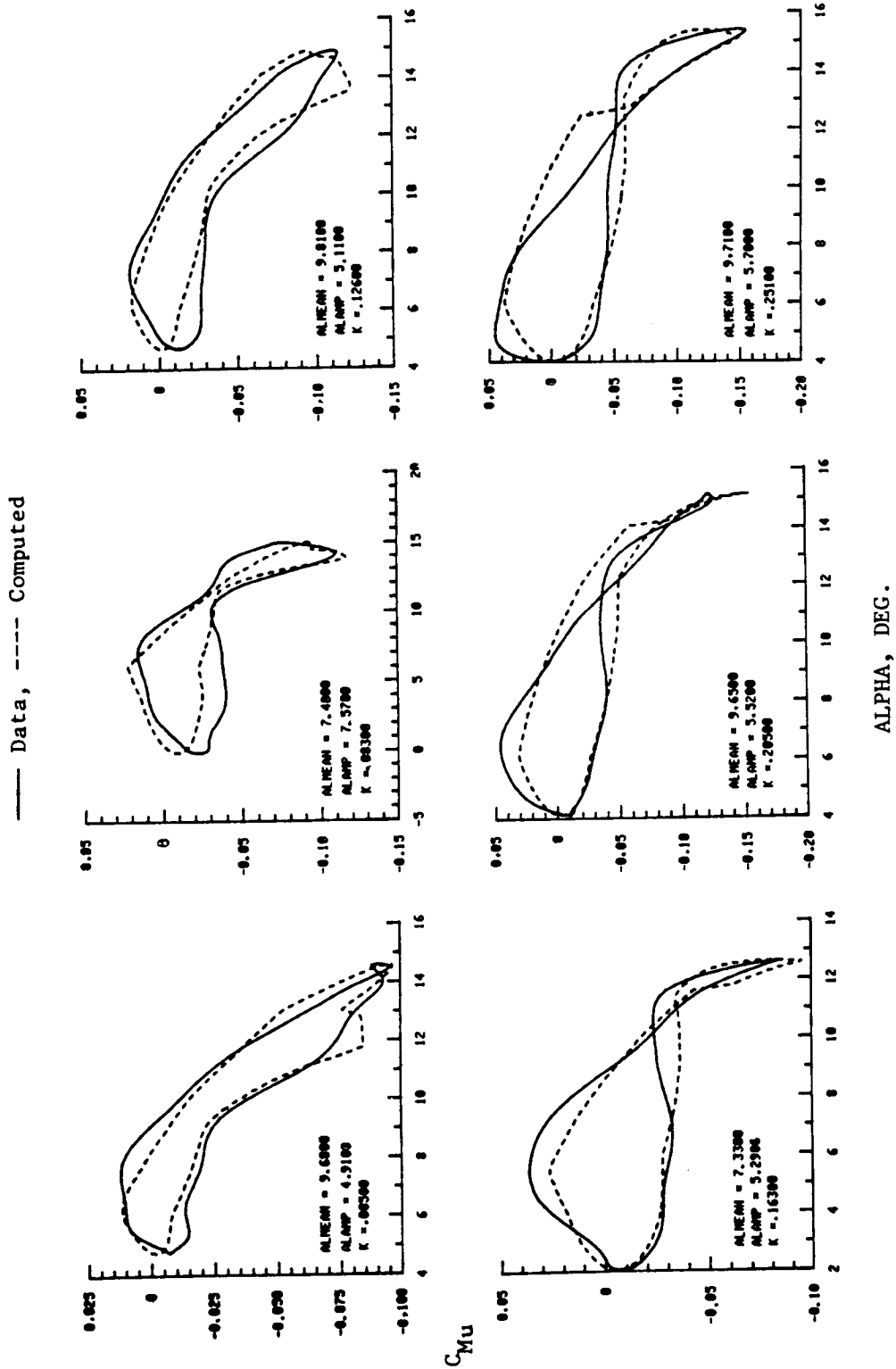
Figure 12b. Comparison of Sythesized Pitching Moment Coefficient Loops with Test Data
V2301-1.58 Airfoil, M = 0.60, $R_n = 6.2 \times 10^6$ Data Set No. 7 in Table I

UNSTEADY UNSTALLED SUBSONIC AERODYNAMICS

The use of quasi-static airloads in the aeroelastic analysis of advanced propeller systems (such as prop-fans) lends itself to simplicity and, hence, economy rather than accuracy. For an accurate quantitative aeroelastic analysis, unsteady aerodynamic forces become indispensible. This can be seen by noting the lift coefficient variations with reduced frequency shown in Fig. 13 for a two-dimensional airfoil at a subsonic Mach number typical of prop-fan operations. The reduced frequency range shown in Fig. 13, moreover, is typical of the vibration modes of real prop-fan blades. The aerodynamic force lag is substantial as implied by the imaginary part of the lift coefficient.

The majority of the available unsteady aerodynamic lift and moment information for airfoils comes from theory or experiment in the (real) frequency domain instead of in the time domain. This is mostly due to the simplicity in mathematics and experimental effort in working in the frequency domain. In order to perform time-history solutions for an aeroelastic problem, however, the frequency domain unsteady aerodynamic data must be properly transformed into the time domain. The frequency domain unsteady aerodynamic data are typically in tabulated or transcendental function form. As a result, it is difficult to perform a transformation which is both accurate and economical. In cases where only eigensolutions are required, there remains a fundamental problem of generalizing data available only in the frequency domain (constant amplitude oscillation) to the complex frequency or Laplace variable domain (decaying and growing oscillations).

In order to overcome the above mentioned difficulties, Pade' approximants have been introduced in the literature as an approximate but consistent way to bridge the gap between the (real) frequency domain usnteady aerodynamic data and the time domain description of the unsteady aerodynamic forces. See, for example, Reference 19. As opposed to the generally transcendental nature of the unsteady aerodynamic data, the Pade' approximants are defined in terms of rational functions that are known to have simple Laplace inversions or inverse Fourier transforms. Besides its mathematical advantage, the Pade' approximant also provides a quick method for interpolating and/or extrapolating the frequency domain data, which are usually limited to some discrete frequencies.

The sources of unsteady aerodynamic data for generating Pade' approximants can be theoretical and/or experimental in nature. If necessary, the data source can even be nonlinear as exemplified by the time domain transonic LTRAN2 code or its advanced versions (References 20 and 21). Such nonlinear sources can be used either in the frequency domain by explicitly making the
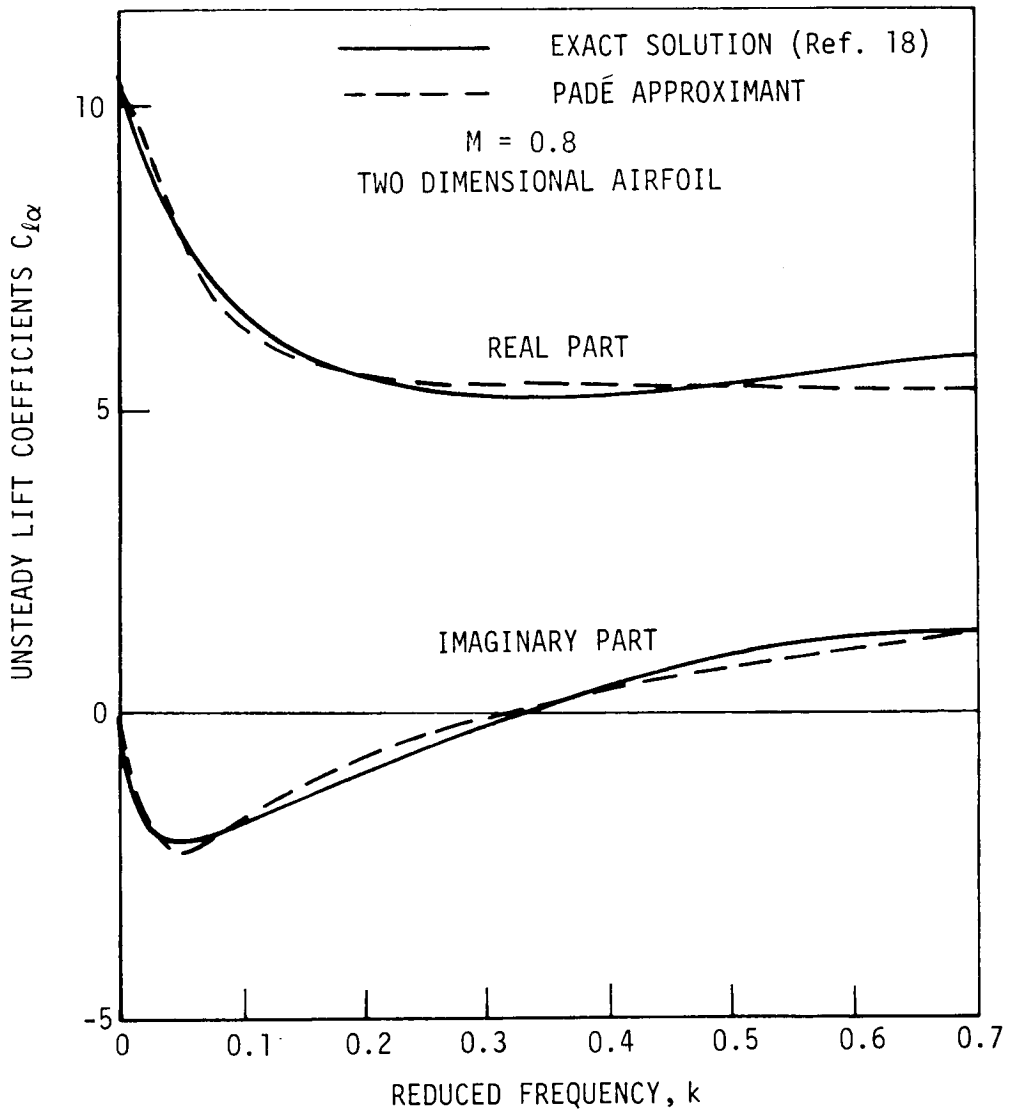
Figure 13. Example of Unsteady Aerodynamic Airfoil Characteristics and Associated Padé Approximation

airfoil motion sinusoidal (in which case only the first harmonic component of the total airfoil is extracted and used), or in the time domain itself using indicial responses. In the latter case, the Pade' form lends itself equally well to an exponential fitting procedure such as Prony's method given in Reference 22.

In the following subsections, the sources of unsteady aerodynamic data used in this study are first described and then the data synthesization procedures for rendering these data to Pade' forms are discussed. Then, in the subsequent subsections, the details of going from the Pade' forms to linear differential equations are described.

Sources of Unsteady Airloads

Either theoretical or experimental data can be used in Pade' approximations. In this report, both data source types were used. The theoretical linear unsteady aerodynamic data source selected is the work of Jordan (Reference 18) for two dimensional flow about an isolated flat plate airfoil. The experimental data source used is that of Davis and Malcolm (Reference 23) for the NACA 64A10 airfoil. The data were put in standard forms according to the following lift and (quarter chord) pitching moment coefficient definitions before synthesization.

$$C_{\ell_h} = \frac{L}{\frac{1}{2}\rho u^2 \bar{h}} \qquad (100a)$$

$$C_{\ell_\alpha} = \frac{L}{\frac{1}{2}\rho u^2 c \bar{\alpha}} \qquad (100b)$$

$$C_{m_h} = \frac{M}{\frac{1}{2}\rho u^2 c \bar{h}} \qquad (100c)$$

$$C_{m_\alpha} = \frac{M}{\frac{1}{2}\rho u^2 c^2 \bar{\alpha}} \qquad (100d)$$

Here $\bar{h}$ and $\bar{\alpha}$ are the airfoil plunging amplitude and the airfoil pitching amplitude, respectively. The pitching motion and the moment are defined throughout this section about the quarter chord. The total lift and moment coefficients are then given simply by the sums of the plunging and pitching results.

77

$$C_\ell = C_{\ell_h} \bar{h} + C_{\ell_\alpha} \bar{\alpha} \tag{101}$$

$$C_m = C_{m_h} \bar{h} + C_{m_\alpha} \bar{\alpha} \tag{102}$$

Synthesization of Data to Pade' Form

The Pade' approximant of any unsteady frequency domain aerodynamic coefficient C is defined as the ratio of two polynomials in complex frequency.

$$C(\omega) = \frac{\sum\limits_{j=1}^{N+1} a_j (i\omega)^j}{\sum\limits_{j=1}^{N} b_j (i\omega)^j} \tag{103}$$

where N is the order of the approximant. The degree of the denominator is lower than that of the numerator by one, because of the known asymptotic behavior at large frequencies.

Physical Constraints

The Pade' coefficients a_j and b_j in Eq. (103) are determined by imposing the following requirements:

(a) The zero frequency data must be satisfied exactly.

(b) The Pade' approximants should approach the piston theory results asymptotically for large frequencies.

(c) The available data (except for zero frequency) will be approximated by Eq. (103) in the least-square sense.

(d) The resultant poles must be stable.

Using basic concepts given in Reference 24, the lift and moment coefficients of plunging and pitching airfoils based on the piston theory can be written in the following form:

$$C = A + i \frac{\omega c}{U} B \tag{104}$$

78

where A and B are frequency independent. These constants (A, B) for both lift and moment coefficients of plunging and pitching airfoils are shown below.

Constants in Force and Moment Coefficients
From Piston Theory

Unsteady Coefficient	A	B
C_{ℓ_h}	0	$-\dfrac{4}{M}$
C_{m_h}	0	$\dfrac{4}{M}(\dfrac{1}{2} - \dfrac{x_s}{c})$
C_{ℓ_α}	$\dfrac{4}{M}$	$\dfrac{4}{M}(\dfrac{1}{2} - \dfrac{x_0}{c})$
C_{m_α}	$\dfrac{4}{M}(\dfrac{x_s}{c} - \dfrac{1}{2})$	$\dfrac{4}{M}(\dfrac{1}{2} - \dfrac{x_0}{c} + \dfrac{1}{2}\dfrac{x_s}{c} - \dfrac{1}{3} - \dfrac{x_s}{c}\dfrac{x_0}{c})$

Note: x_0 = pitching axis location measured from L.E.
x_s = point about which moment is taken
c = full chord

Synthesization Techniques - Least-Square Fit and Weighting Schemes

For simplicity, a two pole Padé approximant is sought, namely, N = 2.

$$C(\omega) = \frac{a(i\omega)^3 + b(i\omega)^2 + c(i\omega) + d}{(i\omega)^2 + e(i\omega) + f}$$

(105)

To satisfy the zero frequency and high frequency limits we have, for $x_s = x_0 = c/4$, the following constraints:

$$d = C(0) \cdot f$$

$$a = 1/\beta$$

where:

$$\beta = \begin{cases} -M/4 & \text{for } C_{\ell_h} \\ M & \text{for } C_{\ell_\alpha} \\ M & \text{for } C_{m_h} \\ -12M/7 & \text{for } C_{m_\alpha} \end{cases}$$

(106)

Therefore, we are left with four unknown constants: b, c, e and f. Let

$$C(\omega) = C_R(\omega) + i\, C_I(\omega)$$

and multiply out Eq. (105) to yield the following real equations.

$$\begin{bmatrix} \omega^2 & 0 & -\omega C_I & C_R - C(0) \\ 0 & \omega & \omega C_R & -C_I \end{bmatrix} \begin{Bmatrix} b \\ c \\ e \\ f \end{Bmatrix} = \begin{Bmatrix} \omega^2 C_R \\ \dfrac{\omega^3}{\beta} - \omega^2 C_I \end{Bmatrix} \tag{107}$$

Least Square Fit

The unsteady aerodynamic coefficient $C(\omega)$ is assumed to be known for n frequency values. Equation (107) in general cannot be satisfied for all frequencies when n > 2. In fact, we would have the following 2n equations for for unknowns:

$$\underset{2n\times4}{[A]} \quad \underset{4\times1}{\{x\}} \quad \underset{2n\times1}{\{B\}} \tag{108a}$$

where:

$$\{x\} = \begin{Bmatrix} b \\ c \\ e \\ f \end{Bmatrix} \tag{108b}$$

The least-square solution for $\{x\}$, however, can be found as the solution of the set of modified equations.

$$\underset{4\times4}{[E]} \quad \underset{4\times1}{\{x\}} = \underset{4\times1}{\{D\}} \tag{109}$$

where:

$$[E] = [A]^T[A] \quad ; \quad [D] = [A]^T[D]$$

Equation (109) is the final required form used to generate the Padé coefficients for both the Jordan theoretical data and the Davis and Malcolm

experimental data, as supplemented by the Jordan data for missing frequencies. It was initially found that the Pade approximants of some of the lift coefficients would not provide stable poles and almost all Pade approximants of the moment coefficients contained unstable poles.

Weighting Schemes

It was believed that the unstable poles might have been caused by the undue weighting to high frequency data in the least-square procedure defined by Eq. (109). This can be seen in the coefficients in Eq. (107). Therefore, several attempts to minimize this undue weighting for high frequencies were made by dividing the two real equations in Eq. (107) by several chosen functions of ω as follows:

Option	Divide 1st Equation by	Divide 2nd Equation by
1	ω^2	ω
2	$\omega^2 \ln \omega$	$\omega \ln \omega$
3	$\omega \ln \omega$	$\omega \ln \omega$
4	ω^2 only for $\omega > 1$	ω only for $\omega > 1$
5	ω^3 only for $\omega > 1$	ω^3 only for $\omega > 1$

As a result of these normalization processes, almost all lift coefficients and most moment coefficients resulted in stable Pade approximants. A further interpolation and extrapolation procedure applied to the poles rendered all Pade approximants stable as required.

Working Forms of Pade Approximants - Partial Fractions

The Pade approximant in Eq. (103) can be written in terms of its partial fractions. Then the total lift coefficient becomes, according to Eq. (101),

$$C_\ell = (A_1 + \frac{A_2 p}{p + \hat{p}_1} + \frac{A_3 p}{p - \hat{p}_2}) \phi + (B_1 p + B_2 + \frac{B_3 p}{p - p_1} + \frac{B_4 p}{p - p_2}) \theta \tag{110}$$

where we have formally replaced the Fourier transform variable $i\omega$ by the Laplace transform variable p. Meanwhile, the inflow angle, ϕ, replaced the plunging velocity variable, $p\bar{h}/c$, and the pitch angle, θ, has replaced old symbol $\bar{\alpha}$. A similar equation holds for the total moment coefficient with generally different constant coefficients and poles in Eq. (9). These coefficients and poles are summarized in Tables IIA through IID.

TABLE IIA – PADÉ APPROXIMANT COEFFICIENTS FOR C_{ℓ_h}

M	a	b	c	d	e	f	$\hat{p}_1$	$\hat{p}_2$	A_1	A_2	A_3
					Jordan (Analytic) Data – (Reference 18)						
0.5	-8.0	-9.17309	-4.52637	0.	2.24101	0.43854	-0.2166	-2.0244	10.3215	-7.4427	5.1212
0.6	-6.66667	-5.86491	-2.91928	0.	1.36726	0.23323	-0.1998	-1.1675	12.5166	-10.4162	4.5663
0.7	-5.71429	-3.02216	-1.58192	0.	0.61048	0.07964	-0.1880	-0.4215	19.8621	-27.6445	13.4967
0.8	-5.0	-1.56463	-0.64227	0.	0.18470	0.00590	-0.0410	-0.1437	108.9316	-139.257	35.3251
0.9	-4.44444	-1.81430	-0.43384	0.	0.16740	0.00066	-0.0041	-0.1633	654.7413	-660.139	9.8417
0.95	-4.21053	-1.81420	-0.44371	0.	0.15568	0.00052	-0.0034	-0.1522	848.629	-856.120	11.7012
1.0	-4.0	-1.61270	0.51616	0.	0.12008	0.00034	-0.0029	-0.1172	1544.945	-1559.80	18.8574
					Davis and Malcolm (Experimental) Data – (Reference 23)						
0.8	-5.0	-1.76515	-0.78794	0.	0.19934	0.00512	-0.0303	-0.1691	153.8842	-175.842	26.957

TABLE IIB – PADÉ APPROXIMANT COEFFICIENTS FOR C_{m_h}

M	a	b	c	d	e	f	$\hat{p}_1$	$\hat{p}_2$	A_1	A_2	A_3
Jordan (Analytic) Data – (Reference 18)											
0.5	2.0	0.20322	0.17254	0.	3.58216	0.84721	-0.2546	-3.3276	-0.2037	0.3201	-2.1164
0.6	1.66667	0.27208	0.17767	0.	2.57283	0.82064	-0.3731	-2.1998	-0.2165	0.4521	-1.9023
0.7	1.42857	0.30670	0.18181	0.	1.80190	0.67914	-0.5369	-1.2650	-0.2677	1.0971	-2.2579
0.8	1.25000	-0.01968	0.04394	0.	1.11650	0.03379	-0.03113	-1.0854	-1.3005	1.3945	-1.3440
0.9	1.11111	0.04779	0.04434	0.	0.78242	0.02060	-0.02728	-0.7551	-2.1523	2.2089	-1.1678
0.95	1.05263	0.20769	0.06517	0.	0.80674	0.01299	-0.01643	-0.7903	-5.0168	4.8773	-0.9132
1.0	1.0	0.59647	0.21073	0.	12.0596	0.03773	-.3214	-1.1738	-5.5845	5.2475	-0.6629
Davis and Malcolm (Experimental) Data – (Reference 23)											
0.8	1.25	-0.13373	0.11839	0.	1.03357	0.08606	-0.0913	-0.9422	-1.3757	1.8147	-1.6890

TABLE IIC – PADÉ APPROXIMANT COEFFICIENTS FOR C_{ℓ_α}

M	a	b	c	d	e	f	P_1	P_2	B_1	B_2	B_3	B_4
					Jordan (Analytic) Data – (Reference 18)							
0.5	2.0	4.93984	1.03056	0.01804	0.21186	0.00207	-0.0103	-0.2016	2.0	7.2552	-2.5224	-0.2167
0.6	1.66667	5.10108	0.85866	0.01256	0.17824	0.00160	-0.00948	-0.1688	1.6667	8.2203	-3.2332	-0.1832
0.7	1.42857	5.29252	0.93964	0.01019	0.15122	0.00116	-0.00809	-0.1431	1.4286	8.7984	-2.6838	-1.0381
0.8	1.25000	5.42277	1.09882	0.01061	0.11288	0.00101	-0.00983	-0.1030	1.2500	10.4720	-0.3592	-4.8311
0.9	1.11111	5.27422	1.21721	0.00523	0.06710	0.00036	-0.00593	-0.0612	1.1111	14.4140	5.5081	-14.7224
0.95	1.05263	4.97463	1.23764	0.00052	0.04753	0.00003	-0.00055	-0.0470	1.0526	20.1220	6.2419	-21.4393
1.0	1.00000	4.67600	1.25900	0.0006	0.02900	0.	0.	-0.029	1.0000	42.7002	0.	-38.0532
					Davis and Malcom (Experimental) Data – (Reference 23)							
0.8	1.25000	5.41924	0.58412	0.001901	0.04442	0.00018	-0.00455	-0.0399	1.2500	10.4720	4.0197	- 9.1279

84

TABLE IID - PADÉ APPROXIMANT COEFFICIENTS FOR C_{m_α}

M	a	b	c	d	e	f	P_1	P_2	B_1	B_2	B_3	B_4
					Jordan (Analytic) Data - (Reference 18)							
0.5	-1.16667	-8.24747	-0.05692	0.	8.32546	0.73019	-0.0886	-8.2368	-1.1667	0.	0.0816	1.3840
0.6	-0.97222	-3.61146	-0.05047	-.00003	3.19234	0.26615	-0.0857	-3.1067	-0.9722	0.	0.0835	-0.5912
0.7	-0.83333	-1.56527	0.05387	0.	1.10341	0.09247	-0.0914	-1.0120	-0.8333	0.	0.2063	-0.8520
0.8	-0.72917	-1.65144	0.36855	0.	0.77129	0.06816	-0.1018	-0.6694	-0.7292	0.	0.9322	-2.0212
0.9	-0.64814	-1.97492	-0.05222	0.00004	0.90858	0.08998	-0.1131	-0.7954	-0.6481	-0.0005	0.2393	-1.6248
0.95	-0.61404	-1.73235	-0.21757	0.00003	0.74256	0.06578	-0.1028	-0.6397	-0.6140	-0.1694	-.6837	-1.1907
1.0	-0.58333	-1.12312	-0.01994	-0.02222	0.16081	0.000148	-0.00093	-0.1599	-0.5833	-150.0000	150.7555	-1.7849
					Davis and Malcom (Experimental) Data - (Reference 23)							
0.8	-0.72917	-1.83388	0.23713	0.	0.95123	0.07001	-0.0904	-0.8708	-0.7292	0.	0.4805	-1.6208

85

Relation of Pade Approximation to Unsteady Decay Parameter

The introduction of the formalized Pade form to the description of unsteady airloads is but a generalization of an approximation to the Wagner function originally formulated by R. T. Jones (Reference 25). In the pre-ceeding section, the unsteady decay parameter, α_w, was defined using a generalized form of this approximation (see Eq. (68)). The resulting "effective" angle-of-attack, α_E, defined using this unsteady decay parameter, is a useful aerodynamic tool in its own right. It can be used independent of the unsteady stalled airloads theory to approximate low frequency un-stalled unsteady airloads. Although the effective angle-of-attack concept assumes that plunging motion can be treated as an equivalent pitch angle, Eq. (66) can still be used to formulate an airloads description similar to that given above in Eqs. (101) and (102):

$$C_\ell = \frac{\pi}{2} \left(\frac{c}{U}\right)\dot{\theta} + C_{\ell_{a_0}}\alpha_E \tag{111}$$

$$C_{m_{c/4}} = -\frac{\pi}{4} \left(\frac{c}{U}\right)\dot{\theta} + \left(C_{m_{a_0}}\right)_{c/4}\alpha_E \tag{112}$$

It can be shown that the Laplace transforms of Eqs. (111) and (112) together with that for the effective angle-of-attack, α_E, result in mathe-matical forms which are identical to Eq. (110). The various constants de-fining the Laplace transformed lift and moment equations, for the Generalized Wagner function (α_E) formulation are given in Table III.

Differential Equation Form

The starting points for formulating practical differential equations for the airloads are the Laplace transformed equations for lift and pitching moment, as typified by Eq. (110). The expressions for both the lift and moment coefficients may then be rewritten in the same abbreviated general form:

$$\Delta C = \left[A_1\phi + A_2x + A_3y + B_1p\theta + B_2\theta + B_3z + B_4w\right] \tag{113}$$

Table III. Padé Coefficients for Generalized Wagner Function

Symbol	C_{ℓ_h}	C_{m_h}
$\hat{P}_1$	$-0.02275\beta^2$	$-0.02275\beta^2$
$\hat{P}_2$	$-0.15\beta^2$	$-0.15\beta^2$
A_1	$C_{\ell_{\alpha_o}}$	$C_{m_{\alpha_o}}$
A_2	$-C_{\ell_{\alpha_o}}(0.165)$	$-C_{m_{\alpha_o}}(0.165)$
A_3	$-C_{\ell_{\alpha_o}}(0.335)$	$-C_{m_{\alpha_o}}(0.335)$
	C_{ℓ_α}	Cm_α
P_1	$-0.02275\beta^2$	$-0.02275\beta^2$
P_2	$-0.15\beta^2$	$-0.15\beta^2$
B_1	$C_{\ell_{\alpha_o}} + 0.5\pi$	$C_{m_{\alpha_o}} - 0.25\pi$
B_2	$C_{\ell_{\alpha_o}}$	$C_{m_{\alpha_o}}$
B_3	$-C_{\ell_{\alpha_o}}(.1648-.0075\beta^2)$	$-C_{m_{\alpha_o}}(.16483 - .0075\beta^2)$
B_4	$-C_{\ell_{\alpha_o}}(.33517 - .10055\beta^2)$	$-C_{m_{\alpha_o}}(.33517-.10055\beta^2)$

$$\beta = \sqrt{1 - M^2}$$

where Δc refers to a perturbational implementation of the Pade' theory, to be discussed in a later section, and where the augmented state variables appearing in Eq. (113) are given by:

$$x = \frac{p\phi}{p - \hat{p}_1} \tag{114}$$

$$y = \frac{p\phi}{p - \hat{p}_2} \tag{115}$$

$$z = \frac{p\theta}{p - p_1} \tag{116}$$

$$w = \frac{p\theta}{p - p_2} \tag{117}$$

The above constants and poles have unique values for lift and for moment as shown in Tables II and III.

For each coefficient, there are generally four Laplace transformed expressions to solve of the form presented in the above equations:

$$x = \frac{p\phi}{p - \hat{p}_1}$$

Since the Laplace operator is invertible, the associated differential equation becomes:

$$px - p\phi = \hat{p}_1 x \tag{118}$$

and then after nondimensionalizing the time differentials by aerodynamic time (chord/velocity) and rearranging:

$$\overset{*}{x} - \left[\frac{\bar{U}}{\bar{c}} \hat{p}_1 \right] x = \overset{*}{\phi} \tag{119a}$$

where $\bar{U}$ and $\bar{c}$ are the nondimensionalized velocity and chord, respectively. Similarly:

88

$$\overset{*}{y} - \left[\frac{\bar{U}}{c} \hat{P}_2 \right] y = \overset{*}{\phi} \tag{119b}$$

$$\overset{*}{z} - \left[\frac{\bar{U}}{c} P_1 \right] z = \overset{*}{\theta} \tag{119c}$$

$$\overset{*}{w} - \left[\frac{\bar{U}}{c} P_2 \right] w = \overset{*}{\theta} \tag{119d}$$

Solving these differential equations over a time step, $\Delta\psi$, gives the following formulas:

$$x_k = x_{k-1} \, e^{\hat{P}_1 \frac{\bar{U}}{c} \Delta\psi} + \frac{\overset{*}{\phi}}{\bar{U}\hat{P}_1/\bar{c}} \left[e^{\hat{P}_1 \frac{\bar{U}}{c} \Delta\psi} - 1 \right] \tag{120a}$$

$$y_k = y_{k-1} \, e^{\hat{P}_2 \frac{\bar{U}}{c} \Delta\psi} + \frac{\overset{*}{\phi}}{\bar{U}\hat{P}_2/\bar{c}} \left[e^{\hat{P}_2 \frac{\bar{U}}{c} \Delta\psi} - 1 \right] \tag{120b}$$

$$z_k = z_{k-1} \, e^{P_1 \frac{\bar{U}}{c} \Delta\psi} + \frac{\overset{*}{\theta}}{\bar{U}P_1/\bar{c}} \left[e^{P_1 \frac{\bar{U}}{c} \Delta\psi} - 1 \right] \tag{120c}$$

$$w_k = w_{k-1} \, e^{P_2 \frac{\bar{U}}{c} \Delta\psi} + \frac{\overset{*}{\theta}}{\bar{U}P_2/\bar{c}} \left[e^{P_2 \frac{\bar{U}}{c} \Delta\psi} - 1 \right] \tag{120d}$$

where (k-1) and (k) refer to successive time steps, where $\Delta\psi$ is the time increment, and where each expression is formulated for both lift and for moment.

Implementation Within the Time-History Solution

The Pade coefficients and poles, computed using the data synthesization techniques discussed above, were included in the G400PROP time-history solution. The Pade approximations of the Jordan (theoretical) and the Davis and Malcolm (experimental) aerodynamic data sets were tabulated for variations in Mach number from 0.5 to 0.95 for Jordan, and for a Mach number of 0.8 for Davis and Malcolm. A linear interpolation scheme was devised in order to obtain Pade values at intermediary Mach numbers.

89

Since the Padé theory is based upon classical small amplitude aerodynamic theory, a perturbational implementation appears warranted. To this end, an option was included to use either perturbational or total (perturbational plus static) pitch and inflow angles in the calculations of Δc_ℓ and Δc_m. The option to use the total angle description in place of the perturbational angle description was included to allow for lack of static airfoil data.

With the perturbational approach, the steady-state values of the pitch and inflow angles are estimated by eliminating the contributions to these angles due to elastic responses. This estimation is accomplished by eliminating the elastic torsion from the pitch angle and the explicit rate dependent terms from the tangential and perpendicular section velocities used to form the inflow angle. Thus, referring to Eqs. (54), (46) and (50) we have:

$$\theta_0 = \theta_N - \sum_{j=1}^{NTM} \tilde{\gamma}_{\theta_j} q_{\theta_j} \tag{121a}$$

$$\phi_0 = \tan^{-1} \left(\frac{U_P + V_{Z6}}{U_T - V_{Y6}} \right) \tag{121b}$$

Therefore the perturbational angles become:

$$\tilde{\theta} = \theta - \theta_0 \quad ; \quad \tilde{\phi} = \phi - \phi_0 \tag{122}$$

at each time step.

These essentially filtered values of $\tilde{\theta}$ and $\tilde{\phi}$ would then be used in computing the Padé Δc_ℓ and Δc_m coefficients, and the $\bar{\theta}$ and $\bar{\phi}$ values would be used to compute a steady-state c_{ℓ_0} and c_{m_0} (from the static airfoil tables). The static c_{ℓ_0} and c_{m_0} would be added to the Padé Δc_ℓ and Δc_m:

$$c_\ell = c_{\ell_0} + \Delta c_\ell \quad ; \quad c_m = c_{m_0} + \Delta c_m \tag{123}$$

The object of this filtering is to produce perturbational angles for use in the Padé calculations which calculate only the transient airloads. Therefore, the filtered option should produce lift and moment coefficients which, with time, approach those of the quasi-steady case. The above

approach therefore uses only perturbational angles-of-attack in computing the unsteady airloads together with estimated steady-state angles-of-attack in computing the steady airloads to determine the overall transient aero-elastic responses.

COUPLING WITH PROPELLER/NACELLE PERFORMANCE ANALYSIS (PANPER)

Overview and Interfacing Issues

PANPER is an analysis developed at UTRC for high speed propeller-nacelle aerodynamic performance prediction*. The program produces induced velocities, in cylindrical coordinates, for use in blade response programs such as G400PROP. PANPER assumes axisymmetric flow and single propeller operation, as opposed to coaxial, counter-rotation duel propeller operation. The induced velocity field provided by PANPER includes the flow distortion effects of the nacelle.

In usage, the G400PROP analysis must be run first, to obtain the various geometric and aerodynamic parameters required by the variable inflow analysis. Since PANPER assumes axisymmetry, these parameters must be the azimuthally averaged values evaluated at the last rotor revolution. A transformation must be made between the "5" coordinate system (preconed and prelead-lagged feathering axis) and the rectilinear coordinate system required by PANPER. Also, the airfoil data used in G400PROP must be modeled in polynomial format for use in PANPER.

Geometric and Aerodynamic Data Required for PANPER

Nondistributed Geometric and Aerodynamic Descriptors

The principal nondistributed parameters which must be conveyed from G400PROP to PANPER are as follows:

1. The number of blades.
2. The blade radius, R, feet.
3. The speed of sound, a_∞, feet/second.
4. The density of air, ρ, lb-sec^2/ft^4.
5. The forward flight speed, V_T, knots.
6. The propeller rotational speed, Ω, rpm.
7. The momentum induced velocity, v_{im}, defined positive in the upflow direction, feet/second.

---

*This program was developed under Contract NAS3-20961 and is to be documented in a two volume set entitled "An Analysis for High Speed Propeller-Nacelle Aerodynamic Performance Prediction".

Distributed Geometric Quantities

The PANPER routine requires distributions of the spanwise segment centers and boundary points at the quarter chord, and in its rectilinear coordinate system. It also requires distributions of the chord and pitch angle in the same coordinate system, referred to herein as the "4" system.

The following material draws upon the earlier sections relating to structural and aerodynamic sweep, and refers to the details shown in Fig. 14. As shown in this figure, the "4" coordinate system is defined by vectors taken locally at the intersection of the segment midchord with the segment boundary. L is the local radius of the midchord-boundary point P, measured from the hub; ξ is the angle which this radius makes with the pre-coned and prelead-lagged feathering axis. The distance measured from the swept G400PROP segment boundaries to the "4" system segment boundaries is referred to as η, where η varies along the chord from 0 at the midchord to η_{LE} at the leading edge and η_{TE} at the trailing edge.

First, the total "5" system deflections must be formed, based upon a combination of the elastic axis location and the elastic bending terms as described in Eqs. (27) and (28), and upon a transformation due to aerodynamic sweep of the arbitrary chordwise locations within the airfoil section. As presented in an above section (see Eq. (44)), the aerodynamic sweep transformation matrix can be defined as:

$$\left[\text{TAS}^{(A)}\right] = \begin{bmatrix} \chi^{(A)} & -\sin\Lambda_{e_5}^{(A)} & \sin\Lambda_{f_5}^{(A)} \\[2ex] \dfrac{\sin\Lambda_{e_5}^{(A)}}{\cos\Lambda_{f_5}^{(A)}} & \dfrac{\chi^{(A)}}{\cos\Lambda_{f_5}^{(A)}} & 0 \\[2ex] \dfrac{-\sin\Lambda_{f_5}^{(A)}\chi^{(A)}}{\cos\Lambda_{f_5}^{(A)}} & \dfrac{\sin\Lambda_{f_5}^{(A)}\sin\Lambda_{e_5}^{(A)}}{\cos\Lambda_{f_5}^{(A)}} & \cos\Lambda_{f_5}^{(A)} \end{bmatrix} \tag{124}$$

where:

$$\chi^{(A)} = \sqrt{1 - \sin^2\Lambda_{e_5}^{(A)} - \sin^2\Lambda_{f_5}^{(A)}} \tag{125}$$

and where the aerodynamic sweep angles are as defined by Eqs. (42) and (43). The arbitrary chordwise locations within the airfoil section are formed using straightforward trigonometric rotations. Using the leading edge of the airfoil section provides the following example:

93
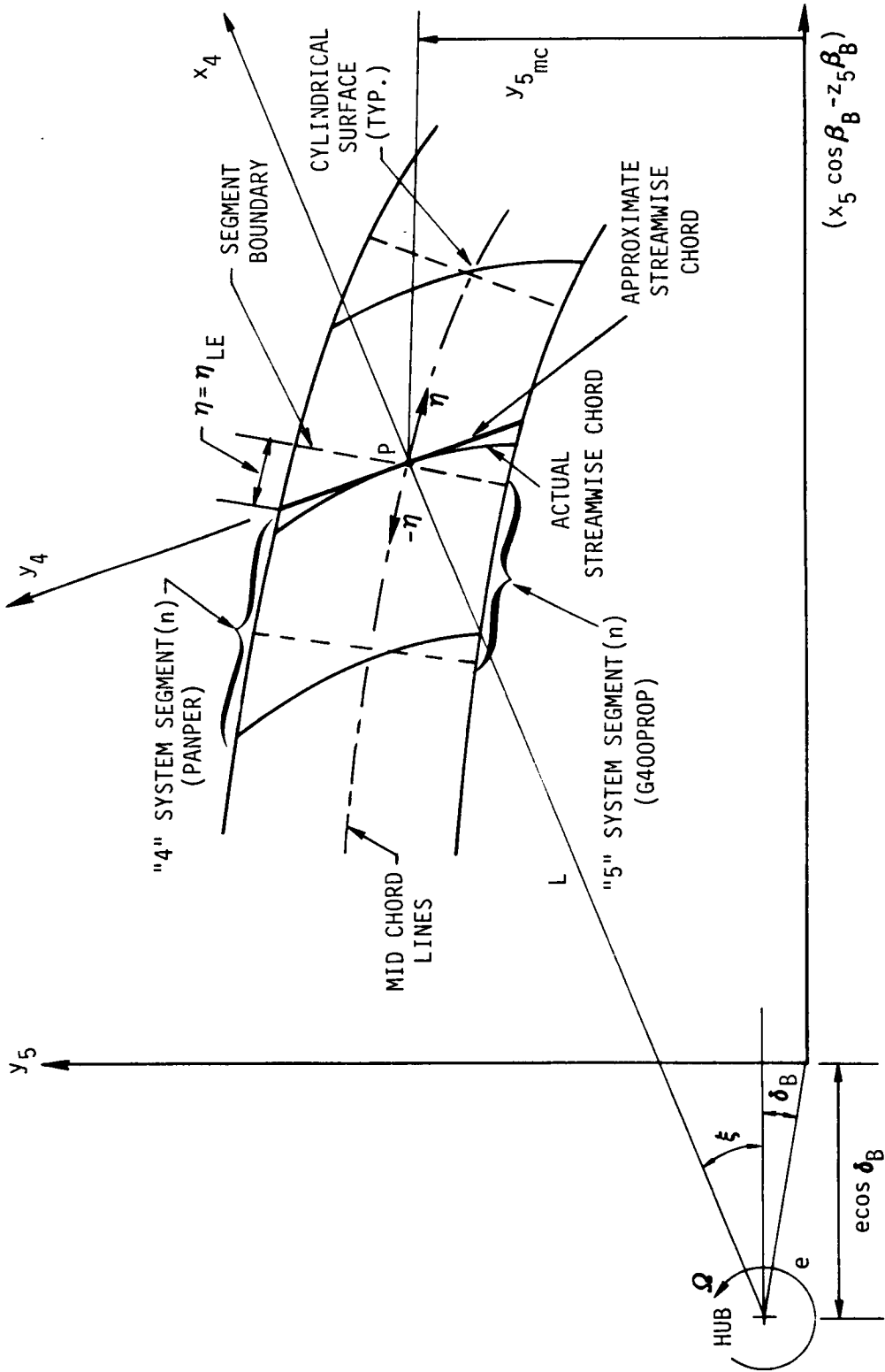
Figure 14. Schematics of the "4" and "5" Coordinate Systems Relating to G400PROP/PANPER Interfacing

$$\begin{Bmatrix} x_5 \\ y_5 \\ z_5 \end{Bmatrix}_{LE} = \begin{Bmatrix} x_5 \\ y_5 \\ z_5 \end{Bmatrix} + \left[TAS^{(A)^{-1}} \right] \begin{Bmatrix} 0 \\ y_{IO_{LE}} \cos \Theta \\ y_{IO_{LE}} \sin \Theta \end{Bmatrix} \qquad (126)$$

where:

$$y_{IO_{LE}} = y_{IO_{QC}} + c/4 \qquad (127)$$

and where $y_{IO_{QC}}$, the edgewise location of the section quarter chord point relative to the elastic axis, is input to the program. Similarly, the total "5" system displacements may be found at other chordwise locations within the airfoil section such as the midchord, the quarter chord, the trailing edge, etc.

Next, in the "5" system, the intersection of the section midchord with the section boundary must be obtained for use in determining the angle ξ and the distance L. The inboard boundary displacements are assumed zero. Direct interpolation is required to obtain the midchord boundary positions at arbitrary spanwise locations (n) along the span, and extrapolation must be used to obtain the outermost midchord boundary point.

$$z_{5_{MCB}}(n) = \frac{z_{5_{MC}}(n) \cdot \Delta x(n-1)}{\Delta x(n) + \Delta x(n-1)} + \frac{z_{5_{MC}}(n-1) \cdot \Delta x(n)}{\Delta x(n) + \Delta x(n-1)} \qquad (128)$$

$$z_{5_{MCB}}(N) = z_{5_{MC}}(N) + (z_{5_{MC}}(N) - z_{5_{MCB}}(N-1)) \qquad (129)$$

where MCB refers to the intersection of the segment midchord with the segment boundary, MC refers to the intersection of the segment midchord with the segment center, the parenthetical indices refer to the segment number, and (N) refers to the last spanwise segment.

Solving for the angle ξ and the distance L:

$$\xi = \tan^{-1} \left[\frac{y_{5_{MCB}}(n) - e\sin\delta_B}{e\cos\delta_B + x_{5_{MCB}}(n)\cos\beta_B - z_{5_{MCB}}(n)\beta_B} \right] \qquad (130)$$

$$L = \sqrt{(y_{5_{MCB}}(n) - e\sin\delta_B)^2 + (e\cos\delta_B + x_{5_{MCB}}(n)\cos\beta_B - z_{5_{MCB}}(n)\beta_B)^2} \qquad (131)$$

95

where Fig. 14 displays the various geometric quantities such as offset, e, prelead-lag, δ_B, precone, β_B, etc.

Once ξ and L have been defined, the "5" system segment boundary displacements may be found, by interpolation, at points along the chord other than the midchord ($\eta_{MC} = 0$). For example, the segment boundary points at the leading edge of the chord may be found based upon the segment midpoints at the leading edge of the chord as follows:

$$
\begin{Bmatrix} x_5 \\ y_5 \\ z_5 \end{Bmatrix}_{LEB_{(n)}} = \frac{(\eta_{LE} + \frac{\Delta x(n)}{2})}{\frac{1}{2}(\Delta x(n+1) + \Delta x(n))} \begin{Bmatrix} x_5 \\ y_5 \\ z_5 \end{Bmatrix}_{LE_{(n+1)}} - \frac{(\eta_{LE} - \frac{\Delta x(n+1)}{2})}{\frac{1}{2}(\Delta x(n+1) + \Delta x(n))} \begin{Bmatrix} x_5 \\ y_5 \\ z_5 \end{Bmatrix}_{LE_{(n)}} \quad (132)
$$

where LEB refers to the intersection of the segment leading edge with the segment boundary, LE refers to the intersection of the segment leading edge with the segment center, and n and n + 1 represent successive spanwise segments. The center leading edge displacements were calculated in Eq. (126). However, η_{LE} remains so far unknown, the solution for which needs the development which follows. (A similar procedure might be followed for any other chordwise position within the airfoil section.)

The coordinate transformation from the "5" system to the "4" system is given by:

$$
\begin{Bmatrix} x_4 \\ y_4 \\ z_4 \end{Bmatrix} = \begin{bmatrix} \cos\beta_B \cos\xi & \sin\xi & -\beta_B\cos\xi \\ -\cos\beta_B \sin\xi & \cos\xi & \beta_B\sin\xi \\ \beta_B & 0 & \cos\beta_B \end{bmatrix} \begin{Bmatrix} x_5 + e\cos\delta_B \\ y_5 - e\sin\delta_B \\ z_5 \end{Bmatrix} \quad (133)
$$

This transformation may be seen from Fig. 14 to be the product of a transformation from the "5" system to the hub coordinate system and a transformation from the hub system to the rectilinear "4" system.

The relationship $x_4 = L$, approximating the streamwise chord line through P, is given by the first row of Eq. (133). In general form:

$$
L = \begin{bmatrix} \cos\beta_B \cos\xi, & \sin\xi, & -\beta_B\cos\xi \end{bmatrix} \begin{Bmatrix} x_1 + \eta x_2 \end{Bmatrix} \quad (134)
$$

where:

$$X_1 = \frac{\frac{\Delta x(n)}{2}}{\frac{1}{2}(\Delta x(n+1)+\Delta x(n))} \begin{Bmatrix} x_5 + e\cos\delta_B \\ y_5 - e\sin\delta_B \\ z_5 \end{Bmatrix}_{(n+1)} + \frac{\frac{\Delta x(n+1)}{2}}{\frac{1}{2}\Delta x(n+1)+\Delta x(n)} \begin{Bmatrix} x_5 + e\cos\delta_B \\ y_5 - e\sin\delta_B \\ z_5 \end{Bmatrix}_{(n)}$$

(135b)

$$X_2 = \frac{2}{\Delta x(n+1)+\Delta x(n)} \begin{Bmatrix} x_5 + e\cos\delta_B \\ y_5 - e\sin\delta_B \\ z_5 \end{Bmatrix}_{(n+1)} - \frac{2}{\Delta x(n+1)+\Delta x(n)} \begin{Bmatrix} x_5 + e\cos\delta_B \\ y_5 - e\sin\delta_B \\ z_5 \end{Bmatrix}_{(n)}$$

Equation (134) represents a linear relationship in η from which, for example, the values for η_{LE} and η_{TE} may be determined. The interpolation procedure of Eq. (132) may then be completed. Having once determined the displacements of the segment boundary points in the "5" system, the boundary point values in the "4" system may be found using Eq. (133).

The intersection of the segment quarter chord with the segment center, in the "4" coordinate system, may be determined to be midway between the intersections of the segment quarter chord with the segment boundary points. Finally, the chord and pitch angles in the "4" system are defined as follows:

$$C_4 = \sqrt{(y_{4_{LEB}} - y_{4_{TEB}})^2 + (z_{4_{LEB}} - z_{4_{TEB}})^2}$$

(136)

$$\theta_4 = \tan^{-1}\left[\frac{z_{4_{LEB}} - z_{4_{TEB}}}{y_{4_{LEB}} - y_{4_{TEB}}}\right]$$

(137)

Distributed Aerodynamic Quantities

The PANPER routine requires that lift and drag coefficients from G400PROP be in polynomial (quadratic) form about the operating angle-of-attack. Thus:

$$C_\ell = C_{\ell_0} + C_{\ell_1}\alpha + C_{\ell_2}\alpha^2$$

(138a)

$$C_d = C_{d_0} + C_{d_1} \alpha + C_{d_2} \alpha^2 \tag{138b}$$

where α varies $\pm 2°$ about the operating condition, and where the coefficients are determined using a Lagrange interpolation approach (Reference 22). It can be shown that:

$$C_{\ell_0} = f(x_1) \left[\frac{x_2 x_3}{8} \right] - f(x_2) \left[\frac{x_1 x_3}{4} \right] + f(x_3) \left[\frac{x_1 x_2}{8} \right] \tag{139a}$$

$$C_{\ell_1} = f(x_1) \left[\frac{-(x_2 + x_3)}{8} \right] + f(x_2) \left[\frac{(x_1 + x_3)}{4} \right] + f(x_3) \left[\frac{-(x_1 + x_2)}{8} \right] \tag{139b}$$

$$C_{\ell_2} = \frac{f(x_1)}{8} - \frac{f(x_2)}{4} + \frac{f(x_3)}{8} \tag{139c}$$

where $f(x_1)$, $f(x_2)$, and $f(x_3)$ are the lift coefficients computed at $(\alpha - 2°)$, α, and $(\alpha + 2°)$, respectively. Similarly, a series form of the drag coefficient may be produced.

The above lift and drag coefficients, along with the geometric quantities and distributions computed earlier, are written into a file chosen by the user for communication between G400PROP and PANPER.

Assimilation of PANPER Generated Components of Variable Inflow

The PANPER routine uses the geometric and aerodynamic data provided by G400PROP to produce induced velocities, in cylindrical coordinates, due to the rotor, rotor wake, and nacelle. The radial induced velocity is defined positive from root to tip, the tangential velocity is defined positive opposite to the direction of rotation, and the axial velocity is defined positive in the normally thrusting direction.

To convert the induced velocities back from the rectilinear "4" coordinate system to G400PROP's "5" system, the inverse of the rotation matrix given in Eq. (133) may be applied. The new transformation matrix is defined as follows:

$$
\left[\text{TR}_{45} \right] = \begin{bmatrix} \cos\beta_B \cos\xi_{mc} & -\cos\beta_B \sin\xi_{mc} & \beta_B \\ \sin\xi_{mc} & \cos\xi_{mc} & 0 \\ -\beta_B \cos\xi_{mc} & \beta_B \sin\xi_{mc} & \cos\beta_B \end{bmatrix} \tag{140}
$$

where ξ_{MC} is defined in a similar manner to ξ, with the exception of its being taken at the midchord center rather than the midchord boundary. The above rotation varies with spanwise location, and is input to PANPER along with the geometric and aerodynamic distributions described above. PANPER uses this transformation to preconvert the calculated induced velocities to "5" system velocities at the G400PROP segment centers, before the data is transferred to G400PROP. These components of the variable inflow are then included in the airload calculations of both the eigensolution and the time-history solution.

EIGENSOLUTION

Review of Basic Methodology

All of the development presented in the previous sections has been
directed to the accurate modeling of the various aeroelastic elements of
rotary wings, and in particular, propellers. This modeling ultimately takes
the form of a collection of nonlinear differential equations of motion. The
two basic types of solution adopted by the G400 analyses for these differen-
tial equations are eigensolutions and time-history solutions.

Basic Solution Types

The purposes of these two solution types are different, yet complementary.
The purpose of the eigensolution is to calculate those inherent, general
characteristics relating to vibration susceptibility (natural frequency and
mode shape), and to stability (characteristic exponent and/or neutral
stability point). The eigensolution is essentially a solution for the so-
called "homogeneous" solution to the differential equations. The purpose of
the time-history solution, on the other hand, is to calculate the specific
responses due to either self-excitation (together with appropriate initial
conditions), or environmental influences (control inputs and/or airflow
distortions).

Of the two, the time-history solution is by far the easier in that all
nonlinearities can be easily retained and a compact, implicit form of the
equations can be used together with a variety of time-marching integration
algorithms. The time-history solution selected for the G400 analyses
(including G400PROP) is relatively simple and is well documented in
Reference 1. Nothing substantially new has been added to this type of
solution in the present study and further descriptions of time-history
solutions per se are, therefore, omitted.

General Characteristics of Eigensolution

The principal reason eigensolutions are relatively more difficult to
achieve is the requirement that the differential equations must be explicitly
linearized. Hence, all the compactness afforded by the implicit formulations
of nonlinearities available with time-history solutions must to a great extent
be abandoned. The great advantage bought with the increased complexity of
setting up an eigensolution, however, is the relatively low cost of solving
the eigensolution compared with time-history solutions.

Within the context of aeroelasticity, there are two basic types of
eigensolutions: frequency domain and (complex) Laplace variable domain. In

the first case, simple harmonic motion is assumed and an appropriate
eigenvalue is defined such that a stability boundary results for a realistic
value of the eigenvalue. The principal advantage of this type of eigen-
solution is that it can use a wide variety of available unsteady aerodynamic
theories and/or experimental data which, owing to simplicity, are defined in
the frequency domain. The principle disadvantage of this type of eigen-
solution is that it can predict neither actual stability levels nor
quantitative stabilizing (or destabilizing) trends. A further disadvantage
of this type of eigensolution is that it provides an aeroelastic description
of a structural member which cannot be easily integrated with transfer
function dynamic descriptions of other structural or control elements.

For the above reasons, the frequency domain eigensolution approach was
rejected in favor of the more general complex frequency (Laplace variable)
type. Thus, the basic form of eigensolution problem considered in the G400
analyses is represented by the following matrix equation:

$$[A]\left\{\overset{**}{Q}\right\} + [B]\left\{\overset{*}{Q}\right\} + [C]\left\{Q\right\} = \left\{0\right\} \tag{141}$$

where the homogeneous solution is given by:

$$\left\{Q\right\} = [\Phi][exp(\lambda\psi)]\left\{\bar{Q}\right\} \tag{142}$$

The mode shapes and complex frequencies are given, respectively, by the
columns of Φ and λ_i $(= \sigma_i \pm i\omega_i)$. The mode shapes are generally complex and,
like the eigenvalues, occur in complex pairs, when not strictly real.

Numerical Considerations

The general solution of Eq. (141) for Φ_i and λ_i, as defined in Eq. (142)
must account for the nonsymmetry of the A, B and C matrices comprising the
eigenvalue problem. Within the G400 analyses, Eq. (141) is solved using the
QZ algorithm method described in References 26 and 27 and available as part
of the EISPACK Matrix Eigensystem Subroutine Package (References 28 and 29).

101

Principal Assumptions

The additional eigensolution development undertaken in this study, to account for structural and aerodynamic sweep, was accomplsihed within the existing mathematical structuring already established for the G400 analyses, as reported in Reference 1. Within this context, the following principal assumptions were used to guide the additional formulations:

1. The elastomechanical modeling of the unswept blade, including linearization about an initially deflected position, is retained. This includes the mode deflection implementation of the ΔEI nonlinear torsion excitation as given by Eq. (30), but only with regard to the elastic curvatures due to modal deflection, v_e'' and w_e''.

2. Within the bending equations, the effects of elastomechanical coupling due to structural sweep can be formulated using the equivalent prebend principle.

3. Within the torsion equation, the couplings due to structural sweep are formulated using the force integration approach of Eq. (40). However, consistent with Assumption 2, the loadings required for Eq. (40) are evaluated using the approximations for small structural sweep.

4. The aerodynamic modeling formulated for large aerodynamic sweep in an above section is used, as formulated, with appropriate linearization.

5. The aerodynamic submatrices comprising Eq. (141) can be accurately (and more practically) evaluated using direct integrations of the various Galerkin weighted partial derivatives (in implicit compact form). This is contrary to the more usual approach of first evaluating numerous integration constants and then forming the matrices from these constants.

Prebend Equivalency Principle

The prebend equivalency principle is a technique whereby existing eigensolution terms formulated for zero elastic axis offset (structural sweep) can be used, with appropriate substitutions, to yield the new structural sweep related terms in the bending equations. The basis of the principle derives from the definitions for the deflection correction functions, Eqs. (4) and (5), discussed in an above section. These deflection correction functions are typically formed from integrations of nonlinear combinations of twist and bending deflection functions. Hence, the integrands of these integrals are of the general form:

$$\Delta w^{(1)} = \int_0^r f(x_1)\, dx_1 \qquad\qquad (143a)$$

where:

$$f(x_1) = \Theta'(x_1)\, v_e(x_1) = (\theta_B' + \theta_e')\, v_e \qquad\qquad (143b)$$

The prebend equivalency principle states that the effect of elastic axis offset is to augment the integrand as if it were an increment to the elastic axis displacement due to bending, but omitting the combination of built-in twist with built-in elastic axis offset:

$$f + \Delta f = \theta_B' v_e + \theta_e'(v_e + y_{IO_{EA}}) \qquad\qquad (144)$$

Perturbations to this equation then become:

$$\delta(f + \Delta f) = \theta_B' \delta v_e \underset{\text{\textcircled{I}}}{} + \theta_e' \delta v_e + v_e \delta\theta_e + y_{IO_{EA}} \delta\theta_e' \underset{\text{\textcircled{IV}}}{} \qquad\qquad (145)$$

The interpretations of these equations is twofold. Equation (144) indicates that for those (nonlinear) terms, which are proportional to finite deflection, analogous terms should arise with elastic axis offset substituted for initial bending deflection. Equation (145) indicates that for those linear terms involving built-in twist (term \textcircled{I}) analogous linear terms should arise involving built-in elastic axis offset (term \textcircled{IV}). Note that the second and third terms are nonliner and contribute nothing to the equivalency principle. Thus, this prinicple must be implemented by examination of both the linear and nonlinear terms appearing in the bending equations. As per the third principal assumption in this section, the effects in the torsion equation are treated in a different manner.

Nonlinear Source Terms

In the original eigensolution formulation summarized in Reference 1, various nonlinear elastomechanical terms emerged which are of the form: q_{v_k}, $(S_\eta \ \delta\eta)$ and q_{w_m}, $(S_\eta \ \delta\eta)$. The quantities q_{v_k}, and q_{w_m}, are the initial generalized (modal) deflections in edgewise bending and flatwise bending, respectively. The general quantities S_η and $\delta\eta$ refer to some appropriate integration constant, and to one of the perturbational response variables, δq_{w_j}, δq_{v_k}, δq_{θ_j} (and/or their time derivations), respectively. The prebend equivalency priinciple as outlined above states that built-in structural sweep, $y_{10_{EA}}$, and $z_{10_{EA}}$, should behave as initial modal bending deflections. Thus,

in the present context the previously derived elastomechanical terms involving q_{w_m} and q_{v_k}, can be used in this heuristic manner to formulate the first set of terms arising from built-in structural sweep (prebends).

Linear Source Terms

The perturbational results of Eq. (145) pertain to those linear elastomechanical terms which are of the form $S_\xi \delta\xi$ where S_ξ is some appropriate built-in twist (θ_B') related integration constant and $\delta\xi$ is a bending perturbational response $(\delta q_{v_k}, \delta q_{w_i},$ or derivatives). The prebend equivalency principle states that the linear terms involving elastic twist $(\delta\theta_e')$ perturbation in the presence of built-in elastic axis offset $(y_{10_{EA}}$ and $z_{10_{EA}})$ should behave the same way as the above $S_\xi d\xi$ terms. The detailed practical implementation of the prebend equivalency principle relating to the nonlinear and linear source terms is summarized in Table IV. Note that with any entered pair of equivalencies, both the functional and its first spanwise derivative are given, were appropriate.

Perturbational Airload Matrices

The perturbational airload matrices and submatrices required for the Eq. (141) eigensolution format are formulated using principal assumptions 4 and 5. The actual calculation of these matrices proceeds in various matrix multiplication steps representing the steps of a chain-rule differentiation procedure. One advantage of this approach is that it maximizes the accuracy in the linearization process because it is implicit, compact and, hence, reasonably tractable. The major steps in this chain-rule, matrix multiplication procedure are described in the following subsection.

Partial Derivative Matrix of Unsteady Airloads

The appropriate starting point for calculating the perturbational aerodynamic matrices is the collection of formulae defining the total load distributions, Eqs. (57) through (61) and (100). This subsection formulates the various partial derivative matrices leading to the partial derivative matrix of airloads with respect to the intermediary (aerodynamic) perturbation vector δZ. Specifically, the following partial derivative matrix is sought:

$$[DFDZ] = \begin{bmatrix} \partial\ p_{a_{z_{10}}}/\partial z_j \\ \hline \partial\ p_{a_{y_{10}}}/\partial z_j \\ \hline \partial\ q_{a_{x_\theta}}/\partial z_j \end{bmatrix} \qquad (146)$$

104

TABLE IV

SUBSTITUTIONS USED FOR IMPLEMENTING PREBEND EQUIVALENCY PRINCIPLE

Bending Functionals	Structural Sweep Substitution
Nonlinear Source Terms	
$\gamma_{w_m'}\, q_{w_m'}; \quad \gamma'_{w_m'}\, q_{w_m'}$	$z_{IO_{EA}}; \quad z'_{IO_{EA}}$
$\gamma'_{v_{k}'}\, q_{v_{k}'}; \quad \gamma'_{v_{k}'}\, q_{v_{k}'}$	$y_{IO_{EA}}; \quad y'_{IO_{EA}}$
$\Delta v_{e_{mj}'}\, q_{w_m'}; \quad \Delta v_{mj}^{(2)'}\, q_{w_m'}$	$\Delta v_{EA_j}; \quad \Delta v_{EA_j}^{(2)'}$
$\Delta w_{e_{kj}'}\, q_{v_k'}; \quad \Delta w_{e_{kj}}^{(2)'}\, q_{v_k'}$	$\Delta w_{EA_j}; \quad \Delta w_{EA_j}^{(2)'}$
$(u_{e_{F_{mm'}}}\, q_{w_m'}\, \delta \overset{*}{q}_{w_m} + u_{e_{E_{kk'}}}\, q_{v_k'}\, \delta \overset{*}{q}_{v_k})$	$(\Delta u_{EA_{F_m}}\, \delta \overset{*}{q}_{w_m} + \Delta u_{EA_{E_k}}\, \delta \overset{*}{q}_{v_k})$
Linear Source Terms	
$\Delta v_{B_m}\, \delta q_{w_m}; \quad \Delta v_{B_m}^{(2)'}\, \delta q_{w_m}$	$\Delta v_{EA_j}\, \delta q_{\theta_j}; \quad \Delta v_{EA_j}^{(2)'}\, \delta q_{\theta_j}$
$\Delta w_{B_k}\, \delta q_{v_k}; \quad \Delta w_{B_k}^{(2)'}\, \delta q_{v_k}$	$\Delta w_{EA_j}\, \delta q_{\theta_j}; \quad \Delta w_{EA_j}^{(2)'}\, \delta q_{\theta_j}$
$\Delta V_k\, \delta q_{v_k}; \quad \Delta V_k^{(2)'}\, \delta q_{v_k}$	$\Delta V_{EA_j}\, \delta q_{\theta_j}; \quad \Delta V_{EA_j}^{(2)'}\, \delta q_{\theta_j}$
$\Delta W_m\, \delta q_{w_m}; \quad \Delta W_m^{(2)'}\, \delta q_{w_m}$	$\Delta W_{EA_j}\, \delta q_{\theta_j}; \quad \Delta W_{EA_j}^{(2)'}\, \delta q_{\theta_j}$

where $P_{a_{y_{10}}}$ and $P_{a_{z_{10}}}$ are, respectively, the airload distributions in the edgewise and flatwise directions:

$$P_{a_{y_{10}}} = P_{a_{y_8}} \cos\Theta + P_{a_{z_8}} \sin\Theta + P_{a_{x_8}} (y'_{6e} \cos\Theta + z'_{6e} \sin\Theta - \Delta\Lambda) \qquad (147a)$$

$$P_{a_{z_{10}}} = -P_{a_{y_8}} \sin\Theta + P_{a_{z_8}} \cos\Theta + P_{a_{x_8}} (z'_{6e} \cos\Theta - y'_{6e} \sin\Theta) \qquad (147b)$$

and δz_j are the elements of the intermediary aerodynamic perturbation vector, $\delta\{Z\}$.

Perturbations of Basic Airloads

The first step in evaluating Eq. (146) is to form the partial derivatives of the "8" coordinate system force airloadings. Using Eq. (57) through (59) one obtains:

106

$$
\begin{Bmatrix} p_{a_{z_8}} \\[2pt] p_{a_{y_8}} \\[2pt] q_{a_{x_8}} \end{Bmatrix}_{\!\delta}
= \frac{\rho c\,\Delta x}{2 m_0}
\left[
\begin{array}{ccc}
-1 & 0 & 0 \\
0 & -1 & 0 \\
y_{loc/4}\cos\Theta & -y_{loc/4}\sin\Theta & c
\end{array}
\right]
\left[
\begin{array}{cccc}
U_N U_T & U_N U_P & U U_P & 0 \\
U_N U_P & -U_N U_T & -U U_T & 0 \\
0 & 0 & 0 & U_N^{2}
\end{array}
\right]
\overbrace{\begin{Bmatrix} c_\ell \\ c_{d_p} \\ c_{d_s} \\ c_m \end{Bmatrix}}^{}_{\!\delta}
$$

$$
+\;
\left[
\begin{array}{cccc}
(U_N c_{d_p} + U c_{d_s}) & U_N c_\ell & (U_T c_\ell + U_P c_{d_p}) & U_P c_{d_s} \\
U_N c_\ell & -(U_N c_{d_p} + U c_{d_s}) & (U_P c_\ell - U_T c_{d_p}) & U_T c_{d_s} \\
0 & 0 & (2 U_N c_m - \kappa\,\dot{\theta}_N^{*}) & 0
\end{array}
\right]
\overbrace{\begin{Bmatrix} U_P \\ U_T \\ U_N \\ U \end{Bmatrix}}^{}_{\!\delta}
$$

$$
+\;
\left[
\begin{array}{cc}
0 & 0 \\
0 & 0 \\
-\,y_{loc/4}\,(p_{a_{z_8}}\sin\Theta + p_{a_{y_8}}\cos\Theta) & -U_N \kappa
\end{array}
\right]
\overbrace{\begin{Bmatrix} \theta_N \\ \theta_N^{*} \end{Bmatrix}}^{}_{\!\delta}
\tag{148}
$$

Of the three contributions to the perturbational "8" coordinate system airloads shown in Eq. (148), only the first two perturbational vectors have to be further expanded to forms relating to components of the δZ vector.

Intermediary Aerodynamic Perturbation Vector

The elements of the intermediary perturbation vector fall into two main groupings: the first relating to blade kinematics, δZ_1, and the second relating to the Padé augmented state variables, δZ_2:

$$\{\delta Z\} = \left\{ \frac{\delta Z_1}{\delta Z_2} \right\} \begin{matrix} \} (12) \\ \} (40) \end{matrix} \qquad \qquad (149a)$$

The twelve (12) elements of Z_1 are respectively defined as:

$$\lfloor Z_1 \rfloor = \lfloor U_{P_5}, U_{T_5}, U_{R_5}, \overset{*}{y}_{6e}, \overset{*}{Z}_{6e}, y'_{6e}, Z'_{6e}, \theta_N, \overset{*}{\theta}_N, y_5, Z_5, U_e \rfloor \qquad (149b)$$

The (maximum of) forty (40) Padé augmented state variables derives from four Padé variables defined each for lift and moment (for a subtotal of eight) taken each with a spanwise shape distribution given by the first five (5) Legendre polynominals. Note that some elements of the Z_1 vector, as defined in Eq. (149) are constant or unused within the scope of the present study and therefore have zero perturbational values, effectively.

Perturbational Section Coefficients

The next step in evaluating the DFDZ matrix (Eq. (146)) is obtaining the partial derivatives of the airfoil section coefficients appearing in Eq. (148), with respect to the element of the intermediary perturbation vector. This in turn depends on the type of unsteady airloading selected and the assumptions made regarding each:

(Quasi-static):

$$\delta \begin{Bmatrix} c_\ell \\ c_{d_p} \\ c_{d_s} \\ c_m \end{Bmatrix} = \begin{Bmatrix} \partial c_\ell / \partial \alpha_N & \partial c_\ell / \partial M \\ \partial c_{d_p} / \partial \alpha_N & \partial c_{d_p} / \partial M \\ 0 & \partial c_{d_s} / \partial M \\ \partial c_m / \partial \alpha_N & \partial c_m / \partial M \end{Bmatrix} \delta \begin{Bmatrix} \alpha_N \\ M_N \end{Bmatrix} \tag{150}$$

(Padé Approximant):

From Eq. (113) the following perturbational form can be written:

$$\delta \begin{Bmatrix} c_\ell \\ c_{d_p} \\ c_{d_s} \\ c_m \end{Bmatrix} = \begin{bmatrix} \partial c_\ell / \partial \phi & \partial c_\ell / \partial \theta_N & 0 & \partial c / \partial \overset{*}{\theta}_N & \partial c_\ell / \partial Z_2 \\ 0 & 0 & 0 & 0 & 0 \\ 0 & 0 & 0 & 0 & 0 \\ \partial c_m / \partial \phi & \partial c_m / \partial \theta_N & 0 & \partial c_m / \partial \overset{*}{\theta}_N & \partial c_m / \partial Z_2 \end{bmatrix} \delta \begin{Bmatrix} \phi_N \\ \theta_N \\ M_N \\ \overset{*}{\theta}_N \\ Z_2 \end{Bmatrix} \tag{151}$$

where δZ_2 again represents the perturbations of the Padé augmented state variables, Eqs. (114) through (117). Note that in the case of the quasi-static airload option, $\delta \alpha_N$ is equal to the sum of $\delta \phi_N$ and $\delta \theta_N$. Both $\delta \phi_N$ and δM_N can be further chain-rule expanded using Eq. (50), (48) and (51):

$$\delta \phi_N = \frac{1}{U_N^2} (U_T \, \delta U_p - U_p \delta U_T) \tag{152}$$

$$\delta M_N = \frac{1}{U_{N_{a_\infty}}} (U_T \, \delta U_T + U_p \delta U_p) \tag{153}$$

Note also that in the case of quasi-static airloads, the $\delta \overset{*}{\theta}_N$ dependency appears in Equation (148) ($\kappa \neq 0$), whereas in the case of Padé approximate airloads, $\kappa = 0$ and the $\overset{*}{\theta}_N$ dependency appears instead in Eq. (151).

109

Perturbation Section Velocities

The last major step in evaluating Eq. (146) is to obtain expressions for the partial derivatives of the various perturbational section velocities appearing in the second contribution to Eq. (148). The appropriate relationship defining these velocities comes from the above section on aerodynamic sweep:

$$
\begin{Bmatrix} U_R \\ -U_T \\ U_P \end{Bmatrix} = \begin{bmatrix} TAS^{(A)} \end{bmatrix} \begin{Bmatrix} U_{R_S} \\ -U_{T_S} \\ U_{P_S} \end{Bmatrix} - \begin{Bmatrix} 0 \\ \overset{*}{y}_{6e} \\ \overset{*}{z}_{6e} \end{Bmatrix} \tag{154}
$$

Taking perturbations of this equation leads to the required perturbations in U_T and U_P. The remaining perturbations in U_N and U come from differentiations of Eqs. (48) and (41):

$$
\delta U_N = \frac{1}{U_N} \left[U_T \delta U_T + U_P \delta U_P \right] \tag{155}
$$

$$
\delta U = \frac{1}{U} \left[U_T \delta U_T + U_P \delta U_P + U_R \delta U_R \right] \tag{156}
$$

Perturbational Equations for Padé Augmented State Variables

Using Eq. (119) as a basis, perturbational forms of the differential equations for the (lift) Padé augmented state vectors can be written as:

$$
\delta \overset{*}{x} - (\frac{U}{c} \hat{p}_1) \delta x = \delta \overset{*}{\phi} \tag{157a}
$$

$$
\delta \overset{*}{y} - (\frac{U}{c} \hat{p}_2) \delta y = \delta \overset{*}{\phi} \tag{157b}
$$

$$
\delta \overset{*}{z} - (\frac{U}{c} p_1) \delta z = \delta \overset{*}{\theta}_N \tag{157c}
$$

$$
\delta \overset{*}{w} - (\frac{U}{c} p_2) \delta w = \delta \overset{*}{\theta}_N \tag{157d}
$$

110

These four differential equations, identical in form, for either the lift or moment perturbational augmented state variables strictly apply at only one spanwise station. For the (NSEG) spanwise stations, there would, for complete accuracy, have to be (8 x NSEG) differential equations (4 for lift and 4 for moment) to be solved simultaneously with the blade modal equations to complete the eigensolution formulation. For this most general case, it appears that a large eigenvalue problem would have to be solved. A practical method for keeping this problem tractable is discussed in the next subsection.

Reduction of Augmented State Variable Degrees-of-Freedom

The (8 x NSEG) degrees-of-freedom due to distinct augmented state variables at each spanwise station can be reduced by expanding the augmented state variables in terms of Legendre polynominals defined along span r. For example:

$$\delta x\,(r,\psi) = \sum_{j=1}^{N} P_{j-1}(r)\,\delta \bar{x}_j(\psi) \tag{158}$$

where the Legendre polynominals are defined as:

$$P_0(r) = 1 \qquad\qquad P_3(r) = 20r^3 - 30r^2 + 12r - 1$$

$$P_1(r) = 2r - 1 \qquad\qquad P_4(r) = 70r^4 - 140r^3 + 90r^2 - 20r + 1$$

$$P_2(r) = 6r^2 - 6r + 1$$

Substitution of Eq. (158) into the differential equation for δx, Eq. (157a) yields:

$$\delta \overset{*}{\bar{x}}_i - (2i-1) \sum_{j=1}^{N} \sigma_{ij}^{(x)}\,\delta \bar{x}_j = (2i-1)\delta f_i(\psi) \tag{159}$$

where:

$$\sigma_{ij}^{(x)} = \int_0^1 (\frac{U}{C})\hat{P}_i(r)P_{i-1}(r)P_{j-1}(r)dr \tag{160a}$$

$$\delta f_i(\psi) = \int_0^1 P_i(r)\,\delta \overset{*}{\phi}(r,\psi)dr \tag{160b}$$

Recalling the definitions for the inflow angle, ϕ:

$$\phi = \tan^{-1}(U_P / U_T)$$

and the normal flow velocity, U_N:

$$U_N^2 = U_P^2 + U_T^2$$

one can easily shown that Eq. (159) becomes:

$$
\delta \overset{*}{x}_i - (2i-1)\sum_{j=1}^{N} \sigma_{ij}^{(x)} \, \delta \overline{x}_j = (2i-1)\int_0^1 P_{i-1}\left[\frac{U_T}{U_N^2}\delta \overset{*}{U}_P - \frac{U_P}{U_N^2}\delta \overset{*}{U}_T \right.
$$

$$
+ \frac{1}{U_N^4}(\overset{*}{U}_T U_P^2 - \overset{*}{U}_T U_T^2 - 2\overset{*}{U}_P U_P U_T)\delta U_P \tag{161}
$$

$$
\left. + \frac{1}{U_N^4}(\overset{*}{U}_P U_P^2 - \overset{*}{U}_P U_T^2 + 2\overset{*}{U}_T U_P U_T)\delta U_T\right]dr
$$

Similarly, one can show the following:

$$
\delta \overset{*}{y}_i - (2i-1)\sum_{j=1}^{N} \sigma_{ij}^{(y)} \, \delta \overline{y}_j = \left[\text{same RHS as eq. 161}\right] \tag{162}
$$

where:

$$
\sigma_{ij}^{(y)} = \int_0^1 (\frac{\overline{U}}{C})\hat{p}_2(r)\, P_{i-1}(r)\, P_{j-1}(r)\,dr \tag{163}
$$

Substituting similar Legendre polynominal expansions into the δz and δw equations in Eqs. (157c) and (157d), and recalling the modal expansion of pitch angle perturbation:

$$
\delta \theta_N = \sum_{j}^{NTM} \overset{\wedge}{\gamma}_{\theta_j}\, \delta q_{\theta_j}
$$

one can easily show the following:

$$\delta \overset{\ast}{z}_i - (2i-1) \sum_{j=1}^{N} \sigma_{ij}^{(z)} \, \delta z_j = (2i-1) \sum_{j} \int_0^1 dr \, P_{i-1}(r) \, \hat{\gamma}_{\theta_j}(r) \, \delta \overset{\ast}{q}_{\theta_j} \qquad (164)$$

$$\delta \overset{\ast}{\bar{w}}_i - (2i-1) \sum_{j=1}^{N} \sigma_{ij}^{(w)} \, \delta \bar{w}_j = \left[\text{same RHS as eq. 164} \right] \qquad (165)$$

where:

$$\sigma_{ij}(z) = \int_0^1 (\frac{U}{C}) p_i(r) \, P_{i-1}(r) \, P_{j-1}(r) dr \qquad (166a)$$

$$\sigma_{ij}^{(w)} = \int_0^1 (\frac{U}{C}) p_2(r) \, P_{i-1}(r) \, P_{j-1}(r) dr \qquad (166b)$$

The smaller set of first order differential equations, Eq. (161), (162), (164) and (165), for optional choice of N in the Legendre polynominal expansion, Eq. (158) can be used to replace the larger the set of differential equations defined by Eq. (157).

Decomposition of Intermediary Perturbation Vector

All of the above development has been directed to the evaluation of Eq. (146) and to the formulation of the Padé augmented state variable equations, both of which are defined in terms of the indermediary perturbation vector, $\delta\{Z\}$. However, the ultimate eigenproblem formulation must be in terms of perturbations of the blade generalized (modal) coordinates (δq_{w_j}, δq_{v_k} and δq_{θ_j}) and the Padé augmented state variables, δZ_2. The method for

113

eliminating the $\delta\{Z\}$ vector and introducing in its place these generalized coordinates is an appropriate second major chain rule, matrix multiplication:

$$\delta\{Z\} = [T_1]\{\delta\overset{*}{Q}_B\} + [T_2]\{\delta Q_B\} + [T_3]\{\delta Q_P\}$$ (167)

where the blade coordinates are given by:

$$\lfloor\delta Q_B\rfloor \equiv \delta\lfloor q_{W_I} \cdots q_{W_{NFM}} \cdots q_{V_I} \cdots q_{V_{NEM}} \cdots q_{\theta_I} \cdots q_{\theta_{NTM}}\rfloor$$ (168a)

and where the weighted Padé augmented variables are given by:

$$\lfloor\delta Q_P\rfloor = \delta\lfloor \bar{x}_j^L, \bar{y}_j^L, \bar{z}_j^L, \bar{w}_j^L, \bar{x}_j^M, \bar{y}_j^M, \bar{z}_j^M, \bar{w}_j^M\rfloor$$ (168b)

The details of the T_1, T_2 and T_3 partial derivative matrices are obtained using the formulation given in the above section on structural twist and sweep, and the above subsection relating to the perturbational forms for the Padé augmented stall variables. While these formulations involve straight-forward partial differentiation, they are quite tedious and presentation of the details herein would contribute little to the clarity or usefulness of this report.

General Application of the Galerkin Method

The remaining formulations required to define the final matrix operations for calculating the required aerodynamic matrices are the approriate Galerkin weighted integrations. Define the generalized (modal) excitation vector commensurate with the vector of generalized coordinates:

$$\delta\{\Xi_B\} = \int_0^1 [\Gamma_B]\delta\begin{Bmatrix} p_{a_{z_{10}}} \\ p_{a_{y_{10}}} \\ q_{a_{x_B}} \end{Bmatrix} dr$$ (169)

where, by Eqs. (146) and (167):

114

$$\delta \begin{Bmatrix} P_{a_{z_{10}}} \\ P_{a_{y_{10}}} \\ q_{a_{x_{10}}} \end{Bmatrix} = \begin{bmatrix} DFDZ \end{bmatrix} \left\{ \begin{bmatrix} T_1 \end{bmatrix} \{\delta \overset{*}{Q}_B\} + \begin{bmatrix} T_2 \end{bmatrix} \{\delta Q_B\} + \begin{bmatrix} T_3 \end{bmatrix} \{\delta Z_2\} \right\} \qquad (170)$$

and where the Galerkin weighting matrix is given by:

$$\begin{bmatrix} \Gamma_B \end{bmatrix} \equiv \begin{bmatrix} (\gamma w_i - \Delta w_i) & \Delta v_i & 0 \\ -\Delta w_k & (\gamma v_k - \Delta v_k) & 0 \\ \Gamma_{z_{\theta_j}} & \Gamma_{y_{\theta_j}} & \hat{\gamma}_{\theta_j} \end{bmatrix} \qquad (171)$$

Finally, the three required perturbational airload matrices can be written as:

$$\begin{bmatrix} BAII \end{bmatrix} = -\int_0^1 \begin{bmatrix} \Gamma_B \end{bmatrix} \begin{bmatrix} DFDZ \end{bmatrix} \begin{bmatrix} T_1 \end{bmatrix} dr \qquad (172)$$

$$\begin{bmatrix} CAII \end{bmatrix} = -\int_0^1 \begin{bmatrix} \Gamma_B \end{bmatrix} \begin{bmatrix} DFDZ \end{bmatrix} \begin{bmatrix} T_2 \end{bmatrix} dr \qquad (173)$$

$$\begin{bmatrix} CAI2 \end{bmatrix} = -\int_0^1 \begin{bmatrix} \Gamma_B \end{bmatrix} \begin{bmatrix} DFDZ \end{bmatrix} \begin{bmatrix} T_3 \end{bmatrix} dr \qquad (174)$$

For completeness, the following additional matrices appropriate to the Padé airloads modeling can be defined:

$$\begin{bmatrix} AA2I \end{bmatrix} = \begin{bmatrix} \partial f / \partial \overset{**}{Q}_B \end{bmatrix} \qquad (175)$$

$$\begin{bmatrix} BA2I \end{bmatrix} = \begin{bmatrix} \partial f / \partial \overset{*}{Q}_B \end{bmatrix} \qquad (176)$$

$$\begin{bmatrix} CA22 \end{bmatrix} = \begin{bmatrix} -\sigma \end{bmatrix} \qquad (177)$$

where the f and σ vectors are ensembles of similar constants defined as by Eqs. (160), (163), (164) and (166).

Structuring Techniques for Semi-Canonical Form

The purpose of this subsection is to integrate the definitions for the various components submatrices given above into the semi-canonical form required by the EISPACK matrix eigensolution algorithms. Specifically, the general form of the perturbational equations of motion, Eq. (141), can be written in its most detailed form:

$$
\begin{bmatrix} A11 & \vline & 0 \\ \hline A12 & \vline & 0 \end{bmatrix} \delta \begin{Bmatrix} \overset{**}{Q}_B \\ \overset{**}{Q}_P \end{Bmatrix} + \begin{bmatrix} B11 + BA11 & \vline & 0 \\ \hline BA21 & \vline & I \end{bmatrix} \delta \begin{Bmatrix} \overset{*}{Q}_B \\ \overset{*}{Q}_P \end{Bmatrix}
$$

$$
+ \begin{bmatrix} C11 + CA11 & \vline & CA12 \\ \hline 0 & \vline & CA22 \end{bmatrix} \delta \begin{Bmatrix} Q_B \\ Q_P \end{Bmatrix} = \begin{Bmatrix} 0 \end{Bmatrix} \tag{178}
$$

· The elastomechanic submatrices, A11, B11 and C11 are obtained from Reference 1 and as outlined above regarding the prebend equivalency principle. The remaining aerodynamic matrices, BA11, CA11, CA12, AA21, BA21, CA22 are given by Eqs. (172) through (177).

The three semi-canonical forms which are now required are those for the vacuum, nonvacuum- quasi-static, and nonvacuum-Padé airload optional calculations.

Vacuum Case

For this case, all aerodynamic matrices are deleted and the resulting semi-canonical form becomes:

$$
\left[\begin{bmatrix} A11 & \vline & B11 \\ \hline 0 & \vline & I \end{bmatrix} \lambda - \begin{bmatrix} 0 & \vline & -C11 \\ \hline I & \vline & 0 \end{bmatrix} \right] \begin{Bmatrix} \lambda \bar{Q}_B \\ \bar{Q}_B \end{Bmatrix} \tag{179}
$$

Nonvacuum, Quasi-Static Airloads Case

For this case, only the principal upper left-hand corner aerodynamic submatrices are retained and the semi-canonical form becomes:

$$
\left[\begin{bmatrix} A11 & \vline & B11 + BA11 \\ \hline 0 & \vline & I \end{bmatrix} \lambda - \begin{bmatrix} 0 & \vline & -C11 - CA11 \\ \hline I & \vline & 0 \end{bmatrix} \right] \begin{Bmatrix} \lambda \bar{Q}_B \\ \bar{Q}_B \end{Bmatrix} \tag{180}
$$

116

Nonvacuum, Padé Approximant Airloads Case

For this most general case, the semi-canonical form becomes:

$$\left[\begin{bmatrix} A11 & B11+BA11 & 0 \\ \hline 0 & I & 0 \\ \hline AA21 & BA21 & I \end{bmatrix} \lambda - \begin{bmatrix} 0 & -C11-CA11 & -CA12 \\ \hline I & 0 & 0 \\ \hline 0 & 0 & CA22 \end{bmatrix}\right] \delta \left\{\begin{matrix} \lambda\bar{Q}_B \\ \bar{Q}_B \\ \bar{Q}_P \end{matrix}\right\} \qquad (181)$$

Note that the maximum dimension of $\bar{Q}_B$ is 10 and that of $\bar{Q}_P$ is 40; thus, the total maximum size of the matrix eigenproblem defined by Eq. (181) is 60 x 60.

117

SAMPLE CALCULATIONS MADE USING G400PROP

The SR-2 Model prop-fan blade was chosen to provide a realistic physical data base for the purpose of demonstrating the capabilities of the G400PROP analysis. This selection was made for two reasons: First, since the SR-2 blade is unswept, complete beam data exists for this prop-fan configuration (in contrast to other, swept prop-fan configurations for which accurate equivalent beam data do not yet exist). Second, results from NASA conducted stall flutter tests of this blade exist and were readily accessible. The appropriate SR-2 blade beam data were assembled and input to the G400PROP analysis, first to determine blade natural frequencies (E159 preprocessor) and then to evaluate coupled mode characteristics and aeroelastic stability. The following subsections describe in turn the blade configuration and selected operating conditions, the uncoupled modal frequency calculations, blade coupled frequencies and mode shapes as calculated by the eigensolution (both without and with sweep), and finally correlation results comparing experimental stall flutter characteristics with the G400PROP predictions.

Description of Selected Blade Configuration
and Operating Conditions

The SR-2 prop-fan propeller model is of solid steel construction, has a .6223 meter diameter, and is configured with eight "shovel tipped" blades (no sweep). The planform of this model design is shown in Figure 15, and a summary of the pertinent geometric and other measured parameters is given in Table V. Also included in this table are the various dynamic parameters which were either calculated or estimated. The blade uncoupled modal frequencies listed were obtained using the E159 preprocessor portion of the code and the frequencies are presented in units of both Hz and per rotor frequency (P), based on the given design tip speed. Rough estimates of the viscous equivalent structural damping values were estimated on the basis of the stall flutter results; these estimates are discussed in greater detail in a subsequent subsection. The torsion stress/torque coefficient, τ/T, at the 19.05 cm spanwise location was calculated using blade geometry and appropriate formulas from Reference 30. The nominal section properties for the SR-2 model blade are then given as functions of nondimensional spanwise location in Figures 16 through 24.
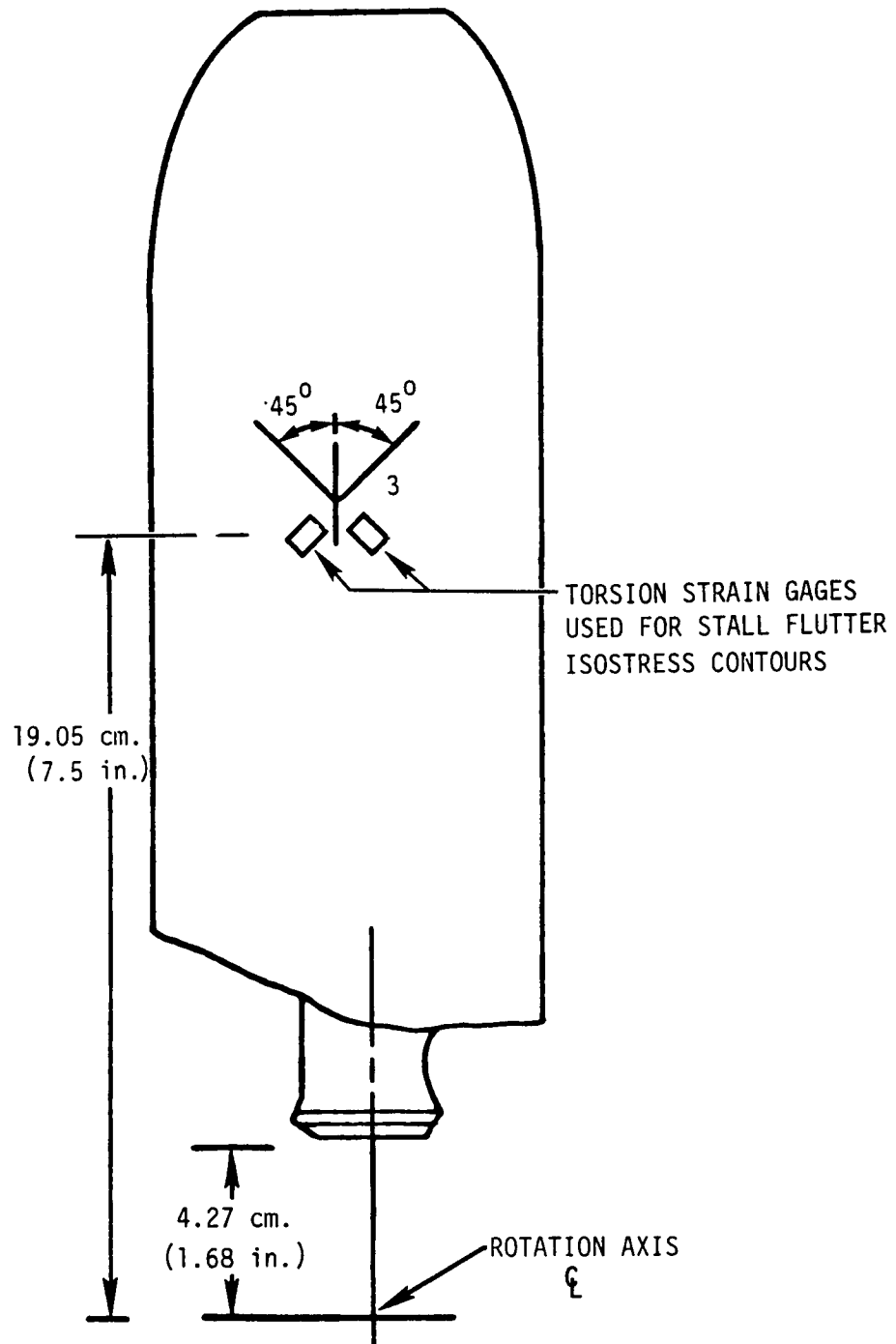
Figure 15. Planform of SR-2 Model Prop-Fan Blade

119

TABLE V

SR-2 MODEL PROP-FAN PHYSICAL PARAMETERS

Design Parameters	Model Values
Tip Speed, ΩR, m/s	277.01
Rotor Speed, Ω, rpm	8500
No. of Blades, b	8
Radius, R, m	.3112
Solidity, σ	.565
Blade Root Offset, e	.1567R
Preconing, β_B, deg	0.1
Prelead-lag, δ_B, deg	0.1
Fabrication Material	4340 stainless steel

Parameters Calculated or Estimated

Uncoupled Mode Natural Frequencies

1st Flatwise Natural Frequency, ω_{w_1}, Hz	233.34 (1.577P)
2nd Flatwise Natural Frequency, ω_{w_2}, Hz	541.94 (3.825P)
3rd Flatwise Natural Frequency, ω_{w_3}, Hz	1037.74 (7.325P)
1st Edgewise Natural Frequency, ω_{v_1}, Hz	1030.59 (7.274P)
1st Torsional Natural Frequency, ω_{θ_1}, Hz	627.64 (4.430P)
2nd Torsional Natural Frequency, ω_{θ_2}, Hz	1246.79 (8.801P)

Structural Critical Damping Ratios

Flatwise Modes	0.008
Edgewise Mode	0.008
Torsion Modes	0.008

Torsion Stress/Pitching Moment

τ/M (@ r = 19.05 cm)	$3.89/cm^3$ ($63.77/in^3$)

120
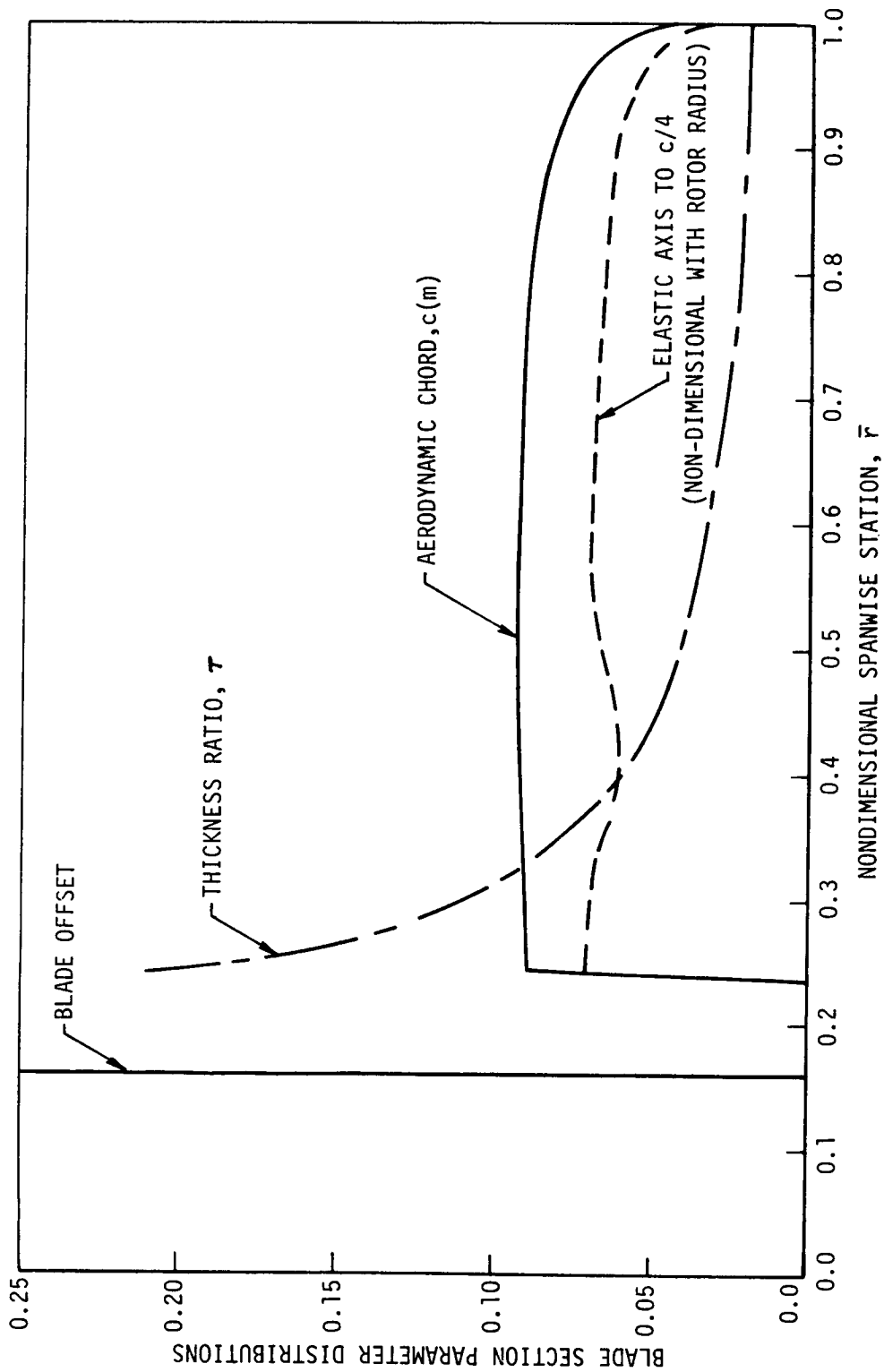
Figure 16. Section Property Distributions for SR-2 Blade
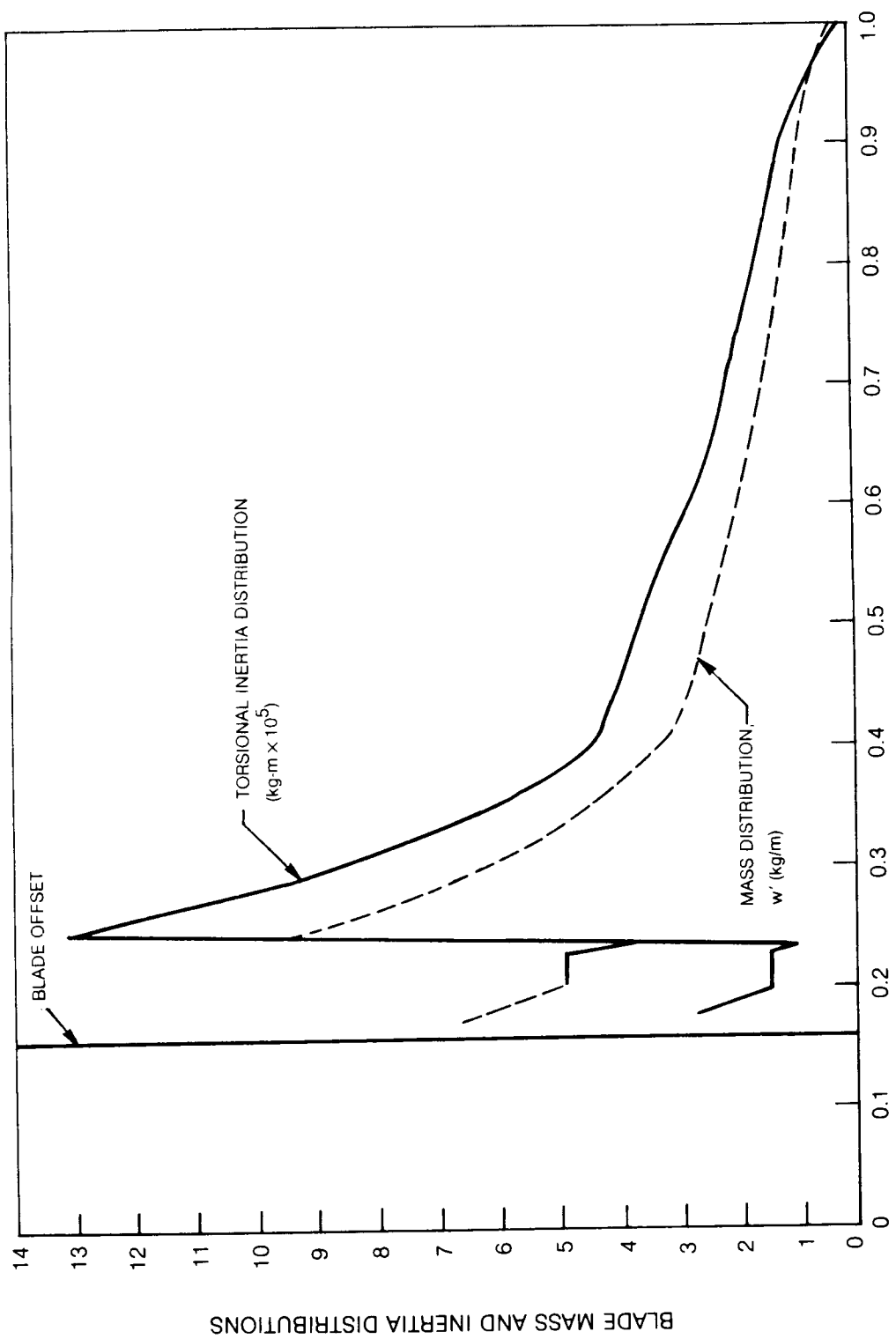
Figure 17. Weight and Inertia Distributions for SR-2 Blade

122

NONDIMENSIONAL SPANWISE STATION, $\bar{r}$

BLADE MASS DISTRIBUTION, w'(kg/m)

BLADE OFFSET
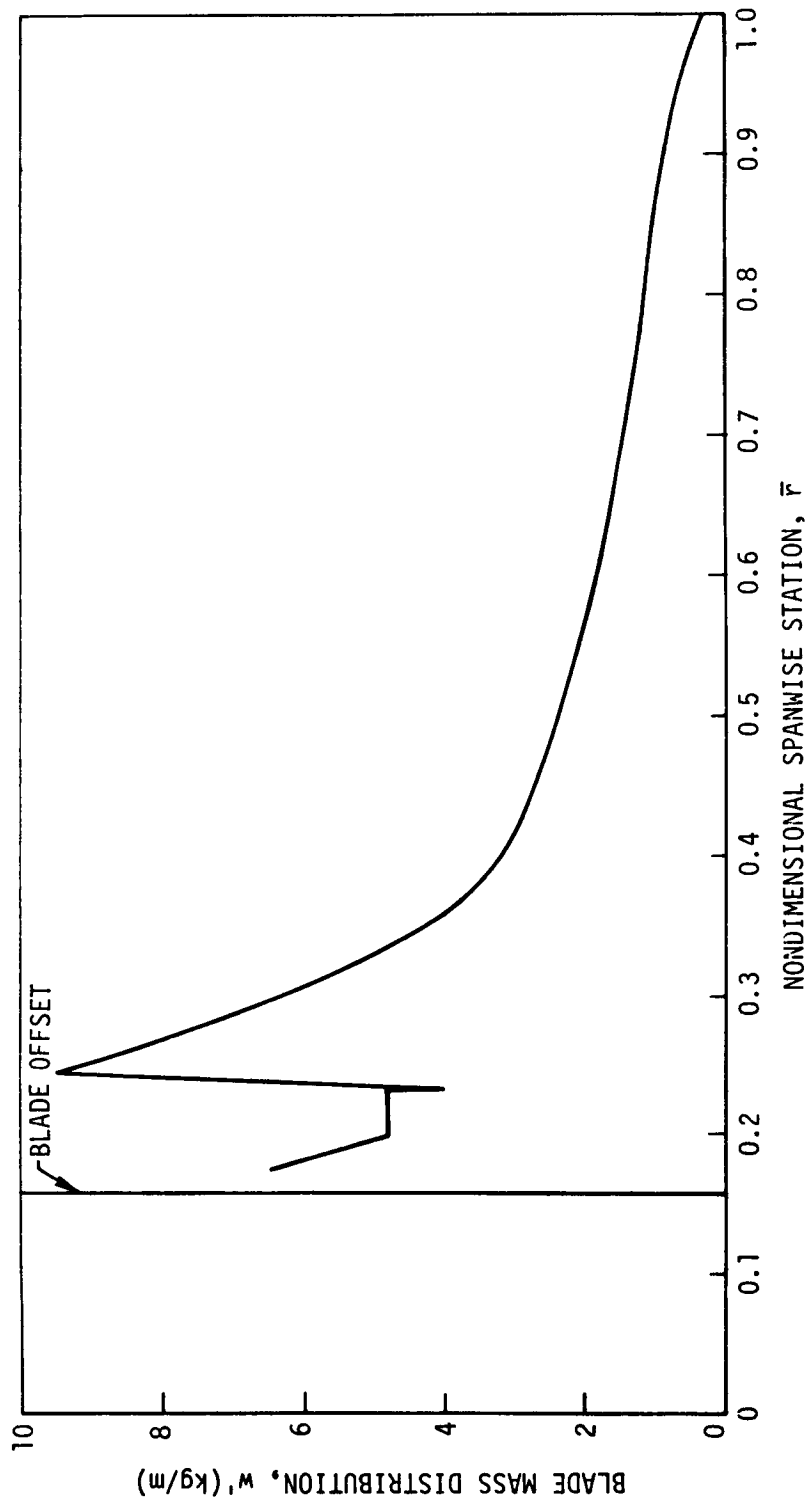
Figure 18. SR-2 Blade Mass Distribution

123
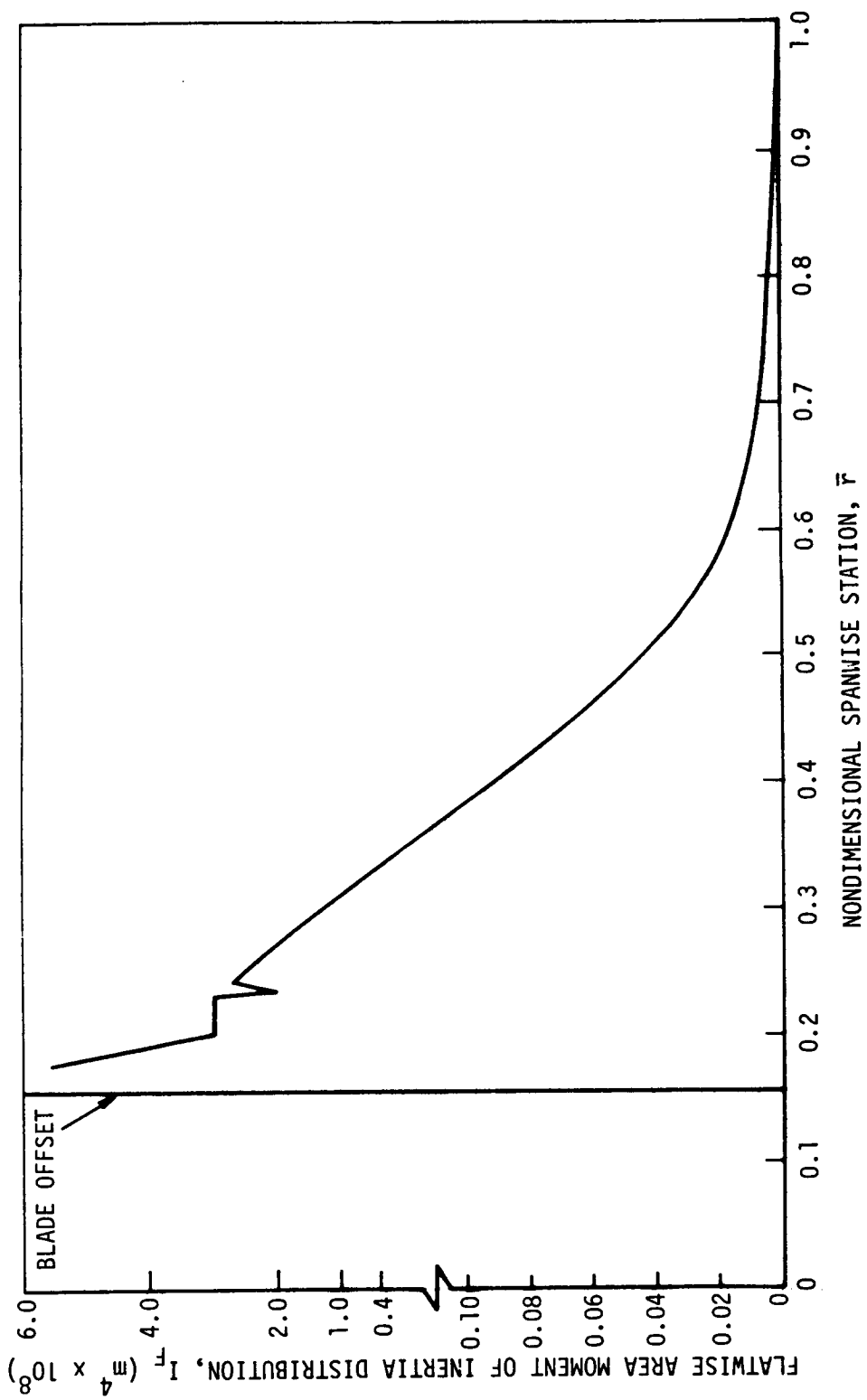
Figure 19. Flatwise Area Moment of Inertia Distribution for SR-2 Blade

NONDIMENSIONAL SPANWISE STATION, $\bar{r}$

EDGEWISE AREA MOMENT OF INERTIA DISTRIBUTION, $I_E(m^4 \times 10^8)$
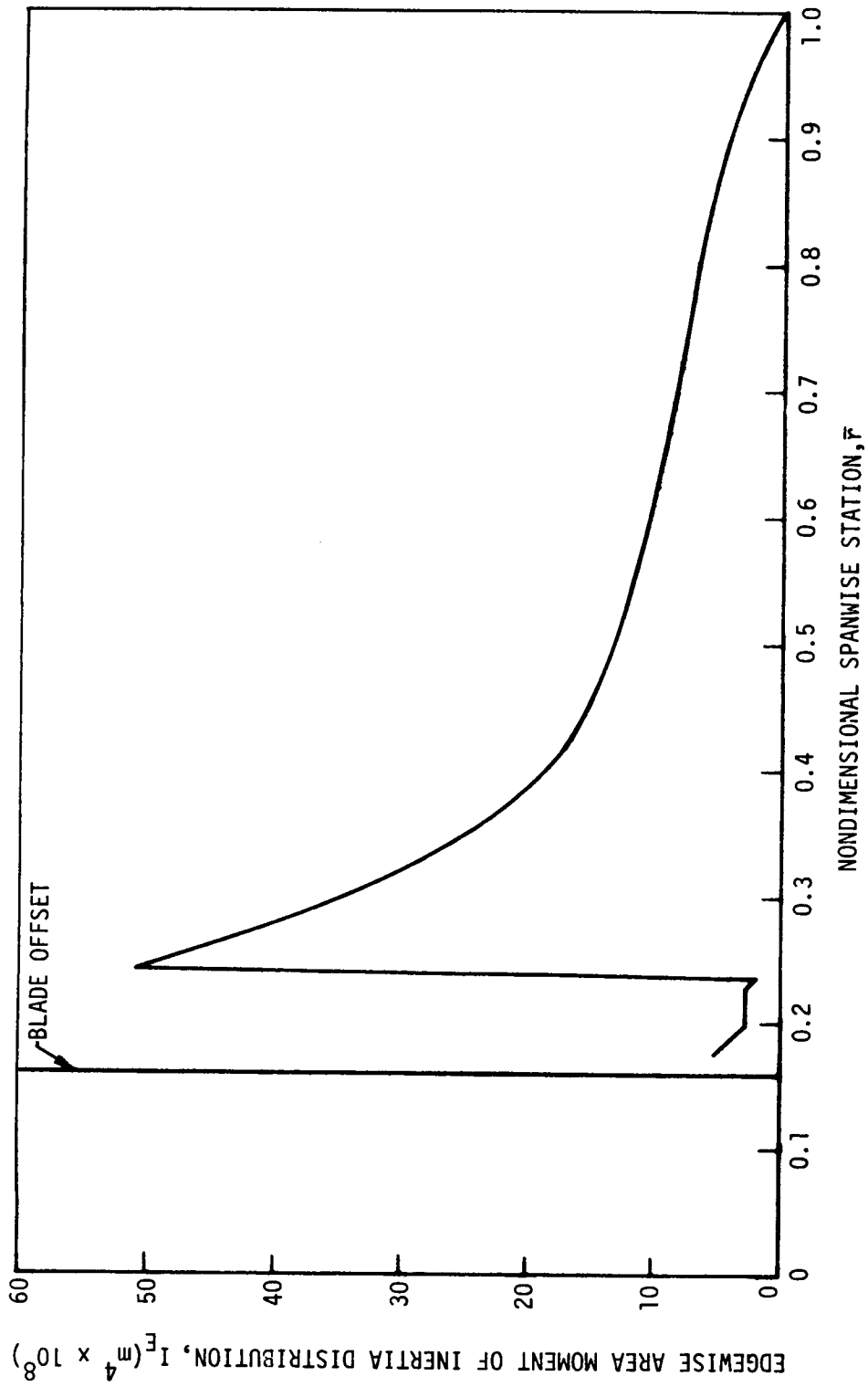
BLADE OFFSET

Figure 20. Edgewise Area Moment of Inertia Distribution for SR-2 Blade
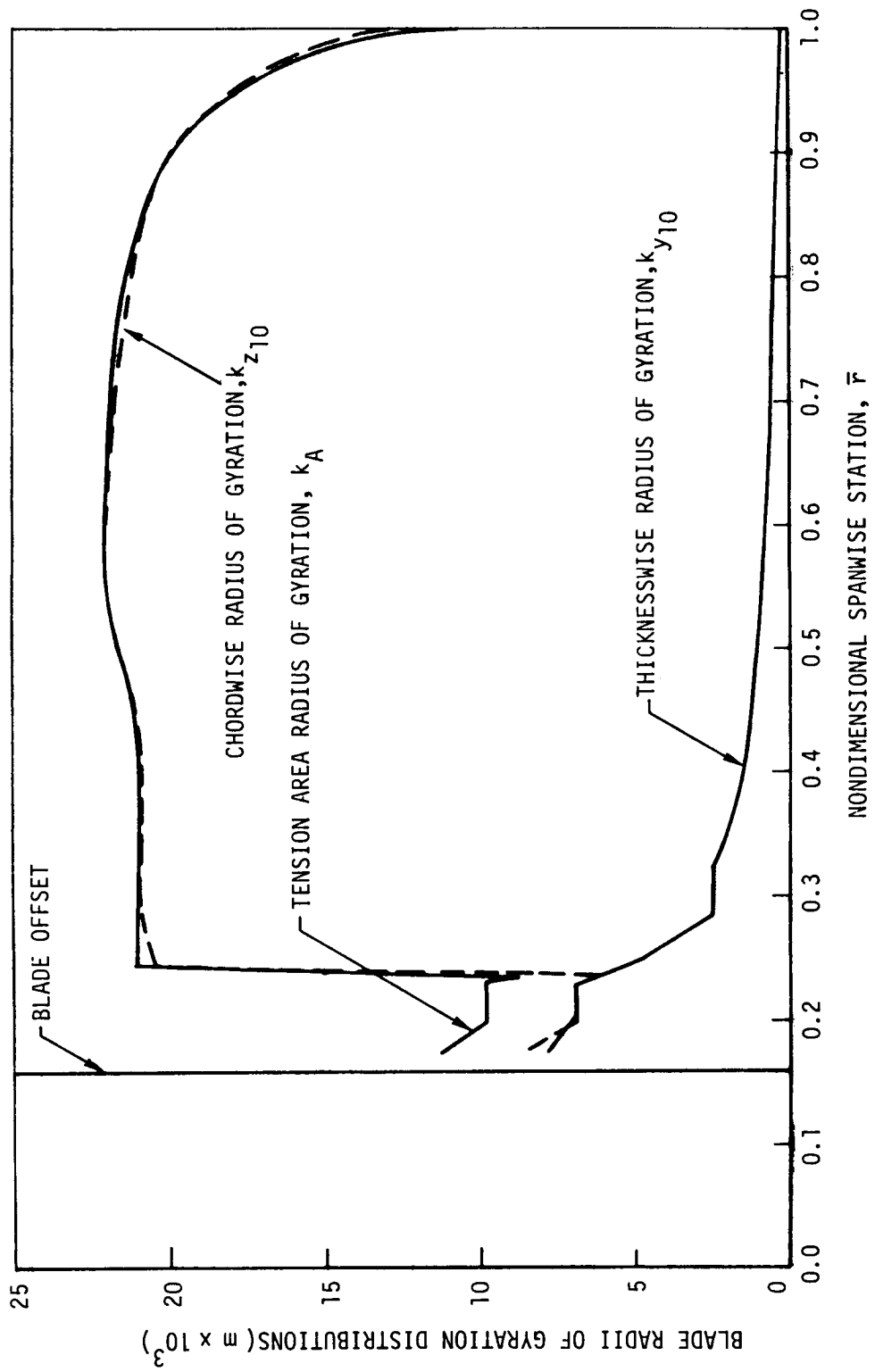
Figure 21. SR-2 Blade Radii of Gyration Distributions
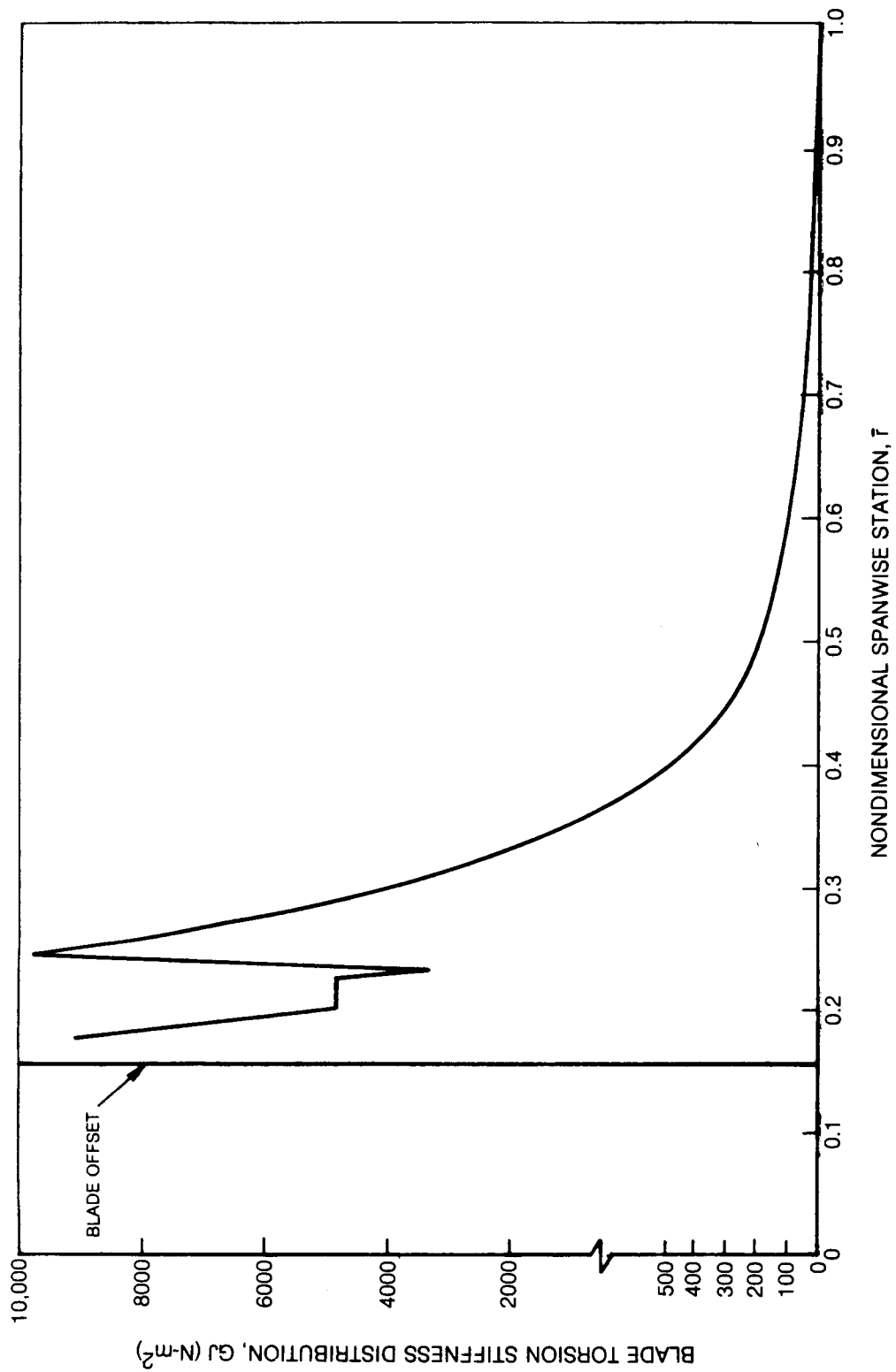
Figure 22. SR-2 Blade Torsion Stiffness Distribution

BLADE OFFSET

NONDIMENSIONAL SPANWISE STATION, r̄

BLADE TORSION STIFFNESS DISTRIBUTION, GJ (N-m²)
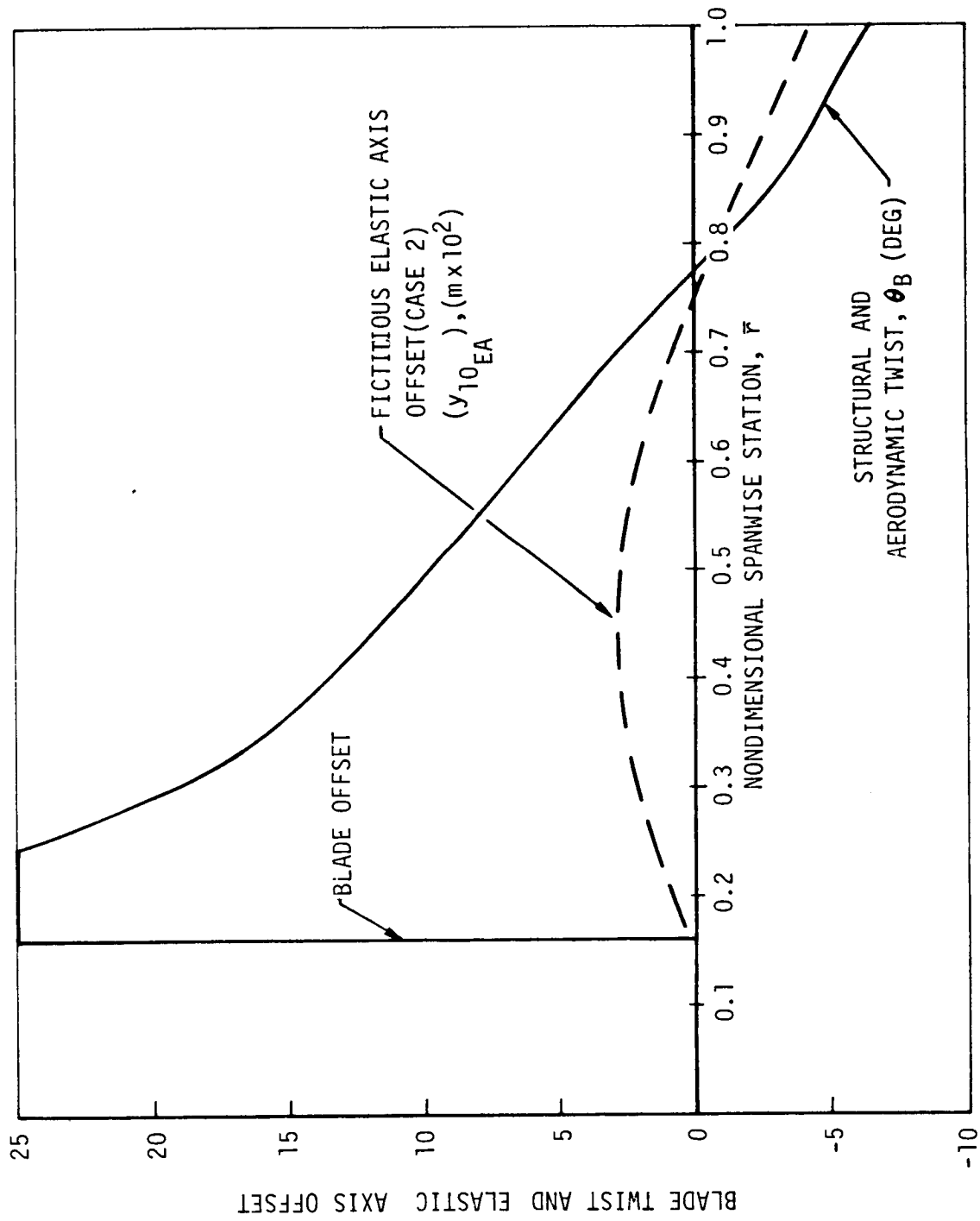
Figure 23. Twist and Fictitious Elastic Offset Distributions for SR-2 Blade
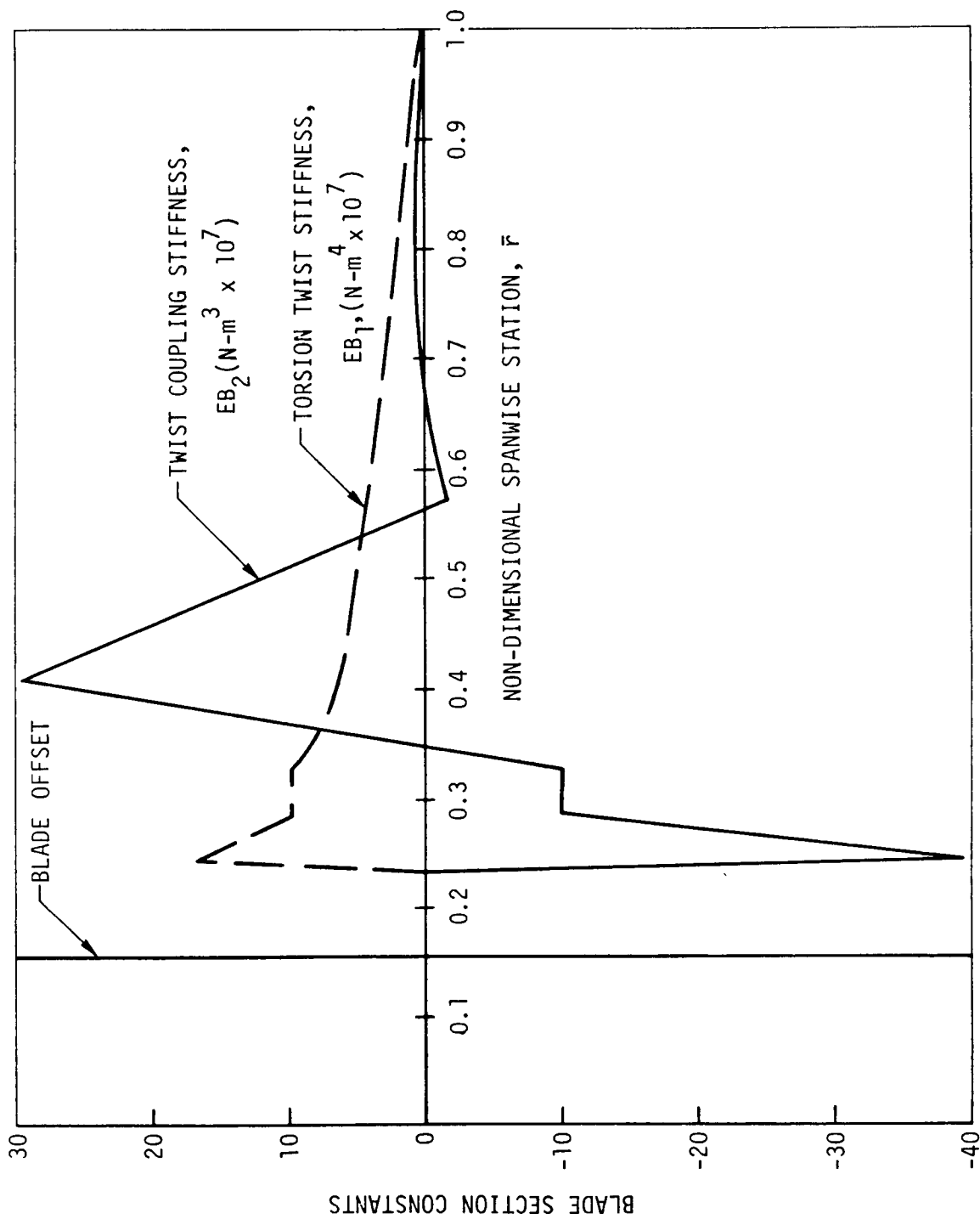
Figure 24. SR-2 Blade Section Twist Stiffness Distributions

129

The seven cases selected to define operating conditions for the SR-2 prop-fan are described in Table VI. The first two conditions are defined by a blade pitch angle and rotor speed representative of unstalled operation, both without and with a fictitious (but representative) structural sweep distribution. These two cases were selected solely as vehicles for demonstrating the capability of the code and are not intended to show any quantitative performance characteristics of the SR-2 blade. While case 1 could potentially be correlated with test data, if such data were available, case 2, with the fictitious structural sweep of 35.3 deg, can only have meaning in a theoretical sense. The purposes of these two cases are, therefore, to demonstrate program operation, as check cases, and to establish qualitative sweep related trends.

The fictitious sweep selected for case 2 was arbitrarily constructed to have a sweep angle of approximately 35.3 deg at and outboard of the 75% span location with parabolic variation inboard to the offset location. This fictitious sweep (elastic axis offset) distribution is shown in Figure 23. The forward flight speed was chosen to maintain an unstalled blade angle-of attack of about 4° at the .75R spanwise location. The number of flatwise, edgewise, and torsion modes used were chosen to exercise the eigensolution to its fullest extent.

The last five conditions shown are identified for the nominal (nonswept) SR-2 blade and are intended for correlation with the stall flutter test results, as discussed in a later subsection. With the seventh correlation case, the edgewise mode was deleted due to the expected inactivity of this relatively high frequency mode, and only the first torsion mode was retained commensurate with the predominantly first torsion mode excitation test results.

The variations in uncoupled blade modal frequencies with tip speed are presented in Figure 25. These frequencies, of course, lack the coupling effects of twist, precone, prelead, etc., which the G400PROP analysis provides.

TABLE VI

SELECTED OPERATING CONDITIONS FOR SR-2 PROP-FAN

$$a_\infty = \begin{array}{l} 352 \text{ mps.} \\ (1155 \text{ fps}) \end{array} = \begin{array}{l} .03066 \text{ Kg/m}^3 \\ (.001914 \text{ lb-sec}^2/\text{ft}^4) \end{array}$$

Case	Blade Pitch Angle, $\theta_{.75R}$, deg	Rotational Speed, Ω, RPM	Forward Flight Speed, V_T, m/s, (Knots)	Structural Sweep, deg	Solution* Type	Modes F-E-T	Fig. No. for Results
1	20	8500	59.52 (115.7)	0	E, UP	3-1-2	26a, 26b, 26c
2**	20	8500	59.52 (115.7)	(35.3)	E, UP	3-1-2	26a, 26b, 26c
3	20	8500	0	0	TH, US	3-1-2	27
4	25	8500	0	0	TH, US	3-1-2	27
5	30	8500	0	0	TH, US	3-1-2	27
6	32	8500	0	0	TH, US	3-1-2	27
7	30	2000	0	0	TH, US	2-0-1	27

* E: eigensolution, TH: time history, UP: unsteady Pade airloads, US: unsteady stalled airloads

** Fictitious sweep case to establish qualitative sweep characteristics
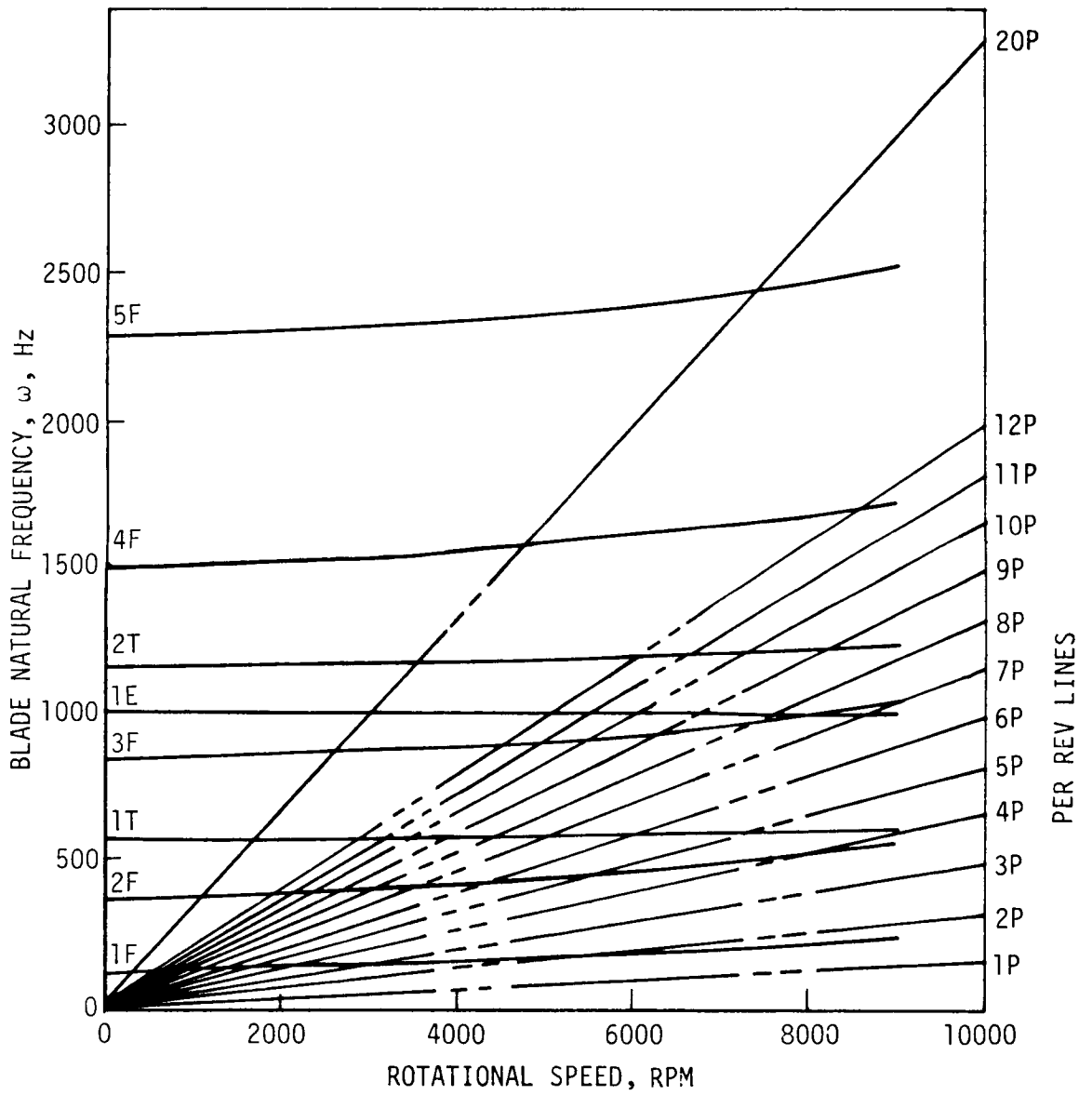
Figure 25. Variation of SR-2 Blade Natural Frequencies with Tip Speed, Uncoupled Modes

Results of Eigensolution

Both cases 1 and 2 were run using the eigensolution analysis to establish satisfactory operation of the code in predicting realistic coupled mode vibration characteristics as well as reasonable aeroelastic stability estimates. The results of these eigensolutions are presented in complementary forms in Table VII and Figures 26a, 26b, and 26c. The table summarizes the <u>eigenvalue</u> results for both the unswept and swept configuration. These consist of the (vacuum) coupled made frequencies, as well as the (nonvacuum) aeroelastic stability damping levels. The three portions of Figure 26 summarize the vacuum case <u>eigenvector</u> results for these two configurations for the six coupled modes. The results are presented in phase-plane format for the three components of tip motion: inplane motion (y_5), out of plane motion (z_5) and pitching (Θ). For each of these modes the results for the nominal (unswept) SR-2 are compared with the corresponding results for the fictitiously swept blade.

Figure 26a shows comparisons of modes 1 and 2 for the swept and unswept configurations. In particular, it can be seen from the phase-plane diagrams that out-of-plane motion is the dominant factor in modes 1 and 2, with significant pitching motion only in mode 2, for both the swept and unswept configurations. This is to be expected since in both configurations mode 1 represents primarily the first flatwise mode (1F), and mode 2 represents the second flatwise mode (2F) with some first torsion mode (1T) coupling. The opposite signs of the inplane (Y5) and out-of-plane (Z5) phase-plane vectors indicate that the bending is primarily flatwise. Also, since the swept blade second mode pitching vector is relatively in phase with the bending, it can be seen that sweep is generating a strong coupling between torsion and flatwise bending as is expected.

Figure 26b shows similar comparisons for modes 3 and 4. The phase-plane vectors illustrate a great deal of pitching motion for modes 3 (1T) and 4 (3F, 1E, 2T), but a significant amount of inplane and out-of-plane motion for both blade configurations only for mode 4. The bending in mode 4 is similarly indicated to be primarily flatwise. Most 3 has a coupled frequency which closely resembles that for pure first torsion mode (1T); this mode is essentially the coupled form of the first torsion mode. Mode 4 has a frequency which is very close to that for third flatwise (3F), first edgewise (1E), and the second torsion (2T) modes.

Figure 26c shows comparisons of mode and 6 for the two blade configurations. Because the Y5 and Z5 components of mode 5 are now in-phase, the bending is indicated to be edgewise. The 5th mode for the swept configuration unexpectedly exhibits a large amount of coupled pitching motion with the second torsion mode (2T). Mode 6 is seen to represent pure second torsion mode (2T), and is thus the coupled form of this mode.

133

EIGENVALUE RESULTS FOR SAMPLE CASES 1 AND 2

Mode	Vacuum		Nonvacuum			
	case 1	case 2	case 1		case 2	
	ω	ω	σ	ω	σ	ω
1	1.511	1.505	-.542	1.449	-.443	2.272
2	3.634	3.608	-.337	3.545	-.428	4.200
3	4.407	4.526	-.348	4.402	-1.407	5.679
4	6.799	6.692	-.269	6.766	-1.619	6.537
5	8.155	7.880	-.155	8.134	-.414	7.525
6	8.789	9.359	-.360	8.780	-.355	9.312

eigenvalue: $\lambda = \sigma \pm i\omega$ (nondimensional with respect to Ω)
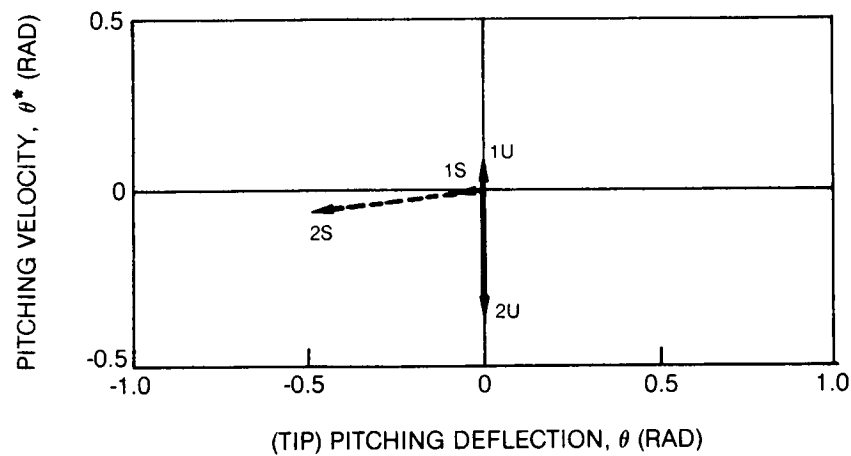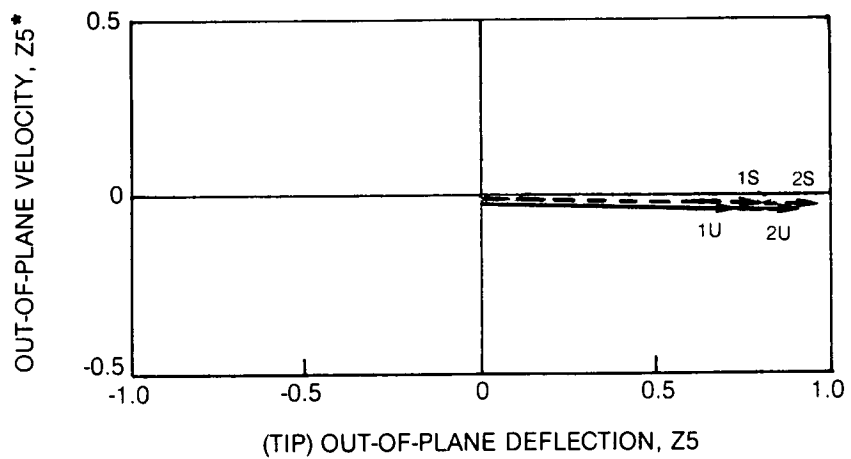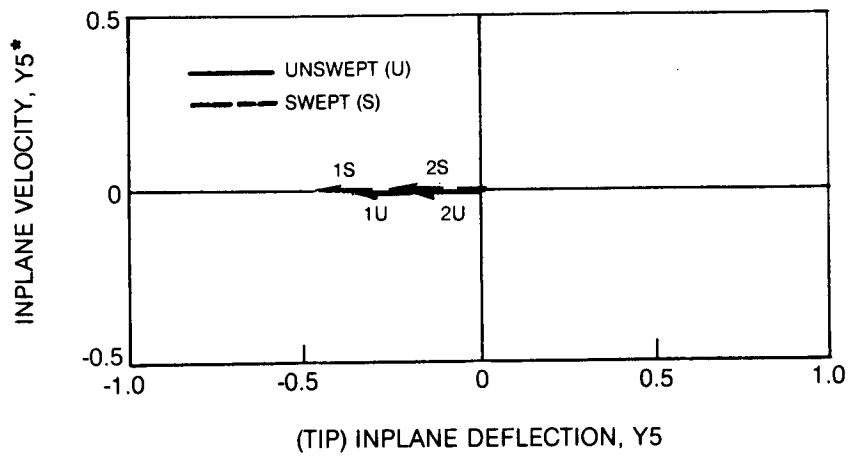
Figure 26a. Coupled Mode Shape Comparisons, at the Tip Section, for Unswept and Swept Blade Configurations, Modes 1 and 2

135
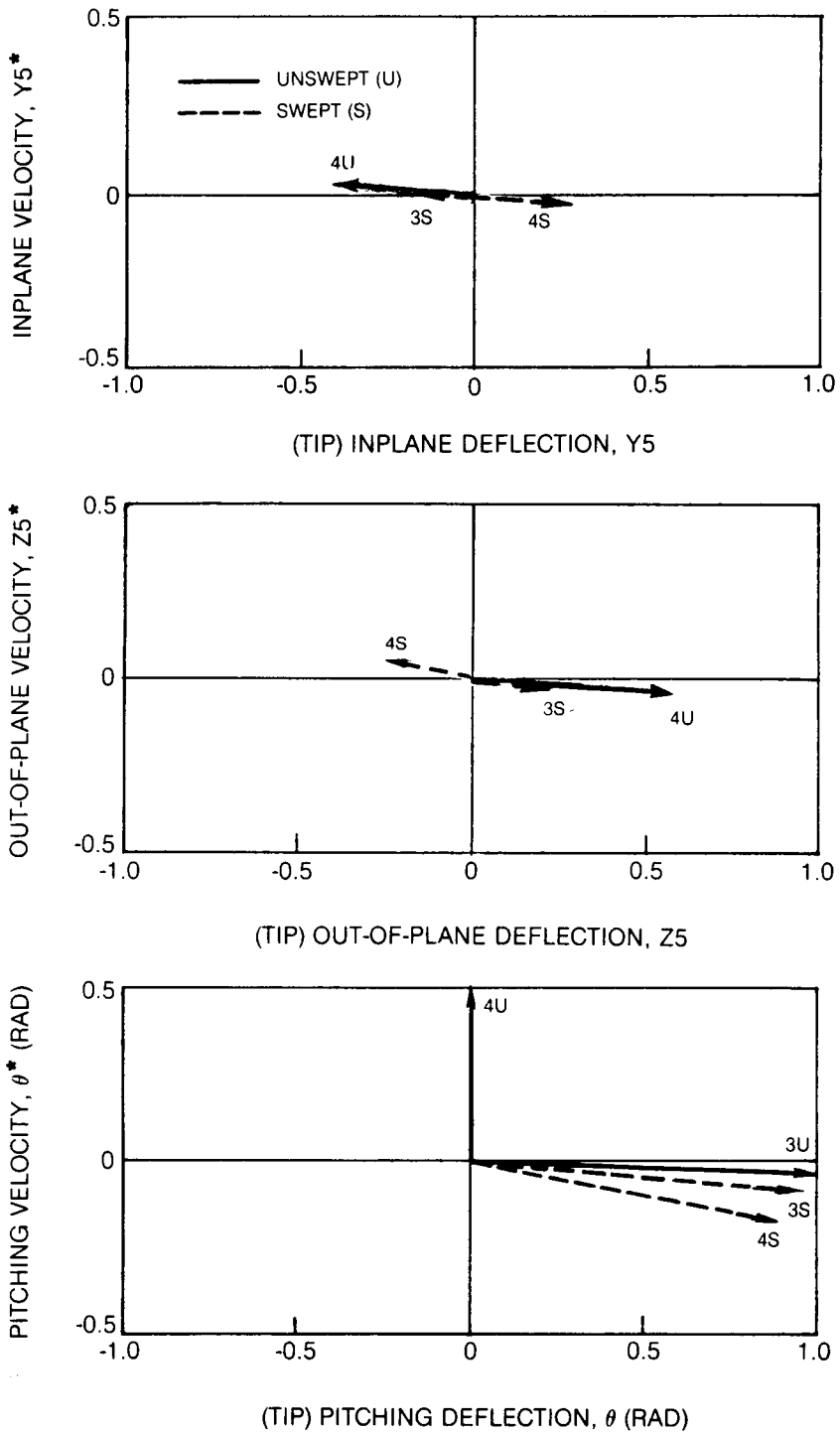
Figure 26b. Coupled Mode Shape Comparisons, at the Tip Section, for Unswept and Swept Blade Configurations, Modes 3 and 4
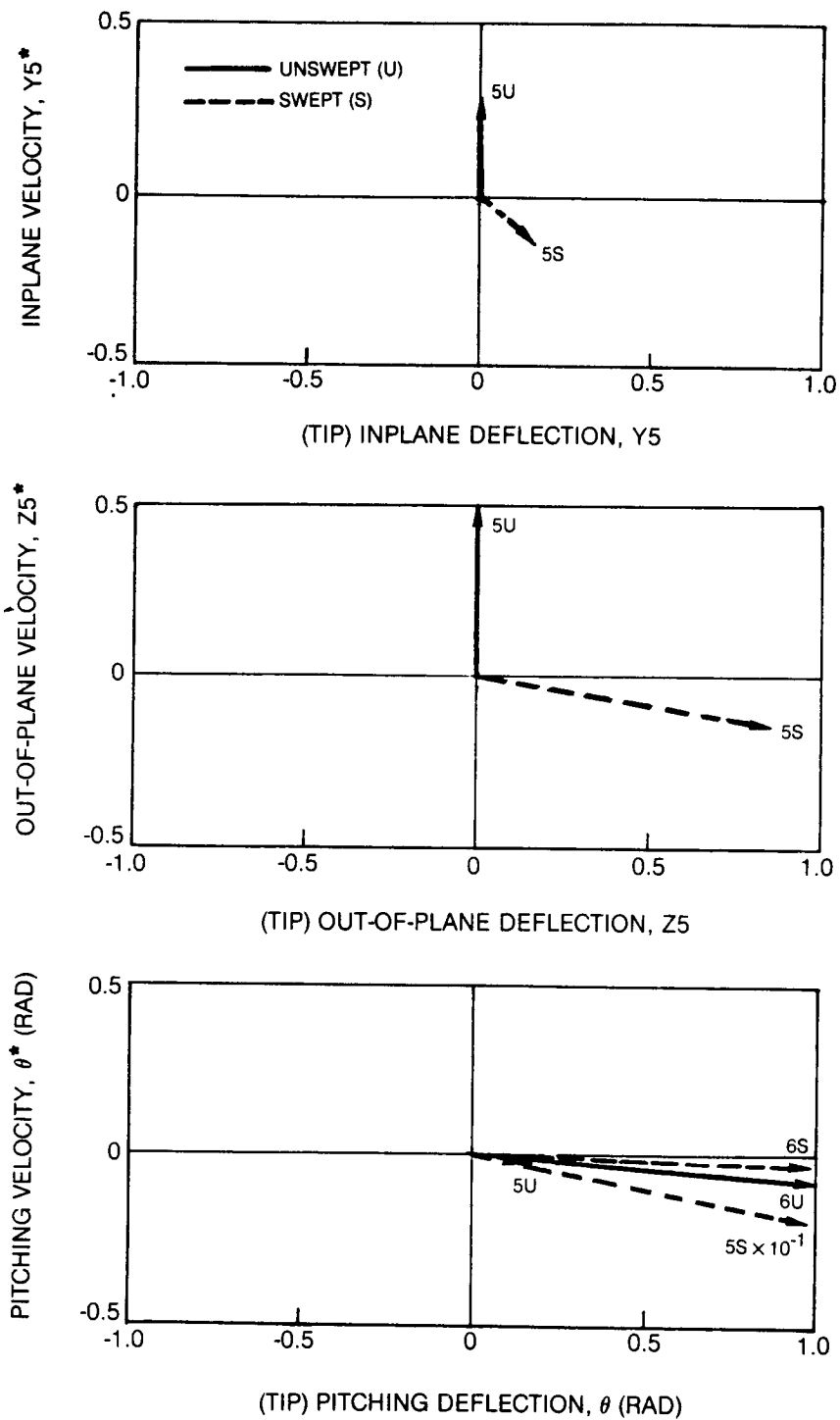
Figure 26c. Coupled Mode Shape Comparisons, at the Tip Section, for Unswept and Swept Blade Configurations, Modes 5 and 6

137

Stall Flutter Correlation Cases

Figure 27 summarizes the experimental and analytic stall flutter results for the statically thrusting SR-2 Prop-Fan model blade. The experimental results are presented in the form of isostress curves for the 1/2 peak-to-peak (1/2PTP) torsion stresses measured at the 19.05 cm spanwise location, as shown in Figure 15. These results were obtained from stall flutter tests on model Prop-Fan configurations.* The reduction of the test data to 1/2PTP torsion stresses was accomplished using the manufacturer's quoted gage factors for the torsion strain gages used.

The analytic G400PROP calculations consist of cases 3 thru 7 given in Table VII and are indicated on Figure 27 by the open or closed square symbols. These five cases were selected with blade pitch angle-rotor speed combinations which would appear to result in both stable and unstable calculated responses. Cases 3 and 7 were selected to overlap partially with case 5 in either blade pitch angle (Case 3) or rotor speed (Case 7). Case 5 was deemed to be a representative condition strongly associated with stall flutter, as opposed to the deep stall buffeting which was observed at significantly higher pitch angles. Correspondingly, Cases 3 and 7 were deemed to be probably stable conditions. Furthermore, in the course of the study, additional conditions, Cases 4 and 6, were introduced to enhance the definition of the apparent stall flutter boundary. In all the G400PROP calculations, the dynamic stall parameters appropriate to the NLR-1 airfoil were used.

In the course of performing the G400PROP calculations, it was noted that the degree of stall flutter response obtainable was a strong function of the values selected for structural damping. With a sufficiently high value of damping (0.02) the blade was stable and a stall flutter condition could not be induced. The final value of damping used (0.008) was selected on the basis that it produced "stable" limit cycle oscillations which neither grew nor diminished once the instability "locked-in."

The final G400PROP calculation results for the five conditions are shown in Figure 27 either with an open or closed symbol denoting stability or instability, respectively. Where appropriate, the calculated 1/2PTP torsion limit cycle torsion stresses are shown parenthetically. Generally, the detailed results of this figure show the correlation between experiment

---

* These tests were performed under contract NA53-22755 and are summarized in UTRC Report R81-335414, "Static Stall Flutter Tests of HSD Prop-Fan Models."
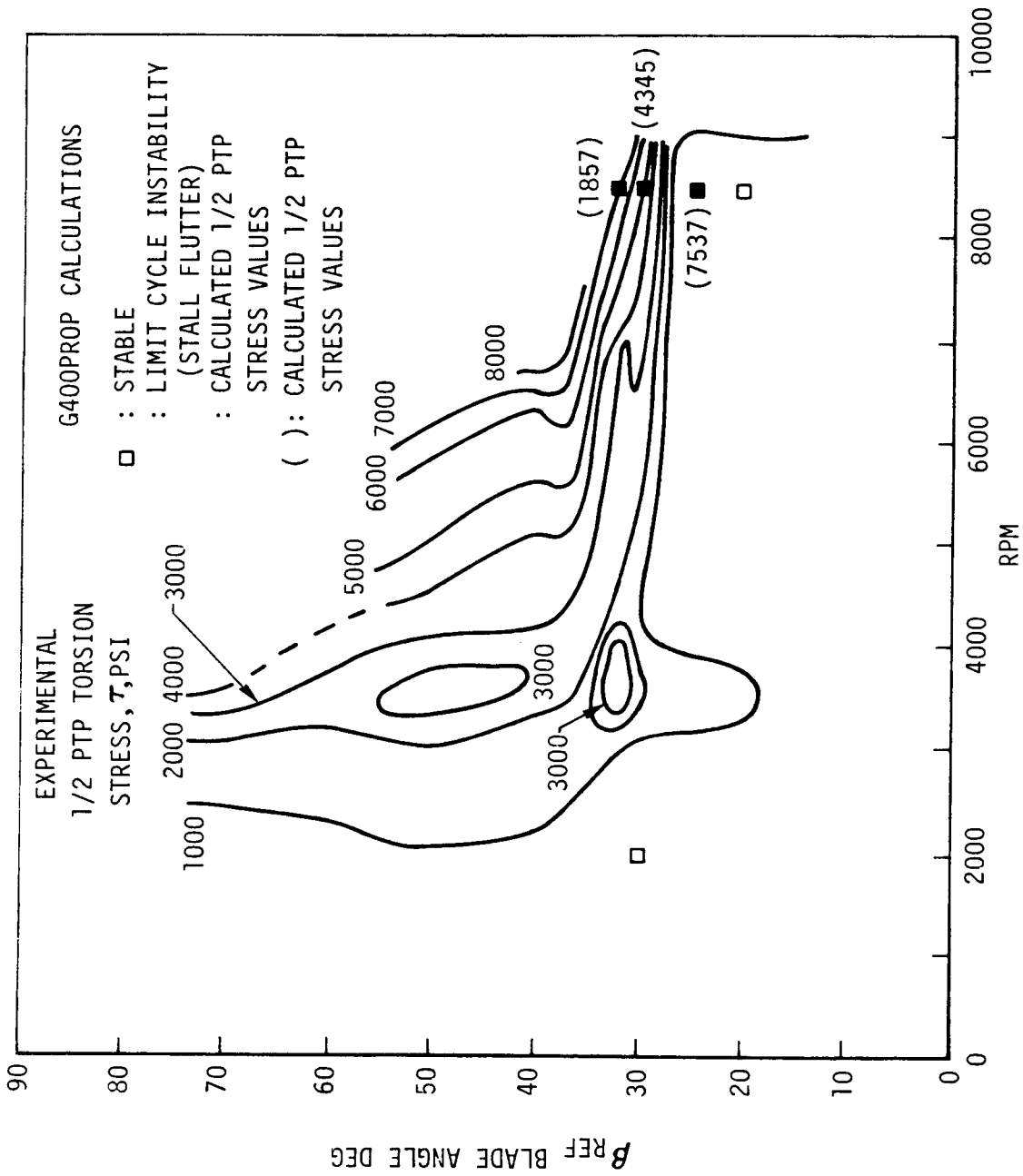
Figure 27. Stall Flutter Correlation Results for the SR-2 Blade and G400PROP Calculations

and analysis to be quite good in that:

(1) Stall flutter was predicted for conditions close to those where it was measured,

(2) Stable conditions were predicted where the propeller was found to be stable, and

(3) The maximum 1/2PTP stress levels correlate well with those measured (despite the disparity in methods used for obtaining the stresses, experiment vs. analysis).

It would appear that the principal disagreement between the experiment and theory is the pitch angle at which the apparent stall flutter boundary occurs; a disparity of about 6 degrees is indicated. Possible reasons for this disparity are as follows:

(1) The inadequacy of using uniform inflow for the statically thrusting condition. Use of the PANPER code to obtain a more realistic flow field for the static thrust condition is practical and could have been used, but was outside the scope of the present study.

(2) The uncertainty in the static stall characteristics of the NACA 16-series airfoil data used.

(3) The unknown impact of cascading effects on the airfoil stall characteristics.

GENERAL DESCRIPTION OF THE G400PROP PROGRAM STRUCTURE

The G400PROP Rotor Aeroelastic Analysis is an extended, special purpose version of the parent G400 analysis described in Reference 1. For application to the special requirements of propellers, the G400 analysis was extended to include an internal preprocessor for uncoupled beam normal modes, the elastomechanics accruing from structural sweep, and an upgraded, more rigorous aerodynamic modeling. This aerodynamic modeling includes aerodynamic sweep, stalled and unstalled unsteady effects, and three-dimensional variable inflow. This version now includes an expanded eigensolution and direct coupling with the PANPER variable inflow analysis. The program was coded in FORTRAN IV and developed on the UNIVAC 1110/81A computer system.

Program Structure

The G400PROP program is structured in a generally conventional hierarchical fashion with an initial routine (MAIN), appropriate modular elements and a collection of utility subroutines and/or functions. Figures 28 through 31 present flowcharts showing the four sequential portions of the G400PROP program structure; each of these figures highlights one of the four major portions of the code. Note that the (A) end terminal depicted in Fig. 38 corresponds to the beginning terminal of Fig. 39, and so on with terminals (B) and (C) with Figs. 29 through 31. In these figures, where appropriate, the names of the subroutines performing the functionally labeled operations, are given parenthetically above their respective functional symbol.

The hierarchical subroutine calling structure is presented in tabular form in Table VIII; this functional structuring also serves to list the elements (subroutine, functions and/or data), contained in the G400PROP code. Note that the hierarchical structure is alternately indicated using indentations with symbols denoting level and/or with parentheses. Note also that this table lists the routines in alphabetical order within any given hierarchy and not with respect to calling order, size or importance. Following this table is Table IX which presents a common block/subroutine cross reference list. Finally, after these two tables the last subsection presents a brief description of each of the G400PROP elements.
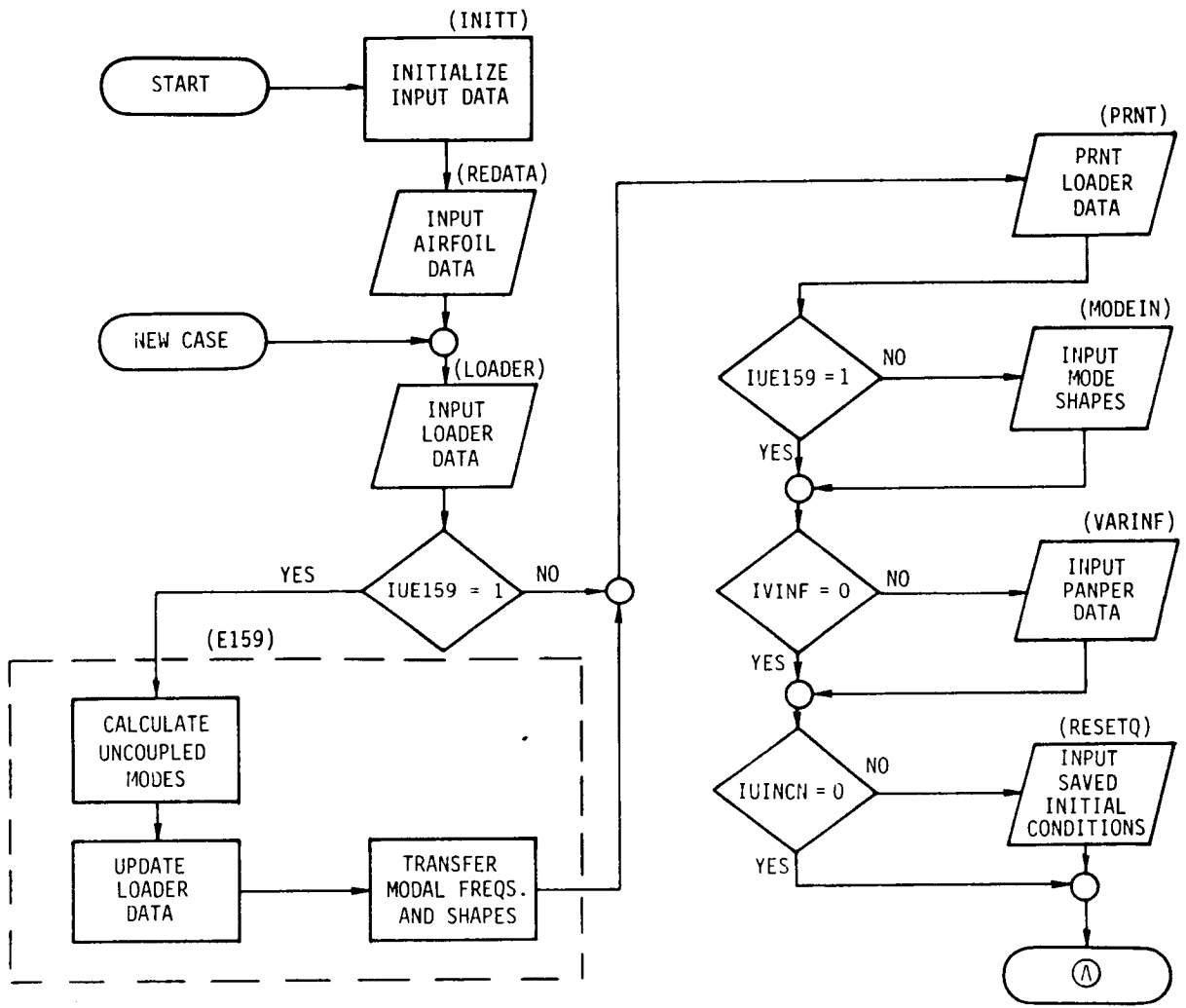
Figure 28. Flowchart for G400PROP — Input and E159 Preprocessor Portions

142
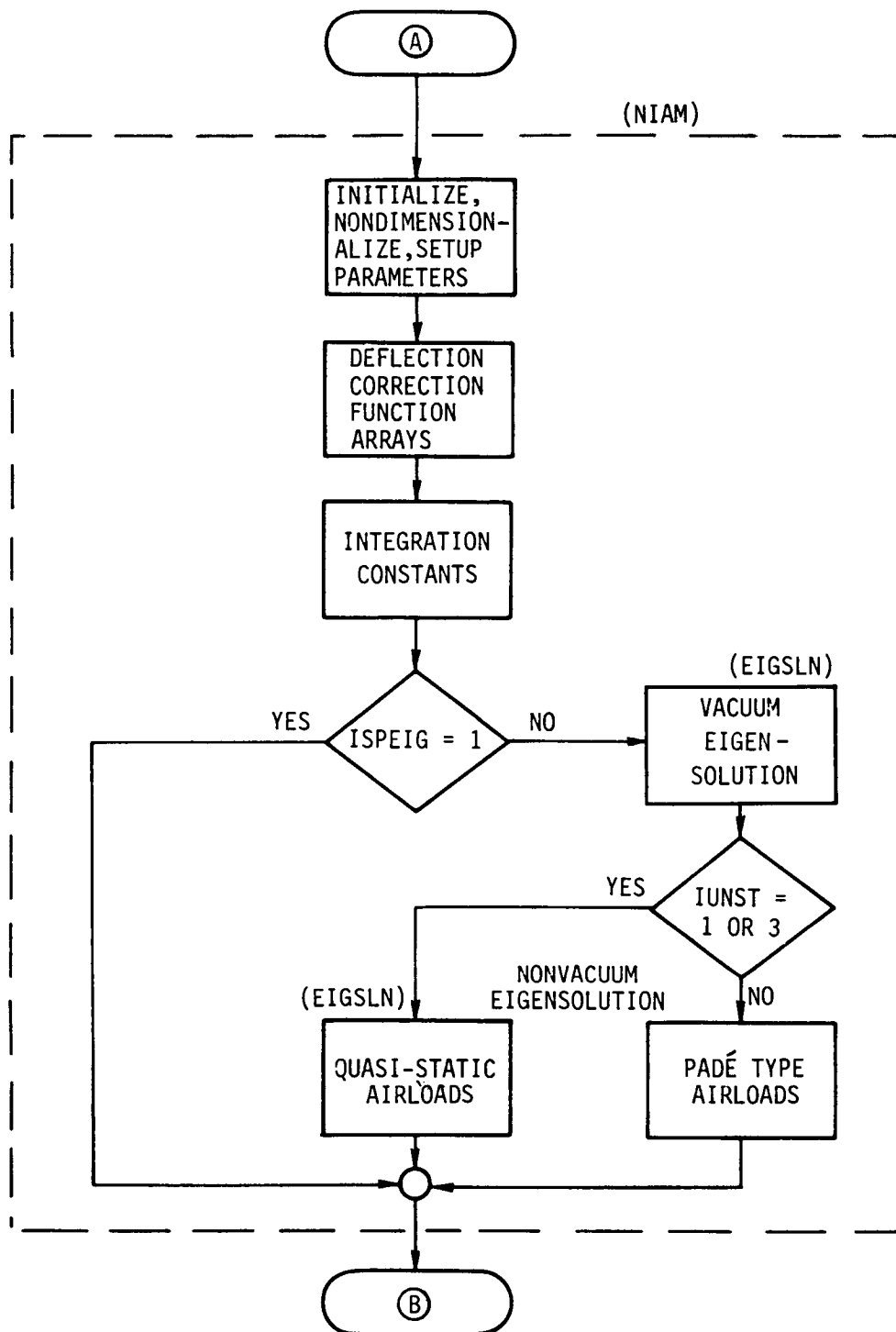
Figure 29. Flowchart for G400PROP-Part I, Eigensolution Portions
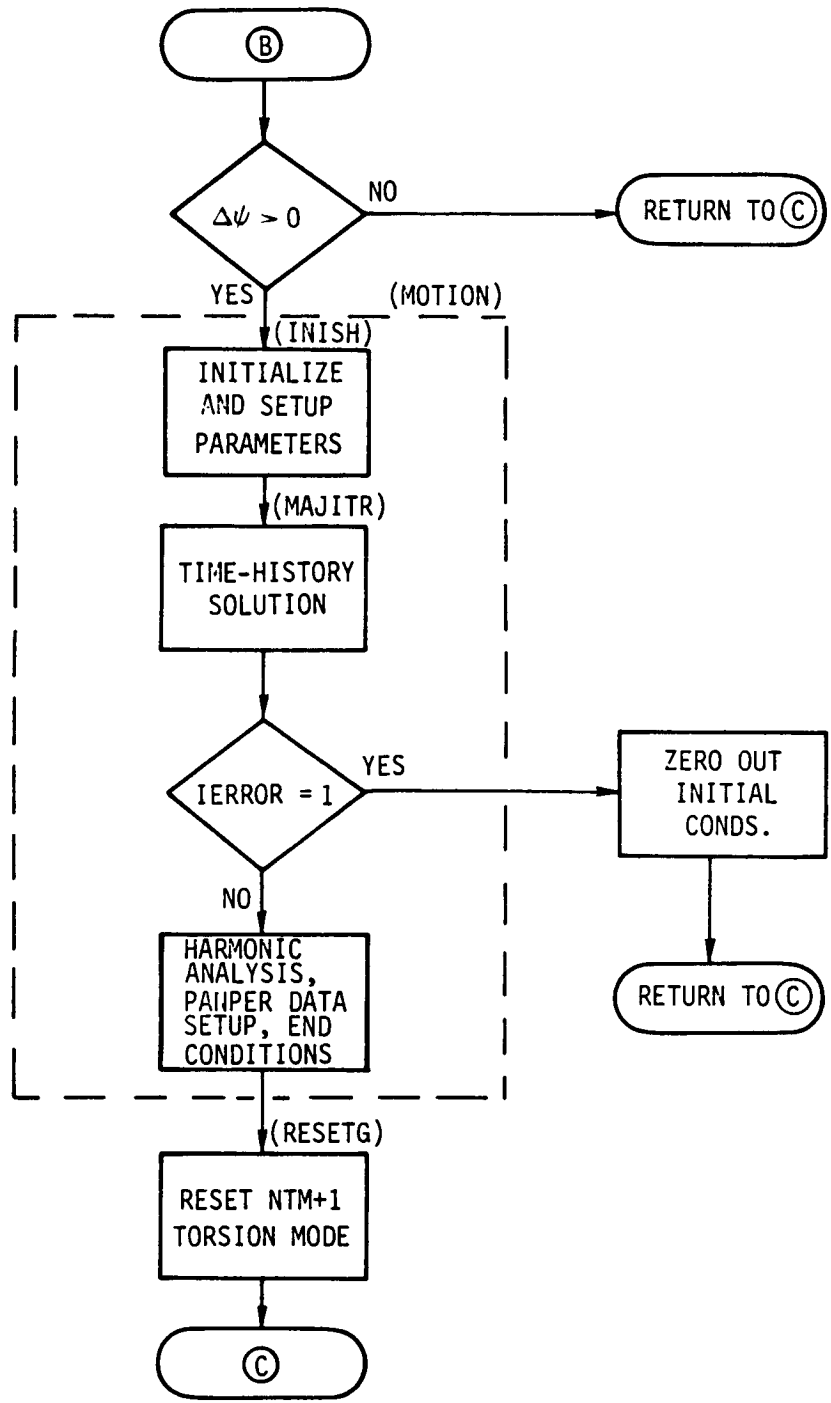
Figure 30. Flowchart for G400PROP-Part II, Time-History Solution Portions

144
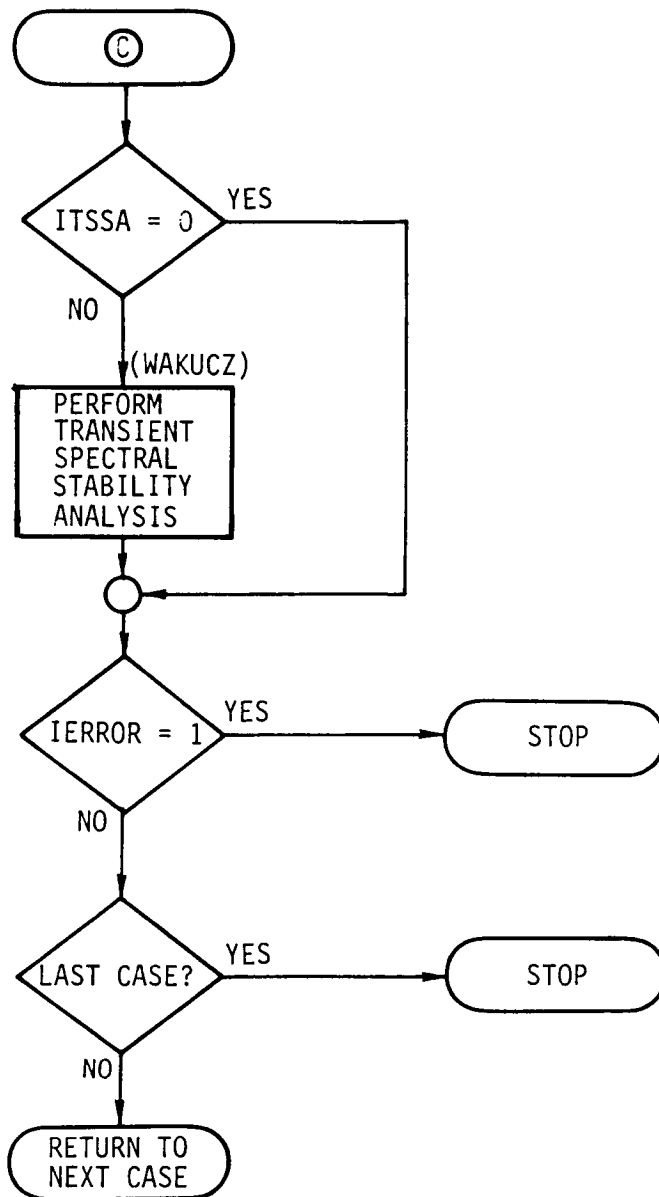
Figure 31. Flowchart for G400PROP-Part III, Transient Spectral Stability Analysis and Program Termination Portions

TABLE VIII

HIERARCHICAL LISTING OF G400PROP ELEMENTS

● MAIN

■ E159

▲ BMFIT
▲ ELAST
▲ INVERT
▲ NFMS

◆ BMEVAL
◆ BMFIT
◆ EIGENE

▼ INVERT
▼ SIMUL

▲ PCHDAT
▲ PCHMØD
▲ TMSS

■ INITT
■ LØADER
■ MØDEIN
■ MØTION

▲ ENDCØN

◆ PNPRSU

▼ BLIN5
▼ DEFLEX
▼ RSPNSS (QQPSET)

◆ QSTHRM (HARM)
◆ RESETQ (SETVAL)
◆ SETVAL

146

TABLE VIII (Cont'd)

▲ INISH

    ◆ ADMCØF
    ◆ DPCHEK

▲ MAJITR

    ◆ AERPRF
    ◆ BLADEL

       ▼ RSPNSS (QQPSET)
       ▼ SETUP
       ▼ SPANS

          ◆ ALFDØT
          ◆ ALWCØM
          ◆ BLIN5
          ◆ DEFLEX
          ◆ HYSDMP
          ◆ PHIDØT
          ◆ REVPAD (PADCØF)
          ◆ SHLDM
          ◆ UNSTCF

             ◗ COEFF3
             ◗ SYNTH3

               ◤ BLIN5
               ◤ GETCDS (INTERP)
               ◤ GETCLS (INTERP)
               ◤ GETCMS (INTERP)
               ◤ SHLDM

    ◆ CRØUTS

147

TABLE VIII (Cont'd)

◆PANMØM (MOMNTM)
◆TABLE
◆TMARCH

     ▼ ADAMS
     ▼ EXTRAP
     ▼ QPPCAL
     ▼ QPPTST
     ▼ STRSSS

-- ▲UNDATA

■NIAM

  ▲ AERØ

    ◆ DEFLEX
    ◆ LNAERØ

      ▼BLIN5
      ▼ SHLDM

    ◆MATRXT
    ◆RSPNSS (QQPSET)

  ▲ AIRPAD

    ◆DEFLEX
    ◆FLGDR
    ◆LNAERO

      ▼BLIN5
      ▼SHLDM

    ◆MATRXT
    ◆PADCØF

TABLE VIII (Cont'd)

◆RSPNESS (QQPSET)

▲ DFYZEA
▲ EIGSLN

◆ FILL2
◆ SØLVE

▼EIGRMC

◆RGG

◗QZHES
◗QZIT
◗QZVAL
◗QZVEC

▼PHASE
▼VECTRS

◆DEFLEX
◆GJR

▲FILL

◆RSPNSS (QQPSET)

▲INTCØF
▲SPNWIZ
▲SPRINT

▲TCØUPL
▲TWØF

■PRNT
■REDATA
■RESETG
■RESETQ

▲SETVAL

TABLE VIII (Cont'd)

■VARINF

■WAKUCZ

    ▲DISCRT
    ▲FFTGEN

       ◆LFCT (NPRM)
       ◆REVERS (SBSCRP)
       ◆SCTAB
       ◆SUBS (SBSCRP)

    ▲LINFIT

    ▲MAXIMZ (IDSCRT)

    ▲MØDULS

    ▲SEARCH

Table IX

Common Block/Subroutine Cross Reference List for G400PROP

Part 1. Common Block Names Per Element

Element	Common Block Names
1. AERØ:	ADERIV, AERØT, BLDDØF, BLDEFL, BLØCKS, CLDMTB, CTTETC, DISTRB, ELASAX, FØRIER, GLAURT, HARRAY, IMISC1, LINEAR, MATRIX1, MISC1, MISC2, MISC3, MISC4, MISC5, MISC6, NLTEXC, PANPER
2. AERPRF:	ADERIV, BLØCKS, DISTRB, DØFVAR, ELASAX, GLAVRT, GUST, HARRAY, IMISC1, LINEAR, MISC1, MISC2, MISC3, MISC4, MISC5, MISC6, PANPER, SPNVAR, TRIM, TRNSNT
3. AIRPAD:	ABC, ADMPAD, ADERIV, AERØT, AGØNY, BLDDØF, BLDEFL, CLDMTB, CTTECT, DISTRB, DISTRC, ELASAX, GLAURT, HARRAY, IMISC1, LINEAR, MATRX1, MISC1, MISC2, MISC3, MISC4, MISC5, MISC6, NLTEXC, PANPER, PADIV
4. ALFDØT:	SYND
5. ALMCØM:	SYNC
6. BLADEL:	ADERIV, BLØCKS, BLDDØF, DISTRB, ELASAX, GLAURT, GUST, HARRAY, IMISC1, LINEAR, MISC1, MISC2, MISC3, MISC4, MISC5, MISC6, SINTS, SINTS2, SPNVAR, TRIM, TRNSNT
7. BLIN5:	BLØCKS, CLDMTB
8. CØEFF3:	ALCH, ARES, ETAS, GETCS, INDEX, INDATA, INDRG, PEAK, PEESP, PLUS, PREDM, QUES, RANG, TABR
9. CRØUTS:	LINEAR
10. DEFLEX:	AERØT, BLDDØF, BLDEFL, BLØCKS, DISTRB, DØFVAR, ELASAX, IMISC1, LINEAR, MATRX1, MISC1, MISC2, MISC4, MISC5, NLTEXC, SPNVAR, YZ5DRV
11. DFYZEA:	ADERIV, BLØCKS, DISTRB, ELASAX, LINEAR, MISC1, MISC3, MISC4
12. DPCHEK:	BLDDØF, MISC1
13. EIGRMC:	LINEAR
14. EIGSLN:	FØRIER, IMISC1, LINEAR
15. ENDCØN:	ADERIV, BLØCKS, DISTRB, DØFVAR, ELASAX, GLAURT, GUST, HARRAY, IMISC1, LINEAR, MISC1, MISC2, MISC3, MISC4, MISC5, SPNVAR, SYNTHP, TRIM, TRNSNT
16. E159:	BLOCKS, DISTRB, LINEAR, MISC1, MSC159, MS159, TØRSN
17. FFTGEN:	FACTØR, INPUT
18. FILL:	BLDDØF, BLØCKS, DISTRB, LINEAR, MISC1, MISC2, MISC3, SINTS, SINTS2
19. FILL2:	ABC, FØRIER, LINEAR, MATRX4, MISC1
20. GETCDS:	DTABLE, INDEX
21. GETCLS:	GTABLE, INDEX
22. GETCMS:	GTABLE, INDEX
23. HYSDMP:	NVDAMP
24. INISH:	ACLMP, ADERIV, ADMPAD, BLDDØF, BLØCKS, DISTRB, DØFVAR, ELASAX, GLAURT, GUST, HARRAY, IMISC1, ISWCH, LINEAR, MISC1, MISC2, MISC3, MISC4, MISC5, MISC6, NVDAMP, PANPER, PNAIR, SAVHAR, SINTS, SPNVAR, SYNC, SYND
25. INITT:	BLØCKS, MISC1, MISC3, MS159, SYNC, SYND, TRIM, TRNSNT

151

Table IX (Cont'd)

Element	Common Block Names											
26. INTCØF:	ADERIV	BLDDØF	BLØCKS	DISTRB	ELASAX	IMISC1	LINEAR	MISC1	MISC2	SINTS	SINTS2	TRIM
27. LNAERØ:	ADERIV	BLØCKS	MISC2									
28. LØADER:	BLØCKS	MISC3										
29. MAIN:	BLDDØF	CLDMTB	DISTRB	DØFVAR	LINEAR	MISC1	MISC3	MS159	TRNSNT			
30. MAJITR:	ADERIV	BLDDØF	BLØCKS	DISTRB	DØFVAR	ELASAX	GLAURT	GUST	HARRAY	IMISC1	LINEAR	MISC1
	MISC3	MISC4	MISC5	MISC6	SPNVAR	TRIM	TRNSNT	PANPER	SPNVAR	MISC1	MISC2	
31. MATRXT:	ADERIV	AERØT	AGONY	BLDEFL	BLDDØF	MISC1	MISC2	DISTRC	ELASAX	GLAURT	HARRAY	
	IMISC1	LINEAR	DISTRB	MATRX1				CLDMTB	MISC6	YZ5DRV	CTTECT	NLTEXC
32. MØDEIN:	BLØCKS	DISTRB										
33. MØTIØN:	ADERIV	BLØCKS	DØFVAR	ELASAX	GLAURT	GUST	MISC1	MISC2	MISC3			
	MISC4	MISC6	NVDAMP	SPNVAR	TRIM	TRNSNT						
34. NIAM:	ABC	ADERIV	ADMPAD	BLDDØF	BLØCKS	CLDMTB	DISTRB	ELASAX	IMISC1	LINEAR	MISC1	MISC2
	MISC3	PANPER	TWIST									
35. PADCØF:	ADERIV	BLØCKS	MISC1	PADIV								
36. PANMØM:	BLØCKS	GLAURT	MISC2	MISC3								
37. PHASE:	LINEAR	MATRX4										
38. PHIDØT:	SYND											
39. PNPRSU:	AVQS	BLDDØF	BLDEFL	BLØCKS	DISTRB	DØFVAR	ELASAX	GUST	HARRAY	LINEAR	IMISC1	MATRX1
	MISC2	MISC4	MISC5	MISC6	NLTEXC	PNAIR						MISC1
40. PRNT:	BLØCKS											
41. QPPCAL:	BLDDØF	DØFVAR	LINEAR									
42. QPPTST:	BLDDØF	DØFVAR										
43. QQPSET:	BLDDØF	DØFVAR										
44. QSTHRM:	BLØCKS	DISTRB	HARRAY	LINEAR	MISC1							
45. REDATA:	CLDMTB	MISC3										
46. RESETG:	BLØCKS	DISTRB	LINEAR	MISC1	TRNSNT							
47. RESETQ:	BLØCKS											
48. REVERS:	FACTOR											
49. REVPAD:	ADMPAD	PADE	PADIV	SINC								
50. RSPNSS:	AVQS	BLDDØF	BLØCKS	DØFVAR	GUST	HARRAY	IMISC1	LINEAR	MISC1	MISC2	MISC4	MISC5
51. SBSCRP:	FACTOR											
52. SCTAB:	INPUT											
53. SETUP:	BLDDØF	BLØCKS	DISTRB	DØFVAR	IMISC1	LINEAR	MISC1	MISC2	MISC4	MISC5		
54. SETVAL:	MISC1	SYNC	SYND									
55. SHLDM:	ADERIV											
56. SØLVE:	ABC	DISTRB	IMISC1	LINEAR	MATRX4							
57. SPANS:	ADERIV	BLDDØF	BLDEFL	BLØCKS	DISTRB	DØFVAR	ELASAX	GLAURT	GUST	HARRAY	IMISC1	LINEAR
	MISC2	MISC3	MISC4	MISC5	MISC6	NLTEXC	NVDAMP	PADE	PADST	PANPER	PNAIR	SPNVAR
	TRIM	TRNSNT	TWIST									
58. SPNWIZ.	BLØCKS	MISC1	SYNTHP									

152

Table IX (Cont'd)

Element	Common Block Names
59. SPRINT:	SINTS SINTS2
60. STRSSS:	BLØCKS BLDDØF DISTRB DØFVAR ELASAX GLAURT HARRAY IMISC1 LINEAR MISC1 MISC2 MISC3 MISC4 MISC5 SPNVAR TRNSNT
61. SUBS:	FACTØR INPUT
62. SYNTH3:	ADERIV ARES ETAS PEAK PEESP PLUS QUES SENDS SYNTHP
63. TABLE:	BLØCKS MISC1 MISC1
64. TCØUPL:	BLOCKJ DISTRB DISTRB MISC2 SINTS
65. TMARCH:	ADERIV BLDDØF BLØCKS DISTRB DØFVAR ELASAX GLAURT HARRAY IMISC1 LINEAR MISC1 MISC2 MISC3 MISC4 MISC5 MISC6 SPNVAR TRIM TRNSNT
66. TMSS:	BLØCKS MISC1 TØRSN
67. TWOF:	BLØCKS DISTRB MISC1
68. UNDATA:	ALCH DTABLE GTABLE INDATA INDRG PREDM RANG TABR
69. UNSTCF:	GETCS SENDS SYNB
70. VARINF:	BLØCKS MISC1 PANPER
71. VECTRS:	BLDDØF BLDEFL CLDMTB DISTRB ELASAX IMISC1 LINEAR MISC1 MISC2 YZ5DRV
72. WAKVCZ:	BLØCKS PLØVAR TRNSNT

153

Table IX (Cont'd)

Part 2. Element Name Per Common Block

Common Block	Element Names
1. ABC:	AIRPAD, INISH, FILL2, NIAM, SØLVE
2. ACL:	
3. ADERIV:	AERØ, SHLDM, AERPRF, SPANS, AIRPAD, SYNTH3, NIAM, DEFLEX, BLADEL, TMARCH, PADCØF, MATRXT, ENDCØN, INISH, INTCØF, LNAERØ, MAJITR, MØTIØN, NIAM, PADCØF
4. ADMPAD:	AIRPAD, INISH, NIAM, DEFLEX, REVPAD
5. AERØT:	AERØ, AIRPAD, AIRPAD, MATRXT, DEFLEX
6. AGØNY:	AIRPAD, MATRXT, UNDATA, SYNTH3
7. ALCH:	CØEFF3
8. ARES:	CØEFF3, SYNTH3
9. AVGQS:	PNPRSU, RSPNSS
10. BLDDØF:	AERØ, QQPCAL, AIRPAD, QPPTST, BLADEL, QQPSET, DEFLEX, RSPNSS, MATRXT, DPCHEK, SETUP, PNPRSU, FILL, SPANS, SPANS, INISH, STRSSS, VECTRS, MAIN, VECTRS, MATRXT, NIAM, PNPRSU
11. BLDEFL:	AERØ, AERPRF, AIRPAD, DEFLEX, BLADEL, MATRXT
12. BLØCKS:	AERØ, LNAERØ, RESETQ, AERPRF, LØADER, RSPNSS, AIRPAD, MAJITR, SETUP, BLINS, MATRXT, BLADEL, MATRXT, SPANS, MAIN, BLIN5, MØDEIN, STRSSS, MATRXT, DEFLEX, MØTIØN, TABLE, NIAM, DFYZEA, NIAM, TCØUPL, REDATA, ENDCØN, PADCØF, TMARCH, VECTRS, E159, PANMØM, TMSS, FILL, PNPRSU, TWØF, INISH, PRNT, VARINF, INITT, QSTHRM, VECTRS, INTCØF, RESETG, WAKUCZ
13. CLDMTB:	AERØ, AIRPAD, MATRXT
14. CTTEC:	AERØ, AIRPAD, AIRPAD
15. DISTRB:	AERØ, MATRXT, TWØF, AERPRF, MØDEIN, VECTRS, AIRPAD, MØTIØN, BLADEL, NIAM, DEFLEX, PNPRSU, DFYZEA, QSTHRM, ENDCØN, RESETG, E159, SETUP, FILL, SØLVE, INISH, SPANS, INTCØF, STRSSS, MAIN, TCØUPL, MAJITR, TMARCH
16. DISTRC:	AIRPAD, MATRXT
17. DØFVAR:	AERPRF, SETUP, BLADEL, SPANS, DEFLEX, STRSSS, ENDCØN, TMARCH, INISH, MAIN, MAJITR, MØTION, PNPRSU, QPPCAL, QPPTST, QQPSET, RSPNSS
18. DTABLE:	GETCDS, UNDATA
19. ELASAX:	AERØ, PNPRSU, AERPRF, SPANS, AIRPAD, STRSSS, BLADEL, TMARCH, DEFLEX, VECTRS, DFYZEA, ENDCØN, INISH, INTCØF, MAJITR, MATRXT, MØTIØN, NIAM
20. ETAS:	CØEFF3, SYNTH3, SUBS
21. FACTØR:	FFTGEN, REVERS, SBSCRP, FILL2
22. FØRIER:	AERØ, EIGSLN
23. GETCS:	CØEFF3, UNSTCF
24. GLAURT:	AERØ, TMARCH, AERPRF, AIRPAD, BLADEL, ENDCØN, INISH, MAJITR, MATRXT, MØTIØN, NIAM, PANMØM, SPANS, STRSSS
25. GTABLE:	GETCLS, GETCMS, UNDATA
26. GUST:	AERPRF, BLADEL, ENDCØN, INISH, MAJITR, MØTIØN, PNPRSU, RSPNSS, SPANS, TMARCH, QSTHRM
27. HARRAY:	AERØ, TMARCH, AERPRF, AIRPAD, BLADEL, ENDCØN, MAJITR, INISH, MØTIØN, PNPRSU, MAJITR, RSPNSS, SPANS, QSTHRM, MØTIØN, INISH, STRSSS

154

Table IX (Cont'd)

Common Block	Element Names
28. IMISC1:	AERO AERPRF AIRPAD BLADEL DEFLEX EIGSLN ENDCØN INISH INTCØF MAJITR MATRXT MØTIØN NIAM PNPRSU RSPNSS SETUP SØLVE SPANS STRSSS TMARCH VECTRS
29. INDATA:	CØEFF3 UNDATA
30. INDEX:	CØEFF3 GETCDS GETCLS GETCMS UNDATA
31. INDRG:	CØEFF3 UNDATA UNDATA
32. INPUT:	FFTGEN SUBS SCTAB
33. ISWCH:	INISH
34. LINEAR:	AERO AERPRF AIRPAD BLADEL CRØUTS DEFLEX EIGRMC EIGSLN ENDCØN E159 FILL FILL2 INISH INTCØF MAIN MAJITR MATRXT MØTIØN NIAM PHASE PNPRSU QPPCAL QSTHRM RESETG RSPNSS SETUP SØLVE SPANS STRSSS TMARCH VECTRS
35. MATRX1:	AERØ AIRPAD DEFLEX MATRXT PHASE SØLVE
36. MATRX4:	FILL2 SØLVE
37. MISC1:	AERØ AERPRF AIRPAD BLADEL DEFLEX DPCHEK ENDCØN E159 FILL FILL2 INISH INITT INTCØF LNAERØ MAIN MAJITR MATRXT MØTIØN NIAM PADCØF PNPRSU QSTHRM RESETG RSPNSS SETUP SETVAL SØLVE SPANS STRSSS TABLE TCØUPL TMARCH TMSS TWØF VARINF VECTRS
38. MISC2:	AERØ AERPRF AIRPAD BLADEL DEFLEX ENDCØN FILL INISH INITT LØADER MAJITR MØTIØN NIAM PANMØM PNPRSU RSPNSS SETUP SPANS STRSSS TCØUPL TMARCH VECTRS
39. MISC3:	AERØ AERPRF AIRPAD BLADEL DEFLEX ENDCØN INISH MAIN MAJITR MATRXT MØTIØN NIAM PANMØM REDATA SPANS STRSSS
40. MISC4:	AERØ AERPRF AIRPAD BLADEL DEFLEX ENDCØN INISH MAJITR MATRXT MØTIØN PNPRSU RSPNSS SETUP SPANS STRSSS TMARCH
41. MISC5:	AERØ AERPRF AIRPAD BLADEL INISH MAJITR MATRXT MØTIØN PNPRSU RSPNSS SETUP SPANS STRSSS TMARCH
42. MISC6:	AERØ AERPRF AIRPAD BLADEL INISH MAJITR MATRXT MØTIØN SPANS TMARCH
43. MSC159:	E159
44. MS159:	E159 INITT MAIN
45. NLTEXC:	AERØ AIRPAD DEFLEX MATRXT MØTIØN SPANS
46. NVDAMP:	BLADEL HYSDMP INISH PNPRSU SPANS
47. PADE:	REVPAD
48. PADIV:	AIRPAD PADCØF REVPAD SPANS
49. PADST:	
50. PANPER:	AERØ AERPRF AIRPAD INISH MAIN NIAM SPANS VARINF
51. PNAIR:	INISH PNPRSU
52. PEAK:	CØEFF3 SYNTH3
53. PEESP:	CØEFF3 SYNTH3
54. PLØVAR:	WAKUCZ
55. PLUS:	CØEFF3 SYNTH3
56. PREDM:	CØEFF3 UNDATA

155

Table IX (Cont'd)

Common Block	Element Names											
57. QUES:	CØEFF3	SYNTH3										
58. RANG:	CØEFF3	UNDATA										
59. SAVHAR:	INISH											
60. SENDS:	SYNTH3	UNSTCF										
61. SINC:	REVPAD											
62. SINTS:	BLADEL	FILL	INISH	INTCØF	SPRINT							
63. SINTS2:	BLADEL	FILL	INTCØF	SPRINT	TCOUPL							
64. SPNVAR:	AERPRF	BLADEL	DEFLEX	ENDCØN	INISH	MAIN	MAJITR	MØTIØN	SPANS	STRSSS	TMARCH	
65. SYNB:	UNSTCF											
66. SYNC:	ALWCØM	INISH	SETVAL									
67. SYND:	ALFDØT	INISH	PHIDØT									
68. SYNTHP	ENDCØN	INISH	SPANS	SYNTH3								
69. TABR:	CØEFF3	UNDATA										
70. TØRSN:	E159	TMSS										
71. TRIM	AERPRF	BLADEL	ENDCØN	INISH	INTCØF	MAJITR	MØTIØN	SPANS	TMARCH			
72. TRNSNT:	AERPRF	BLADEL	ENDCØN	INISH	MAIN	MAJITR	MØTIØN	RESETG	SPANS	STRSSS	TMARCH	WAKUCZ
73. TWIST:	NIAM	SPNWIZ										
74. YZ5DRV:	AIRPAD	DEFLEX	MATRXT	VECTRS								

156

<center>Brief Description of Program Elements</center>

ADAMS

This function implements an algorithm for time integration of any of the time dependent variables.

ADMCOF

This subroutine evaluates the coefficients required for the time integration algorithm.

AERO

This subroutine generates the aerodynamic damping and stiffness matrices for the eigensolution assuming a quasi-static formulation, blade motion and aerodynamic sweep effects.

AERPRF

This subroutine completes the calculations for and outputs the summary of aerodynamic performance quantities.

AIRPAD

This subroutine generates the aerodynamic inertia, damping and stiffness submatrices for the eigensolution assuming a Pade' formulation, blade motion and aerodynamic sweep effects.

ALFDOT

This subroutine calculates the aerodynamic A parameter using backward differencing on the inflow angle and direct knowledge of the time derivative of pitch.

ALWCOM

This subroutine calculates the unsteady decay parameter, $\alpha_{\bar{w}}$, required for the unsteady stalled and generalized Wagner function airloads methodologies.

BLADEL

This subroutine provides the computational loop structuring over number of blades in forming the blade response equations. This loop for G400PROP is presently degenerate and the upper limit on this loop is 1.

<center>157</center>

BLIN5

This subroutine does a tri-variant table look-up of the airfoil section coefficients. The three variables are angle-of-attack, Mach number and spanwise station.

BMEVAL

This subroutine evaluates the bending mode shape and its derivatives at spanwise locations other than where they are calculated in the E159 eigensolution.

BMFIT

This subroutine performs a functional (polynomial) fit of the bending mode shape for use in subroutine BMEVAL for evaluating bending mode shapes at nonstandard spanwise locations.

COEFF3

This subroutine calculates various coefficients needed for the UTRC stalled unsteady airloads methodology.

CROUTS

This subroutine is a compact simultaneous equations solver used for nonteetered rotor configurations. It uses the Crout Reduction method described in Reference 22.

DEFLEX

This subroutine evaluates the spanwise deflections, slopes, velocities, etc. from the modal responses, forms the sweep transformations and, for the eigensolutions, forms various deflection partial derivaties. DEFLEX typically operates within the spanwise loop of the calling subroutine.

DFYZEA

This subroutine forms the spanwise derivative of the structural sweep angles form the input sweep changes per segment length, or from numerical differentiation.

DISCRT

The purpose of this subroutine is to compute the magnitude of the Fourier coefficient, CMAG, of a set of time-history data, as part of the transient spectral stability analysis (TSSA).

DPCHEK

This subroutine tests the input integration steps size for acceptable accuracy, and automatically decreases it if the value is too large.

EIGENE

This subroutine performs the eigensolution of the bending portion of the E159 preprocessor for uncoupled blade frequencies and mode shapes. It uses the method of determinant iteration.

EIGRMC

The purpose of this subroutine is to coordinate the running of the standard nonsymmetric matrix eigensolution subroutine, RGG, to the extent of organizing the root pairs which are caluclated for the main (G400) eigensolution.

EIGSLN

This subroutine coordinates the setup of the main (G400) eigensolution. Specifically, it controls the calculation of the matrices comprising the eigensolution, and the extraction of the eigenvalues.

ELAST

The purpose of this subroutine is to calculate the elastic coefficients for flatwise and edgewise bending for the E159 eigensolution.

ENDCON

This subroutine serves three main functions associated with the completion of the Part II time-history solution: (1) it completes the calculations for median and 1/2 peak-to-peak stresses, (2) it controls the harmonic analyses of responses hub loads and stresses, and (3) it controls the saving of end conditions and other data for use in either the PANPER code or subsequent G400 runs.

EXTRAP

This subroutine effects a "static" solution on any degree-of-freedom whose natural frequency is sufficiently high to approximate the response neglecting the twice time differentiated term in that degree-of-freedom's governing equation.

E159

This subroutine controls the preprocessor calculations of the uncoupled modal frequencies and mode shapes for flatwise and edgewise beam bending, and for torsion responses.

FFTGEN

This subroutine is a standard Fast Fourier Transform calculator, and is used in the transient spectral stability analysis (TSSA).

FILL

The purpose of this subroutine is to fill in the nonaerodynamic portions of the mass, damping and stiffness matrices used in the main (G400) eigensolution.

FILL2

This subroutine arranges the various matrices and submatrices set up by subroutines FILL and AERO or AIRPAD into the semi-canonical form required for eigenvalue extraction by the standard eigensolution solver, RGG.

FLGDR

This function evaluates any of the first five Legendre polynomials.

GETCDS

This subroutine provides internally calculated static aerodynamic drag data in place of user provided static airfoil data for usage in the unsteady stalled airloads calculation.

GETCLS

This subroutine provides internally calculated static aerodynamic lift data for usage in the unsteady stalled airloads calculation.

GETCMS

This subroutine provides internally calculated static aerodynamic
moment data for usage in the unsteady stalled airloads calculation.

GJR

This utility subroutine optionally obtains simultaneous equation solu-
tions and/or matrix inversions using the Gauss-Jordan Reduction method.

HARM

This utility subroutine performs a Fourier (harmonic) Analysis of any
time-history string of data. This harmonic analysis uses a negative cosine
and sine definition for the harmonic components.

HYSDMP

This subroutine calculates the increment to blade edgewise bending
moment to account for hysteretic structural damping. This formation of
structural damping is dependent on edgewise deflection and the signs of
rate and acceleration, but not their magnitudes.

INISH

This subroutine initializes arrays and logic variables, and nondimen-
sionalizes parameters, as required for the time-history solution.

INITT

This subroutine zeros out the various arrays in common "BLOCKS".

INTCOF

This subroutine forms the various elastomechanic integration constants
used in the eigensolution and, to a limited extent, in the time-history
solution.

INTERP

This subroutine is a general purpose linear interpolation calculator.

INVERT

This subroutine is a general purpose matrix inversion, determinant cal-
culator used by the E159 eigensolution.

LFCT

This subroutine finds the prime decomposition of any integer for use with the Fast Fourier Transform subroutine, FFTGEN.

LINFIT

This subroutine performs a least-square fit to results from the transient spectral stability analysis routine, WAKUCZ.

LNAERO

This subroutine calculates partial derivatives of airfoil section coefficients with respect to angle-of-attack and Mach number.

LOADER

The purpose of this subroutine is the loading of the generic loader portion of the input data.

MAIN

This is the main program element and directs all major portions of the solution flow.

MAJITR

This routine contains the time marching computation loop used in the time-history solution; it calls the specialized calculation subroutines needed in this loop.

MATRXT

The purpose of this subroutine is the calculation of various partial derivative matrices used by subroutines AERO and AIRPAD to calculate the aerodynamic portions of the main (G400) eigensolution.

MAXIMZ

The purpose of this subroutine is to maximize the magnitude of the Fourier coefficient as a function of frequency in the vicinity of an identified high response frequency, as part of the transient spectral stability analysis.

MODEIN

This utility subroutine inputs the blade bending and torsion mode shapes and their derivatives with respect to span.

MODULS

The purpose of this utility subroutine is to form the modulus of a vector of Fourier transforms.

MOMNTM

This function evaluates an empirical function joining the two branches of the actuator disk momentum equation across the vortex ring state based on a function given in Reference 31.

MOTION

This subroutine controls all the major elements of the time-history solution.

NFMS

This subroutine controls the calculation of the uncoupled beam bending vibration modes within the E159 eigensolution preprocessor.

NIAM

This subroutine performs the following functions:

1. Performs some of the detailed initializations and/or nondimensionalizations of logic and system parameters.

2. Calculates the deflection correction function arrays which accrue from structural twist and sweep.

3. Controls the calculation of the vacuum and nonvacuum main eigensolutions.

NPRM

This utility subroutine finds the next prime number given the vector of previous primes. It is intended for use with subroutine LFACT.

PADCOF

This subroutine evaluates the Padé coefficients using linear interpolation, as appropriate. It incorporates and optionally selects, the data from either the Jordan data, Davis and Malcolm data, or generalized Wagner function sources.

PANMOM

This subroutine forms the derivative of momentum induced velocity for use in the time-history solution.

PCHDAT

This utility subroutine output punches spanwise array elastomechanical data from the E159 portion of the program for subsequent optional explicit input to the G400 proper part of the program.

PCHMOD

This utility subroutine output punches spanwise mode shape data from the E159 portion of the program for subsequent optional explicit input to the G400 proper portion of the program.

PHASE

This subroutine evaluates the phasing matrices used by the eigensolution for stability analysis.

PHIDOT

This subroutine calculates the time derivative of inflow angles for use in subroutine REVPAD.

PNPRSU

This subroutine forms the geometric and aerodynamic parameters required by the Propeller/Nacelle Variable Inflow Analysis (PANPER).

PRNT

This subroutine provides an echo print output of the Part II input data which pertains to the Inertia, Elastic, Geometric and other Operational Data.

164

QPPCAL

This subroutine calculates the array of response accelerations for output print.

QPPTST

This subroutine tests the system degrees-of-freedom for numerical instabilities. The criteria used to identify such an instability are the occurrence of three sign changes of increasing amplitude in three time steps.

QQPSET

This subroutine sets the blade modal responses and modal rates for a given blade from the vectors of system response amplitudes and rates, respectively.

QSTHRM

This subroutine performs harmonic analyses (using subroutine HARM) of the blade modal responses, hub shears and moments, and blade stresses, after the responses have converged to periodicity.

QZHES

This subroutine is the first step of the QZ algorithm for solving generalized matrix eigenvalue problems, as required by subroutine RGG.

QZIT

This subroutine is the second step of the QZ algorithm for solving generalized matrix eigenvalue problems, as required by subroutine RGG.

QZVAL

This subroutine is the third step of the QZ algorithm for solving generalized matrix eigenvalue problems as required by subroutine RGG.

QZVEC

This subroutine is the fourth step of the QZ algorithm for solving generalized matrix eigenvalue problems as required by subroutine RGG.

REDATA

The prupose of this subroutine is to read the static airfoil data.

RESETG

This subroutine resets torsion mode shapes which might be displaced by the formation of the pseudo-torsion mode.

RESETQ

This subroutine places selected terminal conditions into an array and writes them to a data file for use as initial conditions for subsequent runs.

REVPAD

This subroutine calculates the Pade' augmented state variables used in the time-history solution of the differential equations for unstalled unsteady airloads.

RGG

This utility subroutine calculates the eigenvalues of the generalized nonsymmetrical matrix eigenproblem.

RSPNSS

This subroutine performs the following time-dependent calculations:

1. Forms the blade azimuth angle and various harmonics.

2. Sets the impressed control angle and its time derivatives.

3. Sets the modal response variables from various optional sources.

SBSCRP

This subroutine finds the mixed radix representation of an integer for use in the Fast Fourier Transform.

SCTAB

This utility subroutine exponentiates an angle multiplied by the imaginary vector, i.

SPNWIZ

This function performs a numerical integration between blade section centers of a specific integrand type as required for forming the deflection corrections functions due to structural twist.

SPRINT

This subroutine outputs (as optionally requested) the spanwise integration coefficients. Although most of these coefficients are required only for the eigensolution, some are used in the time-history solution.

STRSSS

This subroutine calculates the spanwise stresses and integrated hub loads optionally using the force integration or mode deflection methods.

SUBS

This subroutine computes appropriate subscripts and exponents for the Fast Fourier Transform.

SYNTH3

This subroutine is a component of the group of elements comprising the unsteady stalled airloads modeling wherein the final calculations of unsteady lift, drag and moment are made.

TABLE

This utility subroutine performs a table look-up and first derivative calculation for use in defining the instantaneous control angle.

TCOUPL

This subroutine calculates the coupled torsion modes arising from optional use of the rigid body degree-of-freedom with the E159 calculated elastic (normal) torsion modes.

TMARCH

This subroutine controls the solution flow for obtaining the time-history solutions. It furthermore tests for numerical instabilities and convergence to periodicity.

TMSS

This subroutine calculates the uncoupled torsion mode shapes and natural frequencies within the E159 eigensolution.

TWOF

This function performs a least-square curve fit calculation on blade twist to facilitate subroutine NIAM in the numerical differentiation of blade twist.

UNDATA

This element contains the empirical coefficients required by subroutine COEFF3 for using the unsteady stalled airloads calculation.

UNSTCF

This subroutine controls the implementation of the unsteady stalled airloads calculation.

VARINF

This subroutine serves as the input/output interface with the PANPER propeller/nacelle variable inflow program.

VECTRS

For any eigenvalue calculated by the main (G400) eigensolution, this subroutine calculates the coupled generalized mode shape and the spanwise components of the physical mode shape.

WAKUCZ

This subroutine performs the transient spectral stability analysis (TSSA) for extracting such stability indicators as characteristic exponent and time to half amplitude from the time-history solutions (see Reference 32).

PROGRAM INPUT DESCRIPTION

The required input to the program consists of the following major
data blocks in order of loading:

I.   Airfoil Data
II.   Inertia, Elastic, Geometric and other Operational Data
III. Blade Mode Shape Data
IV.   Components of Variable Inflow

Details for preparing the data for each of these blocks are given in
the subsections which follow. An additional subsection provides informa-
tion relating to efficient management of the data and to the input and out-
put of restart data using files.

I. Airfoil Data

This data block generally consists of one or more sets of tables of
two-dimensional lift, drag and pitching moment coefficients versus angle-
of-attack for various Mach numbers for up to five (5) arbitrary spanwise
locations. Additionally, if unsteady aerodynamics are used, the static
stall angles and linear coefficient slopes for both lift and pitching
moment are included in this table.

Input Format for First Card(s)

While actual set-up of this data block follows a basic format
(described below), specific variations are required on the first card(s)
of this block depending on optional usage. These variations denote whether
multiple data sets are to be input for respective spanwise locations, a
single set is to be input for use on all spanwise locations, or an analytic
representation of the NACA 0012 airfoil is to be used for all spanwise loca-
tions. Each of these optional usages is described below.

Multiple Spanwise Airfoils

For the case of distinct airfoil characteristics being defined at up to
five (5) multiple spanwise locations, the first card image format is as
follows:

card #1A:

    NA NRCL NRCD NRCM TITLE (optional)   (4I2,A72)

169

where NZ would be ignored so long as the sum of the absolute values of the quantities NRCL, NRCD and NRCM is 4 or greater. The quantities NRCL, NRCD and NRCM are, respectively, the number of radial stations for which multiple c_ℓ, c_d and $c_{m_c/4}$ airfoil data are to be input, as appropriate, each with a minimum absolute value of 1 and a maximum absolute value of 5. Normally, NRCL, NRCD and NRCM are input as positive integer numbers. The program also provides for the optional input of these data as negative values, in which case the extensive output point of these data, as part of the normal case printout, is suppressed. Note that at least one of these three inputs must have an absolute value of 2 or greater. For multiple spanwise section properties, an additional card, following the one described above, is then required, which begins the input of the c_ℓ airfoil data:

card #1B: NZ(1) RADCL(1)   TITLE(optional)   (I2, F8.0, A70)

where NZ(1) is the number of Mach number for which groups of c_ℓ data are to be read in for the first radial station; RADCL(1) is the nondimensional radial station at which the airfoil data is defined.

Single_Airfoil_Description

For the case of a single airfoil to be used for all spanwise locations, a single first card image is input. This card is similar to the card #1A described above, except that the quantities NRCL, NRCD and NRCM are input as zero (or the columns are left blank):

card #1   NZ(1)   0   0   0   TITLE(optional)   (4I2, A72)

In this case the card is interpreted as the first card of the c_ℓ data with the RADCL(1) information omitted (see description above for card #1B).

Analytic_Airfoil_Description

For those optional cases wherein the analytic NACA 0012 airfoil option is evoked (see "S" array location 63 discussed in the following subsection) the first card image must be a single card with blank or zeroed columns 1 through 8. For this option, the remainder of the airfoil data block of data is omitted.

170

Input Format for Subsequent Cards

For those cases wherein tabulated airfoil data are to be input, the subsequent inputs continue the airfoil c_ℓ data initiated with the #1A and/or #1B cards. Thus, the card image set-up defined below is then input NRCL times (or only once, if NRCL = 0):

card #2:

> J N M A(1) CL(2) A(2) CL(2) ... A(4) CL(4)   (I2, 10F7.0)

cards #2+:

> A(5) CL(5) ...   (F9.0, 9F7.0)

.
.
.

> ... A(N) CL(N)   ALSTAL DCLDAO   (F9.0, 9F7.0)

where: J is the number of data entries to be input into each Mach number group. N is the number of angle-of-attack -c_ℓ (abscissae - ordinate) pairs to be input. Normally, a maximum of thirty-four (34) α-c_ℓ pairs may be input; thirty-three (33) pairs are input if the unsteady option is chosen. M is the Mach number appropriate to the data group. A(i) are the N angle-of-attack abscissae in degrees and CL(i) are the N lift coefficient ordinates. ALSTAL and DCLDAO are, respectively, the static stall angle, in degrees, and the lift curve slope at zero angle-of-attack, in per degree; these items are needed only if the unsteady airloads option, (A)64, is invoked with a value of 2. Note that J is fixed-point formatted, but N and M are floating point formatted.

Cards 2 and 2+ are repeated for each successively higher Mach number. A maximum of 12 Mach numbers is allowed and the lowest and highest Mach numbers need not define the total working range as the search technique uses the boundary data for Mach numbers beyond the range input. Thus, repeated data for zero and supersonic Mach numbers are not needed. The lowest Mach number input must contain an angle-of-attack range from -180° to 180° or from 0° to 180° depending on whether or not unsymmetric airfoil data is being input; all higher Mach number data need extend only from -30° to 30° or from 0° to 30° in a similar manner.

The general format described above is repeated for the c_d and $c_{m_c/4}$ subblocks in that order but with either card image #1B or #1A used, depending

on whether multiple airfoil section data are or are not being input (and used). The static stall angles and aerodynamic coefficient curve slopes at zero angle-of-attack are deleted for the c_d subblock. Lastly, note that the total storage allocated for the combined airfoil data is 5000 (which is somewhat less than 2500 abscissa - ordinate point pairs). The maximum storage should be adequate for most applications and can be "budgeted" among the various spanwise sections, as appropriate.

II. Inertia, Elastic, Geometric and Other Operational Data

Generic Load Blocks

This data block includes those items used to define the more detailed dynamic features and/or those which are most likely to vary from case to case. The card image format for these data is as follows:

```
ZZ NN L DATA(L) DATA(L+1) ... DATA(L+4)      (A1, I1, I4, 5F12.0)
```

where: ZZ is an alphameric code item having the value "E", "R", "G", "D", "A", "V", "S", or "-". This alphameric input code determines into which generic loader block the data in the card image will be input. These generic loader blocks store data pertaining respectively to: the E159 preprocessor for calculating blade uncoupled frequencies and modes (see accompanying descriptive material). Radial distributions, Geometric charac-teristics, State Variables (functions of time), and Solution control. NN is the number of data items to be input on a given card; NN must not exceed 5. L is the location or identifying number within the indicated generic loader block of the first data item on the card columns 3-6 right adjusted. DATA(L+1) represents the various data items on the card image, columns 7-18, 19-30, 31-42, 43-54, and 55-66, in the floating point format. The loca-tions or identifying numbers for the various data and control items within each generic loader block are listed below along with definitions and other pertinent comments; note that some data locations are intentionally left blank. These intentionally blank data locations represent inputs defined for other more general versions of the G400 family of aeroelastic analyses but are not appropriate to this specialized propeller version of G400. By not reusing these data locations, the generic loader management permits input compatibility among the various versions of G400.

E159 Preprocessor for Uncoupled Modes

Data input to (E) loader block controls the optional internal calcula-tion of the required uncoupled blade modal data. This calculation thus

serves as a preprocessor for the main body of the G400PROP analysis. Use of this preprocessor is optional to the extent that, if available, these required modal data and related spanwise distributions can be input explicitly, without recourse to the E159 calculation as is described below. Use of the E159 processor within any given G400PROP run, however, enables the calculation and direct transfer of these data for subsequent usage within the main G400 calculations and would need not be explicitly input.

Furthermore, in the input descriptions to follow, there are apparent redundancies with regard to items in the (E) block and similar ones in the (R), (G) and (D) blocks. The redundancies and possible implied ambiguities where they occur are resolved within the program by a deference to the appropriate quantities which are output from the E159 preprocessor. Thus, irregardless of what is initially loaded in the (R), (G) and (D) generic loader data blocks, those quantities output from the E159 preprocessor (and arising from the input (E) loader data) are the ones which are used and subsequently ouptut in the echo listing of the input loader data. Note that in the descriptions to follow, those quantities which are redundantly defined in the (R), (G) and (D) loader blocks are dagger tagged (†). In the event that use of the E159 preprocessor is erronously requested together with explicit input of the modal shape data (see Section III below) the program will detect the ambiguity, print a warning and stop.

E159 Preprocessor Data

(E) Location	Item	Description
1	R	Rotor radius, ft
2	$\bar{e}$	Offset distance of start of elastically deformable portion of rotor blade, nondimensional with respect to R
3	NSEG	Number of segments into which the blade is partitioned
4-23	Δr	Blade breakup distribution of segment lengths, in order from root to tip, maximum of 20, in.
24	NFMC	Number of flatwise bending modes to be calculated
25	NEMC	Number of edgewise bending modes to be calculated
26	NTMC	Number of torsion modes to be calculated
27	(Control)	Make nonzero (1.) to output punch loader data and uncoupled mode shape data for direct input in subsequent runs
28-47	$(I/c)_F$	Section moduli for flatwise bending for sections defined in locations (E) 4-23, root to tip, in^3.
48-67	$(I/c)_E$	Section moduli for edgewise bending for sections defined in locations (E) 4-23, root to tip, in^3.
69	ΩR	Rotor tip speed, ft/sec.
70	(Control)	Make nonzero (1.) to output intermediary E159 calculations for debug purposes.

E159 Preprocessor Data - (Cont'd)

(E) Location	Item	Description
71	$\Delta \omega_{FE}$	Frequency scan interval for flatwise and edgewise bending frequency iteration; default value is .5, rad/sec.
100	N_w	Number of elements in weight distribution, table (equal to twice the number of constant value spanwise increments used).
101-150	$(w', \Delta s)$	Weight distribution table, taken as sequential ordinate-abscissa pairs, root to tip. Generally, this and all other distribution tables should include an extended final (tip) distribution spanwise increment so that the sum of the spanwise increments and the offset exceeds the radius by a sufficient amount to preclude diminution due to numerical round-off. $U(w'_k) =$ lbs/in; $U(\Delta s_k) =$ in.
252	N_{I_F}	Number of elements in flatwise area moment of inertia Table.
253-452	$(I_F, \Delta s)$	Flatwise area moment of inertia table (sec above remarks for w', Δs table); $U(I_{F_k}) = in^4$, $U(\Delta s_k) =$ in.
453	N_{I_E}	Number of elements in edgewise area moment of inertia table.
454-653	$(I_E, \Delta s)$	Edgewise area moment of intetia table (see above remarks for w', Δs table); $U(I_{E_k}) = in^4$, $U(\Delta s_k) =$ in.
655-674	$(x_i)_{NS}$	Stations other than those defined by the input breakup ((E)4-23) for purposes of evaluating the mode shapes.

175

(E) Location	Item	Description
676-695	ΔM_i	Discrete incremental masses added to centers of blade segments (defined by inputs ((E)4-23), lb-sec^2/ft.
696-715	K_{F_i}	Explicit flatwise hinge spring rates at inboard ends of selected blade segments to replace values obtained from input flatwise bending stiffness considerations, lb-ft/rad. (Note:(E) 696 and (E)716 should both be sufficiently large values to approximate infinite stiffness retention of a cantilever beam root boundary conditions.)
716-735	K_{E_i}	Explicit edgewise hinge spring rates at inboard ends of selected blade segments, to replace values obtained from input edgewise bending stiffness considerations, lb ft/rad. (See note above)
736	N_{GJ}	Number of elements in the torsion St. Venant torsion stiffness table.
737-886	$(GJ, \Delta s)$	Torsion stiffness table (see above remarks for w', Δ s table); U (GJ$_k$) = lb-in^2; U(Δs_k) = in.
887	N_{k_A}	Number of elements in spar area radius of inertia table.
888-1037	$(k_A, \Delta s)$	Spar area radius of gyration table (See remarks above for w', Δ s table); U (k_{A_k}) = in., U(Δs_k) = in.
1038	N_{I_θ}	Number of elements in torsional inertia distribution table.

(E) Location	Item	Description
1039-1188	$(I_\theta, \Delta s)$	Torsional inertia distribution table (See remarks above for w', Δs table); $U(I_\theta) = $ lb-sec^2). $U(\Delta s_k) = $ in.
1189	(Control)	Default value implies cantilever attachment at the root. Make (-1.) to activate root torsion spring restraint (input item (E) 1190).
1190	K_{θ_R}	Torsion root spring rate, lb-in/rad. (Note that this input and (D) 34 define a redundant capability. This input item includes the effect of root flexibility in the torsion mode directly, whereas (D) 34 is used to approximate this coupling "after the fact". Consequently, input items (E) 1190 and d(34) should not both be nonzero.
1191	(Control)	Innermost segment which is elastically active in torsion; default is 1.
1192	$\Delta \omega_T$	Frequency scan interval for torsion frequency iteration; default value in 5., rad/sec.
1193	E	Modulus of elasticity; default value is 1×10^7, lb/in^2.
1194	BSCALE	Factor used to scale the stiffness matrix to avoid erroneous zero evaluation of the determinant due to computer underflow or overflow; default value is 10^4. Indication of a need to vary this input is the calculation of bending mode shapes with frequencies equal to multiples of the scan interval (E) 71.

177

(E) Location	Item	Description
1195	(Control)	Make nonzero (1.) to activate the E159 uncoupled mode preprocessor branch of the program.
1541-1560	$k_{y_{10}}$	Thicknesswise mass radii of inertia for selected blade breakup, in. Note that nonzero values will cause the input torsion inertia to be represented by both thickness and chordwise radii of inertia (input items (R) 121-140 and (R) 141-160).
2000	(Control)	Case number for output generated by E159 branch of the program.

Radial Distributions

(R) Location	Item	Description
1-20	† Δx	Nondimensional blade segment lengths, in order from root to tip, maximum of 20 values, starting from the offset location. Accuracy is generally improved if the last segment is small (≤ 0.03).
21-40	† M_i	Mass of each blade segment, lb-sec^2/ft.
41-60	† $(EI)_F$	Flatwise bending stiffness, lb-in^2
61-80	† $(EI)_E$	Edgewise bending stiffness, lb-in^2
81-100	† $(I/c)_F$	Section modulii for flatwise bending, root to tip, in^3.
101-120	† $(I/c)_E$	Section modulii for edgewise bending, root to tip, in^3.
121-140	† $\bar{k}_{y_{10}}$	Thicknesswise mass radii of gyration of blade segments about axis perpendicular to chord line and through the reference axis, root to tip, nondimensional with respect to R.
141-160	† $\bar{k}_{z_{10}}$	Chordwise mass radii of gyration of blade segments about elastic (reference) axis, root to tip, nondimensional with respect to R.
161-180	† $\bar{k}_A$	Area radii of gyration about elastic axis, root to tip, nondimensional with respect to R.
181-200	$\bar{y}_{10_{CG}}$	Distances from elastic axis forward to airfoil section mass centers, root to tip, nondimensional with respect to R.
201-220	$\bar{e}_A$	Distances from reference (elastic) axis forward to edgewise bending neutral axis, root to tip, nondimensional with respect to R.

Radial Distributions (Continued)

(R) Location	Item	Description
221-240	$\bar{y}_{10_{EA}}$	Chordwise distances forward from the (extended) root pitch axis to the built-in elastic axis (defined herein as the locus of section shear centers), nondimensional with respect to R.
241-260	$\Delta\bar{y}_{10_{EA}}$	Built-in chordwise elastic axis offset change per segment (arc) length distribution. This item is a direct statement of the sine of the chordwise (forward) structural sweep angle distribution; if all values of this distribution are input as zero, the sweep angle sine distribution is computed internally using numerical methods from the offset data (R)221-(R)240 , as appropriate.
261-280	$\bar{z}_{10_{EA}}$	Thicknesswise distances from the root pitch axis to the built-in elastic axis (see above items (R)221 - (R) 240), (+) in the normally thrusting direction, nondimensional with respect to R.
281-300	$\Delta\bar{z}_{10_{EA}}$	Built-in thicknesswise elastic axis offset change per segment (arc) length distribution
301-320	EB_1	Torsional stiffness (to be multiplied by twist rate squared), as defined in Reference 4, lb-ft^4.
321-340	EB_2	Torsion to edgewise elastic coupling stiffness (to be multiplied by twist rate), as defined in Reference 4, lb-ft^3.
341-360	τ/M	Constants relating torsional moment to torsional stress, root to tip, in^{-3}.

Radial Distributions (Continued)

(R) Location	Item	Description
361-380	θ_{B_a}	Aerodynamic built-in nonlinear twist angle distribution, deg. Since collective angle is defined at the 75% span location, θ_{B_a} should have a zero value at 75% span. Should the structural twist angle distribution differ from θ_{B_a}, the appropriate data must be loaded into locations (R)381-(R)100; otherwise, θ_{B_a} will be used for both aerodynamic and structural applications.
381-400	θ_{B_s}	Structural built-in nonlinear twist angle distribution, root to tip if different from aerodynamic twist, deg. See remarks above for aerodynamic built-in twist, locations (R)361 - (R)380.
401-420	$\Delta\theta_B$	Built-in (structural) twist angle change per segment length distribution, root to tip deg. Note that this item is a direct statement of the built-in twist rate distribution, θ_B'; if all values of this distribution are input as zero, the twist rate distribution is computed internally using numerical methods from the input twist angle distributions, locations (R)361 - (R)380 or (R)381-(R)400, as appropriate.
421-440	c	Blade chord at center of each segment (use for nonconstant chord blades only), root to tip, ft.
441-460	$\bar{y}_{10_{c/4}}$	Distances from elastic axis forward to airfoil quarter chord position, root to tip, nondimensional with respect to R.
461-480	Λ_s	Aerodynamic built-in sweep angle distribution, positive aft, deg.

181

Radial Distributions (Cont'd)

(R) Location	Item	Description
481-500	$c_{d_{sf}}$	Blade airfoil section <u>skin friction drag coefficient</u>, for use with swept airfoil, skewed flow option.
501-520	$\zeta_{v_{se}}$	Distribution of edgewise nonviscous structural damping ($= g_v/2$, where g_v is the usual structural damping coefficient)
521-540	(Control)	Distribution of explicit airfoil shape similarity index for use with the <u>unsteady stalled airloads</u> option. A zero value denotes a default quasi-static airloads modeling whereas a value of (1., 2., 3.) denotes respective airfoil similarity with the (NLR-1, NACA 0012 (Mod), Vertol 23010-1.58) airfoil sections, all in the mid to high subsonic Mach number range.
541-560	(Control)	Distribution of optional selection modeling with the <u>unsteady unstalled airloads</u>. A value of (0., 1., 2.) denotes Padé approximants evaluated using (generalized Wagner function, analytic Jordan theory, experimental Davis data) aerodynamic sources, respectively.

Geometric Characteristics

(G) Location	Item	Description
1	$\dagger$ ΩR	Rotor tip speed, ft/sec
2	$\dagger$ R	Rotor radius, ft.
3	b	Number of blades
4	$\dagger$ $\bar{e}$	Nondimensional offset distance of start of deformable and/or deflectable portion of rotor blade, e/R
5	$\dagger$ NSEG	Number of blade segments used to define spanwise variable arrays
6	σ	Rotor area solidity (bc/πR)
7	$\theta_{1_{equ}}$	Linear equivalent blade twist angle, i.e., difference between tip and root built-in angles, positive when tip angle is greater (L.E. up) than root angle. Note, this input is the default value when both the built-in twist angle radial distributions have all zero values, deg.
8	c	Blade chord if chord is constant, ft.
10	β_B	Built-in precone angle, deg.
11	δ_B	Built-in prelead angle, deg.

Dynamic Related Parameters

(D) Location	Item	Description
1	NFM	Number of flatwise bending modes to be used (5 max)
2	NEM	Number of edgewise bending modes to be used (3 max)
3	NTM	Number of elastic torsion modes to be used (2 max)
4-8	† $\bar{\omega}_{w_i}$	Flatwise modal frequencies, nondimensional with respect to Ω, in ascending modal order.
10-12	† $\bar{\omega}_{v_k}$	Edgewise modal frequencies, nondimensional with respect to Ω, in ascending modal order
14,15	† $\bar{\omega}_{\theta_j}$	Torsion modal frequencies, nondimensional with respect to Ω, in ascending modal order
30	(Control)	In general, a nonzero value invokes the hysteretic (nonviscous) structural damping formulation in the edgewise bending mode equations. Specifically, make (1., 2.) to use (the constant location (D)31 value, a spanwise distribution of values) in this nonviscous formulation, respectively.
31	$\zeta_{v_{se}}$	Viscous damping equivalent critical damping ratio used to approximate structural damping in all edgewise bending modes
32	$\zeta_{w_{se}}$	Critical (viscous) damping ratio for structural damping in flatwise bending modes
33	$\zeta_{\theta_{se}}$	Critical (viscous) damping ratio for structural damping in torsion modes

Dynamic Related Parameters (Cont'd

(D) Location	Item	Description
34	$K_{\theta_{root}}$	Torsional spring rate connecting root of blade to fixed structure to represent control system flexibility, ft-lb/rad. A nonzero value will automatically introduce the rigid-body feathering degree-of-freedom as an additional "torsion mode".
39	g	Acceleration due to gravity, ft/sec^2; a negative value implies inverted flight.

Aerodynamic Characteristics

(A) Location	Item	Description
1	ρ	Air density, $lb\text{-}sec^2/ft^4$
2	a_∞	Speed of sound, ft/sec
3	B	Tip loss, used to define equivalent momentum area and three-dimensionality corrections to computed two-dimensional airloads near the blade tip.
4	Δc_{d_o}	Increment added to all values of c_d obtained from tabulated airfoil data or from the analytic NACA 0012 data. Airfoil data generally correspond to smooth wind tunnel models and Δc_{d_o} is often used to adjust for the higher drag of production blades; a commonly used value of Δc_{d_o} is 0.002
5	$N_{cut\text{-}out}$	Number of blade segments, starting at inboard end and defining the cut-out region for which the lift and moment coefficients are set to zero.
6	$(c_d)_{cut\text{-}out}$	The drag coefficient used on the first $N_{cut\text{-}out}$ segments.
7	κ_{vim}	Effectivity factor of the induced velocity calculated using actuator disk momentum considerations in calculating inflow angle at a local blade section. Default value is 1., corresponding to conventional usage of momentum actuator disk inflow. This input quantity can be used to approximate the effects caused by real inflow characteristics as modeled by more accurate theories. For such usage, the effectivity would typically be in the range of $1.0 \rightarrow 1.1$

186

Aerodynamic Characteristics (Cont'd)

(A) Location	Item	Description
21	V	Forward flight velocity, kts
22	α_s	Shaft angle-of-attack measured relative to vertical position, deg. Thus, a forward thrusting propeller would generally have the value -90.
28	$\theta_{.75R}$	Blade collective pitch angle as defined at the 75% radius, deg.
29	λ	Mean rotor inflow ratio
30-32	$\bar{v}_o, \bar{v}_{1_c}, \bar{v}_{1_s}$	Initial conditions on the "momentum" induced velocity components comprising a Glauert-like variable inflow description. Note that the "vorticity" variable inflow (controlled by locations (A)65 and (A)66. and the momentum variable inflow can be used separately or simultaneously.
61	(Control)	Make nonzero (1.) if airfoil data for a nonsymmetric airfoil are to be used.
62	(Control)	Make 1., to invoke the radial flow, swept airfoil option.
63	(Control)	Analytic (static) airfoil option. Make nonzero (1.) to use the built-in analytic approximation to the static NACA 0012 airfoil data.

(A) Location	Item	Description
64	(Control)	Unsteady airfoil data option. A zero (default) value invokes the use of the conventional quasi-static airloads description in both the eigensolution and time-history (t-h) solution. Nonzero values invoke the following usages:

1. = generalized Wagner function to define effective angle-of-attack; assumes unstalled aerodynamics, Pade form in eigensolution and tabular airfoil data look-up in t-h solu.;
2. = UTRC synthesized α, A, α_w method in the t-h solu, quasi-static in eigensolution; assumes dynamic stalled aerodynamics (see locations (R) 511-540)
3. = Complete Pade description in eigensolution and t-h solu.; t-h solu. uses filtering to define constant angles-of-attack for use with tabular airfoil data look-up; Pade airloads are then perturbational (see locations (R) 541-560).
4. = Complete Pade description without filtering in t-h solu.; non-perturbational usage with no tabular data look-up.

65	(Control)	Make nonzero (1.) to load (vorticity) induced velocity distributions from the PANPER code using the input unit code specified in input location (S)33.
66	(Control)	Make nonzero (1.) to use the (PANPER) induced velocity distributions loaded as per input locations (A)65 and (S)33.

Aerodynamic Characteristics (Cont'd)

(A) Location	Item	Description
68	(Control)	<u>Generalized Glauert</u> (momentum derived) <u>variable inflow</u> option. A zero value deactivates usage. A value of 1. causes the input induced velocity components to be used as constants; a value of 2. causes the velocity component, $\bar{v}_o$, to be varied to satisfy momentum considerations.
69	(Control)	Input nonzero (1.) to activate use of the <u>tabulated time-histories</u> of <u>incremental control angle</u>, $\angle\theta_{.75}$
70	(Control)	<u>Gust wave option</u>. Make (1., 2.) to use the input gust wave function table as (a gust factor,(ND);an incremental gust velocity, fps), respectively.
71	α_{G_w}	Inclination angle of the gust wave, deg. A positive value implies an upward component.
72	β_{G_w}	Side flow angle of the gust wave, deg. A positive value implies a component from the starboard side.
101	$N_{\Delta\theta_{.75}}$	Number of abscissa-ordinate point pairs used to define time-history of $\Delta\theta_{.75}(t)$; calculation of this time-history is bypassed with a zero value.
102-149	$\Delta\theta_{.75}$	Table of $\Delta\theta_{.75}$ abscissa-ordinate pairs; $U(\Delta\theta_{.75}) = {.75}$ deg.; U (t) = sec.
251	(Control)	Number of abscissa-ordinate point pairs used to define the time-history of the gust wave function; calculation is bypassed with a zero value.

(A) Location	Item	Description
252-299	f_{gust}	Table of gust wave function abscissa-ordinate pairs; $U(f_{gust})$ = (see input loc. (A)70); $U(t)$ = sec.
300	(Control)	<u>Static data utilization</u> option for use with the UTRC α-A-α_w synthesized unsteady stalled airloads. A value of (1., 2.) invokes the use of (input static data, built-in static data) respectively.
301	M_{lower}	Lower Mach number below which the UTRC unsteady airloads method is suppressed.
302	M_{upper}	Upper Mach number above which the UTRC unsteady airloads method is suppressed (0. = no upper limit).
305	(Control)	Input/Output unit code number for <u>restart output of unsteady parameters</u>. (.0 = input/output is suppressed).
306	(Control)	An input value of (0., 1.) causes the UTRC unsteady stalled airloads method to (omit, include), respectively, the calculation of <u>unsteady drag</u>.
307	$(A)_{max}$	Maximum (absolute) value of A parameter used in UTRC unsteady stalled airloads method (0. = no limit)
308	$(\alpha_w)_{max}$	Maximum (absolute) value of unsteady decay parameter, α_w, used in unsteady airloads formulations (0. = no limit)
309	$\bar{\omega}_{\phi}^*$	Frequency used for numerically differentiating inflow angle to calculate A parameter. Typical nonzero values would be blade 1st or 2nd torsion mode frequency. Zero value invokes numerical differentiation algorithm based on standard backward differencing techniques. Nondimensional with respect to Ω.

Aerodynamic Characteristics (Cont'd)

(A) Location	Item	Description
310	(Control)	Number of spanwise shape functions (Legendre polynomials) used for implementation of the Padé airloads in the eigensolution. (default = 1., maximum value = 5.)

State Variables

(V) Location	Item	Description
24	ψ	Initial condition on rotor azimuth, deg.
41–45	$\overset{*}{q}_{w_i}$	Initial conditions on i'th flatwise bending mode (nondimensional) rates
46–48	$\overset{*}{q}_{v_k}$	Initial conditions on k'th edgewise bending mode (nondimensional) rates
49,50	$\overset{*}{q}_{\theta_j}$	Initial conditions on j'th torsion mode (nondimensional) rates.
61–65	q_{w_i}	Initial conditions on i'th flatwise bending mode deflection.
66–68	q_{v_k}	Initial conditions on k'th edgewise bending mode deflections
69,70	q_{θ_j}	Initial conditions on j'th torsion mode deflections.

Solution Control Parameters

(S) Location	Item	Description
1	CASE	
6	(Control)	Make nonzero (1.) to output print the modal integration constants used in the eigensolution and, to a limited extent, in the time-history solution.
7	(Control)	Make nonzero (1.) to suppress the eigensolution
8	$\Delta \psi$	Azimuth increment used in the numerical integration of the dynamic equations, deg. (See section on general information for efficient program usage.)
9	N_F	Number of "flap trials", i.e., maximum number of rotor revolutions for which the blade time-history will be computed in an attempt to obtain convergence to periodicity. If a transient response is desired for only a portion of one rotor revolution the program will compute a time-history solution for any nonzero fractional N_F value input. An identically zero value will cause the time-history solution to be by-passed entirely.
10	ε_F	Flapping tolerance to within which the aeroelastic/dynamic responses must repeat on successive revolutions in order for the motion to be considered converged to periodicity.

Solution Control Parameters (Cont'd)

(S) Location	Item	Description
11	$\Delta\psi_{print}$	Azimuth increment used to present printed output of various pertinent aerodynamic, dynamic and elastic load distributions as well as aeroelastic responses and stresses, deg. This input quantity should be an integral multiple of location(S)8, deg.
12	(Control)	Make nonzero (1.) if the total (transient) time-history is to be output; i.e., responses calculated before convergence to periodicity is obtained.
15	(Control)	Make greater than zero (1.) for first case or when new blade modal data are to be input. Program automatically sets this control number to (-1.) after each loading of modal data.
21	(Control)	Input nonzero (1.) for stress calculations using the mode deflection method. Zero value defaults to force-integration method.
23	(Control)	Make nonzero (1.) if the modal responses and hub shears and moments are to be (negative) Fourier analyzed after periodicity has been obtained.
24	(Control)	Input nonzero (1.) to harmonically analyze and output harmonics of flatwise and edgewise bending stresses.
25	(Control)	Input nonzero (1.) to harmonically analyze and output harmonics of torsional stresses.
26	$\Delta\psi_{plot}$	Azimuth increment used to form the data strings for plotting purposes, deg. This input quantity should be an integral multiple of location (S) 8.

(S) Location	Item	Description
27-31	(Control)	Spanwise segment numbers for which stress data is to be saved for plotting or TSSA purposes (max value = 5.)
32	(Control)	Unit code number of file into which the saved time data strings are to be stored for subseqeunt plot or TSSA purposes (default = 12.)
33	(Control)	File unit code number for data transfer with PANPER code.
34	(Control)	File unit code number for use in saving end conditions for use as initial conditions in subsequent (restart) runs and/or with the PANPER code.
35	(Control)	Stress calculation supression option. Make value equal to (0., 1., 2.) to cause suppression of stress calculations for (nonoutputted responses only, nonoutputted responses and all transient responses, all responses), respectively.
37	(Control)	Selection of responses to be used for eigensolution linearization. Make (0., 1.) to use (initial input modal values, modal values azimuthally averaged from preceeding run), respectively.
41	SR	Sample rate for Transient Spectral Stability Analysis (TSSA). (See Reference 32 for a discussion of this technique.) Every (SR)'th point in a transient time-history is saved for use in a TSSA. A zero value bypasses the TSSA.

Solution Control Parameters (Cont'd)

(S) Location	Item	Description
42-44	(Control)	Channel selection for each of three available for the TSSA. The channels available are: 1-5, flatwise bending modal responses; 6-8, edgewise bending modal responses; 9,10 torsion modal responses; 11, 12 & 13, blade tip vertical, inplane and torsion deflections, respectively. In addition, channels 14 through 28 are available for stability analysis of the blade stresses as selected by input locations (S) 27-31. Thus, channels 14 thru 18 contain the five flatwise stresses, channels 19 thru 23 contain the five edgewise stresses and channels 24 thru 28, the five torsion stresses.
46	ω_L	Lower bound of frequency band chosen for TSSA nondimensional with respect to Ω.
47	ω_U	Upper bound of frequency band chosen for TSSA nondimensional with respect to Ω.
48	(Control)	Initial estimate of percentage of total transient data used in each time displaced data sample block in TSSA.
49	(Control)	Number of transient (time displaced) Fourier coefficient calculations made to establish modal damping in TSSA; maximum value is 200.
50	N_{FREQ}	Number of desired resonant frequencies to be extracted from frequency band defined by input locations (S) 46 and 47.

Solution Control Parameters (Cont'd)

(S) Location	Item	Description
99	(Control)	Location used to end a case or series of cases. Input (+1.) to end the Loader Format data block for the case defined by the Loader data and load additional cases at the conclusiom of that case. Make (-1.) to end the loader data and read no further cases. In both instances the combined aphameric code and word count, ZZ NN (see beginning of this section above) should be either (S1) or (-1). Note: this entry must appear singly on an input card, and that card must be the last card for the case.

Last Card Image for Block II (Loader) Data:

```
 ┌─────────────────────────────────────────────────────────────┐
 /  -1  99  ± 1.                               ( I2, I4, F12.0)  │
 │           ↑                                                   │
 │           │  ┌ +:  other cases follow                         │
 │           └──┤                                                │
 │              └ -:  preceeding data defines last case          │
 └─────────────────────────────────────────────────────────────┘
```
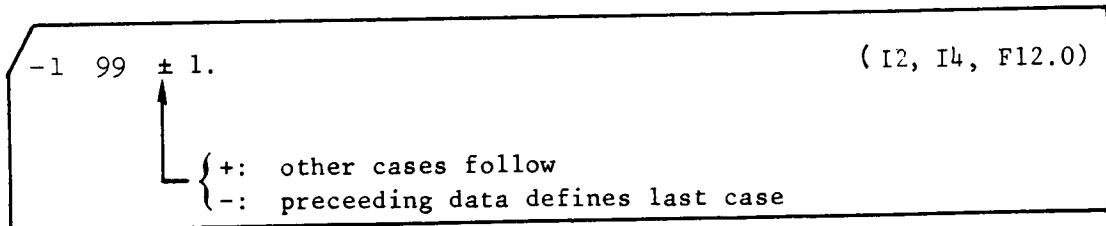
III. Blade Mode Shape Data

     Included in this data are the radial distributions of the blade (uncoupled)
flatwise, edgewise and torsion normal mode shapes and their derivatives. These
quantities are either calculated internally by the (activated) E159 branch of
the program (and not input as part of the input data) or are explicitly input
from some previous source. This previous source can be either the output from
the E159 branch itself (from some previous run), or an equivalent analysis.
In either case, these data are then input in the following card image format:

```
  NFM   NEM   NTM   NSEG                                    (4I4)
```

subsequent cards:

```
  F(i)   F(i+1)    F(i+2)   F(i+3)   F(i+4)          (F18.0, 4F12.0)
```

where: NFM, NEM, and NTM are, respectively, the numbers of flatwise bending,
edgewise bending and torsion normal modes whose mode shapes and derivatives
are to be input. NSEG is the number of blade spanwise stations for which
the input modal data are defined. F(i) are the modal functions listed below
(defined at the i'th spanwise stations). Five entries per card are made
for each F function input for NSEG total entries. The modal functions must
be loaded in the following order:

198

γ_{w_1} (NSEG values, root to tip)

γ'_{w_1} ("   "   "   "   ")

γ''_{w_1} •

γ_{w_2} •
.
                 •
.

.   (NFM flatwise modes)

γ_{v_1}

γ'_{v_1}

γ''_{v_1} (NEM edgewise modes)

γ_{v_2}
.

.

.

γ_{θ_1}

γ'_{θ_1}

γ_{θ_2}
.   (NTM torsion modes)

.

.

IV. Components of Variable Inflow

If location (A)65 of the Aerodynamics Characteristics Loader Block of operational data is nonzero, the following block of variable inflow is loaded in:

card #1:
```
(VINRAD (I), I = 1,8)                          (8F10.0)
```

card #1a:
```
(VINRAD (I), I = 9, 16)                        (8F10.0)
```

card #1b:
```
(VINRAD (I), I = 17, ...)                      (8F10.0)
```

card #2:
```
(VINTAN (I), I = 1, ...)                       (8F10.0)
```

card #3:
```
(VINAC (I), I = 1, ...)                        (8F10.0)
```

VINRAD (I), VINTAN (I), and VINAC (I) are, respectively, the radial, tangential, and axial components of the variable inflow at the I'th radial station, as provided by the PANPER routine. Card image #1a is provided if NSEG > 8. Card image #1b is provided if NSEG > 16, etc. Similarly, card image #2 is repeated until NSEG tangent values are completed, and card image #3 is repeated until NSEG axial values are completed.

V. Multiple Case Runs

The above described data setup defines the correct ordering of required data blocks for a general G400PROP case, or for the G400PROP portion of a more complicated multi-program run stream. When multiple cases are run (while remaining within the G400PROP portion of the run stream) the second and subsequent cases utilize most of the data input for the first case. The following rules apply to the running of mlutiple cases:

200

1. Airfoil data is loaded only for the first case; all subsequent cases within the run use the same tabular data, if analytic data is not used.

2. Only those items within th e operational generic (loader) data which are to be changed from case to case need to be input.

3. Item (S) 99 of the operational data controls the running of subsequent cases; a (+1.) value causes a subsequent case to be loaded whereas a (-1.) value terminates the computer run after the current case.

4. Unless otherwise specified (by a +1. value for operational data item (S) 15) the input modal array data block is used for all cases within the run.

5. Similarly, unless otherwise specified (by a +1, value for operational data item (A)65) and appropriate additional variable inflow data, the input variable inflow data block is used for all cases within the run.

6. Operational data items (S)15 and A(65) discussed above are both automatically set to zero at the conclusion of the data input for every case.

7. Terminal conditions on the blade azimuth angle, item (V) 24, and on the degrees-of-freedom, items (V)41-50 and (V)51-70, for any case are carried over as initial conditions on these quantities for the subsequent case. Thus, for some applications, e.g., investigations of unstable responses, it would be appropriate to reinitialize these items on the subsequent cases.

When solution flow leaves the G400PROP portion of a complex run stream, the ability to carry over terminal conditions (as initial conditions for a subsequent case) and/or any other quantities associated with trim is lost. However, a need still exists for preserving these initial conditions for subsequent reentries to the G400PROP portions of the run stream. As per loader locations (S)34 (described above) these initial conditions are written to and read from the file indicated in this input location.

PROGRAM OUTPUT DESCRIPTION

The complete printed output generated by the G400PROP program can be classified into the following seven major categories:

I.   Listing of Input Airfoil Data
II.   Results of Uncoupled Blade Mode Calculation
III.   Listing of Remaining Input Data
IV.   Parameters Calculated from Input Data
V.   Results of Solution Part I - Eigensolutions
VI.   Results of Solution Part II - Time-History Solution
VII.   Results of Solution Part III - Transient Spectral Stability
          Analysis

This section describes the pertinent output pages associated with each of these categories. Generally, output will always be generated only for the third category. Output for all other categories depends upon optional activation of the uncoupled blade mode calculation, solution parts I, II and/or III, and upon optional suppression of the airfoil data. The subsections which follow describe, in turn, the details of each of these seven categories. Where appropriate, reference is made to descriptions of input items described in an above section.

Listing of Input Airfoil Data

If static airfoil data is input, then a listing of this data will be output for c_ℓ, c_d and $c_{m_{c/4}}$ each with the format shown in Sample Page 1. First, each of the three aerodynamic section coefficient types is appropriately identified with a label. Next, if multiple spanwise airfoil data is input, the radial station at which the data is defined is output. The bulk of the remaining data on Sample Page 1 is the actual airfoil data wherein each column represents data at one Mach number. Within each column, the first line gives the number of angle-of-attack/aerodynamic coefficient pairs defining the functionality; the second line is the Mach number, and the ensuing line pairs are the angle-of-attack/aerodynamic coefficient pairs, where the angles-of-attack are in degrees. This output closely follows the input format description given in an above section. Note that if the number of radial stations for c_ℓ data sets is input negatively, then the total output of the airfoil data is suppressed.

CL TABLE

XCEN = X.XXXXX

| PT. PAIRS | XX.X | XX.X | XX.X | XX.X | XX.X | XX.X | XX.X | XX.X | XX.X | XX.X | XX.X | XX.X |
| MACH NO. | .XXXX | .XXXX | .XXXX | .XXXX | .XXXX | .XXXX | .XXXX | .XXXX | .XXXX | .XXXX | .XXXX | .XXXX |

(data rows of placeholder values: XXX.XXXX / XX.XXXXXX)

Sample Page 1.

Results of Uncoupled Blade Mode Calculation

A requirement for the use of the basic G400 analysis is a set of
uncoupled blade modal data consisting primarily of natural frequencies
and normal mode shapes (and their spanwise derivatives). Since the
initial development of the G400 code (Reference 1), the United Technologies
Corporation program E159 has been added to the G400 code in the form of
a preprocessor. Since the output from the E159 preprocessor impacts on the
Loader data used in the G400 proper portion of the code, it must be run
before the output of the Loader data. Hence, this output category pre-
ceeds the output of the remaining input data.

Sample Page 2 and the top of Sample Page 3 echo data input in the "E"
block of the Generic Loader data. The principal data output on Sample Page
2 are six pairs of columns defining the distributions of pertinent elasto-
mechanic properties starting at the blade root and progressing outward to
the blade tip. The lower, major portion of Sample Page 3 consists of four
columns, the first of which echos the selected blade segment breakup as
nondimensionalized by blade radius. The other three columns present at
each of the selected radial stations, in respective order, the lumped equi-
valent masses, the effective flatwise and edgewise elastic coefficients
(spring rates) as calculated from the input stiffnesses and segment lengths.
These elastic coefficients are used only internally to calculate the natural
modes. Sample Pages 4 and 5 present, for the selected radial stations, the
effective values of those elastic stiffness properties which are used by the
subsequent G400 proper portion of the code. On each of these sample pages,
the columns give the variations of properties together with the correspond-
ing selected blade segment breakup.

Sample Page 6 begins the output of the actual calculations for the
bending modes. The format of Sample Page 6 is used for both flatwise and
edgewise modes and the type of modal data being output is clearly indicated.
The first two rows of Sample Page 6 give the natural frequencies of the
flatwise modes in increasing order. The units of these frequencies, as
given in the first row, is either in rad/sec or per rotor rev depending on
whether the input rotor speed is zero or nonzero, respectively. The second
row values are always the same respective frequencies, but in units of Hz
(cycles/sec). The twelve columns which follow on this sample page consist
first of descriptors for the selected blade radial stations. The second
column (labeled X) gives the nondimensional spanwise stations as measured
from the axis of rotation, whereas the third column (labeled XFH) gives the
similar information, but instead from the offset point. The remaining
three groups of three columns give, for up to three modes, the mode shape
and derivative information, as indicated. The remaining three columns of
output at the bottom of the sample page give, for each respective mode,

OUTPUT FROM UNCOUPLED FREQUENCY AND MODE CALCULATION (E159 BRANCH) CASE NO. = XX

NO. OF FREQUENCIES REQUESTED XXXX FLATWISE XXXX EDGEWISE XXXX TORSIONAL

MODULUS OF ELASTICITY = .XXXX+YYY LBS/IN**2

WEIGHT LBS./IN.	RADIUS OF GYRATION OF SPAR- IN.	IN.	TORS. INERTIA OF BLADE LBS SEC**2	IN.	EDGEWISE AREA MOMENT INERTIA-IN**4	IN.	FLATWISE AREA MOMENT INERTIA-IN**4	IN.	GJ LBS-IN.**2	IN.
.XXXXX+YYY	X.XX	X.XX	.XXXXX-YYY	X.XX	.XXXXX+YYY	X.XX	.XXXXX+YYY	X.XX	.XXXXX+YYY	XX.XX
.XXXXX+YYY	X.XX	X.XX	.XXXXX-YYY	X.XX	.XXXXX-YYY	X.XX	.XXXXX-YYY	X.XX	.XXXXX+YYY	XX.XX
.XXXXX+YYY	X.XX	X.XX	.XXXXX-YYY	X.XX	.XXXXX-YYY	X.XX	.XXXXX-YYY	X.XX	.XXXXX+YYY	XX.XX
.XXXXX+YYY	X.XX	X.XX	.XXXXX-YYY	X.XX	.XXXXX+YYY	X.XX	.XXXXX-YYY	X.XX	.XXXXX+YYY	XX.XX
.XXXXX+YYY	X.XX	X.XX	.XXXXX-YYY	X.XX	.XXXXX+YYY	X.XX	.XXXXX-YYY	X.XX	.XXXXX+YYY	XX.XX
.XXXXX+YYY	X.XX	X.XX	.XXXXX-YYY	X.XX	.XXXXX+YYY	X.XX	.XXXXX-XXX	X.XX	.XXXXX+YYY	XX.XX
.XXXXX+YYY	X.XX	X.XX	.XXXXX-YYY	X.XX	.XXXXX+YYY	X.XX	.XXXXX+YYY	X.XX	.XXXXX+YYY	XX.XX
.XXXXX+YYY	X.XX	X.XX	.XXXXX-YYY	X.XX	.XXXXX+YYY	X.XX	.XXXXX-YYY	X.XX	.XXXXX+YYY	XX.XX
.XXXXX-YYY	X.XX	X.XX	.XXXXX-YYY	X.XX	.XXXXX+YYY	X.XX	.XXXXX-YYY	X.XX	.XXXXX+YYY	XX.XX
.XXXXX-YYY	X.XX	X.XX	.XXXXX-YYY	X.XX	.XXXXX+YYY	X.XX	.XXXXX-YYY	X.XX	.XXXXX+YYY	XX.XX
.XXXXX-YYY	X.XX	X.XX	.XXXXX-YYY	X.XX	.XXXXX+YYY	X.XX	.XXXXX-YYY	X.XX	.XXXXX+YYY	XX.XX
.XXXXX-YYY	X.XX	X.XX	.XXXXX-YYY	X.XX	.XXXXX+YYY	X.XX	.XXXXX-YYY	X.XX	.XXXXX+YYY	XX.XX
.XXXXX-YYY	X.XX	X.XX	.XXXXX-YYY	X.XX	.XXXXX-YYY	X.XX	.XXXXX-YYY	X.XX	.XXXXX+YYY	XX.XX

| TOTALS + E | XX.XX | XX.XX | | XX.XX | | XX.XX | | XX.XX | | XX.XX |

GJ BECOMES FINITE AT THE START OF SEGMENT NO. XX; THE PUSH-ROD IS LOCATED AT THE CENTER OF SEGMENT NO. XX.

Sample Page 2.

OMEGA-R = XXX.XXXX FT./SEC.

OMEGA = XXXXX.XX RPM (XXX.XXXXX CPS)

RADIUS = XXX.XXXX FT.

E/R = XXX.XXXX

FLATWISE AND EDGEWISE SCAN INTERVAL X.XXX

TORSIONAL SCAN INTERVAL X.XX

SCALE FACTOR XXXXX.XXX

ROOT IS RIGID

DELTA X	MASS-SLUGS	FLATWISE ELASTIC COEF. FT-LBS/RAD.	EDGEWISE ELASTIC COEF. FT-LBS/RAD.
.XXXXXX-YYY	.XXXXX	.XXXXXX+YYY	.XXXXXX+YYY
.XXXXXX-YYY	.XXXXXX-YYY	.XXXXXX+YYY	.XXXXXX+YYY
.XXXXXX-YYY	.XXXXXX-YYY	.XXXXXX+YYY	.XXXXXX+YYY
.XXXXXX-YYY	.XXXXXX-YYY	.XXXXXX+YYY	.XXXXXX+YYY
.XXXXXX-YYY	.XXXXXX-YYY	.XXXXXX+YYY	.XXXXXX+YYY
.XXXXXX-YYY	.XXXXXX-YYY	.XXXXXX+YYY	.XXXXXX+YYY
.XXXXXX-YYY	.XXXXXX-YYY	.XXXXXX+YYY	.XXXXXX+YYY
.XXXXXX-YYY	.XXXXXX-YYY	.XXXXXX+YYY	.XXXXXX+YYY
.XXXXXX-YYY	.XXXXXX-YYY	.XXXXXX+YYY	.XXXXXX+YYY
.XXXXXX-YYY	.XXXXXX-YYY	.XXXXXX+YYY	.XXXXXX+YYY
.XXXXXX-YYY	.XXXXXX-YYY	.XXXXXX+YYY	.XXXXXX+YYY
.XXXXXX-YYY	.XXXXXX-YYY	.XXXXXX+YYY	.XXXXXX+YYY
.XXXXXX-YYY	.XXXXXX-YYY	.XXXXXX+YYY	.XXXXXX+YYY
.XXXXXX-YYY	.XXXXXX-YYY	.XXXXXX+YYY	.XXXXXX+YYY
.XXXXXX-YYY	.XXXXXX-YYY	.XXXXXX+YYY	.XXXXXX+YYY
.XXXXXX-YYY	.XXXXXX-YYY	.XXXXXX+YYY	.XXXXXX+YYY
.XXXXXX-YYY	.XXXXXX-YYY	.XXXXXX+YYY	.XXXXXX+YYY
.XXXXXX-YYY	.XXXXXX-YYY	.XXXXXX+YYY	.XXXXXX+YYY
.XXXXXX-YYY	.XXXXXX-YYY	.XXXXXX+YYY	.XXXXXX+YYY
.XXXXXX-YYY	.XXXXXX-YYY	.XXXXXX+YYY	.XXXXXX+YYY
.XXXXXX-YYY	.XXXXXX-YYY	.XXXXXX+YYY	.XXXXXX+YYY
.XXXXXX-YYY	.XXXXXX-YYY	.XXXXXX+YYY	.XXXXXX+YYY
.XXXXXX-YYY	.XXXXXX-YYY	.XXXXXX+YYY	.XXXXXX+YYY

SUM OF THE DELTA XS + EOVR = XXX.XXXX

Sample Page 3.

206

DELTA X	FLATWISE EI/R (LB-IN2)/IN	FLATWISE I/C (IN**3)	EDGEWISE EI/R (LB-IN2)/IN	EDGEWISE I/C (IN**3)
.XXXXXX	.XXXXXX+YYY	.XXXXXX+YYY	.XXXXXX+YYY	.XXXXXX+YYY
.XXXXXX	.XXXXXX+YYY	.XXXXXX+YYY	.XXXXXX+YYY	.XXXXXX+YYY
.XXXXXX	.XXXXXX+YYY	.XXXXXX+YYY	.XXXXXX+YYY	.XXXXXX+YYY
.XXXXXX	.XXXXXX+YYY	.XXXXXX+YYY	.XXXXXX+YYY	.XXXXXX+YYY
.XXXXXX	.XXXXXX+YYY	.XXXXXX+YYY	.XXXXXX+YYY	.XXXXXX+YYY
.XXXXXX	.XXXXXX+YYY	.XXXXXX+YYY	.XXXXXX+YYY	.XXXXXX+YYY
.XXXXXX	.XXXXXX+YYY	.XXXXXX+YYY	.XXXXXX+YYY	.XXXXXX+YYY
.XXXXXX	.XXXXXX+YYY	.XXXXXX+YYY	.XXXXXX+YYY	.XXXXXX+YYY
.XXXXXX	.XXXXXX+YYY	.XXXXXX+YYY	.XXXXXX+YYY	.XXXXXX+YYY
.XXXXXX	.XXXXXX+YYY	.XXXXXX+YYY	.XXXXXX+YYY	.XXXXXX+YYY
.XXXXXX	.XXXXXX+YYY	.XXXXXX+YYY	.XXXXXX+YYY	.XXXXXX+YYY
.XXXXXX	.XXXXXX+YYY	.XXXXXX+YYY	.XXXXXX+YYY	.XXXXXX+YYY
.XXXXXX	.XXXXXX+YYY	.XXXXXX+YYY	.XXXXXX+YYY	.XXXXXX+YYY
.XXXXXX	.XXXXXX+YYY	.XXXXXX+YYY	.XXXXXX+YYY	.XXXXXX+YYY
.XXXXXX	.XXXXXX+YYY	.XXXXXX+YYY	.XXXXXX+YYY	.XXXXXX+YYY
.XXXXXX	.XXXXXX+YYY	.XXXXXX+YYY	.XXXXXX+YYY	.XXXXXX+YYY
.XXXXXX	.XXXXXX+YYY	.XXXXXX+YYY	.XXXXXX+YYY	.XXXXXX+YYY
.XXXXXX	.XXXXXX+YYY	.XXXXXX+YYY	.XXXXXX+YYY	.XXXXXX+YYY
.XXXXXX	.XXXXXX+YYY	.XXXXXX+YYY	.XXXXXX+YYY	.XXXXXX+YYY
.XXXXXX	.XXXXXX+YYY	.XXXXXX+YYY	.XXXXXX+YYY	.XXXXXX+YYY

Sample Page 4.

207

DELTA X	GJEFF/R (LB-IN2)/IN	GJ/R (LB-IN2)/IN	KA/R
.XXXXXX	.XXXXXX+YYY	.XXXXXX+YYY	.XXXXXX-YYY
.XXXXXX	.XXXXXX+YYY	.XXXXXX+YYY	.XXXXXX-YYY
.XXXXXX	.XXXXXX+YYY	.XXXXXX+YYY	.XXXXXX-YYY
.XXXXXX	.XXXXXX+YYY	.XXXXXX+YYY	.XXXXXX-YYY
.XXXXXX	.XXXXXX+YYY	.XXXXXX+YYY	.XXXXXX-YYY
.XXXXXX	.XXXXXX+YYY	.XXXXXX+YYY	.XXXXXX-YYY
.XXXXXX	.XXXXXX+YYY	.XXXXXX+YYY	.XXXXXX-YYY
.XXXXXX	.XXXXXX+YYY	.XXXXXX+YYY	.XXXXXX-YYY
.XXXXXX	.XXXXXX+YYY	.XXXXXX+YYY	.XXXXXX-YYY
.XXXXXX	.XXXXXX+YYY	.XXXXXX+YYY	.XXXXXX-YYY
.XXXXXX	.XXXXXX+YYY	.XXXXXX+YYY	.XXXXXX-YYY
.XXXXXX	.XXXXXX+YYY	.XXXXXX+YYY	.XXXXXX-YYY
.XXXXXX	.XXXXXX+YYY	.XXXXXX+YYY	.XXXXXX-YYY
.XXXXXX	.XXXXXX+YYY	.XXXXXX+YYY	.XXXXXX-YYY
.XXXXXX	.XXXXXX+YYY	.XXXXXX+YYY	.XXXXXX-YYY
.XXXXXX	.XXXXXX+YYY	.XXXXXX+YYY	.XXXXXX-YYY
.XXXXXX	.XXXXXX+YYY	.XXXXXX+YYY	.XXXXXX-YYY
.XXXXXX	.XXXXXX+YYY	.XXXXXX+YYY	.XXXXXX-YYY
.XXXXXX	.XXXXXX+YYY	.XXXXXX+YYY	.XXXXXX-YYY
.XXXXXX	.XXXXXX+YYY	.XXXXXX+YYY	.XXXXXX-YYY

Sample Page 5.

FLATWISE FREQUENCIES = XXX.XXXXX

			XXX.XXXXX CPS				XXX.XXXXX CPS				XXX.XXXXX CPS	
N	X	XFH	// MODE (1)	1ST DERV	2ND DERV	// MODE (2)	1ST DERV	2ND DERV	// MODE (3)	1ST DERV	2ND DERV
XX	.XXXXX	.XXXX	XXX.XXXXX	XXX.XXXXX	XXX.XXXXX	XXX.XXXXX	XXX.XXXXX	XXX.XXXXX	XXX.XXXXX	XXX.XXXXX	XXX.XXXXX
XX	.XXXXX	.XXXX	XXX.XXXXX	XXX.XXXXX	XXX.XXXXX	XXX.XXXXX	XXX.XXXXX	XXX.XXXXX	XXX.XXXXX	XXX.XXXXX	XXX.XXXXX
XX	.XXXXX	.XXXX	XXX.XXXXX	XXX.XXXXX	XXX.XXXXX	XXX.XXXXX	XXX.XXXXX	XXX.XXXXX	XXX.XXXXX	XXX.XXXXX	XXX.XXXXX
XX	.XXXXX	.XXXX	XXX.XXXXX	XXX.XXXXX	XXX.XXXXX	XXX.XXXXX	XXX.XXXXX	XXX.XXXXX	XXX.XXXXX	XXX.XXXXX	XXX.XXXXX
XX	.XXXXX	.XXXX	XXX.XXXXX	XXX.XXXXX	XXX.XXXXX	XXX.XXXXX	XXX.XXXXX	XXX.XXXXX	XXX.XXXXX	XXX.XXXXX	XXX.XXXXX
XX	.XXXXX	.XXXX	XXX.XXXXX	XXX.XXXXX	XXX.XXXXX	XXX.XXXXX	XXX.XXXXX	XXX.XXXXX	XXX.XXXXX	XXX.XXXXX	XXX.XXXXX
XX	.XXXXX	.XXXX	XXX.XXXXX	XXX.XXXXX	XXX.XXXXX	XXX.XXXXX	XXX.XXXXX	XXX.XXXXX	XXX.XXXXX	XXX.XXXXX	XXX.XXXXX
XX	.XXXXX	.XXXX	XXX.XXXXX	XXX.XXXXX	XXX.XXXXX	XXX.XXXXX	XXX.XXXXX	XXX.XXXXX	XXX.XXXXX	XXX.XXXXX	XXX.XXXXX
XX	.XXXXX	.XXXX	XXX.XXXXX	XXX.XXXXX	XXX.XXXXX	XXX.XXXXX	XXX.XXXXX	XXX.XXXXX	XXX.XXXXX	XXX.XXXXX	XXX.XXXXX
XX	.XXXXX	.XXXX	.....	.....	.....	.....	.....	.....	.....	.....	.....
XX	.XXXXX	.XXXX	XXX.XXXXX	XXX.XXXXX	XXX.XXXXX	XXX.XXXXX	XXX.XXXXX	XXX.XXXXX	XXX.XXXXX	XXX.XXXXX	XXX.XXXXX
XX	.XXXXX	.XXXX	XXX.XXXXX	XXX.XXXXX	XXX.XXXXX	XXX.XXXXX	XXX.XXXXX	XXX.XXXXX	XXX.XXXXX	XXX.XXXXX	XXX.XXXXX

SUMMATION(...)DX

(M*G)	.XXXX-YYY	
(M*G*X)	.XXXX-YYY	
(M*G*G)	.XXXX-YYY	
(G)	.XXXX+YYY	.XXXX-YYY	(LB-SEC2/FT2)
(G*X)	.XXXX+YYY	.XXXX-YYY	(LB-SEC2/FT2)
(G*(X**2))	.XXXX+YYY	.XXXX-YYY	(LB-SEC2/FT2)
(G*(X**3))	.XXXX+YYY	.XXXX-YYY
(G*(X**4))	.XXXX+YYY	.XXXX-YYY
(G*(X**5))	.XXXX+YYY	.XXXX-YYY
((G**2)*X)	.XXXX-YYY	.XXXX-YYY
((G*X)**2)	.XXXX+YYY	.XXXX-YYY

Sample Page 6.

209

various internally calculated modal integration constants as indicated by the definitions given parenthetically at the left of the page. Note that G refers to the respective mode shape array given directly above each of these three lower columns.

Sample Page 7 presents for the selected blade breakup the effective values of torsional inertia properties. The second column (labeled IXX) presents the section polar torsion inertia, being the sum of chordwise and thicknesswise mass moments of inertia. The third column presents the difference between the chordwise and thicknesswise mass moments of inertia. This difference of inertia distribution is the one which determines the so-called "propeller moment" torsional stiffening effect. The remaining columns are the mass radius of gyration distributions which, along with the output lumped equivalent masses, produce the values in the second and third columns.

Sample Page 8 presents the actual calculations for the torsion modes. As with the bending mode output, the first two rows of Sample Page 9 give the modal natural frequencies first in either rad/sec or per rotor rev, and then in the second row, cycles/sec. The remaining columns follow closely the format discussed above for the bending modes, except that only the first spanwise derivative is given for each mode. No modal integrations are performed for the torsion modes.

Listing of Remaining Input Data

Output in this category includes a descriptive listing of the Generic Loader data and a listing of the components of variable inflow obtained from the PANPER code. A description of the Generic Loader data output is omitted herein since this output merely duplicates the descriptions already given in even greater detail in a previous section. In Sample Page 9 is shown the listing of the variable inflow input from a data file (prepared by the PANPER code). This output consists of three columns together with a column giving the spanwise station index. The three data columns give the cylindrical coordinate system components of the variable inflow. The positive directions of the components are as follows: radial (VINRAD), positive outward; tangential (VINTAN), positive toward the leading edge; axial (VINAX), positive in the normally thrusting position, and all three components have the units of ft/sec.

Parameters Calculated from the Input Data

In Sample Page 10 is presented data pertaining to the built-in elastic axis offset (structural sweep). The various columns present spanwise

DELTA X	IXX (IN-LB-SEC2)	DELTA(IXX) (IN-LB-SEC2)	KY10 (IN)	KZ10 (IN)
.XXXXXX	.XXXXXX	.XXXXXX	.XXXXXX	.XXXXXX
.XXXXXX	.XXXXXX-YYY	.XXXXXX-YYY	.XXXXXX+YYY	.XXXXXX+YYY
.XXXXXX	.XXXXXX-YYY	.XXXXXX-YYY	.XXXXXX+YYY	.XXXXXX+YYY
.XXXXXX	.XXXXXX-YYY	.XXXXXX-YYY	.XXXXXX+YYY	.XXXXXX+YYY
.XXXXXX	.XXXXXX-YYY	.XXXXXX-YYY	.XXXXXX+YYY	.XXXXXX+YYY
.XXXXXX	.XXXXXX-YYY	.XXXXXX-YYY	.XXXXXX+YYY	.XXXXXX+YYY
.XXXXXX	.XXXXXX-YYY	.XXXXXX-YYY	.XXXXXX+YYY	.XXXXXX+YYY
.XXXXXX	.XXXXXX-YYY	.XXXXXX-YYY	.XXXXXX+YYY	.XXXXXX+YYY
.XXXXXX	.XXXXXX-YYY	.XXXXXX-YYY	.XXXXXX+YYY	.XXXXXX+YYY
.XXXXXX	.XXXXXX-YYY	.XXXXXX-YYY	.XXXXXX-YYY	.XXXXXX+YYY
.XXXXXX	.XXXXXX-YYY	.XXXXXX-YYY	.XXXXXX-YYY	.XXXXXX+YYY
.XXXXXX	.XXXXXX-YYY	.XXXXXX-YYY	.XXXXXX-YYY	.XXXXXX+YYY
.XXXXXX	.XXXXXX-YYY	.XXXXXX-YYY	.XXXXXX-YYY	.XXXXXX+YYY
.XXXXXX	.XXXXXX-YYY	.XXXXXX-YYY	.XXXXXX-YYY	.XXXXXX+YYY
.XXXXXX	.XXXXXX-YYY	.XXXXXX-YYY	.XXXXXX-YYY	.XXXXXX+YYY
.XXXXXX	.XXXXXX-YYY	.XXXXXX-YYY	.XXXXXX-YYY	.XXXXXX+YYY
.XXXXXX	.XXXXXX-YYY	.XXXXXX-YYY	.XXXXXX-YYY	.XXXXXX+YYY
.XXXXXX	.XXXXXX-YYY	.XXXXXX-YYY	.XXXXXX-YYY	.XXXXXX+YYY
.XXXXXX	.XXXXXX-YYY	.XXXXXX-YYY	.XXXXXX-YYY	.XXXXXX+YYY
.XXXXXX	.XXXXXX-YYY	.XXXXXX-YYY	.XXXXXX-YYY	.XXXXXX+YYY

Sample Page 7.

211

TORSION FREQUENCIES = XXXX.XXXXX

N	X	XFH	// MODE (1)	CPS	1ST DERV	// MODE (2)	CPS	1ST DERV	// MODE (3)	CPS	1ST DERV	// MODE (4)	CPS	1ST DERV
			XXXX.XXXXX			XXXX.XXXXX			XXXX.XXXXX			XXXX.XXXXX		
XX	.XXXXX	.XXXXX	XXX.XXXXX	XXX.XXXXX	XXX.XXXXX	XXX.XXXXX	XXX.XXXXX	XXX.XXXXX	XXX.XXXXX	XXX.XXXXX	XXX.XXXXX	XXX.XXXXX	XXX.XXXXX	XXX.XXXXX
XX	.XXXXX	.XXXXX	XXX.XXXXX	XXX.XXXXX	XXX.XXXXX	XXX.XXXXX	XXX.XXXXX	XXX.XXXXX	XXX.XXXXX	XXX.XXXXX	XXX.XXXXX	XXX.XXXXX	XXX.XXXXX	XXX.XXXXX
XX	.XXXXX	.XXXXX	XXX.XXXXX	XXX.XXXXX	XXX.XXXXX	XXX.XXXXX	XXX.XXXXX	XXX.XXXXX	XXX.XXXXX	XXX.XXXXX	XXX.XXXXX	XXX.XXXXX	XXX.XXXXX	XXX.XXXXX
XX	.XXXXX	.XXXXX	XXX.XXXXX	XXX.XXXXX	XXX.XXXXX	XXX.XXXXX	XXX.XXXXX	XXX.XXXXX	XXX.XXXXX	XXX.XXXXX	XXX.XXXXX	XXX.XXXXX	XXX.XXXXX	XXX.XXXXX
XX	.XXXXX	.XXXXX	XXX.XXXXX	XXX.XXXXX	XXX.XXXXX	XXX.XXXXX	XXX.XXXXX	XXX.XXXXX	XXX.XXXXX	XXX.XXXXX	XXX.XXXXX	XXX.XXXXX	XXX.XXXXX	XXX.XXXXX
XX	.XXXXX	.XXXXX	XXX.XXXXX	XXX.XXXXX	XXX.XXXXX	XXX.XXXXX	XXX.XXXXX	XXX.XXXXX	XXX.XXXXX	XXX.XXXXX	XXX.XXXXX	XXX.XXXXX	XXX.XXXXX	XXX.XXXXX
XX	.XXXXX	.XXXXX	XXX.XXXXX	XXX.XXXXX	XXX.XXXXX	XXX.XXXXX	XXX.XXXXX	XXX.XXXXX	XXX.XXXXX	XXX.XXXXX	XXX.XXXXX	XXX.XXXXX	XXX.XXXXX	XXX.XXXXX
XX	.XXXXX	.XXXXX	XXX.XXXXX	XXX.XXXXX	XXX.XXXXX	XXX.XXXXX	XXX.XXXXX	XXX.XXXXX	XXX.XXXXX	XXX.XXXXX	XXX.XXXXX	XXX.XXXXX	XXX.XXXXX	XXX.XXXXX
XX	.XXXXX	.XXXXX	XXX.XXXXX	XXX.XXXXX	XXX.XXXXX	XXX.XXXXX	XXX.XXXXX	XXX.XXXXX	XXX.XXXXX	XXX.XXXXX	XXX.XXXXX	XXX.XXXXX	XXX.XXXXX	XXX.XXXXX
XX	.XXXXX	.XXXXX	XXX.XXXXX	XXX.XXXXX	XXX.XXXXX	XXX.XXXXX	XXX.XXXXX	XXX.XXXXX	XXX.XXXXX	XXX.XXXXX	XXX.XXXXX	XXX.XXXXX	XXX.XXXXX	XXX.XXXXX
XX	.XXXXX	.XXXXX	XXX.XXXXX	XXX.XXXXX	XXX.XXXXX	XXX.XXXXX	XXX.XXXXX	XXX.XXXXX	XXX.XXXXX	XXX.XXXXX	XXX.XXXXX	XXX.XXXXX	XXX.XXXXX	XXX.XXXXX
XX	.XXXXX	.XXXXX	XXX.XXXXX	XXX.XXXXX	XXX.XXXXX	XXX.XXXXX	XXX.XXXXX	XXX.XXXXX	XXX.XXXXX	XXX.XXXXX	XXX.XXXXX	XXX.XXXXX	XXX.XXXXX	XXX.XXXXX
XX	.XXXXX	.XXXXX	XXX.XXXXX	XXX.XXXXX	XXX.XXXXX	XXX.XXXXX	XXX.XXXXX	XXX.XXXXX	XXX.XXXXX	XXX.XXXXX	XXX.XXXXX	XXX.XXXXX	XXX.XXXXX	XXX.XXXXX
XX	.XXXXX	.XXXXX	XXX.XXXXX	XXX.XXXXX	XXX.XXXXX	XXX.XXXXX	XXX.XXXXX	XXX.XXXXX	XXX.XXXXX	XXX.XXXXX	XXX.XXXXX	XXX.XXXXX	XXX.XXXXX	XXX.XXXXX
XX	.XXXXX	.XXXXX	XXX.XXXXX	XXX.XXXXX	XXX.XXXXX	XXX.XXXXX	XXX.XXXXX	XXX.XXXXX	XXX.XXXXX	XXX.XXXXX	XXX.XXXXX	XXX.XXXXX	XXX.XXXXX	XXX.XXXXX
XX	.XXXXX	.XXXXX	XXX.XXXXX	XXX.XXXXX	XXX.XXXXX	XXX.XXXXX	XXX.XXXXX	XXX.XXXXX	XXX.XXXXX	XXX.XXXXX	XXX.XXXXX	XXX.XXXXX	XXX.XXXXX	XXX.XXXXX
XX	.XXXXX	.XXXXX	XXX.XXXXX	XXX.XXXXX	XXX.XXXXX	XXX.XXXXX	XXX.XXXXX	XXX.XXXXX	XXX.XXXXX	XXX.XXXXX	XXX.XXXXX	XXX.XXXXX	XXX.XXXXX	XXX.XXXXX
XX	.XXXXX	.XXXXX	XXX.XXXXX	XXX.XXXXX	XXX.XXXXX	XXX.XXXXX	XXX.XXXXX	XXX.XXXXX	XXX.XXXXX	XXX.XXXXX	XXX.XXXXX	XXX.XXXXX	XXX.XXXXX	XXX.XXXXX
XX	.XXXXX	.XXXXX	XXX.XXXXX	XXX.XXXXX	XXX.XXXXX	XXX.XXXXX	XXX.XXXXX	XXX.XXXXX	XXX.XXXXX	XXX.XXXXX	XXX.XXXXX	XXX.XXXXX	XXX.XXXXX	XXX.XXXXX
XX	.XXXXX	.XXXXX	XXX.XXXXX	XXX.XXXXX	XXX.XXXXX	XXX.XXXXX	XXX.XXXXX	XXX.XXXXX	XXX.XXXXX	XXX.XXXXX	XXX.XXXXX	XXX.XXXXX	XXX.XXXXX	XXX.XXXXX

Sample Page 8.

212

INPUTTED VARIABLE INFLOW DISTRIBUTIONS (OUTPUT FROM PROGRAM PANPER) FPS

SEG. #	VARIABLE RADIAL INFLOW,FPS	VARIABLE TANGENTIAL INFLOW,FPS	VARIABLE AXIAL INFLOW,FPS
XX	XX.XXX	XX.XXX	XX.XXX
XX	XX.XXX	XX.XXX	XX.XXX
XX	XX.XXX	XX.XXX	XX.XXX
XX	XX.XXX	XX.XXX	XX.XXX
XX	XX.XXX	XX.XXX	XX.XXX
XX	XX.XXX	XX.XXX	XX.XXX
XX	XX.XXX	XX.XXX	XX.XXX
XX	XX.XXX	XX.XXX	XX.XXX
XX	XX.XXX	XX.XXX	XX.XXX
XX	XX.XXX	XX.XXX	XX.XXX
XX	XX.XXX	XX.XXX	XX.XXX
XX	XX.XXX	XX.XXX	XX.XXX
XX	XX.XXX	XX.XXX	XX.XXX
XX	XX.XXX	XX.XXX	XX.XXX
XX	XX.XXX	XX.XXX	XX.XXX

Sample Page 9.

ELASTIC AXIS OFFSET DISTRIBUTIONS AND DEFLECTION VECTORS

N	X	Y10EA	Y10EAP	Z10EA	Z10EAP	DUEAO
1	.XXXXX	.XXXXX	.XXXXX	.XXXXX	.XXXXX	.XXXXX
2	.XXXXX	.XXXXX	.XXXXX	.XXXXX	.XXXXX	.XXXXX
3	.XXXXX	.XXXXX	.XXXXX	.XXXXX	.XXXXX	.XXXXX
4	.XXXXX	.XXXXX	.XXXXX	.XXXXX	.XXXXX	.XXXXX
5	.XXXXX	.XXXXX	.XXXXX	.XXXXX	.XXXXX	.XXXXX
6	.XXXXX	.XXXXX	.XXXXX	.XXXXX	.XXXXX	.XXXXX
7	.XXXXX	.XXXXX	.XXXXX	.XXXXX	.XXXXX	.XXXXX
8	.XXXXX	.XXXXX	.XXXXX	.XXXXX	.XXXXX	.XXXXX
9	.XXXXX	.XXXXX	.XXXXX	.XXXXX	.XXXXX	.XXXXX
10	.XXXXX	.XXXXX	.XXXXX	.XXXXX	.XXXXX	.XXXXX
11	.XXXXX	.XXXXX	.XXXXX	.XXXXX	.XXXXX	.XXXXX
12	.XXXXX	.XXXXX	.XXXXX	.XXXXX	.XXXXX	.XXXXX
13	.XXXXX	.XXXXX	.XXXXX	.XXXXX	.XXXXX	.XXXXX
14	.XXXXX	.XXXXX	.XXXXX	.XXXXX	.XXXXX	.XXXXX
15	.XXXXX	.XXXXX	.XXXXX	.XXXXX	.XXXXX	.XXXXX
16	.XXXXX	.XXXXX	.XXXXX	.XXXXX	.XXXXX	.XXXXX
17	.XXXXX	.XXXXX	.XXXXX	.XXXXX	.XXXXX	.XXXXX
18	.XXXXX	.XXXXX	.XXXXX	.XXXXX	.XXXXX	.XXXXX
19	.XXXXX	.XXXXX	.XXXXX	.XXXXX	.XXXXX	.XXXXX
20	.XXXXX	.XXXXX	.XXXXX	.XXXXX	.XXXXX	.XXXXX

Sample Page 10.

distribution as identified by segment number (N), and spanwise station (X). The third and fourth columns give the edgewise offset information for the elastic axis offset and the fifth and sixth colums give the corresponding flatwise elastic axis offset information. The quantities Y10EAP and Z10EAP are derived quantities and are actually the sines of the structural sweep angles in the edgewise and flatwise senses. For small angles, these quantities become the slopes (first derivatives) of the offset locations (Y10EA and Z10EA). The quantity DUEAO represents the foreshortening array needed to restore the equivalent straight beam back to the originally structurally swept position.

In Sample Page 11 are shown typical modal information for the input flatwise and edgewise bending modes. For each such mode, the (nondimensional) modal frequency and input mode shape and spanwise derivatives are listed. In addition, the listing presents the various derived incremental deflection correction function vectors which account for blade twists (see Eqs. (7) through (14)), and for radial foreshortening. Within a flatwise modal information group, the DVB and DVE arrays correspond to those first order Δv spanwise functions due to built-in twist and torsional modal twist, respectively. The DWWBB, DWWBC and DWWCC arrays correspond to the second order ΔW functions. The various arrays DV2BP, DV2EP, DWW2BBP, DW2BCP and DWW2CCP are the first spanwise derivations of the second components (those with superscript "2") of the above discussed arrays, DVB, DVE, ..., respectively. The DUEAF deflection array corresponds to the bending deflection linear foreshortening accruing from built-in structural sweep (see Eq. (30)). The UWE deflection arrays correspond to the flatwise bending nonlinear foreshortening (see Eq. (33)). Within the edgewise modal information group, the various arrays, DWB, DWE, ... etc., correspond to similarly defined spanwise functions involving twist, structural sweep and the edgewise modal deflection and spanwise derivative arrays. On Sample Page 12 are presented the input torsion modal arrays and natural frequencies together with the derived pseudo-torsion mode shape (as defined in Reference 1) and spanwise derivative. Also presented are the first and second order deflection correction functions accruing from structural sweep.

Results of Solution Part I - Eigensolution

Sample Pages 13 through 17 present the pertinent details of results from the eigensolutions. There are two-distinct eigensolutions calculated and the two results are identified, respectively, by the following labels:

1. LINEARIZED NONLINEAR VACUUM CASE
2. LINEARIZED NONLINEAR NONVACUUM CASE

215

LINEAR AND NONLINEAR MODAL DEFLECTION VECTORS

FLATWISE MODE 1   MODAL FREQUENCY = XXX.XXXX

N	X	GW	GWP	GWPP	DVB	DV2BP	DWWBB	DWW2BBP	DWWBC	DWW2BCP	DWWCC	DWW2CCP
1	X.XXXXX	X.XXXXX	X.XXXXX	X.XXXXX	X.XXXXX	X.XXXXX	X.XXXXX	X.XXXXX	X.XXXXX	X.XXXXX	X.XXXXX	X.XXXXX
2	X.XXXXX	X.XXXXX	X.XXXXX	X.XXXXX	X.XXXXX	X.XXXXX	X.XXXXX	X.XXXXX	X.XXXXX	X.XXXXX	X.XXXXX	X.XXXXX
3	X.XXXXX	X.XXXXX	X.XXXXX	X.XXXXX	X.XXXXX	X.XXXXX	X.XXXXX	X.XXXXX	X.XXXXX	X.XXXXX	X.XXXXX	X.XXXXX
.	X.XXXXX	X.XXXXX	X.XXXXX	X.XXXXX	X.XXXXX	X.XXXXX	X.XXXXX	X.XXXXX	X.XXXXX	X.XXXXX	X.XXXXX	X.XXXXX
.	X.XXXXX	X.XXXXX	X.XXXXX	X.XXXXX	X.XXXXX	X.XXXXX	X.XXXXX	X.XXXXX	X.XXXXX	X.XXXXX	X.XXXXX	X.XXXXX
.	X.XXXXX	X.XXXXX	X.XXXXX	X.XXXXX	X.XXXXX	X.XXXXX	X.XXXXX	X.XXXXX	X.XXXXX	X.XXXXX	X.XXXXX	X.XXXXX
N	X.XXXXX	X.XXXXX	X.XXXXX	X.XXXXX	X.XXXXX	X.XXXXX	X.XXXXX	X.XXXXX	X.XXXXX	X.XXXXX	X.XXXXX	X.XXXXX

LINEAR RADIAL DEFLECTION VECTOR DUE TO ELASTIC AXIS OFFSET (DUEAF), AND

QUADRATIC DEFLECTION VECTORS DUE TO TORSION MODAL TWIST (DVE(1,J), DV2EP(1,J)) AND TO FLATWISE BENDING (UWE(1,M))

J = (1), (2), (3)   /   M = (1), (2), (3), (4)   /   UWE

N	X	DUEAF	DVE (1)	DV2EP (1)	DVE (2)	DV2EP (2)	DVE (3)	DV2EP (3)	DVVBC (1)	DVV2BCP (2)	DVVCC (3)	DVV2CCP (4)
1	X.XXXXX	X.XXXXX	X.XXXXX	X.XXXXX	X.XXXXX	X.XXXXX	X.XXXXX	X.XXXXX	X.XXXXX	X.XXXXX	X.XXXXX	X.XXXXX
2	X.XXXXX	X.XXXXX	X.XXXXX	X.XXXXX	X.XXXXX	X.XXXXX	X.XXXXX	X.XXXXX	X.XXXXX	X.XXXXX	X.XXXXX	X.XXXXX
3	X.XXXXX	X.XXXXX	X.XXXXX	X.XXXXX	X.XXXXX	X.XXXXX	X.XXXXX	X.XXXXX	X.XXXXX	X.XXXXX	X.XXXXX	X.XXXXX
.	X.XXXXX	X.XXXXX	X.XXXXX	X.XXXXX	X.XXXXX	X.XXXXX	X.XXXXX	X.XXXXX	X.XXXXX	X.XXXXX	X.XXXXX	X.XXXXX
.	X.XXXXX	X.XXXXX	X.XXXXX	X.XXXXX	X.XXXXX	X.XXXXX	X.XXXXX	X.XXXXX	X.XXXXX	X.XXXXX	X.XXXXX	X.XXXXX
.	X.XXXXX	X.XXXXX	X.XXXXX	X.XXXXX	X.XXXXX	X.XXXXX	X.XXXXX	X.XXXXX	X.XXXXX	X.XXXXX	X.XXXXX	X.XXXXX
N	X.XXXXX	X.XXXXX	X.XXXXX	X.XXXXX	X.XXXXX	X.XXXXX	X.XXXXX	X.XXXXX	X.XXXXX	X.XXXXX	X.XXXXX	X.XXXXX

EDGEWISE MODE 1   MODAL FREQUENCY = XXX.XXXX

N	X	GV	GVP	GVPP	DWB	DW2BP	DVVBB	DVV2BBP	DVVBC	DVV2BCP	DVVCC	DVV2CCP
1	X.XXXXX	X.XXXXX	X.XXXXX	X.XXXXX	X.XXXXX	X.XXXXX	X.XXXXX	X.XXXXX	X.XXXXX	X.XXXXX	X.XXXXX	X.XXXXX
2	X.XXXXX	X.XXXXX	X.XXXXX	X.XXXXX	X.XXXXX	X.XXXXX	X.XXXXX	X.XXXXX	X.XXXXX	X.XXXXX	X.XXXXX	X.XXXXX
3	X.XXXXX	X.XXXXX	X.XXXXX	X.XXXXX	X.XXXXX	X.XXXXX	X.XXXXX	X.XXXXX	X.XXXXX	X.XXXXX	X.XXXXX	X.XXXXX
.	X.XXXXX	X.XXXXX	X.XXXXX	X.XXXXX	X.XXXXX	X.XXXXX	X.XXXXX	X.XXXXX	X.XXXXX	X.XXXXX	X.XXXXX	X.XXXXX
.	X.XXXXX	X.XXXXX	X.XXXXX	X.XXXXX	X.XXXXX	X.XXXXX	X.XXXXX	X.XXXXX	X.XXXXX	X.XXXXX	X.XXXXX	X.XXXXX
.	X.XXXXX	X.XXXXX	X.XXXXX	X.XXXXX	X.XXXXX	X.XXXXX	X.XXXXX	X.XXXXX	X.XXXXX	X.XXXXX	X.XXXXX	X.XXXXX
N	X.XXXXX	X.XXXXX	X.XXXXX	X.XXXXX	X.XXXXX	X.XXXXX	X.XXXXX	X.XXXXX	X.XXXXX	X.XXXXX	X.XXXXX	X.XXXXX

LINEAR RADIAL DEFLECTION VECTOR DUE TO ELASTIC AXIS OFFSET(DUEAE), AND,

DEFLECTION VECTORS DUE TO ELASTIC (MODAL) TWIST, DWE(1,J), DW2EP(1,J), AND TO EDGEWISE BENDING, UVE(1,M)

J = (1), (2), (3)   UVE

N	X	DUEAE	DWE (1)	DW2EP (1)	DWE (2)	DW2EP (2)	DWE (3)	DW2EP (3)	UVE
1	X.XXXXX	X.XXXXX	X.XXXXX	X.XXXXX	X.XXXXX	X.XXXXX	X.XXXXX	X.XXXXX	X.XXXXX
2	X.XXXXX	X.XXXXX	X.XXXXX	X.XXXXX	X.XXXXX	X.XXXXX	X.XXXXX	X.XXXXX	X.XXXXX
3	X.XXXXX	X.XXXXX	X.XXXXX	X.XXXXX	X.XXXXX	X.XXXXX	X.XXXXX	X.XXXXX	X.XXXXX
.	X.XXXXX	X.XXXXX	X.XXXXX	X.XXXXX	X.XXXXX	X.XXXXX	X.XXXXX	X.XXXXX	X.XXXXX
.	X.XXXXX	X.XXXXX	X.XXXXX	X.XXXXX	X.XXXXX	X.XXXXX	X.XXXXX	X.XXXXX	X.XXXXX
.	X.XXXXX	X.XXXXX	X.XXXXX	X.XXXXX	X.XXXXX	X.XXXXX	X.XXXXX	X.XXXXX	X.XXXXX
N	X.XXXXX	X.XXXXX	X.XXXXX	X.XXXXX	X.XXXXX	X.XXXXX	X.XXXXX	X.XXXXX	X.XXXXX

Sample Page 11.

TORSION MODE 1   MODAL FREQUENCY =   .XXXXX

N	X	GT	GTP	DVEA	DV2EAP	DWEA	DW2EAP	DVVEA	DVV2EAP	DWWEA	DWW2EAP
1	.XXXX	.XXXX	.XXXX	.XXXX	.XXXX	.XXXX	.XXXX	.XXXX	.XXXX	.XXXX	.XXXX
2	.XXXX	.XXXX	.XXXX	.XXXX	.XXXX	.XXXX	.XXXX	.XXXX	.XXXX	.XXXX	.XXXX
3	.XXXX	.XXXX	.XXXX	.XXXX	.XXXX	.XXXX	.XXXX	.XXXX	.XXXX	.XXXX	.XXXX
4	.XXXX	.XXXX	.XXXX	.XXXX	.XXXX	.XXXX	.XXXX	.XXXX	.XXXX	.XXXX	.XXXX
5	.XXXX	.XXXX	.XXXX	.XXXX	.XXXX	.XXXX	.XXXX	.XXXX	.XXXX	.XXXX	.XXXX
6	.XXXX	.XXXX	.XXXX	.XXXX	.XXXX	.XXXX	.XXXX	.XXXX	.XXXX	.XXXX	.XXXX
7	.XXXX	.XXXX	.XXXX	.XXXX	.XXXX	.XXXX	.XXXX	.XXXX	.XXXX	.XXXX	.XXXX
8	.XXXX	.XXXX	.XXXX	.XXXX	.XXXX	.XXXX	.XXXX	.XXXX	.XXXX	.XXXX	.XXXX
9	.XXXX	.XXXX	.XXXX	.XXXX	.XXXX	.XXXX	.XXXX	.XXXX	.XXXX	.XXXX	.XXXX
10	.XXXX	.XXXX	.XXXX	.XXXX	.XXXX	.XXXX	.XXXX	.XXXX	.XXXX	.XXXX	.XXXX
11	.XXXX	.XXXX	.XXXX	.XXXX	.XXXX	.XXXX	.XXXX	.XXXX	.XXXX	.XXXX	.XXXX
12	.XXXX	.XXXX	.XXXX	.XXXX	.XXXX	.XXXX	.XXXX	.XXXX	.XXXX	.XXXX	.XXXX
13	.XXXX	.XXXX	.XXXX	.XXXX	.XXXX	.XXXX	.XXXX	.XXXX	.XXXX	.XXXX	.XXXX
14	.XXXX	.XXXX	.XXXX	.XXXX	.XXXX	.XXXX	.XXXX	.XXXX	.XXXX	.XXXX	.XXXX
15	.XXXX	.XXXX	.XXXX	.XXXX	.XXXX	.XXXX	.XXXX	.XXXX	.XXXX	.XXXX	.XXXX
16	.XXXX	.XXXX	.XXXX	.XXXX	.XXXX	.XXXX	.XXXX	.XXXX	.XXXX	.XXXX	.XXXX
17	.XXXX	.XXXX	.XXXX	.XXXX	.XXXX	.XXXX	.XXXX	.XXXX	.XXXX	.XXXX	.XXXX
18	.XXXX	.XXXX	.XXXX	.XXXX	.XXXX	.XXXX	.XXXX	.XXXX	.XXXX	.XXXX	.XXXX
19	.XXXX	.XXXX	.XXXX	.XXXX	.XXXX	.XXXX	.XXXX	.XXXX	.XXXX	.XXXX	.XXXX
20	.XXXX	.XXXX	.XXXX	.XXXX	.XXXX	.XXXX	.XXXX	.XXXX	.XXXX	.XXXX	.XXXX

PSEUDO-TORSION MODE

N	X	GT	GTP	DVEA	DV2EAP	DWEA	DW2EAP	DVVEA	DVV2EAP	DWWEA	DWW2EAP
1	.XXXX	.XXXX	.XXXX	.XXXX	.XXXX	.XXXX	.XXXX	.XXXX	.XXXX	.XXXX	.XXXX
2	.XXXX	.XXXX	.XXXX	.XXXX	.XXXX	.XXXX	.XXXX	.XXXX	.XXXX	.XXXX	.XXXX
3	.XXXX	.XXXX	.XXXX	.XXXX	.XXXX	.XXXX	.XXXX	.XXXX	.XXXX	.XXXX	.XXXX
4	.XXXX	.XXXX	.XXXX	.XXXX	.XXXX	.XXXX	.XXXX	.XXXX	.XXXX	.XXXX	.XXXX
5	.XXXX	.XXXX	.XXXX	.XXXX	.XXXX	.XXXX	.XXXX	.XXXX	.XXXX	.XXXX	.XXXX
6	.XXXX	.XXXX	.XXXX	.XXXX	.XXXX	.XXXX	.XXXX	.XXXX	.XXXX	.XXXX	.XXXX
7	.XXXX	.XXXX	.XXXX	.XXXX	.XXXX	.XXXX	.XXXX	.XXXX	.XXXX	.XXXX	.XXXX
8	.XXXX	.XXXX	.XXXX	.XXXX	.XXXX	.XXXX	.XXXX	.XXXX	.XXXX	.XXXX	.XXXX
9	.XXXX	.XXXX	.XXXX	.XXXX	.XXXX	.XXXX	.XXXX	.XXXX	.XXXX	.XXXX	.XXXX
10	.XXXX	.XXXX	.XXXX	.XXXX	.XXXX	.XXXX	.XXXX	.XXXX	.XXXX	.XXXX	.XXXX
11	.XXXX	.XXXX	.XXXX	.XXXX	.XXXX	.XXXX	.XXXX	.XXXX	.XXXX	.XXXX	.XXXX
12	.XXXX	.XXXX	.XXXX	.XXXX	.XXXX	.XXXX	.XXXX	.XXXX	.XXXX	.XXXX	.XXXX
13	.XXXX	.XXXX	.XXXX	.XXXX	.XXXX	.XXXX	.XXXX	.XXXX	.XXXX	.XXXX	.XXXX
14	.XXXX	.XXXX	.XXXX	.XXXX	.XXXX	.XXXX	.XXXX	.XXXX	.XXXX	.XXXX	.XXXX
15	.XXXX	.XXXX	.XXXX	.XXXX	.XXXX	.XXXX	.XXXX	.XXXX	.XXXX	.XXXX	.XXXX
16	.XXXX	.XXXX	.XXXX	.XXXX	.XXXX	.XXXX	.XXXX	.XXXX	.XXXX	.XXXX	.XXXX
17	.XXXX	.XXXX	.XXXX	.XXXX	.XXXX	.XXXX	.XXXX	.XXXX	.XXXX	.XXXX	.XXXX
18	.XXXX	.XXXX	.XXXX	.XXXX	.XXXX	.XXXX	.XXXX	.XXXX	.XXXX	.XXXX	.XXXX
19	.XXXX	.XXXX	.XXXX	.XXXX	.XXXX	.XXXX	.XXXX	.XXXX	.XXXX	.XXXX	.XXXX
20	.XXXX	.XXXX	.XXXX	.XXXX	.XXXX	.XXXX	.XXXX	.XXXX	.XXXX	.XXXX	.XXXX

Sample Page 12.

In both cases, those nonlinear inertial and elastic terms appearing in equations of motions are linearized about the input response variables as determined by end conditions from a previous run or by the input initial conditions from the "V" generic loader block. In the first case, all aerodynamic terms are omitted; this calculation is for the purpose of obtaining the "coupled" modal characteristics. In the second case, the full aerodynamic description is retained; this calculation is for the purpose of analysis for aeroelastic stability. In both cases, the eigensolution problem is stated in terms of an inertia (A) matrix, a damping (B) matrix, and a stiffness (C) matrix, and these matrices are output for both cases. Furthermore, for both cases, the extracted eigensolutions (coupled roots and frequencies) are listed by root pairs.

Linearized Nonlinear Vacuum Case

On the upper half of Sample Page 13 are presented the spanwise distributions of the major nondimensionalized dynamic and structural properties used throughout the program (both for eigensolutions and time-history solutions). The X and XCEN arrays are the nondimensional distances of the centers of the segments from the offset and the rotor axis, respectively. The QUAD array constitutes the integration weighting numbers for spanwise integration. The THETA-STR array is the pitch angle distribution of the structural principal axes and has the units of degrees; in general, it differs from the aerodynamic pitch angle distribution appearing on another sample page. The two arrays, TWIST-BLT and TWIST-TOT, are the nondimensional structural twist rate distributions of the built-in twist and the total twist (including initial elastic response), respectively; these arrays have the units of radians. The quantities TENSB, EIYB, EIZB and MASSB are, respectively, the blade tension, flatwise bending stiffness, edgewise bending stiffness and mass distributions, all nondimensionalized by appropriate combinations of R, Ω and m_0. The (Y10NA)/c and Y10CG)/c arrays are, respectively, the distributions of edgewise bending neutral axis and mass center offset distances from the elastic axis nondimensionalized by chord (rather than radius).

On the bottom half of Sample Page 13 begins the output for the linearized nonlinear vacuum case with the three matrices defining the eigenproblem. On Sample Page 14 are presented the output formats for the cases wherein the roots are either complex conjugates (top half) or a pair of real-valued numbers (bottom half). For each root, the eigenvector or GENERALIZED MODE SHAPE is presented, normalized to the largest amplitude. In the case of a complex conjugate pair, the eigenvector is evaluated using only the complex root with the positive imaginary part. The number of elements in this vector is identical with the dimension of the A, B, and C matrices and represent, in order, the coupled relative responses

218

PART I. EIGENSOLUTIONS OF VARIOUS LINEARIZATIONS OF EQUATION SET - CHARACTERISTIC ROOTS AND COUPLED MODE SHAPES

RADIAL DISTRIBUTIONS OF GEOMETRIC, DYNAMIC AND STRUCTURAL QUANTITIES

N	X	XCEN	QUAD	THETA-STR	TWIST-BLT	TWIST-TUT	TENSB	EIYB	EIZB	(Y10NA)/C	MASSB	(Y10CG)/C
1	.XXXX	.XXXX	.XXXX	.XXXX	.XXXX	.XXXX	.XXXX	.XXXX	.XXXX	.XXXX	.XXXX	.XXXX
2	.XXXX	.XXXX	.XXXX	.XXXX	.XXXX	.XXXX	.XXXX	.XXXX	.XXXX	.XXXX	.XXXX	.XXXX
3	.XXXX	.XXXX	.XXXX	.XXXX	.XXXX	.XXXX	.XXXX	.XXXX	.XXXX	.XXXX	.XXXX	.XXXX
4	.XXXX	.XXXX	.XXXX	.XXXX	.XXXX	.XXXX	.XXXX	.XXXX	.XXXX	.XXXX	.XXXX	.XXXX
5	.XXXX	.XXXX	.XXXX	.XXXX	.XXXX	.XXXX	.XXXX	.XXXX	.XXXX	.XXXX	.XXXX	.XXXX
6	.XXXX	.XXXX	.XXXX	.XXXX	.XXXX	.XXXX	.XXXX	.XXXX	.XXXX	.XXXX	.XXXX	.XXXX
7	.XXXX	.XXXX	.XXXX	.XXXX	.XXXX	.XXXX	.XXXX	.XXXX	.XXXX	.XXXX	.XXXX	.XXXX
8	.XXXX	.XXXX	.XXXX	.XXXX	.XXXX	.XXXX	.XXXX	.XXXX	.XXXX	.XXXX	.XXXX	.XXXX
9	.XXXX	.XXXX	.XXXX	.XXXX	.XXXX	.XXXX	.XXXX	.XXXX	.XXXX	.XXXX	.XXXX	.XXXX
10	.XXXX	.XXXX	.XXXX	.XXXX	.XXXX	.XXXX	.XXXX	.XXXX	.XXXX	.XXXX	.XXXX	.XXXX
11	.XXXX	.XXXX	.XXXX	.XXXX	.XXXX	.XXXX	.XXXX	.XXXX	.XXXX	.XXXX	.XXXX	.XXXX
12	.XXXX	.XXXX	.XXXX	.XXXX	.XXXX	.XXXX	.XXXX	.XXXX	.XXXX	.XXXX	.XXXX	.XXXX
13	.XXXX	.XXXX	.XXXX	.XXXX	.XXXX	.XXXX	.XXXX	.XXXX	.XXXX	.XXXX	.XXXX	.XXXX
14	.XXXX	.XXXX	.XXXX	.XXXX	.XXXX	.XXXX	.XXXX	.XXXX	.XXXX	.XXXX	.XXXX	.XXXX
15	.XXXX	.XXXX	.XXXX	.XXXX	.XXXX	.XXXX	.XXXX	.XXXX	.XXXX	.XXXX	.XXXX	.XXXX
16	.XXXX	.XXXX	.XXXX	.XXXX	.XXXX	.XXXX	.XXXX	.XXXX	.XXXX	.XXXX	.XXXX	.XXXX
17	.XXXX	.XXXX	.XXXX	.XXXX	.XXXX	.XXXX	.XXXX	.XXXX	.XXXX	.XXXX	.XXXX	.XXXX
18	.XXXX	.XXXX	.XXXX	.XXXX	.XXXX	.XXXX	.XXXX	.XXXX	.XXXX	.XXXX	.XXXX	.XXXX
19	.XXXX	.XXXX	.XXXX	.XXXX	.XXXX	.XXXX	.XXXX	.XXXX	.XXXX	.XXXX	.XXXX	.XXXX
20	.XXXX	.XXXX	.XXXX	.XXXX	.XXXX	.XXXX	.XXXX	.XXXX	.XXXX	.XXXX	.XXXX	.XXXX

LINEARIZED NONLINEAR VACUUM CASE

A MATRIX

```
.XXX-YYY  .XXX-YYY  .XXX-YYY  .XXX-YYY
.XXX-YYY  .XXX-YYY  .XXX-YYY  .XXX-YYY
.XXX-YYY  .XXX-YYY  .XXX-YYY  .XXX-YYY
.XXX-YYY  .XXX-YYY  .XXX-YYY  .XXX-YYY
.XXX-YYY  .XXX-YYY  .XXX-YYY  .XXX-YYY
```

B MATRIX

```
.XXX-YYY  .XXX-YYY  .XXX-YYY  .XXX-YYY
.XXX-YYY  .XXX-YYY  .XXX-YYY  .XXX-YYY
.XXX-YYY  .XXX-YYY  .XXX-YYY  .XXX-YYY
.XXX-YYY  .XXX-YYY  .XXX-YYY  .XXX-YYY
.XXX-YYY  .XXX-YYY  .XXX-YYY  .XXX-YYY
```

C MATRIX

```
.XXX-YYY  .XXX-YYY  .XXX-YYY  .XXX-YYY
.XXX-YYY  .XXX-YYY  .XXX-YYY  .XXX-YYY
.XXX-YYY  .XXX-YYY  .XXX-YYY  .XXX-YYY
.XXX-YYY  .XXX-YYY  .XXX-YYY  .XXX-YYY
.XXX-YYY  .XXX-YYY  .XXX-YYY  .XXX-YYY
```

Sample Page 13.

ROOTS (X, X) = .XXXX +-I .XXXXX ZETA = .XXXXX WN = .XXXX

GENERALIZED MODE SHAPE

	X	Y5	Y5*	Z5	Z5*	THETA	THETA*
{RE}		.XXX	.XXX	.XXXX	.XXXX	.XXXX	
{IM}		.XXX	.XXX	.XXXX	.XXXX	.XXXX	

PHYSICAL MODE SHAPE

N	X	Y5	Y5*	Z5	Z5*	THETA	THETA*
1	.XXXX	.XXXX	.XXXX	.XXXX	.XXXX	.XXXX	.XXXX
2	.XXXX	.XXXX	.XXXX	.XXXX	.XXXX	.XXXX	.XXXX
3	.XXXX	.XXXX	.XXXX	.XXXX	.XXXX	.XXXX	.XXXX
4	.XXXX	.XXXX	.XXXX	.XXXX	.XXXX	.XXXX	.XXXX
5	.XXXX	.XXXX	.XXXX	.XXXX	.XXXX	.XXXX	.XXXX
6	.XXXX	.XXXX	.XXXX	.XXXX	.XXXX	.XXXX	.XXXX
7	.XXXX	.XXXX	.XXXX	.XXXX	.XXXX	.XXXX	.XXXX
8	.XXXX	.XXXX	.XXXX	.XXXX	.XXXX	.XXXX	.XXXX
9	.XXXX	.XXXX	.XXXX	.XXXX	.XXXX	.XXXX	.XXXX
10	.XXXX	.XXXX	.XXXX	.XXXX	.XXXX	.XXXX	.XXXX
11	.XXXX	.XXXX	.XXXX	.XXXX	.XXXX	.XXXX	.XXXX
12	.XXXX	.XXXX	.XXXX	.XXXX	.XXXX	.XXXX	.XXXX
13	.XXXX	.XXXX	.XXXX	.XXXX	.XXXX	.XXXX	.XXXX
14	.XXXX	.XXXX	.XXXX	.XXXX	.XXXX	.XXXX	.XXXX
15	.XXXX	.XXXX	.XXXX	.XXXX	.XXXX	.XXXX	.XXXX
16	.XXXX	.XXXX	.XXXX	.XXXX	.XXXX	.XXXX	.XXXX
17	.XXXX	.XXXX	.XXXX	.XXXX	.XXXX	.XXXX	.XXXX
18	.XXXX	.XXXX	.XXXX	.XXXX	.XXXX	.XXXX	.XXXX
19	.XXXX	.XXXX	.XXXX	.XXXX	.XXXX	.XXXX	.XXXX
20	.XXXX	.XXXX	.XXXX	.XXXX	.XXXX	.XXXX	.XXXX

ROOTS (X, X) = .XXXXX ; (1)

GENERALIZED MODE SHAPE

X	Y5	Z5	THETA
.XXXXX	.XXX	.XXX	.XXX
	.XXX	.XXX	.XXX

PHYSICAL MODE SHAPE

N	X	Y5	Z5	THETA
1	.XXXX	.XXXX	.XXXX	.XXXX
2	.XXXX	.XXXX	.XXXX	.XXXX
3	.XXXX	.XXXX	.XXXX	.XXXX
4	.XXXX	.XXXX	.XXXX	.XXXX
5	.XXXX	.XXXX	.XXXX	.XXXX
6	.XXXX	.XXXX	.XXXX	.XXXX
7	.XXXX	.XXXX	.XXXX	.XXXX
8	.XXXX	.XXXX	.XXXX	.XXXX
9	.XXXX	.XXXX	.XXXX	.XXXX
10	.XXXX	.XXXX	.XXXX	.XXXX
11	.XXXX	.XXXX	.XXXX	.XXXX
12	.XXXX	.XXXX	.XXXX	.XXXX
13	.XXXX	.XXXX	.XXXX	.XXXX
14	.XXXX	.XXXX	.XXXX	.XXXX
15	.XXXX	.XXXX	.XXXX	.XXXX
16	.XXXX	.XXXX	.XXXX	.XXXX
17	.XXXX	.XXXX	.XXXX	.XXXX
18	.XXXX	.XXXX	.XXXX	.XXXX
19	.XXXX	.XXXX	.XXXX	.XXXX
20	.XXXX	.XXXX	.XXXX	.XXXX

Sample Page 14.

of the (NFM) flatwise modes, (NEM) edgewise modes, and the (NTM) torsion modes. The arrays labeled PHYSICAL MODE SHAPE consist of the relative span-wise distributions of inplane (Y5), out-of-plane (Z5) and pitching (THETA) deflection components of the coupled mode shape. The quantities labeled Y5*, Z5* and THETA* are the velocity or 90 degree out-of-phase components of their respective deflection components. The Y5, Y5*, Z5 and Z5* modal deflections and velocities are nondimensionalized by R and Ω, whereas THETA and THETA* have the units of radians.

Linearized Nonlinear Nonvacuum Case

Sample Page 15 presents the output format appropriate to the aero-dynamically effective eigensolution and is labeled LINEARIZED NONLINEAR NONVACUUM CASE. Since there exist two optional forms of static airfoil data (analytic NACA 0012 or input tables) as well as two optional forms of unsteady aerodynamic methodology available to the eigensolution (quasi-static or Pade) an appropriate label is output on this sample page based upon the option inputs selected. On the upper half of Sample Page 15 are presented the spanwise distributions of the major aerodynamic characteristics used to define the pertrubational airloads in the eigenproblem. The X and XCEN arrays are defined the same as in Sample Page 13. The units of the CHORD array are feet. The angle-of-attack descriptors, THETA-AERO, PHI and ALPHA are, respectively, the geometric aerodynamic pitch angle (can be different from the structural principal axis pitch angle), the inflow angle, and the resulting section angle-of-attack, all in degrees. These angles are calculated using the input initial conditions for the response variable deflections and velocities. The resulting Mach number (MACH) and section coefficients (CL, CD and CM) are used to define the linearization point about which perturbational airloads are defined. The quantity KAPPA/U is the span-wise variation in aerodynamic moment damping coefficient which, when multiplied by the local pitch rate, approximates the potential flow un-steady pitching moment coefficient. The quantity (Y10C/4)/C is the span-wise distribution of quarter chord offset from the elastic axis nondimen-sionalized by chord (not radius). The lower half of Sample Page 15 and all of Sample Page 16 present the output format for the A, B and C matrices which is similar to the format for the vacuum case matrices. In those cases wherein the Pade airloads modeling option is invoked (as indicated in these sample pages), the eigensolution dynamic matrices are augmented to include submatrices resulting from perturbational Pade airload augmented state variables. These augmented state variables each are governed by their own dynamic equations which, together with the differential equations for the blade dynamics, define submatrix partitioning within each of the now augmented A, B and C matrices. Thus, the two A matrices shown in Sample Page 15 are, respectively, the upper left and lower left submatrices com-prising the augmented A matrix. Sample Page 16 contains the similar outputs

221

LINEARIZED NONLINEAR NONVACUUM CASE

*** UNSTEADY (UNSTALLED) AIRLOADS VIA PADE IMPLEMENTATION ARE USED IN FOLLOWING CASE ***

RADIAL DISTRIBUTIONS OF GEOMETRIC AND AERODYNAMIC QUANTITIES

N	X	XCEN	CHORD	THETA-AERO	PHI	ALPHA	MACH	CL	CD	CM	KAPPA/U	(Y10C/4)/C
1	.XXXX	.XXXX	.XXXX	XX.XXX	XXX.XXX	XX.XXX	.XXX	.XXXX	.XXXX	.XXXX	.XXXX	.XXXX
2	.XXXX	.XXXX	.XXXX	XX.XXX	XXX.XXX	XX.XXX	.XXX	.XXXX	.XXXX	.XXXX	.XXXX	.XXXX
3	.XXXX	.XXXX	.XXXX	XX.XXX	XXX.XXX	XX.XXX	.XXX	.XXXX	.XXXX	.XXXX	.XXXX	.XXXX
4	.XXXX	.XXXX	.XXXX	XX.XXX	XXX.XXX	XX.XXX	.XXX	.XXXX	.XXXX	.XXXX	.XXXX	.XXXX
5	.XXXX	.XXXX	.XXXX	XX.XXX	XXX.XXX	XX.XXX	.XXX	.XXXX	.XXXX	.XXXX	.XXXX	.XXXX
6	.XXXX	.XXXX	.XXXX	XX.XXX	XXX.XXX	XX.XXX	.XXX	.XXXX	.XXXX	.XXXX	.XXXX	.XXXX
7	.XXXX	.XXXX	.XXXX	XX.XXX	XXX.XXX	XX.XXX	.XXX	.XXXX	.XXXX	.XXXX	.XXXX	.XXXX
8	.XXXX	.XXXX	.XXXX	XX.XXX	XXX.XXX	XX.XXX	.XXX	.XXXX	.XXXX	.XXXX	.XXXX	.XXXX
9	.XXXX	.XXXX	.XXXX	XX.XXX	XXX.XXX	XX.XXX	.XXX	.XXXX	.XXXX	.XXXX	.XXXX	.XXXX
10	.XXXX	.XXXX	.XXXX	XX.XXX	XXX.XXX	XX.XXX	.XXX	.XXXX	.XXXX	.XXXX	.XXXX	.XXXX
11	.XXXX	.XXXX	.XXXX	XX.XXX	XXX.XXX	XX.XXX	.XXX	.XXXX	.XXXX	.XXXX	.XXXX	.XXXX
12	.XXXX	.XXXX	.XXXX	XX.XXX	XXX.XXX	XX.XXX	.XXX	.XXXX	.XXXX	.XXXX	.XXXX	.XXXX
13	.XXXX	.XXXX	.XXXX	XX.XXX	XXX.XXX	XX.XXX	.XXX	.XXXX	.XXXX	.XXXX	.XXXX	.XXXX
14	.XXXX	.XXXX	.XXXX	XX.XXX	XXX.XXX	XX.XXX	.XXX	.XXXX	.XXXX	.XXXX	.XXXX	.XXXX
15	.XXXX	.XXXX	.XXXX	XX.XXX	XXX.XXX	XX.XXX	.XXX	.XXXX	.XXXX	.XXXX	.XXXX	.XXXX
16	.XXXX	.XXXX	.XXXX	XX.XXX	XXX.XXX	XX.XXX	.XXX	.XXXX	.XXXX	.XXXX	.XXXX	.XXXX
17	.XXXX	.XXXX	.XXXX	XX.XXX	XXX.XXX	XX.XXX	.XXX	.XXXX	.XXXX	.XXXX	.XXXX	.XXXX
18	.XXXX	.XXXX	.XXXX	XX.XXX	XXX.XXX	XX.XXX	.XXX	.XXXX	.XXXX	.XXXX	.XXXX	.XXXX
19	.XXXX	.XXXX	.XXXX	XX.XXX	XXX.XXX	XX.XXX	.XXX	.XXXX	.XXXX	.XXXX	.XXXX	.XXXX
20	.XXXX	.XXXX	.XXXX	XX.XXX	XXX.XXX	XX.XXX	.XXX	.XXXX	.XXXX	.XXXX	.XXXX	.XXXX

A MATRIX

```
.XXX-YYY .XXX-YYY .XXX-YYY .XXX-YYY    .XXX-YYY .XXX-YYY .XXX-YYY
.XXX-YYY .XXX-YYY .XXX-YYY .XXX-YYY    .XXX-YYY .XXX-YYY .XXX-YYY
.XXX-YYY .XXX-YYY .XXX-YYY .XXX-YYY    .XXX-YYY .XXX-YYY .XXX-YYY
.XXX-YYY .XXX-YYY .XXX-YYY .XXX-YYY    .XXX-YYY .XXX-YYY .XXX-YYY
.XXX-YYY .XXX-YYY .XXX-YYY .XXX-YYY    .XXX-YYY .XXX-YYY .XXX-YYY

.XXX-YYY .XXX-YYY .XXX-YYY .XXX-YYY    .XXX-YYY .XXX-YYY .XXX-YYY
.XXX-YYY .XXX-YYY .XXX-YYY .XXX-YYY    .XXX-YYY .XXX-YYY .XXX-YYY
.XXX-YYY .XXX-YYY .XXX-YYY .XXX-YYY    .XXX-YYY .XXX-YYY .XXX-YYY
.XXX-YYY .XXX-YYY .XXX-YYY .XXX-YYY    .XXX-YYY .XXX-YYY .XXX-YYY
.XXX-YYY .XXX-YYY .XXX-YYY .XXX-YYY    .XXX-YYY .XXX-YYY .XXX-YYY
.XXX-YYY .XXX-YYY .XXX-YYY .XXX-YYY    .XXX-YYY .XXX-YYY .XXX-YYY
.XXX-YYY .XXX-YYY .XXX-YYY .XXX-YYY    .XXX-YYY .XXX-YYY .XXX-YYY
.XXX-YYY .XXX-YYY .XXX-YYY .XXX-YYY    .XXX-YYY .XXX-YYY .XXX-YYY
.XXX-YYY .XXX-YYY .XXX-YYY .XXX-YYY    .XXX-YYY .XXX-YYY .XXX-YYY
.XXX-YYY .XXX-YYY .XXX-YYY .XXX-YYY    .XXX-YYY .XXX-YYY .XXX-YYY
.XXX-YYY .XXX-YYY .XXX-YYY .XXX-YYY    .XXX-YYY .XXX-YYY .XXX-YYY
```

Sample Page 15.

B MATRIX

.XXX-YYY	.XXX-YYY	.XXX-YYY	.XXX-YYY	.XXX-YYY	.XXX-YYY
.XXX-YYY	.XXX-YYY	.XXX-YYY	.XXX-YYY	.XXX-YYY	.XXX-YYY
.XXX-YYY	.XXX-YYY	.XXX-YYY	.XXX-YYY	.XXX-YYY	.XXX-YYY
.XXX-YYY	.XXX-YYY	.XXX-YYY	.XXX-YYY	.XXX-YYY	.XXX-YYY
.XXX-YYY	.XXX-YYY	.XXX-YYY	.XXX-YYY	.XXX-YYY	.XXX-YYY
.XXX-YYY	.XXX-YYY	.XXX-YYY	.XXX-YYY	.XXX-YYY	.XXX-YYY

C MATRIX

.XXX-YYY	.XXX-YYY	.XXX-YYY	.XXX-YYY	.XXX-YYY	.XXX-YYY
.XXX-YYY	.XXX-YYY	.XXX-YYY	.XXX-YYY	.XXX-YYY	.XXX-YYY
.XXX-YYY	.XXX-YYY	.XXX-YYY	.XXX-YYY	.XXX-YYY	.XXX-YYY
.XXX-YYY	.XXX-YYY	.XXX-YYY	.XXX-YYY	.XXX-YYY	.XXX-YYY
.XXX-YYY	.XXX-YYY	.XXX-YYY	.XXX-YYY	.XXX-YYY	.XXX-YYY

Sample Page 16.

223

A PHASING MATRIX

```
.XXXXE-YY  .XXXXE-YY  .XXXXE-YY  .XXXXE-YY  .XXXXE-YY
.XXXXE-YY  .XXXXE-YY  .XXXXE-YY  .XXXXE-YY  .XXXXE-YY
.XXXXE-YY  .XXXXE-YY  .XXXXE-YY  .XXXXE-YY  .XXXXE-YY
.XXXXE-YY  .XXXXE-YY  .XXXXE-YY  .XXXXE-YY  .XXXXE-YY
.XXXXE-YY  .XXXXE-YY  .XXXXE-YY  .XXXXE-YY  .XXXXE-YY
.XXXXE-YY  .XXXXE-YY  .XXXXE-YY  .XXXXE-YY  .XXXXE-YY
```

B PHASING MATRIX

```
.XXXXE-YY  .XXXXE-YY  .XXXXE-YY  .XXXXE-YY  .XXXXE-YY
.XXXXE-YY  .XXXXE-YY  .XXXXE-YY  .XXXXE-YY  .XXXXE-YY
.XXXXE-YY  .XXXXE-YY  .XXXXE-YY  .XXXXE-YY  .XXXXE-YY
.XXXXE-YY  .XXXXE-YY  .XXXXE-YY  .XXXXE-YY  .XXXXE-YY
.XXXXE-YY  .XXXXE-YY  .XXXXE-YY  .XXXXE-YY  .XXXXE-YY
.XXXXE-YY  .XXXXE-YY  .XXXXE-YY  .XXXXE-YY  .XXXXE-YY
```

C PHASING MATRIX

```
.XXXXE-YY  .XXXXE-YY  .XXXXE-YY  .XXXXE-YY  .XXXXE-YY
.XXXXE-YY  .XXXXE-YY  .XXXXE-YY  .XXXXE-YY  .XXXXE-YY
.XXXXE-YY  .XXXXE-YY  .XXXXE-YY  .XXXXE-YY  .XXXXE-YY
.XXXXE-YY  .XXXXE-YY  .XXXXE-YY  .XXXXE-YY  .XXXXE-YY
.XXXXE-YY  .XXXXE-YY  .XXXXE-YY  .XXXXE-YY  .XXXXE-YY
.XXXXE-YY  .XXXXE-YY  .XXXXE-YY  .XXXXE-YY  .XXXXE-YY
```

Sample Page 17.

224

for the augmented B and C matrices. The two B matrices are, respectively, the upper left and lower left submatrices comprising the augmented B matrix. The two C matrices are, respectively, the upper left and upper right submatrices comprising the augmented C matrix. With the exception of the lower right C submatrix, which is always a diagonal matrix, all other submatrices are null and their output is suppressed. The eigenvalues calculated for the nonvacuum cases are output in the same format as is described above for Sample Page 14.

Should one of the roots in the nonvacuum eigensolution be unstable, as indicated by a positive root or real part of a complex pair, an output listing of the force phasing matrices appropriate to the instability is generated and outputted as depicted in Sample Page 17. These matrices, having the same size as the A, B, and C dynamic matrices, enable the various destabilizing forces to be identified; descriptive material for their definition and interpretation are contained in Reference 33.

Results of Solution Part II - Time-History Solutions

Sample Pages 18 through 22 present the pertinent details of the results from the time-history solutions (i.e., transient aeroelastic responses). The first row of parameters following the page title represents, for the subsequent time-history solution, the parameters defining the flight condition. These consist of the various control angles (in degrees), the inflow and advance ratios, LAMBDA and MU, respectively, and the initial nondimensionalized values of the "momentum" induced velocity components. The remainder of Sample Page 18 comprises the typical azimuthal listing; this listing is output for every azimuth angle which is a multiple of the print azimuth increment, loader input (S)11.

Azimuthal Printouts

The first line appearing on all subsequent azimuthal printouts gives the rotor azimuth angle, revolution number and time. In addition, the three components of the instantaneous Glauert (momentum induced) inflow are output. The remainder of the azimuthal printout consists of 3 main groups of result quantities. The first of the three groups on this sample page lists the spanwise distributions of the pertinent aerodynamic quantities, the format of which depends on the choice of unsteady airloads modeling selected (input location (S)64).

Unsteady Airloads Utilizing an Equivalent Angle-of-Attack

Unsteady airloads options wherein the airloads depend on a single "effective" angle-of-attack are: i) the quasi-static modeling ((A)64 = 0.),

225

PART II. TIME HISTORY SOLUTION OF COMPLETE (NONLINEAR) EQUATION SET – AEROELASTIC TRANSIENT RESPONSES

A1S .XXX   B1S .XXX   THETA 75 XX.XXX   LAMBDA .XXXXX   MU .XXX   LAMBDA 0 = .XXXX   V0 .XXXXX   LAMBDA 1C = .XXXX   V1C .XXXXX   LAMBDA 1S = .XXX   V1S .XXXX

PSI(1)= .X DEG   REV= X   TIME= .XX SEC

N	XCEN	PHTLLDA	THTL1	PHI	ALPHA	MACH	DCL	DCM	CL	CD	CM	SAZ5	SAY5	MAX5	MAY5
1	.XXX	.XXX	.XXX	XX.XX	X.XX	.XXX	.XX	.XX	.XX	.XX	.XX	.XX	.XX	.XXX	.XX
2	.XXX	.XXX	.XXX	XX.XX	X.XX	.XXX	.XX	.XX	.XX	.XX	.XX	.XX	.XX	.XXX	.XX
3	.XXX	.XXX	.XXX	XX.XX	X.XX	.XXX	.XX	.XX	.XX	.XX	.XX	.XX	.XX	.XXX	.XX
4	.XXX	.XXX	.XXX	XX.XX	X.XX	.XXX	.XX	.XX	.XX	.XX	.XX	.XX	.XX	.XXX	.XX
5	.XXX	.XXX	.XXX	XX.XX	X.XX	.XXX	.XX	.XX	.XX	.XX	.XX	.XX	.XX	.XXX	.XX
6	.XXX	.XXX	.XXX	XX.XX	X.XX	.XXX	.XX	.XX	.XX	.XX	.XX	.XX	.XX	.XXX	.XX
7	.XXX	.XXX	.XXX	XX.XX	X.XX	.XXX	.XX	.XX	.XX	.XX	.XX	.XX	.XX	.XXX	.XX
8	.XXX	.XXX	.XXX	XX.XX	X.XX	.XXX	.XX	.XX	.XX	.XX	.XX	.XX	.XX	.XXX	.XX
9	.XXX	.XXX	.XXX	XX.XX	X.XX	.XXX	.XX	.XX	.XX	.XX	.XX	.XX	.XX	.XXX	.XX
10	.XXX	.XXX	.XXX	XX.XX	X.XX	.XXX	.XX	.XX	.XX	.XX	.XX	.XX	.XX	.XXX	.XX
11	.XXX	.XXX	.XXX	XX.XX	X.XX	.XXX	.XX	.XX	.XX	.XX	.XX	.XX	.XX	.XXX	.XX
12	.XXX	.XXX	.XXX	XX.XX	X.XX	.XXX	.XX	.XX	.XX	.XX	.XX	.XX	.XX	.XXX	.XX
13	.XXX	.XXX	.XXX	XX.XX	X.XX	.XXX	.XX	.XX	.XX	.XX	.XX	.XX	.XX	.XXX	.XX
14	.XXX	.XXX	.XXX	XX.XX	X.XX	.XXX	.XX	.XX	.XX	.XX	.XX	.XX	.XX	.XXX	.XX
15	.XXX	.XXX	.XXX	XX.XX	X.XX	.XXX	.XX	.XX	.XX	.XX	.XX	.XX	.XX	.XXX	.XX
16	.XXX	.XXX	.XXX	XX.XX	X.XX	.XXX	.XX	.XX	.XX	.XX	.XX	.XX	.XX	.XXX	.XX
17	.XXX	.XXX	.XXX	XX.XX	X.XX	.XXX	.XX	.XX	.XX	.XX	.XX	.XX	.XX	.XXX	.XX
18	.XXX	.XXX	.XXX	XX.XX	X.XX	.XXX	.XX	.XX	.XX	.XX	.XX	.XX	.XX	.XXX	.XX
19	.XXX	.XXX	.XXX	XX.XX	X.XX	.XXX	.XX	.XX	.XX	.XX	.XX	.XX	.XX	.XXX	.XX
20	.XXX	.XXX	.XXX	XX.XX	X.XX	.XXX	.XX	.XX	.XX	.XX	.XX	.XX	.XX	.XXX	.XX

N	XCEN	VERT. DEFL.	INPLANE DEFL.	TORSION DEFL.	SDZ5	SDY5	MDX5	MEX9	FLATWISE STRESS	EDGEWISE STRESS	CORNER STRESS	TORSION STRESS	TORSION MOMENT
1	.XXX	.XXX	.XXX	.XXX	.XXX	.XXX	XX.XX	.XXX	XXX.	XXX.	XXX.	.XXX	XXX.XX
2	.XXX	.XXX	.XXX	.XXX	.XXX	.XXX	XX.XX	.XXX	XXX.	XXX.	XXX.	.XXX	XXX.XX
3	.XXX	.XXX	.XXX	.XXX	.XXX	.XXX	XX.XX	.XXX	XXX.	XXX.	XXX.	.XXX	XXX.XX
4	.XXX	.XXX	.XXX	.XXX	.XXX	.XXX	XX.XX	.XXX	XXX.	XXX.	XXX.	.XXX	XXX.XX
5	.XXX	.XXX	.XXX	.XXX	.XXX	.XXX	XX.XX	.XXX	XXX.	XXX.	XXX.	.XXX	XXX.XX
6	.XXX	.XXX	.XXX	.XXX	.XXX	.XXX	XX.XX	.XXX	XXX.	XXX.	XXX.	.XXX	XXX.XX
7	.XXX	.XXX	.XXX	.XXX	.XXX	.XXX	XX.XX	.XXX	XXX.	XXX.	XXX.	.XXX	XXX.XX
8	.XXX	.XXX	.XXX	.XXX	.XXX	.XXX	XX.XX	.XXX	XXX.	XXX.	XXX.	.XXX	XXX.XX
9	.XXX	.XXX	.XXX	.XXX	.XXX	.XXX	XX.XX	.XXX	XXX.	XXX.	XXX.	.XXX	XXX.XX
10	.XXX	.XXX	.XXX	.XXX	.XXX	.XXX	XX.XX	.XXX	XXX.	XXX.	XXX.	.XXX	XXX.XX
11	.XXX	.XXX	.XXX	.XXX	.XXX	.XXX	XX.XX	.XXX	XXX.	XXX.	XXX.	.XXX	XXX.XX
12	.XXX	.XXX	.XXX	.XXX	.XXX	.XXX	XX.XX	.XXX	XXX.	XXX.	XXX.	.XXX	XXX.XX
13	.XXX	.XXX	.XXX	.XXX	.XXX	.XXX	XX.XX	.XXX	XXX.	XXX.	XXX.	.XXX	XXX.XX
14	.XXX	.XXX	.XXX	.XXX	.XXXX	.XXX	XX.XX	.XXX	XXX.	XXX.	XXX.	.XXX	XXX.XX
15	.XXX	.XXX	.XXX	.XXX	.XXX	.XXX	XX.XX	.XXX	XXX.	XXX.	XXX.	.XXX	XXX.XX
16	.XXX	.XXX	.XXX	.XXX	.XXX	.XXX	XX.XX	.XXX	XXX.	XXX.	XXX.	.XXX	XXX.XX
17	.XXX	.XXX	.XXX	.XXX	.XXX	.XXX	XX.XX	.XXX	XXX.	XXX.	XXX.	.XXX	XXX.XX
18	.XXX	.XXX	.XXX	.XXX	.XXX	.XXX	XX.XX	.XXX	XXX.	XXX.	XXX.	.XXX	XXX.XX
19	.XXX	.XXX	.XXX	.XXX	.XXX	.XXX	XX.XX	.XXX	XXX.	XXX.	XXX.	.XXX	XXX.XX
20	.XXX	.XXX	.XXX	.XXX	.XXX	.XXX	XX.XX	.XXX	XXX.	XXX.	XXX.	.XXX	XXX.XX

	QW1	QW2	QW3	QW4	QW5	QV1	QV2	QV3	QT1	QT2	BETA	DELTA
(*)	.XXX-YYY	.XXX-YYY	.XXX-YYY	.XXX-YYY	.XXX-YYY	.XXX-YYY	.XXX-YYY	.XXX-YYY	.XXX-YYY	.XXX-YYY	.XXX-YYY	.XXX-YYY
(**)	.XXX-YYY	.XXX-YYY	.XXX-YYY	.XXX-YYY	.XXX-YYY	.XXX+YYY	.XXX-YYY	.XXX-YYY	.XXX-YYY	.XXX-YYY	.XXX-YYY	.XXX-YYY
XI	.XXX-YYY	.XXX-YYY	.XXX-YYY	.XXX-YYY	.XXX-YYY	.XXX-YYY	.XXX-YYY	.XXX-YYY	.XXX-YYY	.XXX-YYY	.XXX-YYY	.XXX-YYY

Sample Page 18.

ii) the unstalled generalized Wagner functions modeling ((A)64 = 1.), and
iii) the UTRC synthesized unsteady stalled modeling ((A)64 = 2.). For
these cases, the first seven aerodynamic quantities are: LAMBDAS, GAMMA,
PHI, ALPHA, MACH, A, and ALPHAW. These quantities are, respectively, the
aerodynamic sweep angle due only to radial flow (in degrees), the total
aerodynamic sweep angle including structural sweep (in degrees), the in-
flow angle and angle-of-attack (both in degrees), Mach number, nondimen-
sional angle-of-attack rate, and the unsteady decay parameter (in degrees).

Unsteady Airloads Utilizing the Padé Formulation

The Padé airload options inherently assume that the pitch and plunge
of the airfoil are independent variables defining the airloads. For either
of the Padé options ((A)64 = 3. or 4.), the first seven aerodynamic quan-
tities are those shown in Sample Page 18: PHTILDA, THTIL, PHI, ALPHA, MACH,
DCL and DCM. The first four of these quantities are, respectively, the per-
turbational inflow and pitch angles away from the mean values defining
the mean angle-of-attack, the total inflow angle, and the total angle-of-
attack, all in degrees. The remaining three items are, respectively, the
Mach number, and the pertrubational unsteady lift and moment coefficients.
If input item (A)64 is equal to 3., the analysis filters out the steady
(low frequency) parts of the inflow and pitch angles so as to use the Padé
airloads on only the perturbational airloads (static airloads on the filtered
low frequency angles). If input item (A)64 is equal to 4., the Padé air-
loads description is used on the total inflow and pitch angles and the per-
turbational coefficients become the total coefficients.

Remainder of Azimuthal Printout

The aerodynamic coefficients CL, CD and CM are self-explanatory and non-
dimensional. The airload distributions in the z_5 and y_5 directions, SAZ5
and SAY5, respectively, have the units of lb/in., the aerodynamic pitching
moments about the x_5 and y_5 axes, MAX5 and MAY5, respectively, have the units
of lb-in./in. The second of the three groups on Sample Page 18 lists per-
tinent spanwise distributions of a structural dynamic nature. The vertical
and inplane deflections are those, respectively, in the z_5 and y_5 directions
and have the units of in. The torsional deflection has the units of deg.
The quantities SDZ5, SDY5 and MDX5 are "semi-dynamic" load distributions.
These distributions are dimensionally the same as those resulting from aero-
dynamics, but arise instead from all the dynamic effects except the doubly
time differentiated ones. The quantity MEX9 is the nonlinear elastic torsion
moment distribution as calculated using the ΔEI implementation (Eq. (38));
it too has the units of lb-in./in. All stress quantities have the units of
$lb/in.^2$, whereas the torsion moment has the units of lb-in. The third of
the three groups on Sample Page 18 lists the modal responses, their non-
dimensional time derivatives and "right-hand-side" excitations. Specifically,

227

for each modal response variable (column) are given the instantaneous displacement, velocity, acceleration and generalized excitation (elements on right-hand side of the modal equation).

After the time-history solution has either converged to periodicity or run to maximum flapping trials (input location (S)9), various integrated loads are calculated for one final blade revolution to form the aerodynamic performance and stress results depicted in Sample Page 19. For each of eight performance quantities, results are presented in nondimensional coefficient form, in nondimensional form divided by solidity, and in actual dimensional form. Note that ten dimensional quantities are listed and the units are lb for forces and lb-ft for moments, as appropriate. The quantity EQU. DRAG (lb) represents the combined power expended by the rotor due to rotor rotation (torque) and translation (drag) divided by flight speed.

The next line duplicates the parameters defining the flight condition and includes additional quantities which depend on the integrated performance for evaluation. At the beginning of the time-history calculation, it is not known which part of the inflow ratio being used is due to ram effects and which due to momentum induced effects. Once the integrated rotor thrust is calculated, however, the induced portion of the inflow can then be calculated using the simple usual momentum formula derived for flight in an infinite continuum. The complementary portion of the inflow represents the ram effect from which the shaft angle-of-attack ALPHA S, in degrees, can be calculated. The quantity VEL ACT is the actual forward flight velocity, in knots, consistent with the advance ratio used and the shaft angle-of-attack. For finite forward flight speeds EQU. L/D is the lift divided by the equivalent drag; for hovering cases this quantity is the figure of merit. PAR. AREA, the rotor parasite (drag) area, in square feet is the rotor drag divided by dynamic pressure. The control angles, A1S, B1S, THETA 75 and the shaft angle-of-attack all have the units of degrees. The power absorbed by the propeller from the airstream in kilowatts is given by the quantity KWATT. It will always be of opposite sign from the horsepower. The remainder of Sample Page 19 consists of reductions of the various stresses given in the azimuthal printout in terms of median and 1/2 peak-to-peak values.

Once the time-history solution has converged to periodicity, the program optionally performs harmonic analyses of the azimuthal variations of various response quantitites. The outputs of these harmonic analyses are depicted in Sample Pages 20 through 22. In each of these sample pages, the harmonic information for each response variable is contained in the appropriate horizontal band of five rows. The harmonics are listed by columns up to a maximum of 10 harmonics. All harmonic analysis output depicted on

228

AERODYNAMIC PERFORMANCE AND STRESSES

	H FORCE	Y FORCE	THRUST	ROLL. MOM.	PITCH MOM.	TORQUE	LIFT	PROP. FORCE	HORSEPOWER	EQU. DRAG
C{}/SIG	X.XXXXXXXX	X.XXXXXXXX	X.XXXXXXXX	X.XXXXXXXX	X.XXXXXXXX	X.XXXXXXXX	X.XXXXXXXX	X.XXXXXXXX	X.XXXXXXXX	
C{}	X.XXXXXXXX	X.XXXXXXXX	X.XXXXXXXX	X.XXXXXXXX	X.XXXXXXXX	X.XXXXXXXX	X.XXXXXXXX	X.XXXXXXXX	X.XXXXXXXX	
DIMENS.	XXX.XX	XXX.XX	XXX.XX	XXX.XX	XXX.XX	XXX.XX	XXX.XX	XXX.XX	XXX.XX	XXX.XX

A1S	B1S	THETA 75	EFF. LAMBDA	EFF. MU	ACT. VEL	ALPHA S	EQU. L/D	PAR. AREA	KILOWATTS
X.XXX	X.XXX	XX.XXX	X.XXXXX	X.XXX	XXX.XX	XXX.XXX	X.XXX	X.XXX	XXXX.XX

N	X CEN	MEDIAN STRESSES / FLATWISE	EDGEWISE	1/2 PTP STRESSES / FLATWISE	EDGEWISE	MAX CORNER STRESSES	TORSION MOMENTS / MEDIAN	1/2 PTP
XX	.XXXX	XXXX.	XXXX.	XXXX.	XXXX.	XXXX.	XXXX.	XXX.XX
XX	.XXXX	XXXX.	XXXX.	XXXX.	XXXX.	XXXX.	XXXX.	XXX.XX
XX	.XXXX	XXXX.	XXXX.	XXXX.	XXXX.	XXXX.	XXXX.	XXX.XX
XX	.XXXX	XXXX.	XXXX.	XXXX.	XXXX.	XXXX.	XXXX.	XXX.XX
XX	.XXXX	XXXX.	XXXX.	XXXX.	XXXX.	XXXX.	XXXX.	XXX.XX
XX	.XXXX	XXXX.	XXXX.	XXXX.	XXXX.	XXXX.	XXXX.	XXX.XX
XX	.XXXX	XXXX.	XXXX.	XXXX.	XXXX.	XXXX.	XXXX.	XXX.XX
XX	.XXXX	XXXX.	XXXX.	XXXX.	XXXX.	XXXX.	XXXX.	XXX.XX
XX	.XXXX	XXXX.	XXXX.	XXXX.	XXXX.	XXXX.	XXXX.	XXX.XX
XX	.XXXX	XXXX.	XXXX.	XXXX.	XXXX.	XXXX.	XXXX.	XXX.XX
XX	.XXXX	XXXX.	XXXX.	XXXX.	XXXX.	XXXX.	XXXX.	XXX.XX
XX	.XXXX	XXXX.	XXXX.	XXXX.	XXXX.	XXXX.	XXXX.	XXX.XX
XX	.XXXX	XXXX.	XXXX.	XXXX.	XXXX.	XXXX.	XXXX.	XXX.XX
XX	.XXXX	XXXX.	XXXX.	XXXX.	XXXX.	XXXX.	XXXX.	XXX.XX

Sample Page 19.

229

HARMONIC ANALYSIS OF BLADE RESPONSES

	A0	1	2	3	4	5	6	7	8	9	10
QW1	X.XXXE-YY	X.XXXE-YY	X.XXXE-YY	X.XXXE-YY	X.XXXE-YY	X.XXXE-YY	X.XXXE-YY	X.XXXE-YY	X.XXXE-YY	X.XXXE-YY	X.XXXE-YY
QW2	X.XXXE-YY	X.XXXE-YY	X.XXXE-YY	X.XXXE-YY	X.XXXE-YY	X.XXXE-YY	X.XXXE-YY	X.XXXE-YY	X.XXXE-YY	X.XXXE-YY	X.XXXE-YY
QW3	X.XXXE-YY	X.XXXE-YY	X.XXXE-YY	X.XXXE-YY	X.XXXE-YY	X.XXXE-YY	X.XXXE-YY	X.XXXE-YY	X.XXXE-YY	X.XXXE-YY	X.XXXE-YY
QV1	X.XXXE-YY	X.XXXE-YY	X.XXXE-YY	X.XXXE-YY	X.XXXE-YY	X.XXXE-YY	X.XXXE-YY	X.XXXE-YY	X.XXXE-YY	X.XXXE-YY	X.XXXE-YY
QV2	X.XXXE-YY	X.XXXE-YY	X.XXXE-YY	X.XXXE-YY	X.XXXE-YY	X.XXXE-YY	X.XXXE-YY	X.XXXE-YY	X.XXXE-YY	X.XXXE-YY	X.XXXE-YY
QT1	X.XXXE-YY	X.XXXE-YY	X.XXXE-YY	X.XXXE-YY	X.XXXE-YY	X.XXXE-YY	X.XXXE-YY	X.XXXE-YY	X.XXXE-YY	X.XXXE-YY	X.XXXE-YY

Sample Page 20.

HARMONIC ANALYSIS OF HUB SHEARS AND MOMENTS

	AO	1	2	3	4	5	6	7	8	9	10
LONG. SHR	XX.X										
LAT. SHR	XX.X										
VERT. SHR	XX.X										
ROLL MOMT	XX.X										
PITCH MOMT	XX.X										
YAW MOMT	XX.X										

Sample Page 21.

231

HARMONIC ANALYSIS OF FLATWISE STRESSES

Sample Page 22.

232

these sample pages assume a negative harmonic content form in keeping with the (negative) harmonic form conventionally assumed for the blade pitch control and rigid flapping angles. For each harmonic of response variable five quantities are output; these quantities are, respectively, the (negative) cosine and sine components, the equivalent amplitude and phase angle, and lastly, the amplitude of the harmonic relative to all the other harmonic amplitudes output. Sample Page 20 depicts the harmonic analyses of the dimensionless modal response variables selected wherein $QW(I)$, $QV(K)$ and $QT(J)$ are, respectively, the (I) flatwise, (K) edgewise and (J) torsional uncoupled mode responses.

Sample Page 21 depicts the harmonic analyses of the total shears and moments exerted by one blade to the hub. In contrast to the steady hub loads listed in the AERODYNAMIC PERFORMANCE AND STRESSES output (Sample Page 19) which are calculated by integrating only the aerodynamic load distributions, the total hub loads, which are herein harmonically analyzed, are calculated by similarly integrating the combined aerodynamic and the dynamic load distributions. The longitudinal, lateral and vertical hub shears comprising the first three quantities of this sample page all have the dimensions of lb and are defined in the x_1-(aft), y_1-(starboard), and z_1- (up and along axis of rotation) axis directions, respectively. The roll, pitch and yaw moments comprising the latter three quantities on this sample page have the dimensions of lb-ft and are defined positive (using the right-hand rule) about the x_1-, y_1-, and z_1-axes, respectively. Note that the aerodynamic rolling moment whose output is depicted in Sample Page 19 is defined positive starboard side down and is opposite from the harmonically analyzed total rolling moment depicted in Sample Page 21. Sample Page 22 depicts the harmonic analysis of the flatwise stresses at the center of each of the spanwise segments. A similar output listing is provided for both edgewise and torsional stresses.

<div align="center">

Results of Solution Part III - Transient
Spectral Stability Analysis

</div>

Transient time-history solutions are often difficult to interpret for quantitative stability information. This is due to the fact that the total responses so calculated inherently consist of several component modes simultaneously and transiently approaching (or departing from) multi-harmonic periodicity with a wide range of natural frequencies and inherent damping levels. The extraction of the component responses at discrete frequencies in order to examine their individual attenuation characteristics is the purpose of the Transient Spectral Stability Analysis (TSSA) portion of Program G400PROP. The details of this analysis, which utilizes Fourier Transform techniques, are beyond the scope of this report but are treated in Reference 32.

Essentially the TSSA first performs Fourier transformations of selected time-history data strings, which have been previously generated in the time-history solution portion of the analysis (Solution Part II) and appropriately saved. The purpose of the Fourier Transform is to identify, within these time-histories, those frequencies whose amplitudes are relatively largest and which are herein denoted as "resonances". The TSSA then calculates the transient behavior of the extracted amplitudes of these resonances over the time-history time interval and estimates equivalent linear stability indices (characteristic exponent, critical damping ratio, and time to half amplitude).

Sample Pages 23 and 24 depict the output typically generated by the TSSA. The sequence of output depicted is duplicated for each of the transient response channels selected. Sample Page 23 depicts the output generated by the Fourier Transform frequency indentification portion of the TSSA. Shown at the top of the page is the transient response channel being analyzed and the frequency range wherein resonance identification is desired (input locations (S)46 and 47). The series of five output items to follow consist of parameters defining the numerical Fourier transform; note that the results of the TSSA incorporate a time nondimensionalization based on rotor speed, Ω. The tabulation of the Fourier Transform follows wherein, for each frequency (harmonic of the fundamental as determined by the total nondimensional time interval), the real and imaginary parts, the square of the amplitude and the logarithm to the base 10 of the amplitude are outputted. Generally, this tabulation will consume more than the one page indicated in Sample Page 23. After this listing is completed, those frequencies and their respective square amplitudes which are found to be resonances, as defined above, are listed.

Aside from their several nonlinearities, the dynamic equations of motion for propeller blades implicitly contain several linear aerodynamic terms which, under conditions of yawed flight, can become periodic. It is not expected then, that the aeroelastic time-history responses generated by these equations should manifest Floquet Theory characteristics (see Reference 34). In particular, the Fourier Transform is capable of identifying "multiple resonances" which are separated by (plus or minus) multiples of the rotor frequency and which would be found to have approximately the same damping level as measured by characteristic exponent. Hence, the resonant frequencies found by the resonance search are further screened to extract only those frequencies with distinct noninteger values and which, within the set having the same noninteger values, have the largest transform magnitudes. These extracted frequencies are herein denoted "fundamental resonances" and are the only ones examined further for stability in the TSSA.

PART III. TRANSIENT SPECTRAL STABILITY ANALYSES OF SELECTED AEROELASTIC TRANSIENT RESPONSES

TRANSIENT RESPONSE CHANNEL NO. XX - FOURIER TRANSFORM AND RESONANT FREQUENCY IDENTIFICATION

DESIRED FREQUENCY RANGE = X.XX TO X.XX (/REV)

```
NUMBER OF POINTS IN TIME SERIES =        XXX
          (ND) TIME INCREMENT =      X.XXXXX    RAD
              LENGTH OF INTERVAL =  XX.XXXXX    RAD
            FUNDAMENTAL FREQUENCY =   X.XXXXX   /REV
               HIGHEST FREQUENCY = XX.XXXXX    /REV
```

RESONANCE FREQUENCIES FOUND BY SEARCH ROUTINE

```
1    .XXXXXXX+YYY     .XXXXXXX+YYY
2    .XXXXXXX+YYY     .XXXXXXX+YYY
3    .XXXXXXX+YYY     .XXXXXXX+YYY
4    .XXXXXXX+YYY     .XXXXXXX+YYY
5    .XXXXXXX+YYY     .XXXXXXX+YYY
6    .XXXXXXX+YYY     .XXXXXXX+YYY
7    .XXXXXXX+YYY     .XXXXXXX+YYY
8    .XXXXXXX+YYY     .XXXXXXX+YYY
9    .XXXXXXX+YYY     .XXXXXXX+YYY
```

RESONANT FREQUENCIES DETERMINED TO BE FUNDAMENTALS

```
1    .XXXXXXX+YYY
2    .XXXXXXX+YYY
3    .XXXXXXX+YYY
4    .XXXXXXX+YYY
```

Sample Page 23.

235

Sample Page 24 depicts the results of frequency fine tuning and
response stability estimation for each of the fundamental resonances ex-
tracted earlier in the TSSA. The results for each of these frequencies are
presented in columnar fashion. The top horizontal blocks of output represent
the frequency fine-tuning results. Of most practical importance are the
values labeled OPTIMIZED FREQUENCY which are, in nondimensional (per rotor
rev) form, the best estimates of the frequency of the fundamental resonant
frequencies. These frequencies are obtained by an optimization technique,
the details of which are beyond the scope of this report. The remainder
of the output depicted on this sample page (for each fundamental resonance)
consists of three horizontal blocks of output representing various estimates
of the effective damping characteristics. These three types of blocks are
best explained by considering, for each of the fundamental responses indicated
in Sample Page 24, the variation in the natural logarithm of the magnitude
of resonant frequency content with (nondimensional) time. If these ampli-
tude logarithms attenuate with time, then the response with that frequency
content (mode) is deemed stable, and conversely the slope of that attenua-
tion with time is a measure of the effective linear damping; in the analysis
this slope is obtained by a simple least-square fit. It may happen that the
variation of amplitude logarithms with time is neither monotonic increasing
nor decreasing in which case a condition of maximum or minimum amplitude
is defined. By weighting the least-square fit either uniformly or with an
appropriate function accentuating the initial or terminal ends of the ampli-
tude logarithms data string, the three latter horizontal blocks of output
depicted in Sample Page 24 are generated. Within each of these blocks, the
first quantity depicted is the nondimensional CHARACTERISTIC EXPONENT, which
is analogous to and interpreted in the same way as the real part of the
eigenvalue discussed in the output for Solution Part I. The REVS to (MAX/
MIN) AMPL is an indication of the asymptotic behavior of the component re-
sponse. STANDARD DEVIATION is the root-mean-squared error achieved in the
least-square curve-fit and is an indication of the regularity of the ampli-
tude logarithm function and of the accuracy of the stability estimation.
Based upon the OPTIMIZED FREQUENCY outputted at the top of the sample page,
the equivalent CRITICAL DAMPING RATIO is calculated from the characteristic
exponent using standard formulas. Finally, the output item labeled REVS TO
HALF AMPLITUDE is the third alternate way in which the equivalent linear
damping result is presented.

In Sample Page 25 is depicted the typical additional page of output
generated at the beginning of every case following the first case of a
multiple case sum. The two columns depict, respectively, the location num-
bers and data values for the newly input data distinguishing the present
case from the previous one. This feature is intended solely as an ease of
usage output to assist in data management.

236

TRANSIENT RESPONSE CHANNEL NO. XX - RESONANT FREQUENCY FINE TUNING AND CRITICAL DAMPING RATIO CALCULATIONS

INITIAL PERCENTAGE	XX.XX			
INITIAL NO. OF DATA PTS.	XXX			
NO. FOURIER COEF. CALCS.	XXX			
FINAL NO. OF DATA PTS.	XXX	XXX	XXX	XXX
INITIAL FREQUENCY ESTIMATE				
(/REV)	X.XXXXX	X.XXXXX	X.XXXXX	X.XXXXX
OPTIMIZED FREQUENCY				
(/REV)	X.XXXXX	X.XXXXX	X.XXXXX	X.XXXXX
HARMONIC	XX	XX	XX	XX
UNIFORMLY WEIGHTED CHARACTERISTICS				
CHARACTERISTIC EXPONENT	X.XXXXX	X.XXXXX	X.XXXXX	X.XXXXX
REVS TO (MAX/MIN) AMPL.	XX.XXXXX	XX.XXXXX	XX.XXXXX	XX.XXXXX
STANDARD DEVIATION	X.XXXXX	X.XXXXX	X.XXXXX	X.XXXXX
CRITICAL DAMPING RATIO	X.XXXXX	X.XXXXX	X.XXXXX	X.XXXXX
REVS TO HALF AMPLITUDE	XXXXX.XXXXX	XXXXX.XXXXX	XXXXX.XXXXX	XXXXX.XXXXX
INITIAL END WEIGHTED CHARACTERISTICS				
CHARACTERISTIC EXPONENT	X.XXXXX	X.XXXXX	X.XXXXX	X.XXXXX
REVS TO (MAX/MIN) AMPL.	XX.XXXXX	XX.XXXXX	XX.XXXXX	XX.XXXXX
STANDARD DEVIATION	X.XXXXX	X.XXXXX	X.XXXXX	X.XXXXX
CRITICAL DAMPING RATIO	X.XXXXX	X.XXXXX	X.XXXXX	X.XXXXX
REVS TO HALF AMPLITUDE	XXXXX.XXXXX	XXXXX.XXXXX	XXXXX.XXXXX	XXXXX.XXXXX
TERMINAL END WEIGHTED CHARACTERISTICS				
CHARACTERISTIC EXPONENT	X.XXXXX	X.XXXXX	X.XXXXX	X.XXXXX
REVS TO (MAX/MIN) AMPL.	XX.XXXXX	XX.XXXXX	XX.XXXXX	XX.XXXXX
STANDARD DEVIATION	X.XXXXX	X.XXXXX	X.XXXXX	X.XXXXX
CRITICAL DAMPING RATIO	X.XXXXX	X.XXXXX	X.XXXXX	X.XXXXX
REVS TO HALF AMPLITUDE	XXXXX.XXXXX	XXXXX.XXXXX	XXXXX.XXXXX	XXXXX.XXXXX

Sample Page 24.

237

PROGRAM G400PROP.- CASE 2 OF A MULTI-CASE RUN. INPUT DATA REPRESENTING CHANGES TO THE PREVIOUS CASE ARE AS FOLLOWS:

```
XXXX    .XXXXXXE+YY
XXXX    .XXXXXXE+YY
XXXX    .XXXXXXE+YY
XXXX    .XXXXXXE+YY
XXXX    .XXXXXXE+YY
XXXX    .XXXXXXE+YY
XXXX    .XXXXXXE+YY
XXXX    .XXXXXXE+YY
XXXX    .XXXXXXE+YY
XXXX    .XXXXXXE+YY
XXXX    .XXXXXXE+YY
XXXX    .XXXXXXE+YY
XXXX    .XXXXXXE+YY
XXXX    .XXXXXXE+YY
```

Sample Page 25.

PROGRAM BACKGROUND MATERIAL

General Information to Facilitate Operation
of Program and Improve Efficiency

Aside from considerations of the details of the aeroelastic modeling which are covered in various above sections and in Reference 1 and 3, additional attention should be paid to maximizing both the efficiency and accuracy of the implemented numerical solutions of the dynamic equations. This subsection presents material describing areas of concern with respect to these numerical methods, and more importantly, ways of dealing with them by proper input procedures.

Blade Segment Selection

Two decisions must be made in selecting a proper distribution of blade segment lengths: how many segments should be used, and where segments should be either sparsely or densely packed. The G400PROP code incorporates a maximum number of twenty segments, up from the maximum of fifteen offered in the earlier versions of G400 (References 1 and 3). Capability to use twenty segments should not be confused with a general need to use all this capability in every application.

Various criteria can be used to guide the program user in making an efficient blade breakup selection:

1. Generally any one segment should not exceed 15 percent of the span. This criterion is subjective in that it is based on accumulated user experience.

2. The segment density should be greatest at the innermost portion of the blade for the E159 part of the program (uncoupled mode calculations) and at outermost portion for the G400 proper part of the program. The requirement for greater blade detail at the root blade portion in the E159 calculation stems from the fact that here the elastic strain energy is most heavily concentrated and has the most variability. It follows that accurate modeling of the equivalent springs used in E159 is enhanced by a finer breakup here. The requirement for greater blade detail in the blade tip portion in the G400 proper calculations stems from the concentration here of inertial and aerodynamic loadings. The aerodynamic loads are especially subject to greatest variability at the tip sections.

239

3. The segment density should be also guided by the specific details of the blade in question. Any blade portion which has locally concentrated properties should have greater segment density. Also, segment boundaries should be selected to conform to the geometry inherent in the blade planform.

4. With some initial extra effort in the preparatory stage, an efficient breakup can be used wherein the need for a dense breakup at the root can be relaxed in the G400 proper portion of the code. This effort consists of first running the E159 preprocessor separately with a dense breakup at the root to maximize the accuracies of the natural frequencies. Then, various inboard segments are selectively eliminated or modified from the mode shapes and other distributed data before subsequent input to G400 proper part of the code. In this manner the elastic modeling accuracy is preserved (through retention of the accurate natural frequencies) while reducing the all over segment count used in the more expensive G400 proper aeroelastic calculation.

Input of Differentiated Data

The coordinate transformations formulated for G400 require two sets of spanwise differentiated data which must be explicitly gleaned from the geometry of the blade design: structural twist rate and structural sweep rate. Although the G400 codes provide for internal numerical differentiations of these quantities, actual designs often include abrupt spanwise variation which cannot be so differentiated efficiently. Consequently, the G400 input list includes a direct input of rate related data, and use of this input is generally recommended for increased accuracy.

The method selected for input of rate data on these items is based on the assumption that the rates are constant over their respective segment lengths. To make the input numbers more meaningful and to minimize data preparation calculations by the user, the rate data are input as respective changes in the variables (either twist angle and/or elastic axis offset) over each segment length. Thus, the actual derivatives are calculated internally by division by each segment length and the user is freed of this chore. One advantage of this input format is that the resulting numerical values input provides a quick check of the data. All such changes can be easily summed to yield the integrated change over the whole blade, for comparison with input root to tip values of the variables themselves.

Temporal Numerical Integration

As discussed in Reference 1, temporal integration of the higher differ-
entiated response variables to obtain the lower ones is achieved in the
G400PROP program using a variant of the Adams integration algorithm. The
selected algorithm is defined by means of the azimuthal integration step
size, $\nabla\psi$, and the integration frequency, $\bar{\omega}$.

The integration step size should be an integral divisor of 360; a proper
choice depends on the maximum coupled frequency inherent in the various aero-
elastic responses. A reasonable upper limit for $\nabla\psi$ is 30 divided by the max-
imum such frequency in per rev. Values of $\nabla\psi$ greater than this upper limit
will compromise the integration accuracy and, for sufficiently large values,
will cause the computed responses to develop "numerical" instabilities. As
a corollary, a check on any response which is predicted to be unstable by
the analysis, is to rerun the case with a reduced integration step size to
test for the possibility of the unstable response being merely a numerical
instability.

For each response degree-of-freedom a different integration frequency,
$\bar{\omega}$, is used in the integration algorithm; this frequency is, for each of the
elastic modes, the respective input natural frequencies (locations (D)4-8,
(D)10-12, and (D)14,15. In addition to defining modal stiffnesses and in-
tegration frequencies, the input frequencies serve yet another purpose. As
noted above, the proper value of integration step size, $\nabla\psi$, varies inversely
with the maximum modal frequency. Thus, run times (caused by reduced step
size) will significantly increase as any one modal frequency increases.
Since any degree-of-freedom exhibiting a large natural frequency tends to
respond quasi-statically, i.e., as if the acceleration ($\overset{**}{q}$) term were neg-
ligible, a reasonable approximation to the response calculation is to avoid
the numerical integration of the $\overset{**}{q}$ term entirely and treat the response
quasi-statically. This option can be invoked for any such high frequency
mode by input of a negative frequency; a negative sign will not affect the
proper usage of the frequency in the calculation of the dynamic equations.
Note that this optional response calculation can be invoked singly or in
combination for any of the elastic modal responses (negative values in any
of locations (D)4-8, 10-12, and 14-15).

State Vector Initial Conditions

For many applications useful results can be obtained from the G400PROP
code with little or no attention paid to the input of initial conditions
(all elements of the (V) Loader block and locations 30-32 of the (A) Loader
block). Three situations exist, however, wherein appropriate and accurate
initial conditions should be input to maximize the usefulness of the analysis.

241

Stability Calculations for Configurations With Strong Nonlinearities

The literature abounds with examples of indentifiable classes of rotor instabilities which involve some form of essential nonlinearity. The inclusion of such nonlinear characteristics in a comprehensive aeroelastic analysis such as G400PROP typically requires making the stability calculations for the blade in its predeflected equilibrium position. This is true for some forms of instability which are best analyzed using the time-history solution, and it is especially true for those for which the eigensolution is most appropriate. Because the time-history solution inherently includes modelings of all excitations it is the logical tool to use for obtaining these equilibrium conditions. The principal difficulty with this approach is that these equilibrium conditions are governed by the same equations of motion which govern the transients, including any instability should it exist. Hence, the presence of an inherent instability can interfere with any attempt to obtain the equilibrium conditions, and some form of filtering, to suppress the unstable transient, is therefore required. The G400PROP code does not have an explicitly dedicated filtering algorithm for this purpose, however, and some other ad hoc measure must be used. Two such measures which could be used are briefly described below:

1. Use of exaggerated amounts of structural damping ((D) loader block locations 31-33) in a precalculation run using the time-history solution. By artificially increasing these damping levels by at least one order of magnitude the inherent instability transient responses can be quenched while leaving the final equilibrium point solution unaffected. The end conditions from this precalculation run define the equilibrium initial conditions for a subsequent stability run which would, of course, include the restored values of structural damping.

2. Use of the quasi-static solution on one of the degrees-of-freedom critical to the instability in a precalculation run (see the above subsection). The time-history solution would then be used in a manner similar to the above described method.

Calibrated Excitations of Transients

For those cases wherein the instabilities are best investigated using the time-history solution, the initial conditions provide a convenient method for exciting the transient responses in an unambiguous and calibrated manner. This can be accomplished by selecting a critical degree-of-freedom and assigning to it a rate initial condition ((V) loader block locations 41-50) equal to its (nondimensional) natural frequency times an appropriate amplitude (in radians).

242

Restart Calculations

For some cases involving time-history calculations insufficient rotor
revolutions may have been selected to define the dynamic phenomenon under
study and a continuation of the case is required. To this end use should be
made of the built-in feature of the G400PROP code to record end conditions
on the control angles, components of induced velocity and the blade deflec-
tion state vector. The code provides for automatic output of punched card
images at the end of the run and, if Loader location (S) 34 is input with
a nonzero value appropriate to an available file unit number, to that file
as well. Note, however, that these end conditions will be so recorded only
if the run makes a normal completion. Premature aborting of the run because
of excessive response amplitudes, for example, will suppress this output.
Finally, once the end conditions are recorded they can then be used as
initial conditions for subsequent runs.

Computer Run Times and Storage Requirements

Typical Run Times

The run times required for making typical calculations with the G400PROP
code depend on two main factors: the computer type and the extent of the
aeroelastic problem being solved. This subsection provides information which
should be of help in bracketing the run time to be expected in any specific
application. Clearly the run times are in proportion to the degree of so-
phistication selected from what is avilable in the code. For example, use
of analytic static airfoil data, quasi-static airloads and reduced numbers
of both modes and radial stations will significantly reduce the run time,
albeit at an expense in accuracy. The data presented in Table X was obtained
from running various problem configurations with the code on the UTRC UNIVAC
1110/81A. Usage of the program with complete variation of all possible com-
binations of options is clearly impractical since it would require a prohib-
itively large number of runs. The cases selected for inclusion in Table X,
however, should help in identifying the costs of major calculation features.
The following points can be made from the results of Table X:

1. Eigensolutions are roughly an order of magnitude cheaper than time-
   history solutions.

2. The inclusion of Padé airloads increases the run time of eigensolu-
   tions roughly 50%.

3. Significant reductions of time are obtainable by proper tailoring
   of the run to only those capabilities needed.

243

TABLE X

Typical Run Times for G400PROP on UNIVAC 1110/81A Computer

Solution Capability Used	1	2	3	4	5	6	7	8	9	10
1. E159 Preprocessor	Y	N	N	N	N	N	N	N	N	N
2. Problem Size: NSEG	20	20	20	20	20	15	20	20	20	20
NFM	3	3	3	2	2	2	3	2	2	2
NEM	1	1	1	0	0	0	1	0	0	0
NTM	2	2	2	1	0	0	2	1	1	1
3. Eigensolution	N	Q	P	N	N	N	N	N	N	N
4. Time-History Solution	N	N	N	Y	Y	Y	Y	Y	Y	Y
$\Delta\psi$				1.25	2.5	2.5	1.25	1.25	1.25	1.25
max. revs				10	10	10	10	10	10	10
unsteady airloads				Q	Q	Q	S	P	S	S
5. TSSA	N	N	N	N	N	N	N	N	N	Y
Total CPU time (min:sec)	0:37.5	0:07.6	0:11.5	5:23.0	2:19.2	1:42.6	13:15.2	6:45.5	10:13.1	10:19.0

Sample Case Number

Y: yes
N: no
Q: quasi-static
P: Pade approximant
S: unsteady stalled

4. The additional cost of running the transient spectral stability analysis (TSSA) is minimal. For the TSSA activated sample case 10, 256 point time series were used with a moving block size of 60% and the use of 100 block displacement calculations.

Storage Requirements

The storage requirements for the G400PROP code as installed on the UNIVAC 1110/81A are as follows: total IBANK (instruction required storage) is approximately 75K (decimal) locations and the DBANK (data required storage) is approximately 146K locations for a total of ∿221K. The program lends itself reasonably well to overlay techniques and these storage requirements have been reduced to ∿45K IBANK and 105K DBANK for a total of ∿150K on the UNIVAC. A major identifiable driver on these storage requirements is the eigensolution capability which requires 46K additional directly identifiable storage in the overlay structure. For purposes of comparison with other computers, G400PROP was written and compiled in FORTRAN 77, and one location on the UNIVAC 1110/81A consists of a 36 bit word.

REFERENCES

1. Bielawa, R. L.: Aeroelastic for Helicopter Rotor Blades with Time-Variable, Nonlinear Structural Twist and Multiple Structural Redundancy-Mathematical Derivation and Program User's Manual. NASA CR-2638, February 1976.

2. Bielawa, R. L.: A Second Order Nonlinear Theory of the Aeroelastic Properties of Helicopter Rotor Blades in Forward Flight. Ph.D. Thesis, Massachusetts Institute of Technology, June 1965.

3. Bielawa, R. L.: Aeroelastic Analysis for Helicopter Rotors With Blade Appended Pendulum Vibration Absorbers - Mathematical Derivations and Program User's Manual. NASA CR-165896, June 1982.

4. Houbolt, J. C., and G. W. Brooks: Differential Equations of Motion for Combined Flapwise Bending, Chordwise Bending and Torsion of Twisted Non-uniform Rotor Blades. NACA Report 1346, October 1956.

5. Hodges, D. H. and E. H. Dowell: Nonlinear Equations of Motion for the Elastic Bending and Torsion of Twisted Nonuniform Rotor Blades. NASA TN D-7818, December 1974.

6. Rosen, A. and P. P. Friedmann: Nonlinear Equations of Equilibrium for Elastic Helicopter or Wind Turbine Blades Undergoing Moderate Deformation. UCLA School of Engineering and Applied Science Dpt. UCLA-ENG-7718 (NASA CR-159478), December 1978.

7. Rosen, A.: The Effect of Initial Twist on the Torsional Rigidity of Beams - Another Point of View, ASME Journal of Applied Mechanics, Vol. 47, 1980, pp. 389-392.

8. Hodges, D. H.: Torsion of Pretwisted Beams due to Axial Loading, ASME Journal of Applied Mechanics, Vol. 47, 1980, pp. 393-397.

9. Shield, R. T.: Extension and Torsion of Elastic Bars With Initial Twist, ASME Journal of Applied Mechanics, Vol. 49, 1982, pp. 779-786.

10. Bisplinghoff, R. H., H. Ashley, and R. L. Halfman: Aeroelasticity. Addison - Wesley Publishing Company, Inc., 1957.

11. Bielawa, R. L.: Blade Stress Calculations - Mode Deflection vs. Force Integration, Journal of the American Helicopter Society, Vol. 24, No. 3, July 1978.

12. Gangwani, S. T.: Prediction of Dynamic Stall and Unsteady Airloads on Rotor Blades. Journal of the American Helicopter Society, Vol. 27, No. 4, October 1982, pp. 57-64. Also Preprint No. 81-1, AHS, 37th Annual National Forum, New Orleans, LA., May 1981.

13. Dadone, L. U.: Two-Dimensional Wind Tunnel Test of an Oscillating Rotor Airfoil, Vol. II. NASA CR-2915, December 1977.

14. Gray, L. and J. Liiva: Two-Dimensional Tests of Airfoils Oscillating Near Stall, Vol. II, Data Report. USAAVLAB TR-68-13B, USAAMRDL, Ft. Eustis, VA., April 1968.

15. Beddoes, T. S.: A Synthesis of Unsteady Aerodynamic Effects Including Stall Hysteresis. Vertica, Vol. 1, pp. 113-123, 1976.

16. Carlson, R. G., G. L. Commerford, and P. H. Mirick: Dynamic Stall Modeling and Correlation with Experimental Data on Airfoils and Rotors. Presented at the AHS/NASA Specialists' Meeting on Rotorcraft Dynamics, NASA SP-352, Rotorcraft Dynamics, Paper 2, February 1979.

17. Gangwani, S. T.: Synthesized Airfoil Data Method for Prediction of Dynamic Stall and Unsteady Airloads. NASA CR-3672, February 1983.

18. Jordan, P. F.: Aerodynamic Flutter Coefficients for Subsonic, Sonic and Supersonic Flow (linear Two Dimensional Theory), RAE RM No. 2932, April 1953.

19. Vepa, R.: Finite State Modeling of Aeroelastic Systems, NASA CR-2779, February 1977.

20. Ballhaus, W. F. And P. M. Goorjian: Implicit Finite Difference Computations of Unsteady Transonic Flows About Airfoils, AIAA Journal, Vol. 15, No. 12, December 1977, pp. 1728-1735.

21. Ballhaus, W. F. and P. M. Goorjian: Efficient Solution of Unsteady Transonic Flows About Airfoils, Paper No. 14, AGARD Conference Proceedings No. 226, Unsteady Airload in Separated and Transonic Flows, 1978.

22. Hildebrand, F. B.: Introduction to Numerical Analysis. McGraw-Hill Book Co., Inc., New York, N. Y., 1956.

23. Davis, S. D. and G. N. Malcolm: Experimental Unsteady Aerodynamics of Conventional and Supercritical Airfoils, NASA TM 81221, August 1980.

24. Lighthill, M. J.: Oscillating Airfoils at High Mach Number, Journal of the Aeronautical Sciences, Vol. 20, No. 6, June 1953.

25. Jones, R. T.: The Unsteady Lift of a Wing of Finite Aspect Ratio, NACA Report 681, 1940.

26. Moler, C. B. and G. W. Stewart: An Algorithm for Generalized Matrix Eigenvalue Problems, SIAM Journal of Numerical Analysis, Vol. 10, No. 2, April 1973.

27. Ward, R. C.: An Extension of the QZ Algorithm for Solving the Generalized Matrix Eigenvalue Problem. NASA-TN-D7305, July 1973.

28. Smith, B. T., et al: Lecture Notes in Computer Science, No. 6, Matrix Eigensystem Routines - EISPACK Guide. Springer-Verlag, Berlin, 1976.

29. Garbow, B. S., et al: Lecture Notes in Computer Science, No. 51, Matrix Eigensystem Routines - EISPACK Guide Extention. Springer-Verlag, Berlin, 1977.

30. Roark, R. J. and W. C. Young: Formulas for Stress and Strain. McGraw-Hill Book Co., New York, 1975, pp. 294.

31. Gessow, A. and G. C. Myers: Aerodynamics of the Helicopter. Frederick Ungar Publishing Co., New York, 1967

32. Kuczynsky, W. A.: Inflight Rotor Stability Monitor. NASA Symposium on Flutter Testing Techniques, NASA Flight Research Center, Edwards AFB, California, October 1975.

33. Bielawa, R. L.: Dynamic Analysis of Multi-Degree-Of-Freedom Systems Using Phasing Matrices. American Helicopter Society/NASA Specialists Meeting on Rotorcraft Dynamics Proceedings, No. 4, Moffett Field, California, 1974.

34. Hall, W. E.: Application of Floquet Theory to the Analysis of Rotary Wing VTOL Stability. SUDDAR No. 400, Stanford University Center for Systems Research. (NASA Contract NAS-25143), 1973.

1. Report No. NASA CR-3729	2. Government Accession No.	3. Recipient's Catalog No.
4. Title and Subtitle Aeroelastic Analysis for Propellers - Mathematical Formulations and Program User's Manual		5. Report Date December 1983
		6. Performing Organization Code
7. Author(s) R. L. Bielawa, S. A. Johnson, R. M. Chi, and S. T. Gangwani		8. Performing Organization Report No. UTRC83-6
		10. Work Unit No.
9. Performing Organization Name and Address United Technologies Research Center East Hartford, Connecticut 06108		11. Contract or Grant No. NAS3-22753
		13. Type of Report and Period Covered Contractor Report
12. Sponsoring Agency Name and Address National Aeronautics and Space Administration Washington, D.C. 20546		14. Sponsoring Agency Code 535-03-12 (E-1799)

15. Supplementary Notes

Final report. Project Manager, Oral Mehmed, Structures and Mechanical Technologies Division, NASA Lewis Research Center, Cleveland, Ohio 44135.

16. Abstract

Mathematical development is presented for a specialized propeller dedicated version of the United Technologies Corporation G400 Rotor Aeroelastic Analysis. This specialized analysis, G400PROP, simulates aeroelastic characteristics particular to propellers such as structural sweep, aerodynamic sweep and high subsonic unsteady airloads (both stalled and unstalled). Detailed formulations are presented for these expanded propeller related methodologies. Results are presented of limited application of the analysis to realistic blade configurations and operating conditions which include stable and unstable stall flutter test conditions. Sections are included for enhanced program user efficiency and expanded utilization. This material includes (1) a detailed description of the structuring of the G400PROP FORTRAN coding, (2) a detailed description of the required input data, (3) a detailed description of the output results, and (4) general information to facilitate operation and improve efficiency.

17. Key Words (Suggested by Author(s)) Propellers Rotor aeroelasticity Structural sweep Unsteady airloads Stall flutter	18. Distribution Statement Unclassified - Unlimited STAR Category 39

19. Security Classif. (of this report) Unclassified	20. Security Classif. (of this page) Unclassified	21. No. of pages 253	22. Price* A12